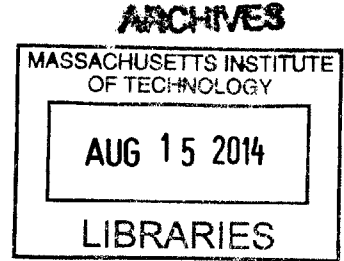


Chemical Kinetic Modeling of Oxy-Fuel Combustion of Sour Gas for Enhanced Oil Recovery

by

Dominik Bongartz

B.Sc. Mechanical Engineering
RWTH Aachen University, 2012



Submitted to the Department of Mechanical Engineering
in partial fulfillment of the requirements for the degree of

Master of Science in Mechanical Engineering

at the

MASSACHUSETTS INSTITUTE OF TECHNOLOGY

June 2014

© Massachusetts Institute of Technology 2014. All rights reserved.

Signature redacted

Author

Department of Mechanical Engineering

May 9, 2014

Signature redacted

Certified by

Ahmed F. Ghoniem

Ronald C. Crane (1972) Professor of Mechanical Engineering

Thesis Supervisor

Signature redacted

Accepted by

David E. Hardt,

Ralph E. and Eloise F. Cross Professor of Mechanical Engineering

Chairman, Department Committee on Graduate Theses

Chemical Kinetic Modeling of Oxy-Fuel Combustion of Sour Gas for Enhanced Oil Recovery

by

Dominik Bongartz

Submitted to the Department of Mechanical Engineering
on May 9, 2014, in partial fulfillment of the
requirements for the degree of
Master of Science in Mechanical Engineering

Abstract

Oxy-fuel combustion of sour gas, a mixture of natural gas (primarily methane (CH_4)), carbon dioxide (CO_2), and hydrogen sulfide (H_2S), could enable the utilization of large natural gas resources, especially when combined with enhanced oil recovery (EOR). Chemical kinetic modeling can help to assess the potential of this approach. In this thesis, a detailed chemical reaction mechanism for oxy-fuel combustion of sour gas has been developed and applied for studying the combustion behavior of sour gas and the design of power cycles with EOR.

The reaction mechanism was constructed by combining mechanisms for the oxidation of CH_4 and H_2S and optimizing the sulfur sub-mechanism. The optimized mechanism was validated against experimental data for oxy-fuel combustion of CH_4 , oxidation of H_2S , and interaction between carbon and sulfur species. Improved overall performance was achieved through the optimization and all important trends were captured in the modeling results.

Calculations with the optimized mechanism suggest that increasing H_2S content in the fuel tends to improve flame stability through a lower ignition delay time. Water diluted oxy-fuel combustion leads to higher burning velocities at elevated pressures than CO_2 dilution or air combustion, which also facilitates flame stabilization. In a mixed CH_4 and H_2S flame, H_2S is oxidized completely as CH_4 is converted to carbon monoxide (CO). During CO burnout, some highly corrosive sulfur trioxide (SO_3) is formed. Quenching of SO_3 formation in the combustor can only be achieved at the expense of higher CO emissions.

The modeling of a gas turbine cycle showed that oxy-fuel combustion leads to SO_3 concentrations that are one to two orders of magnitude lower than in air combustion and will thus suffer much less from the associated corrosion problems. Slightly fuel-rich operation is most promising for achieving the low CO and oxygen (O_2) concentrations required for EOR while further minimizing SO_3 . Carbon dioxide dilution is better for achieving low O_2 in the EOR stream while H_2O gives the better combustion efficiency.

Thesis Supervisor: Ahmed F. Ghoniem

Title: Ronald C. Crane (1972) Professor of Mechanical Engineering

Acknowledgments

I would like to thank Professor Ghoniem for his guidance and support throughout my Master's program. His confidence and vast knowledge and experience in the field of combustion and energy conversion have been a source of inspiration and his advice has been invaluable for my work.

I am also grateful to Dr. Santosh Shanbhogue, who has been extremely helpful with all my questions ranging from software problems over combustion and energy systems to presentation techniques and scientific writing. It was a great pleasure to be working on this project with him and my fellow Master's student Nadim Chakroun.

My colleagues at the Reacting Gas Dynamics Lab and my friends and housemates have contributed much to making my time at MIT one of the most memorable periods of my life and I would like to thank them for everything.

Finally, I would like to my family - most of all my parents and my sister Nicola - and my girlfriend Hanna, as well as my good friends in the Old World for their never ending love, understanding, and patience. I could not have done this without them.

The funding of this work by Siemens Energy, Inc is gratefully acknowledged.

Contents

Abstract	3
Acknowledgments	5
1 Introduction	11
1.1 Sour Gas as an Energy Source	11
1.2 Oxy-Fuel Combustion for Enhanced Oil Recovery	12
1.3 Combustion Modeling	13
1.4 Thesis Goals and Outline	15
2 Literature Review	17
2.1 Impact of the Combustion Products	18
2.1.1 Oil Well and Pipeline Requirements	18
2.1.2 Oxy-Fuel Combustion of Methane	19
2.1.3 Sulfur Species	24
2.1.4 Interactions Between Carbon and Sulfur Species	30
2.1.5 Summary: Combustion Products	31
2.2 Flame Stability	32
2.2.1 Oxy-Fuel Combustion of Methane	32
2.2.2 Hydrogen Sulfide Combustion	44
2.2.3 Interactions Between the Two Fuels	45
2.2.4 Summary: Flame Stability	46
2.3 Conclusion	47
3 Chemical Reaction Mechanism Development	49
3.1 Basic Reaction Mechanisms	50

3.1.1	Methane Mechanism	50
3.1.2	Hydrogen Sulfide Mechanism	53
3.2	Mechanism Optimization	54
3.2.1	Thermodynamic Data	55
3.2.2	Chemical Kinetic Data	55
3.3	Model Validation	61
3.3.1	Oxy-Fuel Combustion of Methane	62
3.3.2	Hydrogen Sulfide Combustion	64
3.3.3	Interaction	70
3.4	Conclusion	74
4	Characteristics of Sour Gas Combustion	77
4.1	Adiabatic Flame Temperature	77
4.2	Ignition Delay Time	79
4.3	Laminar Burning Velocity	83
4.3.1	Impact of the Combustion Mode	84
4.3.2	Impact of the Fuel Composition	88
4.3.3	Influence of Pressure	90
4.4	Premixed Flame Structure	94
4.4.1	General Structure	94
4.4.2	Impact of the Combustion Mode	96
4.4.3	Impact of the Fuel Composition	99
4.4.4	Flame Thickness	100
4.5	Conclusion	101
5	Kinetic Modeling of a Sour Gas Power Cycle	103
5.1	Model Development	104
5.1.1	Power Cycle and Boundary Conditions	104
5.1.2	Performance Measures	106
5.1.3	Reactor Network Model	108

5.2	Flame Zone Design	110
5.2.1	Equilibrium Trends	111
5.2.2	Chemical Time Scales	113
5.3	Dilution Zone Design	115
5.3.1	Dilution Cooling Rate	116
5.3.2	Formation of Sulfur Trioxide During Cooling	122
5.4	Influence of the Equivalence Ratio	125
5.5	Conclusion	127
6	Conclusions	131
6.1	Summary	131
6.2	Suggested Future Work	132
	References	135
A	Reaction Mechanism	149
A.1	Optimized Sulfur Reactions	149
A.2	Recommended Sour Gas Mechanism	151
A.2.1	Thermodynamic Data	151
A.2.2	Chemical Kinetic Data	161

Chapter 1

Introduction

Continuous supply with energy in the desired forms is one of the basic needs of our modern society. The demand for power is increasing rapidly because of the growth of the world population and the fast economic development of large countries like India and China. This trend is expected to continue well into the twenty-first century [1].

Fossil fuel sources, which currently account for more than 80% of the world primary energy consumption, are limited and their use is causing growing concern because of the role of carbon dioxide (CO_2) emissions in global warming. It is therefore of prime importance to develop new technologies for ensuring future energy supply at an affordable cost while minimizing environmental impact.

One potential new energy source that could help address this issue is sour gas. The use of this unusual fuel for electricity generation could be enabled by oxy-fuel combustion. Investigating the potential of this approach by means of numerical modeling is the purpose of the present thesis.

This chapter first provides some general information on sour gas and oxy-fuel combustion technology. Next, the general approaches to combustion modeling used in this work are presented. The final section states the research objectives and introduces the structure of the thesis.

1.1 Sour Gas as an Energy Source

Sour gas is a kind of natural gas that contains large amounts of hydrogen sulfide (H_2S) and CO_2 . The volume fractions of these contaminants usually vary between 0% and 30% each,

with the exact composition differing widely between different gas fields [2]. Both substances are considered undesirable if the gas is to be used for electricity generation. Carbon dioxide lowers the heating value of the gas which makes it more expensive to transport and more difficult to burn. Hydrogen sulfide is both corrosive and toxic and its combustion can produce sulfur compounds that cause corrosion of the plant hardware and for which strict emission standards have been imposed.

Expensive purification processes are necessary to reduce the mole fractions of CO_2 and H_2S to acceptable levels before using the gas in a conventional power plant. Because of these difficulties, a significant fraction of the world wide natural gas resources is currently unusable [3]. Keeping in mind the increasing demand for energy, finding an economically viable way of using these resources is becoming more and more attractive.

1.2 Oxy-Fuel Combustion for Enhanced Oil Recovery

Oxy-fuel combustion is a promising technology to address the problems associated with the use of sour gas. It has recently received increasing attention as one of the possible ways of implementing carbon capture and sequestration (CCS), the other ones being post-combustion capture, pre-combustion capture and electrochemical separation [4]. In oxy-fuel combustion, the fuel is burned in pure oxygen (O_2) and some diluent that is added to moderate the temperatures. In the most common cycle designs, this diluent is either CO_2 , water (H_2O), or a mixture of the two. The exhaust stream exiting the combustor thus consists mainly of CO_2 and H_2O . After running it through a turbine to generate power, the H_2O can easily be removed by condensation. The remaining stream of CO_2 can be sequestered, which has been proposed as a means to mitigate climate change, or used in enhanced oil recovery (EOR) [5]. In EOR, the CO_2 is injected into a depleted oil field to reduce the viscosity of the oil and increase the amount of oil that can be extracted from it.

Using oxy-fuel combustion with EOR for generating electricity from sour gas is expected to be beneficial in several ways:

- The problem of a low heating value can be overcome by reducing the amount of diluent

that is recycled to the combustor, thus enhancing flame stability.

- Oxy-fuel cycles are likely to operate with little to no excess oxygen [6], which might alleviate the corrosion issues caused by the sulfur-containing combustion products.
- Through the use of the CO₂ in EOR an additional revenue stream can be generated to counteract the additional cost and complexity of an oxy-fuel power plant compared to a conventional one [7].
- In EOR the exhaust gases are not discharged into the atmosphere but sequestered in an oil field. This might eliminate the need to extract the products of hydrogen sulfide combustion as well as change the constraints for other pollutants.
- Aging oil fields are a common source of sour gas. By using this gas close to the field in an oxy-fuel process, the life of the field can be extended while additionally generating electricity from an otherwise unusable byproduct.

So far, this technology has never been implemented and has not even been treated explicitly in the scientific literature. It is hence necessary to further investigate this approach to evaluate its potential. Since many difficulties that might be encountered in the process like the formation of corrosive combustion products or difficulties in flame stabilization are related to chemical effects, it is of special importance to have chemistry models that can predict the combustion behavior at the desired conditions. In particular, such chemistry models can be used to verify if the claimed advantages of using an oxy-fired concept over conventional air-combustion actually exist and what diluent is the most promising.

1.3 Combustion Modeling

The ideal way to investigate realistic gas turbine combustors in a numerical analysis would be the use of full-scale three dimensional computational fluid dynamics (CFD) with a detailed chemical reaction mechanism that includes all important chemical species and reactions. Despite the continuing increase in computational power, this is still not feasible for technologically relevant Reynolds numbers because of the stiffness caused by the chemical reactions

and the huge amount of computational effort needed for the computation of the turbulent flow field. Therefore, three general modeling approaches have emerged for describing chemically reacting flows.

The first approach consists in conducting full-scale CFD while using a description of the combustion chemistry in as simplified a way as possible. These simplistic chemistry models generally fall into two categories [8]:

1. Global mechanisms consisting of few (typically 1-4) steps that are postulated based on an understanding of the combustion chemistry. The reaction rate parameters are obtained by fitting some sort of experiment. The validity of such models is usually limited to the kind of situation that was used for the parameter determination.
2. Reduced mechanisms that are derived from a corresponding detailed mechanism. The reduction procedure usually involves the elimination of species and reactions that are not important for the situations of interest and subsequent application of quasi steady-state and partial equilibrium assumptions. Reduced mechanisms are usually somewhat larger than global mechanisms (e.g. 5-15 steps) and also contain a number of algebraic expressions for the concentration of minor species in addition to the differential equations.

This approach is useful for assisting the design of a combustor by predicting flame shape, flame length, temperature distribution and distributions of major species. However, such calculations cannot be expected to give accurate descriptions for the concentrations of minor species, which may include some important pollutants.

The second approach for obtaining useful information about the reactive flow is to keep the full detailed chemical reaction mechanism and simplify the flow field instead. This approach uses a network of simplified reactor models such as well stirred reactors (WSR) or plug flow reactors (PFR) to approximate a real combustor and possibly even the flow path of the flue gas including turbines and heat exchangers. The setup of the reactor network can be based on physical intuition and residence time considerations [9, 10] or on a previous CFD simulation using simplified chemistry [11, 12]. Since the chemistry is represented in all

necessary detail, even minor species can be predicted.

Finally, one can also use detailed chemistry in models of canonical situations that do not refer to any specific geometry but provide general insights about the fuel-oxidizer system of interest. Such models describe for example a freely propagating 1-D laminar flame, the ignition of a homogeneous gas mixture, or a gas stream that experiences a certain temperature profile along its flow path. This can be useful for validating detailed reaction mechanisms and obtaining information on how different gas compositions and operating conditions affect both flame stability and emissions.

Up to now, no chemistry model for oxy-fuel combustion of sour gas is available in the literature. Since a detailed reaction mechanism can be used both in the canonical situations for predicting general parameters and in the reactor network approach and can also form the basis of reduced mechanisms for use in CFD, the development and validation of such a mechanism seems to be a good first step towards understanding the combustion behavior of sour gas under oxy-fuel conditions.

1.4 Thesis Goals and Outline

The goal of this work is twofold. First, a chemistry model for sour gas combustion should be developed and validated to provide a tool for investigating the concept. Second, this model should be used in reactor network models and computing standard combustion parameters for evaluating the potential of the technology and providing indications on the most promising implementation as far as chemical effects are concerned.

After a summary of the initial literature review in Chapter 2, Chapter 3 describes the development and validation of a detailed reaction mechanism for sour gas. In Chapter 4, this mechanism is used to predict some basic combustion properties of sour gas, and in Chapter 5 to evaluate the behavior in different power cycles using a simplified reactor network model. Chapter 6 gives a summary of the main findings and provides an outlook on suggested future work on the topic.

Chapter 2

Literature Review

The main challenges of this project with respect to the combustion process are caused by the unusual fuel with varying composition and possibly high contents of H_2S and CO_2 , and the fact that the combustion does not take place in air but in O_2 with some diluent other than nitrogen (N_2). In this context, the goal of the literature review is to highlight what is known about problems that might be encountered and what conditions seem promising for ensuring stable combustion at the desired temperature while producing minimal emissions. This can also indicate which phenomena a good chemistry model should be able to predict.

So far, oxy-fuel combustion of sour gas itself has not been treated explicitly in the scientific literature. In fact, even regular air combustion of sour gas has not received much attention, at least not in the context of power generation. However, there are three related fields in the literature that we can draw on. First, oxy-fuel combustion of regular or 'sweet' natural gas has received increasing attention in recent years. Second, there is interest in sulfur chemistry in the context of the Claus process. The Claus process is widely used to convert H_2S that has been extracted from fossil fuels to solid sulfur. However, the operating conditions of this process differ considerably from what is typical for gas turbine combustors. The main differences are that in the Claus plants are operated extremely fuel rich (equivalence ratio of $\Phi = 3$ versus $\Phi = 1$ in oxy-fuel combustion) to achieve the partial oxidation needed for producing solid sulfur, and at lower pressure (close to atmospheric versus up to 15 – 30 atm in a gas turbine). Thus, one has to be careful when adopting results from these investigations. Third, a number of researchers have worked on the formation of SO_x in power plants because of its role as a regulated air pollutant and in causing severe corrosion problems.

This chapter gives an overview of what can be found in these fields on the complexities

related to emissions, the impact of the combustion products on the plant hardware, flame stabilization, and potential stability issues.

2.1 Impact of the Combustion Products

This section summarizes the findings on the impact of the combustion products, including the special restrictions imposed by the intended use of the exhaust stream in EOR, the impact of the typical oxy-fuel diluents on CH₄ combustion, the nature of the sulfur combustion products, and issues arising from the interaction of carbon and sulfur species.

2.1.1 Oil Well and Pipeline Requirements

Since in EOR the exhaust gases are not released into the atmosphere but pumped into an oil well, the allowable concentrations of certain substances are different from the ones in conventional power plants. They are determined by the compatibility with the well, the plant hardware, and the pipelines rather than by the interactions with the atmosphere.

So far, there is no consensus as to what the quality requirements of CO₂ streams for EOR should be. Table 2.1 shows the specifications used by two existing and one planned project, demonstrating the range of compositions.

There are different reasons for the limitation of these components. Carbon monoxide (CO), N₂, and O₂ are known to increase the so-called Minimum Miscibility Pressure (MMP) that is required to inject the CO₂ into the oil well.

Table 2.1: CO₂ purity specifications for existing and planned (*) EOR projects. Data taken from [13, 14].

Component	Kinder Morgan	Weyburn	Gullfaks*
CO ₂	95 %	96 %	99.5 %
CO		1000 ppm	< 10 ppm
O ₂	10 ppm	< 50 ppm	< 10 ppm
H ₂ S	10 – 200 ppm	9000 ppm	
SO _x			< 10 ppm
Hydrocarbons	< 5 %	3 %	100 ppm
N ₂	< 4 %	< 300 ppm	< 0.48 %

Oxygen is particularly harmful because it can also cause overheating at the injection point due to oxidation, increase the oil viscosity through chemical reactions, or enhance the growth of bacteria in the field. Therefore, de Visser et al. [13] recommend to limit the O_2 to less than 100 ppm. Pipitone and Bolland [14] found that such low concentrations cannot be achieved with conventional CO_2 purification systems such as flash units and distillation columns for gas-fired or coal-fired power plants operating with the typical 2 – 6 % excess O_2 .

Injection of H_2S along with the CO_2 has been used for many years as a cheap way of disposing of H_2S . On the other hand, little is known about the co-injection of SO_2 [15].

Apart from the restrictions for injection into the oil well, the CO_2 also has to be transported safely from the power plant to the injection site. De Visser et al. [13] compiled recommendations for the purity of CO_2 for transportation in pipelines (see Table 2.2).

Table 2.2: CO_2 purity recommendations for pipelines. Data taken from [13].

Component	Concentration
CO_2	> 95.5 %
CO	2000 ppm
H_2O	500 ppm
H_2S	200 ppm
Total of N_2 , Ar, H_2	< 4 %

In this case, the limits for CO and H_2S are based on the health hazard in case of sudden pipeline leakages. The water content is limited by the formation of carbonic acid and the solution of hydrogen sulfide, both of which cause corrosion problems. In the presence of SO_2 , even stricter limits on the water content may be necessary. Stanger and Wall [15] studied the thermodynamic data of O_2 , H_2O , and SO_2 in compressed CO_2 and found that even for small concentrations of SO_2 , sulfuric acid will form with any water available rather than carbonic acid. Therefore, they suggest a maximum water content of 50 ppm instead of 500 ppm.

2.1.2 Oxy-Fuel Combustion of Methane

The use of a diluent other than N_2 in oxy-fuel combustion has a significant impact on the combustion products. If CO_2 is used as a diluent, the working fluid of the cycle will consist

mainly of CO₂ with a small portion (on the order of 20%) of H₂O, while in the case of H₂O dilution the working fluid is basically steam with roughly 10% of CO₂. Besides having significant consequences for the design of the cycle and the turbomachinery, this might also impact the formation of undesired substances.

Ideally, NO_x formation should not be an issue in oxy-fuel combustion since the oxidizer does not contain any nitrogen. Therefore, NO_x is not considered in the following section. However, it should be kept in mind that some nitrogen could be introduced in the system through imperfect air separation for the production of oxygen, contamination of the fuel, and air ingress during the process.

The more important harmful species in oxy-fuel combustion of CH₄ are CO and O₂. Any CO or O₂ present in the flue gas signifies a waste of fuel or energy used for oxygen production, respectively. Furthermore, as discussed above, the allowable concentrations of both substances are restricted for EOR. The emissions of these species in oxy-fuel combustion using CO₂ or H₂O as a diluent is discussed in this section.

Carbon Dioxide Dilution

Glarborg and Bentzen [16] found significantly increased CO concentrations in a CH₄ flow reactor at all equivalence ratios (Φ) when using CO₂ dilution instead of N₂ dilution (see Figure 2-1). Through chemical kinetics simulations, they found that oxy-fuel conditions at medium to high temperatures lead to the formation of CO mainly through



A similar observation was made by Heil et al. [17] who measured the concentrations of CO and O₂ in their burner for non-premixed flameless combustion of CH₄. They found an increase in the CO concentrations at the combustor outlet of a factor of three for oxy-fuel operation as compared to air combustion. Oxygen emissions were comparable for both combustion modes.

A number of studies have been reported on the emission behavior of CO₂ diluted oxy-fuel

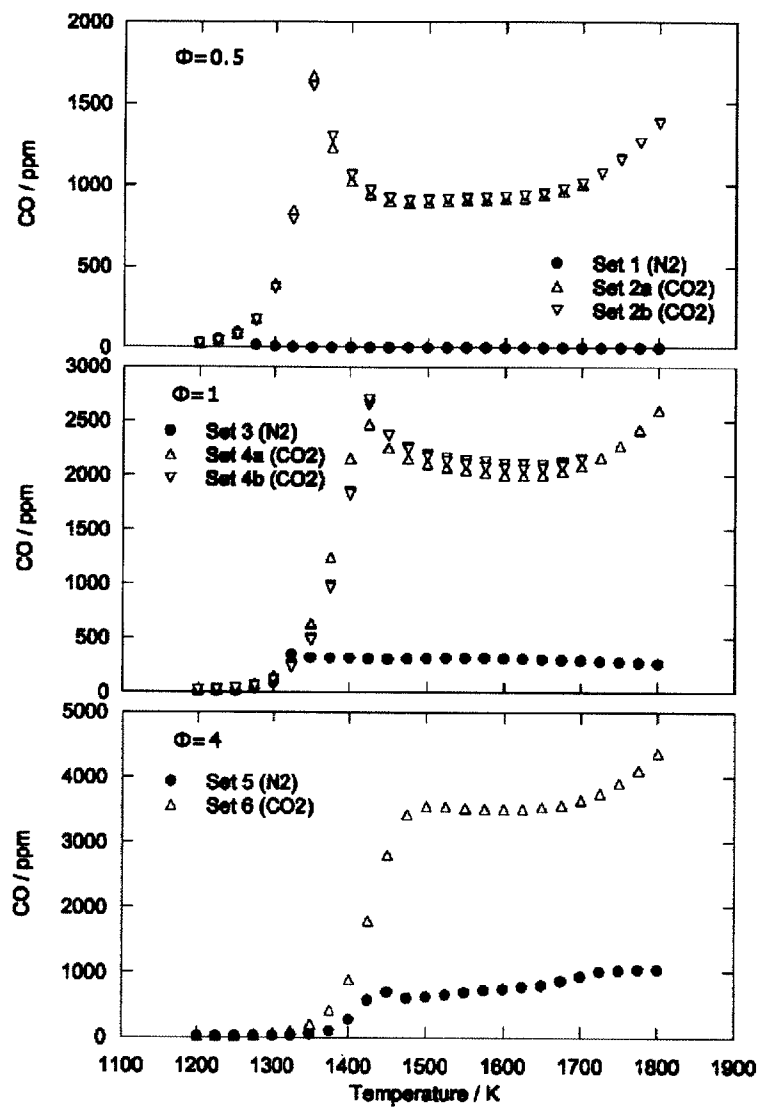


Figure 2-1: Increased CO concentrations in a CH₄ flow reactor with CO₂ dilution as compared to N₂ dilution. Adopted from [16], modified.

combustion in gas turbine combustors. Williams et al. [18] studied CO emissions from a pre-mixed swirl stabilized combustor and found a sharp increase in CO emissions above $\Phi = 0.95$ and a slight increase when raising the O_2 concentration from 30 to 35%. In a similar investigation, Li et al. [19] found that CO and O_2 emissions follow opposite trends with increasing equivalence ratio and oxygen concentration (see Figure 2-2). The authors explained the decrease of the unburned O_2 emissions with increasing initial oxygen concentration by the higher flame speed leading to more complete combustion.

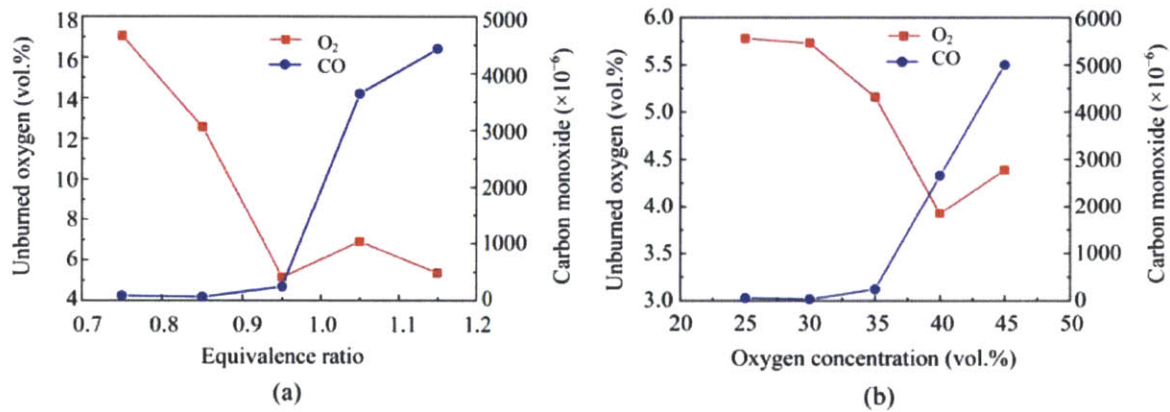


Figure 2-2: CO and O_2 emissions from a premixed swirl-stabilized combustor follow opposite trends with varying equivalence ratio and oxygen concentration. a) Fixed oxygen concentration of 30%. b) Fixed equivalence ratio of 0.95. Adopted from [19].

This observation on the O_2 emissions is in contrast to the findings of Amato et al. [20, 21]. They conducted a comprehensive study on the emissions of CO and O_2 in a similar combustor at atmospheric pressure and found that for a fixed equivalence ratio the concentrations of both substances increase with increasing adiabatic flame temperature, which corresponds to an increasing initial O_2 concentration (see Figure 2-3). The temperature dependence of the emissions is far weaker than what is predicted by thermodynamic equilibrium calculations. In agreement with the previous studies, increasing the equivalence ratio was found to increase CO and decrease O_2 emissions. These trends could be reproduced qualitatively with chemical kinetics calculations using a fixed residence time of 40 ms, but there were still quantitative differences. Chemical kinetics calculations at 15 atm suggest that both CO and O_2 emissions will decrease with increasing pressure. This is caused by lower equilibrium concentrations and faster chemical kinetics at higher pressure.

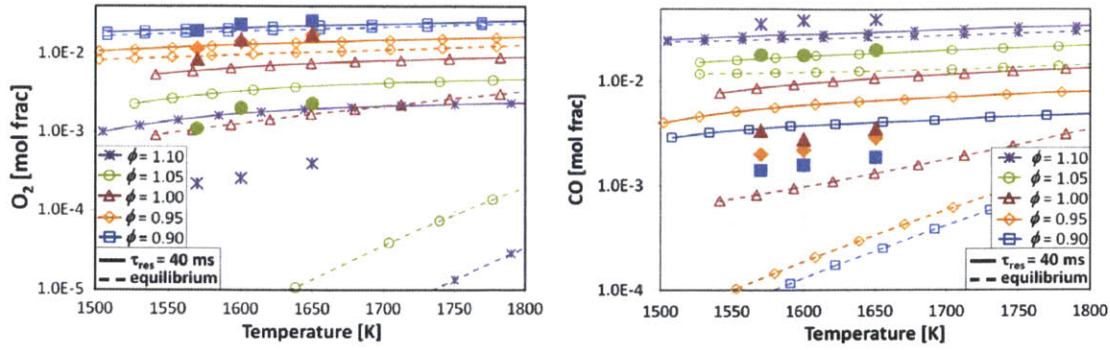


Figure 2-3: Both CO and O₂ emissions from a swirl-stabilized combustor increase with the adiabatic flame temperature. Adopted from [21].

Water Dilution

Bhargava et al. [22] investigated the influence of steam addition on the CO emissions of a CH₄-air flame in a gas turbine combustor at elevated pressure and found that for a given flame temperature there is no dependence of the CO emissions on the steam content.

A study on a swirl stabilized combustor in H₂O diluted oxy-combustion mode by Chorpening et al. [23] showed that similar to CO₂ dilution the CO emissions increase sharply close to $\Phi = 1$ while O₂ decreases slightly with increasing equivalence ratio.

Comparison

Richards et al. [24] compared the CO emissions of H₂O and CO₂ diluted oxy-fuel combustion using equilibrium and chemical kinetics calculations for elevated pressure and temperature. They found that H₂O dilution leads to significantly lower equilibrium CO levels than CO₂ dilution, and that the burnout time required to reach 1.1 times this equilibrium concentration is shorter. However, they point out that in both cases the CO levels are not unreasonably high and the burnout times are within the typical range for gas turbine combustors.

During the development of the reheat combustor for the CES oxy-fuel power cycle [25], Lewis et al. [26, 27] used a reactor network of a swirl stabilized combustor consisting of a WSR and a PFR in series to investigate CO emissions. They concluded that CO₂ dilution gave higher emissions and required longer residence times. For both diluents, there was a

dilution ratio that gave minimum emissions and about 10% of excess O_2 was needed for acceptable CO burnout.

Recently, Abián et al. [28] compared the chemical pathways by which CO_2 and H_2O influence CO oxidation. They found that while CO_2 tends to slow down the oxidation under all conditions because of the consumption of OH radicals, H_2O can either inhibit or enhance the oxidation depending on its concentration.

2.1.3 Sulfur Species

The primary combustion product of hydrogen sulfide is SO_2 . In the presence of excess oxygen, a few percent of this SO_2 are usually further oxidized to sulfur trioxide (SO_3) [29, 30]. Under fuel-rich conditions, formation of solid deposits of elementary sulfur has been observed [31, 32]. Sulfur trioxide is particularly troublesome because it is known to cause different kinds of corrosion that can damage the plant hardware. This section therefore focuses on the formation of SO_3 and its role in the related corrosion mechanisms.

Sulfur Trioxide Formation

Sulfur trioxide is thermodynamically favored at lower temperatures, but in most cases its formation is kinetically limited (see Figure 2-4).

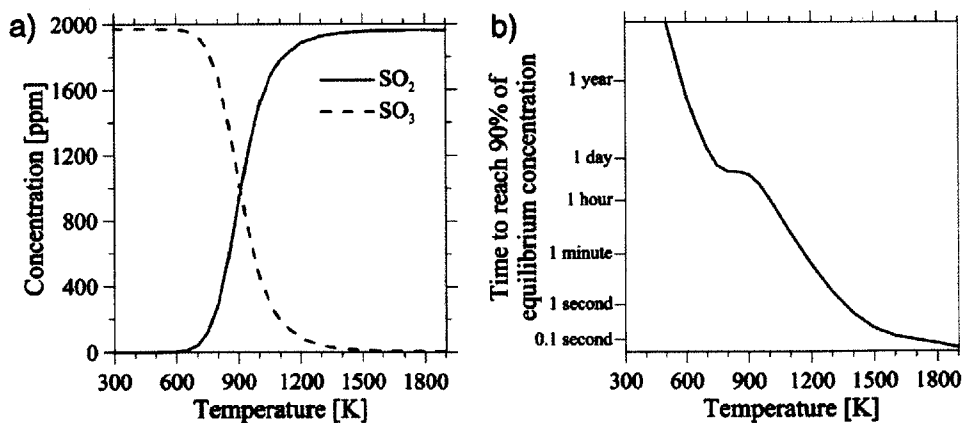


Figure 2-4: Sulfur trioxide formation is kinetically limited. a) Equilibrium concentrations. b) Time scale for reaching equilibrium. Adopted from [33], modified.

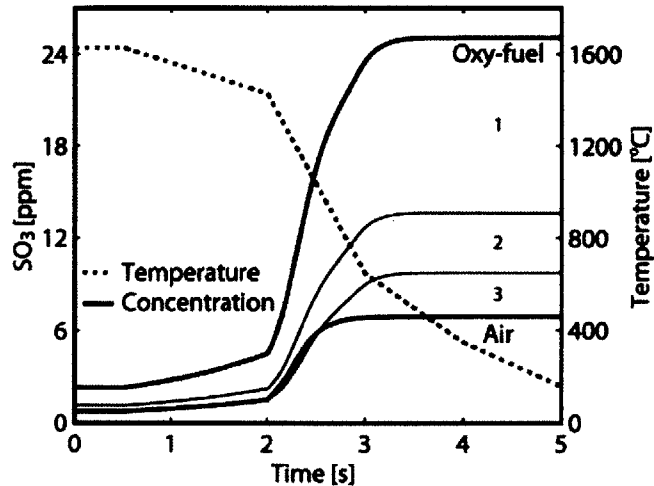
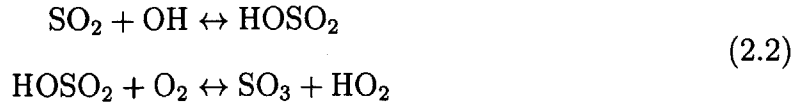


Figure 2-5: Increased SO_3 concentration in CO_2 diluted oxy-fuel combustion of lignite. The areas 1–3 denote the different effects leading to the increase. Adopted from [29].

Fleig et al. [29] investigated the SO_2/SO_3 conversion in the context of pulverized coal combustion using chemical kinetics and found that SO_3 formation can be increased under CO_2 diluted oxy-fuel conditions (see Figure 2-5). They attribute this increase to three effects, the relative importance of which is indicated by the areas 1 to 3 in Figure 2-5:

1. Since they assume that part of the flue gas is recycled to control the flame temperatures before any desulfurization process has taken place, the oxidizer mixture already contains SO_2 . This increases the overall SO_2 concentration and thus the probability of SO_3 formation.
2. Due to the higher heat capacity of the diluent compared to nitrogen, the volume flow rate of the diluent is lower to match the flame temperatures of air combustion. Therefore, the same amount of sulfur in the fuel leads to higher concentrations in the flue gas.
3. As discussed in Section 2.1.2, the presence of large amounts of CO_2 in the oxidizer changes the radical pool mainly through the reaction $\text{CO}_2 + \text{H} \leftrightarrow \text{CO} + \text{OH}$, thus increasing the amount of OH radicals. According to their analysis, this enhances the formation of SO_3 through the following reactions:



Water in the flue gas can lead to a further increase in SO_3 formation [33, 34].

The calculations of Fleig et al. [29] show that almost all of the SO_3 is formed during the cooling of the flue gas from 1500 K to 1000 K. The amount of SO_3 formed can be decreased through higher cooling rates and reduced excess oxygen (see Figure 2-6). All of these results were also confirmed experimentally for propane flames with SO_2 injection [35].

Finally, SO_3 can also be formed through heterogeneous reactions. Especially iron oxide has been found to catalyze the conversion of SO_2 to SO_3 [36].

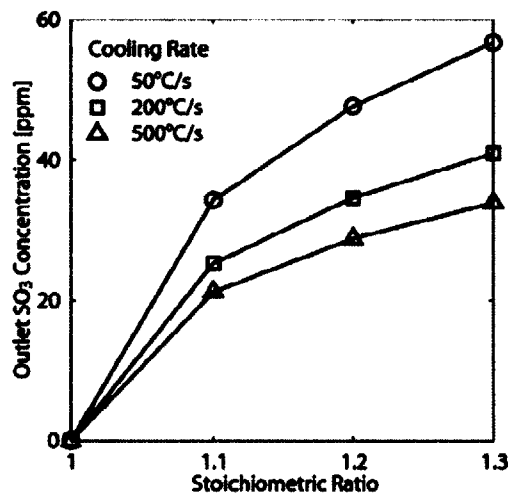


Figure 2-6: The formation of SO_3 decreases with the stoichiometry ratio ($= 1/\Phi$) and increases with the cooling rate. Adopted from [29].

Cold-End Corrosion

Cold end corrosion (also referred to as sulfuric acid corrosion) is a common problem in coal-fired power plants, heat recovery steam generators or oil-fired boilers [15, 37–39]. As the flue gas produced in the combustion of a sulfur-containing fuel is cooled, almost all of the SO_3 combines with the water vapor to form sulfuric acid (H_2SO_4) [39, 40]. If the temperature

drops below the dew point of the sulfuric acid, which is usually on the order of 400 – 500 K, the acid can condense on surfaces and cause strong corrosion.

This acid dew point temperature limits air preheating in coal-fired power plants to avoid corrosion in the air preheater, the electrostatic precipitator (ESP), and the ductwork to the flue gas desulfurization unit [37]. Ganapathy [41] pointed out that it is not the temperature of the flue gas itself that has to drop below the acid dew point to cause condensation of sulfuric acid, but the temperature of the wall. Especially in the case of heat recovery steam generators or boilers, where the critical surfaces are heat exchangers used to heat water or steam, this temperature is determined rather by the fluid on the other side of the wall than by the exhaust gas. Thus, cold end corrosion can occur even at gas temperatures higher than the dew point.

Several correlations have been proposed to predict the acid dew point, such as the ones by Verhoff and Banchero [42], Okkes [43] or ZareNezhad [44]. All of these are based on empirical data and calculate the acid dew point based on the partial pressures of SO_3 and H_2O . If these partial pressures are unknown, it is suggested to use the values encountered in chemical equilibrium at 1273 K, assuming that the kinetics of the SO_2/SO_3 freeze below this temperature. Looking at measurements for different power plants in both air and oxy-fuel combustion, Stanger [15] pointed out that this is a rather conservative estimate.

The ZareNezhad correlation is the most recent one and was found to be more accurate than the other correlations [44]. Figure 2-7 shows that the calculated sulfuric acid dew point increases with both increasing SO_3 and H_2O content in the flue gas. The dependence on the SO_3 is very strong for concentrations under 100 ppm. Increasing the water content above 20 – 30 % does not change the dew point much.

Even more recently, ZareNezhad [45] provided a generalized correlation for calculating the dew point of the most important acids encountered in the flue gases of power plants, including sulfurous acid. The sulfurous acid dew point shows a similar behavior as the sulfuric acid dew point with a weak dependence on the SO_2 concentration instead of SO_3 . However, the sulfurous acid dew point is always more than 50 K lower than the sulfuric acid dew point, making it less problematic.

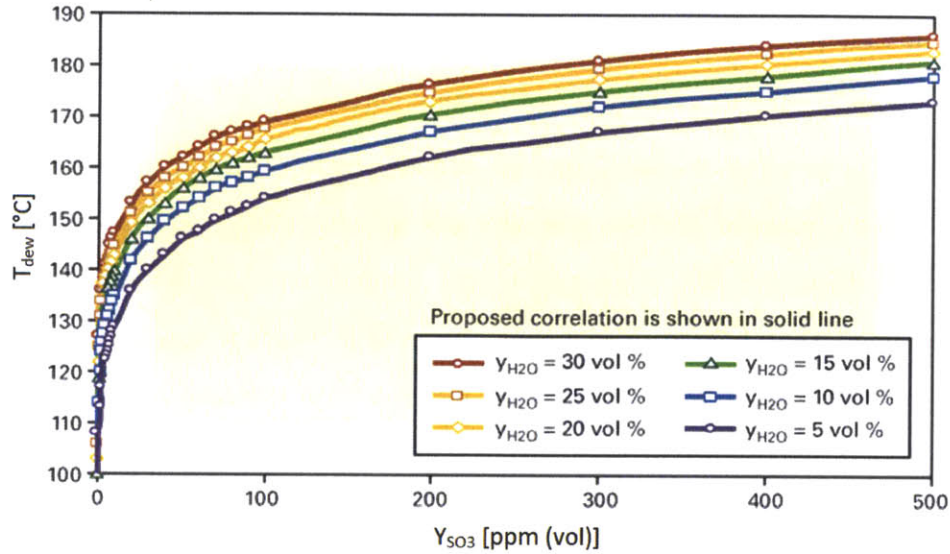


Figure 2-7: The sulfuric acid dew point as predicted with the ZareNezhad correlation increases with the SO_3 and H_2O concentrations. Adopted from [44], modified.

It should be noted that the measurements upon which this correlation is based were taken for compositions ranging from 0 – 500 ppm SO_3 and 5 – 35 % H_2O [15] so that it is not obvious whether the observations are applicable to oxy-fuel combustion with water dilution where the flue gas can contain up to 90 % H_2O . Furthermore, all the data presented in the literature is taken at atmospheric pressure as most studies were focused on coal-fired power plants. In our case, the regions where cold end corrosion could occur are not necessarily at atmospheric pressure since the corrosive gases are the working fluid of the cycle instead of being simply a carrier of thermal energy.

When sulfuric acid condensation occurs, the actual corrosion rate depends on the temperature of the surface and the concentration of SO_3 . The maximum corrosion rates are typically encountered several degrees below the dew point [41, 44]. Therefore, Gomes [46] suggested to non-dimensionalize the gas temperature with the acid dew point in order to characterize the corrosion risk in four classes ranging from 'no corrosion' to 'extreme corrosion'. The maximum corrosion rate decreases if the amount of SO_3 in the gas is reduced [38]. According to an EPRI report [37], the lowest concentrations for which corrosion problems have been reported in power plants are around 20 ppm.

Hot Corrosion

Hot corrosion (also known as fireside corrosion) is a problem commonly encountered in gas turbines that is also due to combustion products containing sulfur [47]. There are two different types of hot corrosion that occur at different temperatures and have different causes [48].

High-temperature hot corrosion (HTHC, or type I hot corrosion) generally occurs between 1100 and 1200 K and is initiated by the formation of a liquid alkali sulfate film on the turbine blades and guide vanes. The temperature range in which it occurs coincides approximately with the range in which these substances are liquid [48]. A number of chemical reaction due to the molten salt film leads to the destruction of the protective oxide film of the surface and the subsequent attack of the base material which can ultimately result in mechanical failure.

The most important agent is Na_2SO_4 , which can be formed through the reaction of sodium and SO_2 in the presence of excess O_2 [49]. The sodium may come with the combustion air in the form of sodium chloride or other compounds, e.g. from seawater or runway dust in the case of aircraft engines. The exact mechanism of formation and whether it is formed in the gas phase and condenses on the blades or is formed via heterogeneous surface reaction has been the subject of extensive discussions in the literature.

Steinberg and Schofield [50] investigated the reaction of sodium with sulfur in hydrogen flames both experimentally and numerically, using SO_2 for lean flames and H_2S for rich flames as a sulfur source. They did not find significant amounts of Na_2SO_4 and estimated that it would take about 100 ppm of sodium for its formation in the gas phase, concluding that heterogeneous formation must be the cause for hot corrosion phenomena. Subsequently, to investigate this heterogeneous formation they analyzed the deposition of salts in hydrogen and propane flames with different sulfur concentrations and sodium salts [51]. They found pure Na_2SO_4 to be the main constituent of the deposited material regardless of the sulfur and sodium sources or flame conditions used. In their experiment, the deposition rate turned out to depend on the sodium concentration by the first order. It was found to be independent of the sulfur content, the fuel and the equivalence ratio. Again, they confirmed that no gaseous Na_2SO_4 was present. Nevertheless, Glarborg and Marshall [52] presented a chemical

mechanism for the homogeneous formation of alkali sulfates through the reaction of alkali chlorides or alkali hydroxides with sulfur oxides. They stated that although this formation pathway is believed not to be important in typical combustion applications, it might play a role in different situations such as biomass combustion, where the occurrence of alkali sulfate aerosols has been reported. For the gas phase formation, the rate-limiting step appears to be the SO_2/SO_3 conversion.

Low-temperature hot corrosion (LTHC, or type II hot corrosion) occurs between 900 and 1000 K and in addition to Na_2SO_4 it is mainly caused by CoSO_4 . CoSO_4 is formed through the reaction of cobalt from the blade material and SO_3 from the gas. Therefore, while being more resistant against HTHC, cobalt-based alloys favor the occurrence of LTHC [49].

Several remedies have been suggested against hot corrosion apart from proper alloy selection (e.g. adding chromium) and the use of protective coatings. One possibility is the washing of the turbine components that are prone to hot corrosion to avoid the accumulation of salts. This is part of the maintenance procedures for aircraft engines, but the suggested intervals (at least once a month) are too short to be applied to power plants that are designed for continuous operation. A second way of avoiding hot corrosion is to keep the air free of salt. It has been suggested that the sodium content should be less than 0.008 ppm by weight to eliminate hot corrosion. This could be achieved with high-efficiency air filters. Also, the content of sodium and potassium as well as vanadium in the fuel should be controlled [49].

2.1.4 Interactions Between Carbon and Sulfur Species

One interesting effect related to the interaction of carbon and sulfur species is the inhibition of CO oxidation by SO_2 . Dagaut et al. [53] investigated this in a jet stirred reactor and in a flow reactor at atmospheric pressure and temperatures of 800 – 1400 K. They found that the oxidation of the CO/H_2 mixtures is slower in the presence of SO_2 , especially for stoichiometric and fuel-rich conditions (see Figure 2-8). According to their analysis, at

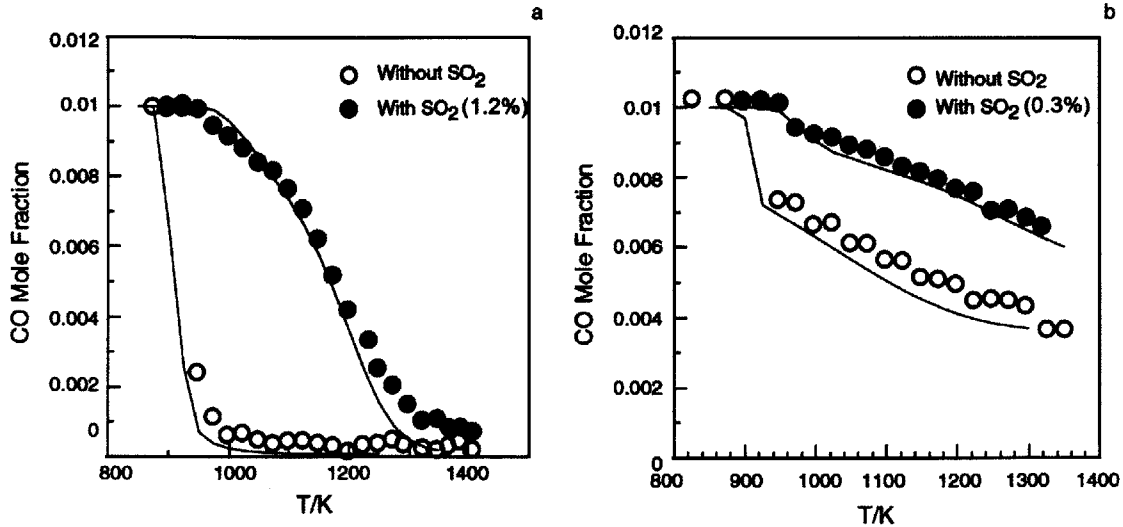
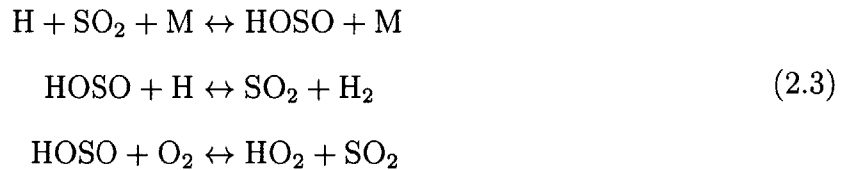


Figure 2-8: Inhibiting effect of SO_2 on the oxidation of a CO/H_2 mixture in a flow reactor at stoichiometric (a) and fuel-rich (b) conditions. Adopted from [53], modified.

stoichiometric conditions and 1200 K this inhibition is mostly due to the reactions



which correspond to a recombination of H radicals. A similar inhibition was also found in a CO_2 atmosphere [54]. This could cause increased CO and possibly also O_2 emissions when burning sour gas.

On the other hand, the presence of combustible carbon species such as CH_4 or CO has been found to enhance SO_2 to SO_3 conversion under certain conditions because of the associated increase in radical concentrations [34].

2.1.5 Summary: Combustion Products

In oxy-fuel combustion for EOR, the allowable concentrations of product species is determined by the compatibility with the plant hardware, the oil well, and the pipelines.

In terms of CH_4 combustion, both CO and O_2 have to be limited to ppm levels. Operation

close to stoichiometric conditions thus seems promising for achieving a good compromise. From equilibrium and chemical kinetics calculations, water dilution appears to be better for achieving low CO levels than CO₂ dilution, which is known to enhance CO formation through CO₂+H=CO+OH. However, there is little data on emissions of H₂O diluted oxy-fuel combustors. The presence of SO₂ in the flue gas could lead to a further increase in CO and possibly O₂ concentrations due to catalyzed radical removal.

The main concern associated with H₂S combustion is the formation of SO₃, which can lead to high temperature corrosion in gas turbines or cold end corrosion in heat exchangers and low pressure turbines. Both high CO₂ and H₂O content could increase SO₃ formation through chemical effects. The exact amounts of SO₃ formed will depend strongly on the cycle design. Operation close to stoichiometry or even slightly rich and fast cooling of the flue gas will help alleviate corrosion problems. The presence of combustible carbon species like CO or CH₄ can catalyze SO₃ formation under certain conditions.

2.2 Flame Stability

This second section deals with flame stabilization, highlighting the characteristics of CH₄ oxy-combustion, what is known on stabilizing H₂S flames, and interactions between the fuels.

2.2.1 Oxy-Fuel Combustion of Methane

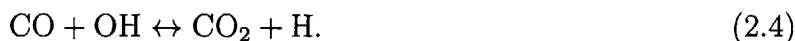
The recent interest in oxy-fuel combustion of natural gas in gas turbines has led to a number of publications on the stability of CH₄/O₂/diluent flames. Important parameters such as the laminar burning velocity and ignition delay times have been investigated for both H₂O and CO₂ diluted flames. Because of the fact that higher cycle efficiencies are expected for CO₂ dilution [55], most studies on the stability of actual combustors have focused on carbon dioxide dilution. However, the first real power plant using oxy-fuel combustion of methane has been built using water dilution [25, 56]. These experiences are reported in the following sections. A brief review of flame stabilization at very high pressures is also included since some of the proposed oxy-fuel cycles operate at unusually high combustor pressure [55].

Carbon Dioxide Dilution

If the N_2 in the combustion air is simply replaced by CO_2 (i.e. 21% O_2 and 79% CO_2 in the oxidizer), the burning velocity of CH_4 is reduced substantially as was first shown by Zhu et al. [57] (e.g. about 87% slower at $\Phi = 1$). This must be considered in the design of a combustor and could make flame stabilization more challenging. The reduction in the burning velocity can be attributed to three effects [18, 58, 59]:

1. The thermodynamic and transport properties of N_2 and CO_2 are different. Most importantly, the isobaric heat capacity of CO_2 is much higher than that of N_2 (e.g. 68% higher at 1500 K [60]). For the same diluent concentration, this leads to much lower flame temperatures.
2. Carbon dioxide is not completely inert but participates in some chemical reactions that influence the burning velocity.
3. The thermal radiation characteristics of CO_2 are different from the ones of N_2 .

Liu et al. [59] investigated the chemical effect of CO_2 dilution on the laminar burning velocity of methane. Using the GRI Mech 3.0, they computed burning velocities both with CO_2 dilution and with a modified substance that has the same properties as CO_2 but does not participate in any reactions (see Figure 2-9). There is a considerable difference in the burning velocities using the real and modified CO_2 , proving that chemical reactions of CO_2 do play a role. Analyzing the chemical pathways, they found the most important reaction to be



Large amounts of CO_2 in the mixture lead to an increased consumption of H radicals. Therefore, this reaction competes with the main chain branching reaction of the H-O-system $H + O_2 \leftrightarrow O + OH$, which slows down the fuel consumption. Kishore et al. [61] and Halter et al. [62] both investigated the effect of increasing addition of nitrogen or carbon dioxide as a diluent to air on the laminar burning velocity of methane using different experimental

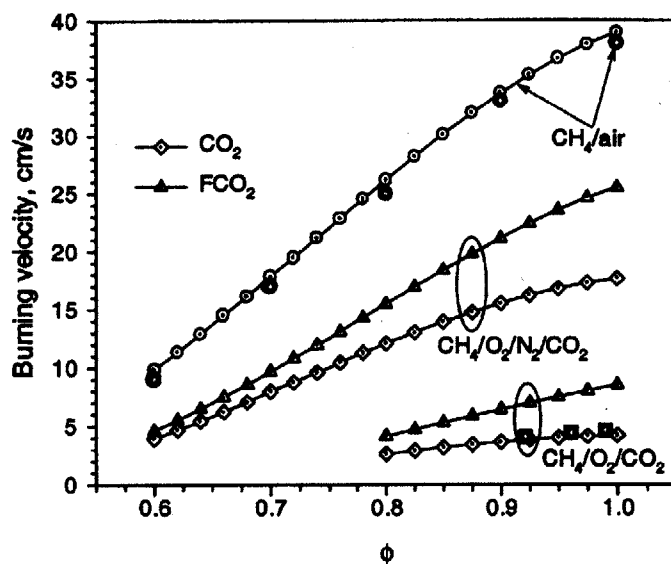


Figure 2-9: The chemical effect of CO₂ dilution on the burning velocity of methane. FCO₂ denotes the modified, inert version of CO₂. Adopted from [59], modified.

methods. They confirmed that the burning velocity decreases faster for carbon dioxide addition than for nitrogen addition. Halter et al. also quantified the relative contribution of increased heat capacity and chemical reactions on the decrease of the laminar burning velocity. They found the importance of the chemical effect to decrease with increasing amounts of diluent in the mixture.

The effect of the altered radiation characteristics has also received some attention. Carbon dioxide is much more effective at emitting and absorbing thermal radiation than nitrogen. This could lead to either increased heat loss of the flame or enhanced pre-heating of the reactants. Numerical investigations of the extinction limits of strained premixed and non-premixed CH₄/O₂/CO₂ flames showed that while significant preheating can in fact occur, the net effect seems to be narrower extinction limits due to increased heat loss [63, 64]. For predicting this effect correctly, the statistical narrow-band model (SNB) was found to perform much better than the optically thin model (OTM) that is often used in air combustion [63–65].

Another important parameter giving indications for flame stabilization is the ignition delay time. Levy et al. [66] investigated the ignition delay of CH₄ experimentally with addition of different diluents in shock tubes for temperatures in the range of 1350 – 1800 K

and pressures of 5 – 10 bar. For a fixed diluent and oxygen concentration by volume, they could not detect a dependance of the ignition delay on the type of diluents added. However, their data is limited to relatively small contents of CO₂ and H₂O (on the order of 5%). Thiessen et al. [67] simulated constant volume autoignition of CH₄ using N₂ and CO₂ dilution. While the ignition delay increases with increasing diluent concentration, they also found the difference between the ignition delays for N₂ and CO₂ dilution to be extremely small (see Figure 2-10). Using a modified CO₂ version with the thermodynamic and transport properties of N₂, they found the physical properties of CO₂ to lead to a increase in the ignition delay because of the lower temperatures. However, this is balanced by the chemical effect that speeds up the reaction in the early stages of combustion. This is in agreement with earlier work on this topic [68]. In a sensitivity analysis, they found the main impact of CO₂ during that stage to be the enhanced third body efficiency compared to N₂. The reactions involving CO₂ directly such as the one responsible for the decrease of the laminar burning velocity don't become important until relatively late in the combustion process and therefore have negligible impact on the ignition delay.

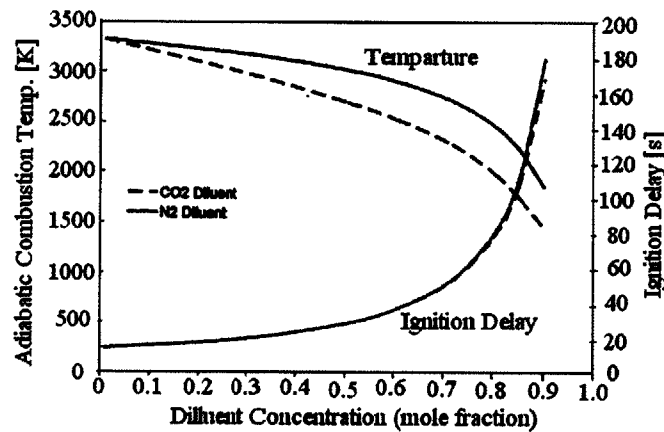


Figure 2-10: Constant volume ignition delay of methane for initial conditions of $T = 800$ K, $p = 1$ atm and $\Phi = 1$. Adopted from [67].

Very recently, a number of studies has been conducted on the stability of actual combustors using geometries that are similar to the ones used in gas turbines. Amato et al. [58] investigated blowoff of premixed CH₄/O₂/CO₂ flames as compared to CH₄/O₂/N₂ and CH₄/Air flames in a swirl-stabilized gas turbine model combustor [69]. They operated the combustor

at atmospheric pressure close to stoichiometry ($\Phi = 0.9 - 1.1$) using different CO_2 or N_2 concentrations to vary the adiabatic flame temperature. For the same inlet flow velocity, they found $\text{CH}_4/\text{O}_2/\text{CO}_2$ to blow off at higher temperatures than CH_4/Air flames. For both $\text{CH}_4/\text{O}_2/\text{CO}_2$ and $\text{CH}_4/\text{O}_2/\text{N}_2$ flames, mixtures closer to stoichiometric compositions were easiest to blow off (see Figure 2-11). This might at first sound counterintuitive since in air flames equivalence ratios close to stoichiometry usually produce the strongest flames. The difference is that in air combustion, varying the equivalence ratio means varying the flame temperature with the highest temperatures occurring close to stoichiometric conditions. In the case of $\text{CH}_4/\text{O}_2/\text{CO}_2$ flames, the flame temperature can be controlled by varying the diluent composition. At stoichiometric conditions, the highest dilution is necessary to achieve a given flame temperature, which slows down the kinetics.

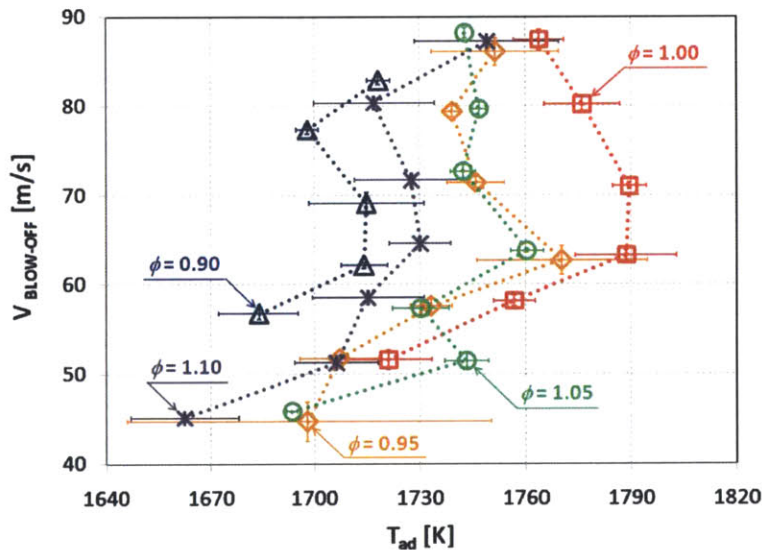


Figure 2-11: Blowoff of $\text{CH}_4/\text{O}_2/\text{CO}_2$ flames in a gas turbine model combustor. Adopted from [58].

The unexpected negative slope of the blowoff data of Amato et al. (cf. Figure 2-11) occurring at higher velocities was also observed by Shroll [70] who suggested this might be caused by a transition to turbulence. Amato et al. found that the blowoff trends for oxy-combustion can be predicted reasonably well using a Damköhler number $\text{Da} = \tau_{\text{flow}}/\tau_{\text{chem}}$ with a chemical time scale based on the extinction strain rate (see Figure 2-12). Using this method, they also predicted blowoff trends for an elevated pressure of 15 bar. The difference

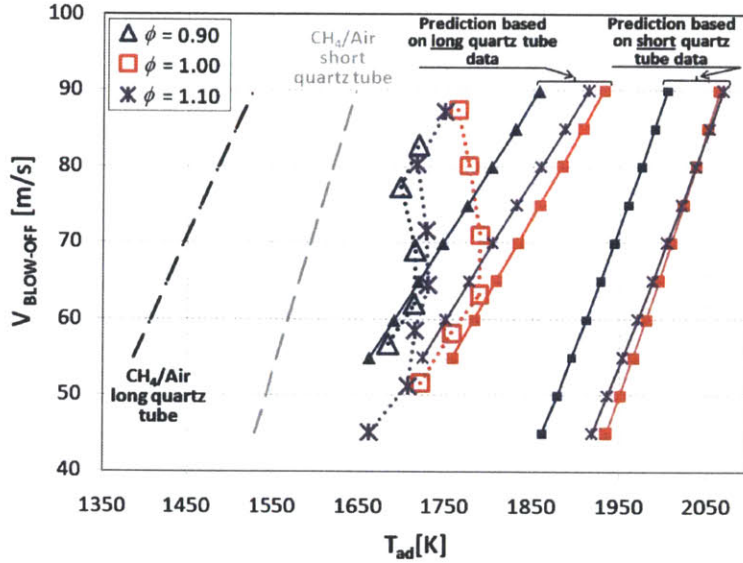


Figure 2-12: Blowoff trends of $\text{CH}_4/\text{O}_2/\text{CO}_2$ flames can be predicted qualitatively using a chemical time scale $\tau_{\text{chem}} = 1/\kappa_{\text{ext}}$. Adopted from [58].

in the adiabatic flame temperature at blowoff between oxy-fuel and air combustion for a specific inlet velocity is considerably smaller at higher pressure. This suggests that the problem of decreased static stability in oxy-fuel combustion might not be as severe at the higher pressures at which gas turbine combustors are usually operated.

Kutne et al. [71] studied the behavior of partially premixed $\text{CH}_4/\text{O}_2/\text{CO}_2$ flames in a gas turbine model combustor at atmospheric pressure varying Reynolds number, equivalence ratio and oxygen concentration. They were unable to stabilize flames at oxygen concentrations lower than 22%. They found that increasing oxygen concentrations to improved the stability of their combustor, although even for 30% O_2 the flame was still less stable than an air flame. This led them to the conclusion that oxy-fuel combustion in combustors designed for air combustion might not be feasible and that special configurations and strategies have to be developed. Seepana and Jayanti [72] were able to stabilize a CO_2 diluted flame in a swirl combustor with 20.9% O_2 in the oxidizer as compared to 14.8% O_2 when using N_2 dilution.

Shroll et al. [70, 73] investigated the dynamic stability of premixed $\text{CH}_4/\text{O}_2/\text{CO}_2$ flames in a swirl-stabilized combustor at atmospheric pressure. The general behavior was found to be similar to air combustion, which is in agreement with the findings of Ditaranto and Hals [74].

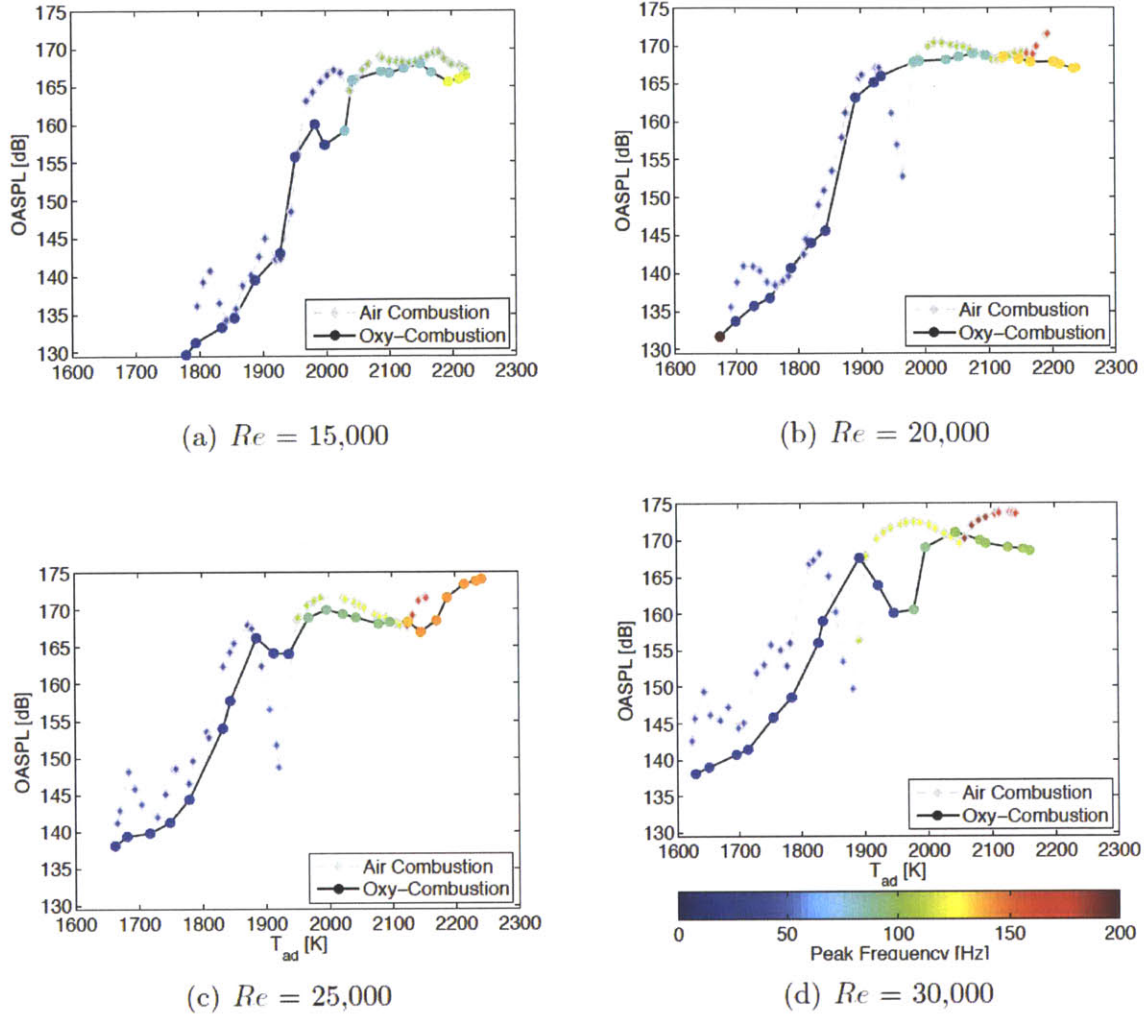


Figure 2-13: Overall sound pressure levels in a swirl stabilized combustor are similar for air and oxy-combustion for the same adiabatic flame temperature. Adopted from [70].

The change of the overall sound pressure level as well as the transition to different limit cycles associated with different flame shapes occurred at similar adiabatic flame temperatures (see Figure 2-13). The difference in the frequencies of the limit cycle corresponds approximately to the change in the speed of sound of the mixture due.

On the other hand, a study by Li et al. [19] in a swirl-stabilized combustor found different acoustic instabilities in air and oxy-fuel combustion, with CO_2 leading to instabilities over a wider range of conditions.

A few studies have been reported on alternative combustion concepts for CO₂ diluted oxy-fuel combustion. Heil et al. [17, 75] demonstrated the flameless non-premixed combustion of CH₄ in an oxy-fuel environment using a commercial 25 kW recuperative burner. They operated the combustor successfully at an equivalence ratio of 0.87 and O₂ concentrations in the oxidizer of 21 and 18% with an estimated inlet temperature of 900 K. Stable combustion at the desired combustor temperature of 1170 K was achieved and the temperature distribution was relatively homogeneous.

Chen and Zheng [76] numerically investigated the combustion of biogas, which they modeled as a mixture of 40% CH₄ and 60% CO₂, under oxy-fuel conditions using a Mild Combustion concept. Similar to flameless combustion, Mild Combustion is characterized by a high inlet temperature of the reactants and a low temperature increase due to the combustion. They found that for preheat temperatures higher than 1200 K, Mild Combustion can be sustained at very low O₂ concentrations.

Water Dilution

The effect of water vapor addition on the laminar burning velocity of methane has also been subject of a few studies. Mazas et al. [77] measured laminar burning velocities of CH₄/O₂/N₂/H₂O flames at atmospheric pressure for equivalence ratios from 0.5 to 1.5, water vapor concentrations of 0 to 20% and O₂ concentrations in the oxidizer of 21 to 100%. They found that the burning velocity decreases linearly with increasing water vapor concentration. The slope becomes less steep for higher O₂ concentrations and equivalence ratios close to unity, that is for higher flame temperatures. The linear behavior was confirmed in a study by Boushaki et al. [78] for small water concentrations. Using simulations with a modified H₂O species that does not take part in any reactions, Mazas et al. [77] showed that the chemical reactions of water tend to reduce the burning velocity. It was found that the slower kinetics are mainly due to the enhanced third body efficiency of H₂O compared to N₂ (16:1) for the reaction



which competes with the main chain branching reaction $\text{H} + \text{O}_2 \leftrightarrow \text{OH} + \text{O}$. Also, the reduction in the O atom concentration due to the enhanced reaction



competes with the reaction $\text{CH}_4 + \text{O} \leftrightarrow \text{CH}_3 + \text{OH}$, which further decreases the CH_4 consumption [77, 79]. Babkin and V'yun [80] investigated the influence of pressure on the effect of water addition, finding a stronger decrease in the burning velocity at higher pressures.

Regarding the ignition delay time, the previously mentioned study by Levy et al. [66] showed that water causes no measurable changes under the conditions of the experiment (1350 – 1800 K, 5 – 10 atm, $\Phi \approx 0.3$, 4% H_2O).

Not many specific experimental results on the stability of H_2O diluted oxy-fuel flames in gas turbine combustors using water dilution have been reported. However, the feasibility of stabilizing a flame under these conditions has been proven through the development of combustors for use in the CES power cycle [23, 24, 27, 81]. Both the primary combustor (called 'gas generator') and a reheat combustor have been successfully tested. The reheat combustor is based on the can-style combustor of the GE J79 gas turbine and uses a combination of sudden expansion and swirl, similar to the model combustor used for the investigation of CO_2 diluted flames [23, 69]. Since NO_x emissions are not expected to be a problem, a diffusion flame is employed (the oxygen and the water are mixed prior to the fuel injection). First test results presented by Chorpening et al. [23] revealed no thermoacoustic instabilities. They operated the combustor at 10 atm and a power of 1 MW using an equivalence ratio of $\Phi = 0.9$ and a steam to oxygen ratio of 5.6:1 (molar). This ratio was chosen to enable ignition and was lower than the ratio of 8:1 that was originally planned to give a flame temperature of 1480 K. Subsequent development and testing were presented by Anderson et al. [81]. Figure 2-14 shows a schematic of the combustor design at this stage. This combustor, too, was successfully tested producing a stable flame. The measured pressure drop across the combustor was 5.5 to 6.0%. However, using the desired steam to oxygen ratio of 8:1, they had to lower the equivalence ratio to $\Phi = 0.67$ to get stable combustion.

The gas generator for the CES power cycle is a platelet type combustor based on a

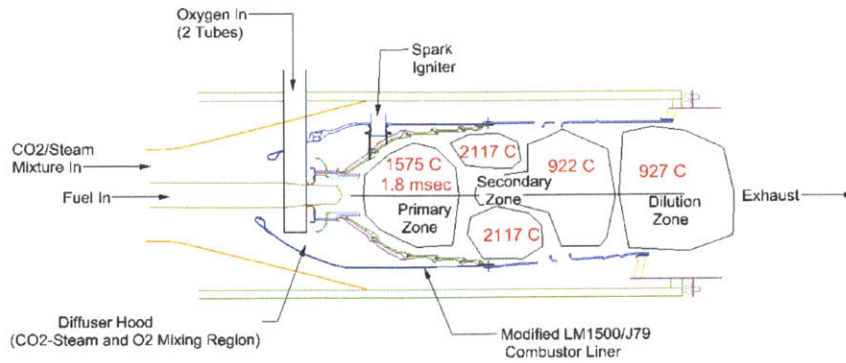


Figure 2-14: Oxy-fuel reheat combustor for the CES cycle. Adopted from [81].

rocket engine [82]. The oxygen and the natural gas along with some water are premixed and injected in the combustor through a stack of platelets with thin channels. The rest of the water is injected along the combustor to moderate the temperature and cool the walls. The specifications of the current version of the GG12 gas generator are a thermal power of 200 MW, a pressure of 62 bar and an outlet temperature of 2030 K [83]. The pressure drop of 15 % is considerably larger than for conventional gas turbines (typically $\leq 5\%$). A similar concept is planned for the reheat combustor in another generation of the CES cycle.

Comparison

Based on the laminar burning velocity, no direct comparison of the stabilization characteristics of CO_2 and H_2O diluted methane flames has been published. Looking at the burning velocity of hydrogen, Le Cong and Dagaut [84] compared the two diluents using their own reaction mechanism and found that the reduction is somewhat stronger in the case of CO_2 dilution (see Figure 2-15). The direct comparison of the results of the different studies presented in the previous sections is difficult, mainly because of the different preheat temperatures used. The static and dynamic stability of CO_2 diluted oxy-fuel flames in gas-turbine combustors is much better documented than for H_2O diluted flames. Nevertheless, the only actual combustor that is currently being developed for use in a gas turbine is based on water dilution. So far, both diluents have required the use of higher combustion temperatures than in air combustion to maintain a stable flame.

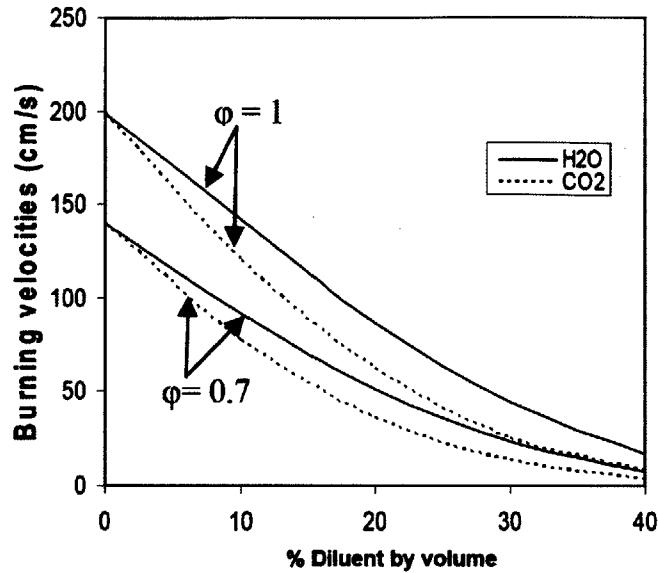


Figure 2-15: The laminar burning velocity of hydrogen-air flames decreases faster for CO₂ addition than for H₂O addition. Adopted from [84], modified.

High Pressure Combustion

One feature of the oxy-fuel cycles for natural gas that have been proposed is that some of them operate at exceptionally high combustor pressures [55]. In the case of the water cycle, the combustor pressure of 83 bar is even higher than the critical point of both CH₄ (46 bar) and O₂ (50 bar) [60]. The influence of high pressures on the laminar burning velocity of methane in air was investigated by Iijima and Takeno [85]. The burning velocity decreases with increasing pressure, which will make it even more difficult to stabilize a flame (see Figure 2-16). Their results also indicate that this problem might be alleviated by increasing the preheat temperature. Eberius and Kick [86] measured burning velocities of methane in air up to 100 bar showing that the decrease continues at these high pressures. They successfully stabilized a conical premixed flame at these extreme pressures in a nozzle burner with a jet diameter of 1.5 mm for slightly fuel-rich conditions ($\Phi \geq 1.1$). Flame stability was good up to 70 bar, beyond this pressure fluctuations occurred which they suggested to mitigate by using an even smaller nozzle.

The combustion of methane in liquid oxygen (LOX) at high pressures has received some

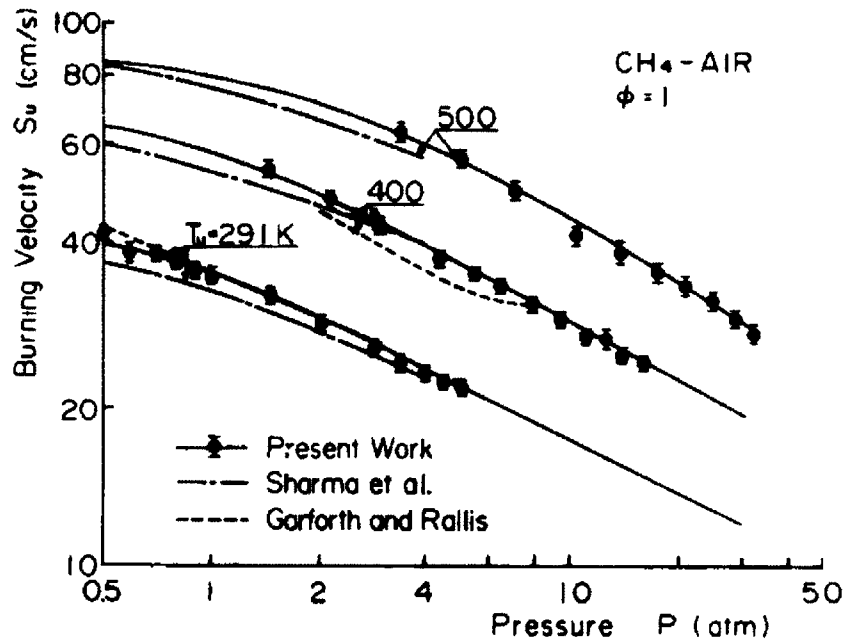


Figure 2-16: The laminar burning velocity of methane-air flames decreases with pressure and increases with the preheat temperature. Adopted from [85], modified.

attention in the literature due to the recent interest in the use of methane as a fuel for rocket propulsion. Lux and Haidn [87] investigated the stabilization of CH_4/LOX flames in a coaxial diffusion type nozzle burner at an equivalence ratio of $\Phi = 1.17$. They were able to stabilize flames at different pressures up to 60 bar and the flame structure did not change significantly with pressure. Other studies have observed a more compact flame for increasing pressures [88, 89].

Salgues et al. [90] compared CH_4/LOX combustion in a similar burner to burners with a swirling oxygen flow in the inner tube for $p = 41$ bar and $\Phi = 1.33$. They found that the swirl burner led to shorter flames with a higher spread angle and to a higher combustor efficiency measured by the chamber pressure.

The third type of combustor commonly used in liquid propellant rocket engines is based on jet impingement, similar to the one employed by CES. A larger number of small injector holes create impinging jets of oxygen and fuel that enable an intense mixing and subsequent combustion [91]. So far, the use of methane in this kind of combustor has not yet been documented in the literature. Compared to the coaxial jet and swirling combustor, this

combustor concept leads to a higher pressure drop [92]. When used in a power plant, this could be detrimental to the efficiency.

2.2.2 Hydrogen Sulfide Combustion

Due to the fact that hydrogen sulfide is not commonly used as a fuel, no work has been reported on the stabilization of H₂S flames in combustors similar to the ones used in gas turbines. However, some important combustion parameters of H₂S are known, although the amount and accuracy of the data available are limited.

Zabetakis [93] reports that the flammability limits of H₂S in air at atmospheric pressures are wider than those of CH₄, especially on the rich side (4 – 44% vs. 5 – 15% for their setup).

The laminar burning velocity of H₂S in air at atmospheric pressure has been the subject of a few early experimental studies (see Figure 2-17). There is considerable scatter in the data, with values at $\Phi = 1$ ranging from 27 cm/s to 48 cm/s. This is on the same order as the maximum burning velocity of CH₄ in air (≈ 40 cm/s [57]). The dependence on the equivalence ratio is also similar to hydrocarbons. The modeling studies of Vervisch et al. [94] and Zhou et al. [32] show some discrepancies with the experiment even when considering the spread of the data. For the former, the dependence on the equivalence ratio is not well reproduced on the rich side, while for the latter the value at stoichiometric conditions is somewhat too high.

The ignition delay time of H₂S was measured by Bradley and Dobson [99] in a H₂S-O₂-Ar mixtures in shock waves for temperatures of 1350 – 2450 K. They measured different induction times for the appearance of OH and SO₂ and reported different results for a high-temperature region and a low temperature region. Frenklach et al. [100] took similar measurements over the temperature range 950 – 1200 K, also looking at the effect of water vapor in the mixture. They found that water accelerates the explosion, although they refrained from presenting quantitative results due to the large scatter of their data. They also presented regressions for the data of Bradley and Dobson, stating that while the low-temperature results do not agree with their own, the extrapolation of the high-temperature results does.

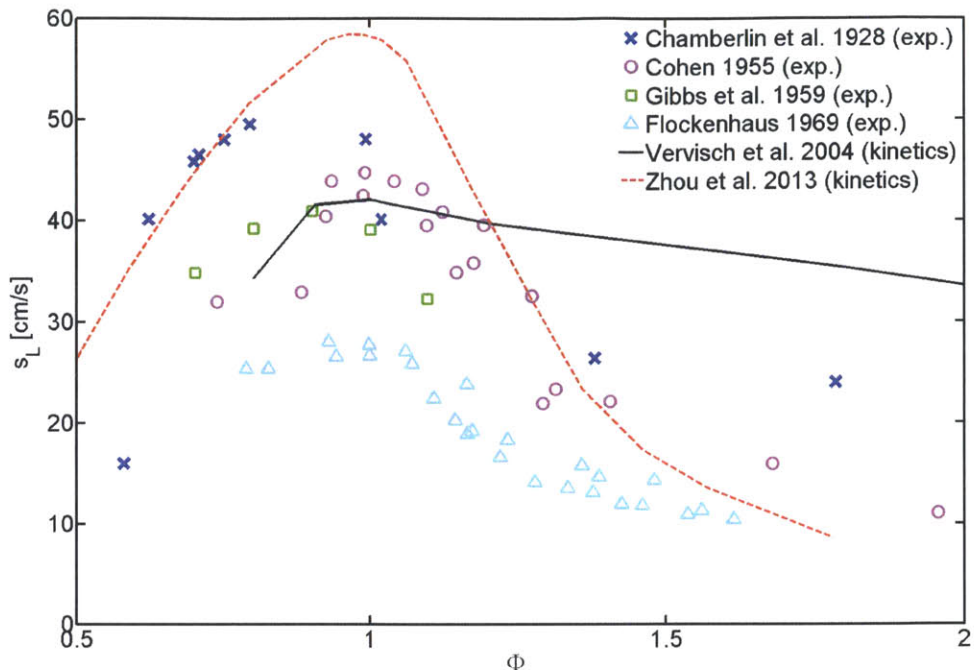


Figure 2-17: Flame speed of hydrogen sulfide in air. Data taken from [32, 94–98].

2.2.3 Interactions Between the Two Fuels

The simultaneous oxidation of CH_4 and H_2S has been investigated numerically and experimentally by Chin et al. [101] in the context of the Claus process, where CH_4 can occur as a contaminant in the feed gas. They found that H_2S oxidation proceeds significantly faster than CH_4 oxidation and that H_2S successfully competes for O_2 in a fuel-rich environment (see Figure 2-18): the fraction of H_2S that is converted is larger and additional O_2 will mostly be consumed by H_2S and not by CH_4 .

Experimental studies on propane/air flames by Kurz [102–104] showed that addition of H_2S can reduce the laminar burning velocity below the values found for either pure propane or pure H_2S . Easier blowout was also observed for propane flames with added H_2S . One possible explanation for this behavior could be the inhibition of CO oxidation by SO_2 mentioned in Section 2.1.4.

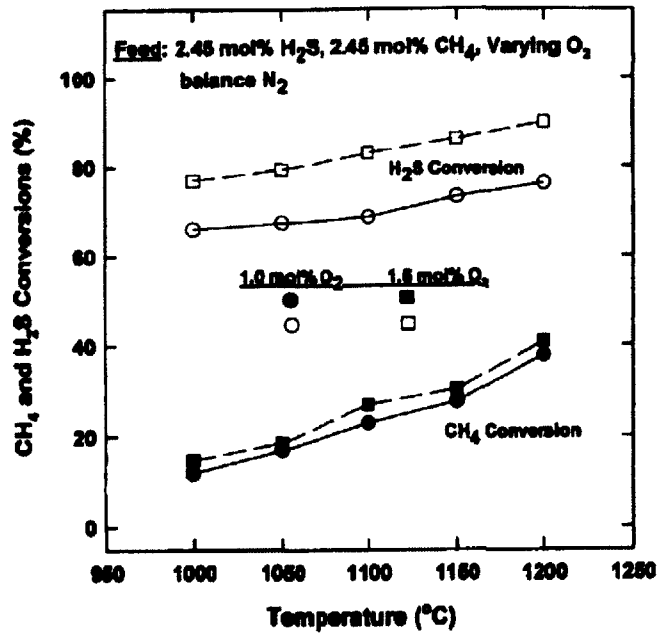


Figure 2-18: H_2S is converted faster than CH_4 in a flow reactor at fuel-rich conditions ($\Phi = 9$, $\Phi = 6$). Adopted from [101].

2.2.4 Summary: Flame Stability

The stability of CH_4 oxy-fuel flames is strongly impacted by the diluent. The different heat capacities of H_2O and CO_2 lead to different flame temperatures, which has a strong impact on the flame speed. Especially CO_2 also has a chemical effect due to the increased H radical consumption through $\text{CO}_2 + \text{H} = \text{CO} + \text{OH}$, which slows down the kinetics. Furthermore, the radiative properties of CO_2 alter the heat transfer characteristics, possibly leading to further destabilization due to increased heat loss. Oxy-fuel flames with CO_2 dilution blow off more easily than air flames and show similar dynamic instabilities. Judging from the laminar burning velocity, H_2O dilution seems to be better for flame stability. Although little experimental data has been reported, the first commercial oxy-fuel combustor operates with H_2O dilution.

The high combustor pressure of some proposed oxy-fuel cycles could exacerbate the difficulties in flame stabilization. This can be counteracted through increased preheating. Platelet type burners may provide an alternative for high pressure flame stabilization at

the expense of an increased combustor pressure drop.

Little is known on the stability characteristics of H_2S . Its flame speed in air is similar to CH_4 and its flammability limits are somewhat wider. On the other hand, H_2S has been found to be detrimental to the stability of propane flames and SO_2 is known to catalyze H radical removal.

2.3 Conclusion

A thorough review of the literature highlighted some of the difficulties that could be encountered in oxy-fuel combustion of sour gas. The following conclusions can be drawn for the design of a power plant from a combustion point of view:

The requirements on the combustion products are determined by the oil well and the plant hardware. For the oil well, this means that both CO and O_2 have to be limited to ppm levels. A major concern related to the combustion products of H_2S is the formation of SO_3 because of its role in different corrosion mechanisms.

Regarding the selection of a diluent, H_2O appears to be more promising than CO_2 . Unlike H_2O , CO_2 leads to a strong decrease in the flame speed of CH_4 due to both thermal and chemical effects. Carbon dioxide diluted oxy-fuel flames blow off more easily than air flames and can encounter similar dynamic instabilities. Little is known about the stability of H_2O diluted oxy-fuel flames, but their feasibility has been demonstrated by the development of the first commercial oxy-fuel combustor.

In terms of CO and O_2 emissions, H_2O dilution also seems to be superior to CO_2 dilution judging from chemical kinetics calculations. However, one general point that should be taken into account when considering emissions from oxy-fuel combustion is the fate of the pollutants as they pass through the cycle. This leads to different conclusions for CO_2 and H_2O dilution which may be illustrated through the following example:

For a given flame temperature, comparable amounts of diluent have to be fed to the combustor for CO_2 and H_2O dilution. Assuming a diluent concentration of 70 %, the exhaust gas will consist of roughly 80 % CO_2 and 20 % H_2O for carbon dioxide dilution and 10 % CO_2

and 90 % H₂O for water dilution. When the water is condensed out of the flue gas before the remaining CO₂ stream is sent to the oil well, most of the pollutants will remain in the CO₂ stream. Thus, if the concentration of some pollutant (e.g. CO) at the combustor outlet is x ppm for both cycles, at the injection site it will be $1.25 \cdot x$ ppm for CO₂ dilution and $10 \cdot x$ ppm for H₂O dilution. On the other hand, for CO₂ dilution the rest of the pollutants is recycled to the combustor which may or may not lead to an increased concentration of these substances. Therefore, it is essential for an unbiased comparison of H₂O versus CO₂ diluted power cycles to look not only at the combustion process but at the whole cycle. This is particularly important when considering SO₃ formation, which mostly occurs during the cooling of the flue gases.

Regarding the design of a combustor, the high pressures that are suggested for several oxy-fuel cycles represent an additional challenge because of the associated decrease in flame speed. However, flame stabilization in shear or swirl burners has been demonstrated up to supercritical pressures. Platelet burners may improve stability at very high pressure at the expense of a high pressure drop.

It is not clear how the stability of the flame will be impacted when H₂S is added to the fuel. While H₂S itself has similar combustion properties as CH₄, it might have an inhibiting effect on CH₄ oxidation. This inhibition could also cause increased CO and O₂ emissions.

In terms of the operating conditions, it seems promising to operate at stoichiometric or even slightly rich conditions. Stoichiometric operation leads to a good compromise between CO and O₂ emissions, hence avoiding to waste fuel or energy for O₂ generation. Operating slightly rich could help comply with the very low O₂ levels allowable for EOR and be beneficial for avoiding SO₃ formation. To further decrease SO₃ formation, the flue gas should be cooled as quickly as possible between 1500 K and 1000 K.

Chapter 3

Chemical Reaction Mechanism Development

The literature review presented in the previous chapter revealed some of the chemical effects that are of special importance for oxy-fuel combustion of sour gas. Based on these findings, a good chemical reaction mechanism for use in this project should fulfill the following requirements:

- Capture the effects of CO_2 or H_2O diluted oxy-fuel conditions on the laminar burning velocity and the ignition delay time of CH_4 over a range of temperatures.
- Predict the formation and consumption of CO and O_2 under oxy-fuel conditions with reasonable accuracy.
- Give a good prediction for the laminar burning velocity and ignition delay time of H_2S over a range of temperatures and for different diluents.
- Predict the formation of SO_3 under the conditions of interest.
- Capture possible interactions between carbon and sulfur species and reproduce the correct relative oxidation speed of CH_4 and H_2S .

Up to now, no chemistry model that performs satisfactorily in all of these situations has been presented in the literature. This chapter describes the development of a reaction mechanism for sour gas, aiming at closing this gap. First, the carbon and sulfur mechanisms that were chosen as a basis for the sour gas mechanism are presented. Next, the tuning of the sulfur

part is described in detail. Finally, the performance of the resulting mechanism in many relevant situations is presented. All modeling was done using CHEMKIN-PRO [105].

3.1 Basic Reaction Mechanisms

As a general approach, we have chosen to first combine one mechanism for CH_4 and one for H_2S combustion that are available in the literature. In choosing the mechanisms, the main criterion was the demonstrated performance in the situations of interest mentioned above. The resulting combined mechanism contains 75 species and 570 reactions.

3.1.1 Methane Mechanism

Methane is one of the best studied fuels because of its simplicity and importance as main constituent of natural gas, and a considerable number of reaction mechanisms has been presented for describing its oxidation in flames. However, virtually all of these were developed and tested for air combustion. It is only very recently that growing interest in oxy-fuel combustion has led to a few studies investigating the suitability of the established mechanisms for simulating oxy-fuel conditions.

After reviewing the relevant literature, we have chosen the GRI-Mech 3.0 [106] (53 species, 325 reactions), which is one of the most widely used and best tested CH_4 mechanisms currently available. It has been used successfully to predict the reduction in laminar burning velocity in methane-air flames with CO_2 addition [61, 62] (see Figure 3-1) and H_2O addition [77, 78] and in H_2O diluted oxy-fuel flames [77] (see Figure 3-2) at atmospheric pressure with satisfactory precision. However, the stronger decrease through water addition at higher pressures observed in the experiments is somewhat underpredicted [79] (cf. Figure 3-4). The mechanism can also correctly predict the influence of different diluents on the ignition delay time of CH_4 (see Figure 3-3).

The most promising alternative is the mechanism presented by Le Cong et al. [107] (131 species, 1043 reactions), which is based on an existing hydrocarbon mechanism and was optimized for incorporating the effects of high H_2O and CO_2 concentrations. It was

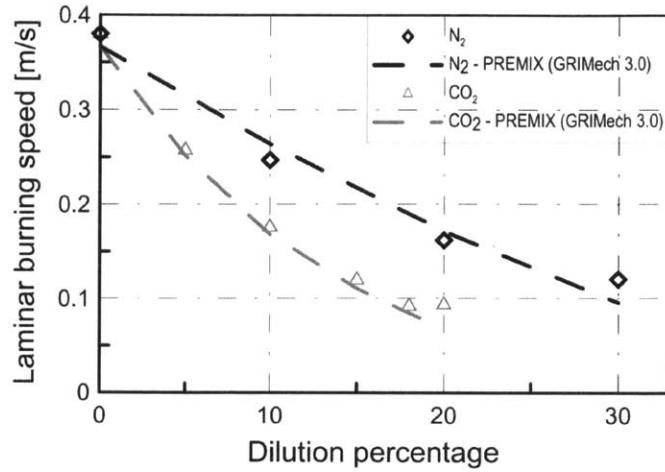


Figure 3-1: The GRI-Mech 3.0 (lines) can predict the decrease in the laminar burning velocity of stoichiometric CH₄-air flames with addition of CO₂ in the experiment (symbols) of Halter et al. [62]. Adopted from [62].

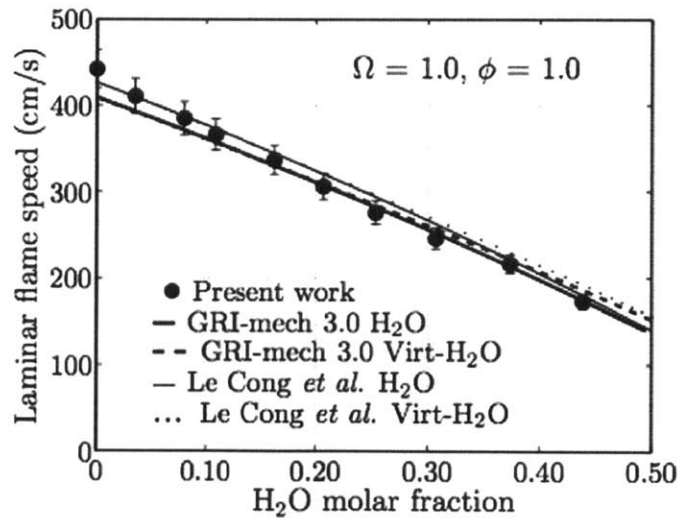


Figure 3-2: The GRI-Mech 3.0 (solid line) can predict the laminar burning velocity for stoichiometric CH₄ oxy-fuel flames with water dilution in the experiment (symbols) of Mazas et al. [77]. Adopted from [77].

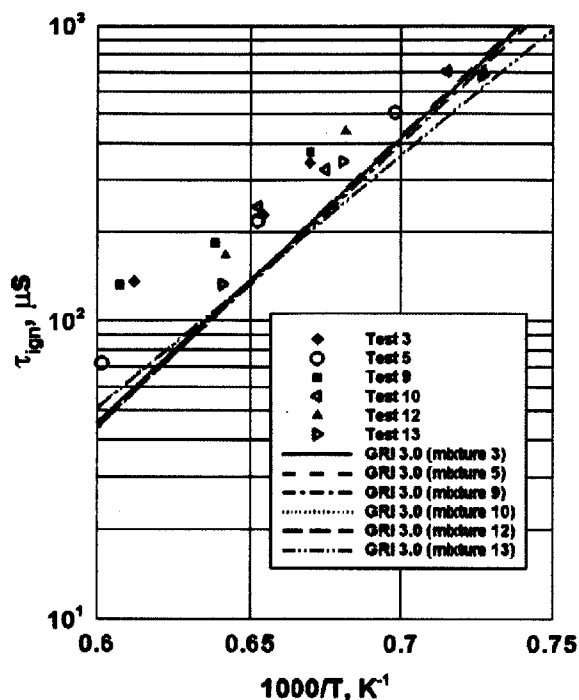


Figure 3-3: The GRI-Mech 3.0 (lines) predicts no dependence of the ignition delay time of CH_4 on the type of diluent in agreement with the experimental data (symbols) of Levy et al. [66]. Adopted from [66].

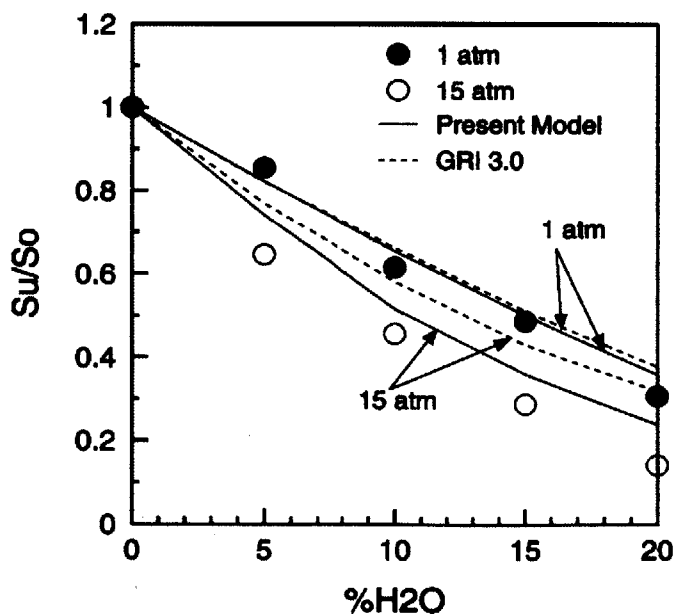


Figure 3-4: The Le Cong mechanism (solid line) performs slightly better than the GRI-Mech 3.0 (dashed line) at predicting the stronger decrease of the burning velocity of CH_4 air flames with H_2O addition at higher pressure in the experiment (symbols) of Babkin and V'yun [80]. Adopted from [79].

validating by predicting burning velocities and ignition delay for CH_4 and H_2 combustion in air in the presence of H_2O . In most cases, it gives results that are similar to the GRI-Mech 3.0, but it performs slightly better at predicting the influence of H_2O on the burning velocity at increased pressure [79] (see Figure 3-4).

3.1.2 Hydrogen Sulfide Mechanism

Since hydrogen sulfide is not commonly used as a fuel, the number of reaction mechanisms available in the literature is much more limited and the reaction pathways are less well established than for CH_4 . However, there has been a growing interest in sulfur chemistry in recent years in the context of the Claus process and SO_x formation in coal-fired power plants. Building on early modeling work of Frenklach et al. [100], Tsuchiya et al. [108], and Glarborg et al. [30], a number of sulfur mechanisms have been proposed. These include the work of Alzueta et al. [54, 109], the Leeds sulfur mechanism [110], and the mechanism presented by Cerru et al. [111, 112].

For building the sour gas mechanism, we have chosen the mechanism recently presented by Zhou et al. [32] (44 species, 227 reactions), which currently represents one of the most comprehensive sulfur mechanisms. It puts more emphasis on disulfur species, which were found to be particularly important near stoichiometric conditions. The authors tested it with reasonable success for the flow reactor experiment presented in the same paper, the burning velocity of H_2S in air, H_2S pyrolysis, and predicting the structure of a premixed H_2S -air flame. The basic sulfur oxidation pathways of the mechanism are shown schematically in Figure 3-5. The main pathway goes from H_2S over the mercapto radical (SH) and sulfur monoxide (SO) to SO_2 , with some of the sulfur being in the form of atomic sulfur (S) as an intermediate step. As mentioned above, if the O_2 excess is reduced (i.e. when approaching stoichiometry) disulfur species like S_2 , HSS , and HSSH become more important.

However, only the reactions containing sulfur species were adopted from this mechanism since the O-H reactions are already contained in the GRI-Mech 3.0. These reactions that determine the O-H radical pool are important for both CH_4 and H_2S oxidation and hence provide a means of interaction between the two fuels. The mechanism does not include

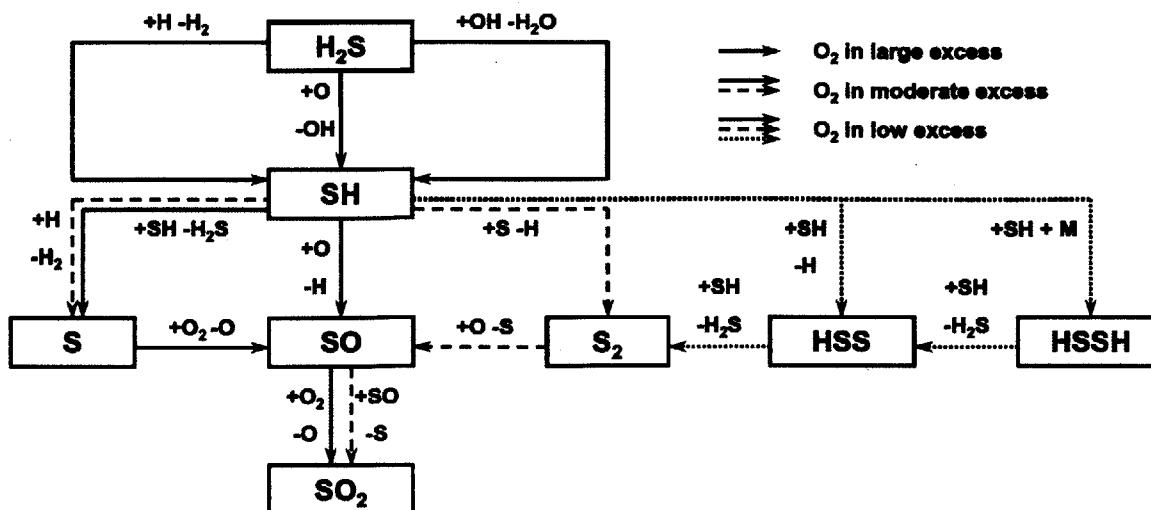


Figure 3-5: The main oxidation pathway in the H₂S oxidation mechanism of Zhou et al. [32] goes from H₂S over SH and SO to SO₂, with other pathways becoming more important close to $\Phi = 1$. The pathways shown were the dominant ones in the flow reactor experiment of Zhou et al. Adopted from [32], modified.

any species containing both carbon and sulfur such as COS or CS₂, the influence of which Cerru et al. [111] found to be negligible.

3.2 Mechanism Optimization

Testing the basic combined mechanism revealed discrepancies between experiment and modeling that we considered too large for important combustion parameters of H₂S such as laminar burning velocity and ignition delay time. These discrepancies are not caused by the O-H chemistry that is now taken from the GRI-Mech 3.0, but occur for the complete original sulfur mechanism as well. This motivated the tuning of the sulfur mechanism to improve the agreement with experiments under relevant conditions. Unlike for hydrocarbon combustion, for sulfur compounds there is considerable uncertainty not only in the reaction mechanisms but also in the thermochemistry [113]. Therefore, both the thermodynamic and chemical kinetic data were considered.

3.2.1 Thermodynamic Data

The large scatter in the thermodynamic data of sulfur species becomes immediately apparent when comparing the data used by Zhou et al. [32] to other recent mechanisms and databases such as, for example, the sulfur mechanism of Alzueta and coworkers [54] and the continuously updated thermodynamic database of Goos et al. [114]. Especially for species containing both sulfur and oxygen such as HSO, HOSO, or HOSO₂, the values for the heat capacity at 300 K and the enthalpy and entropy of formation differ by up to 15 % between the different sources. However, the only molecule for which the differences in the thermodynamic data influenced our computational results significantly is the mercapto radical (SH).

We have chosen to change the value for the enthalpy of formation of SH from $\Delta h_{f,SH}^{298} = 34.2$ kcal/mol, which is used in the Zhou mechanism [32] based on the experiments of Shiell et al. [115], to $\Delta h_{f,SH}^{298} = 33.8$ kcal/mol. This new value leads to improved agreement between our modeling and the experimental data for the laminar burning velocity of H₂S (see Figure 3-6) and the H₂S flow reactor experiment of Zhou et al. [32] (see Figure 3-7), and is in agreement with the recommendations of Goos et al. [114] and Denis [116]. The Goos et al. database [114] recommends the value $\Delta h_{f,SH}^{298} = 33.9 \pm 0.1$ kcal/mol, which is based on the calculations of Császár et al. [117]. In an extensive review on sulfur thermochemistry, Denis [116] compared recent computational and experimental values and suggested a value of $\Delta h_{f,SH}^{298} = 34.0 \pm 0.3$ kcal/mol.

Because of this change, we also had to modify the rate parameters for the high-pressure limit of the reaction $SH + SH (+M) = HSSH (+M)$ since they were originally determined from the backward reaction using the equilibrium constant, which is affected by the thermodynamic data [118]. The new rate is only about half as fast and has a higher activation energy.

3.2.2 Chemical Kinetic Data

In order to further improve the performance of the mechanism, we conducted an automated optimization of the chemical kinetic data of the sulfur submechanism. The cases for which

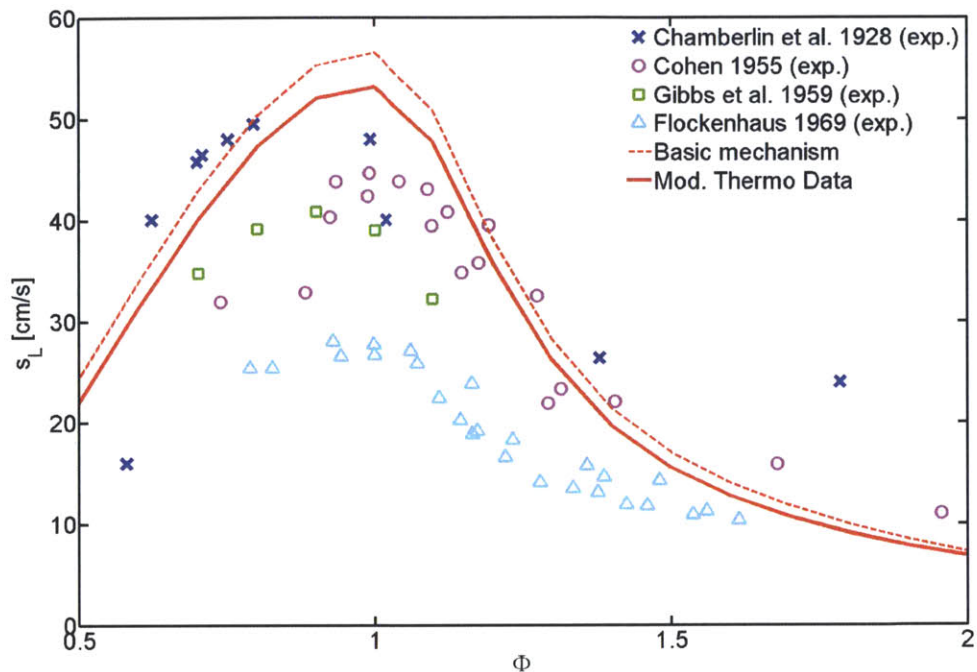


Figure 3-6: The modified thermodynamic data for SH leads to improved agreement for the laminar burning velocity of H_2S in air with the experimental data from [32, 94–98].

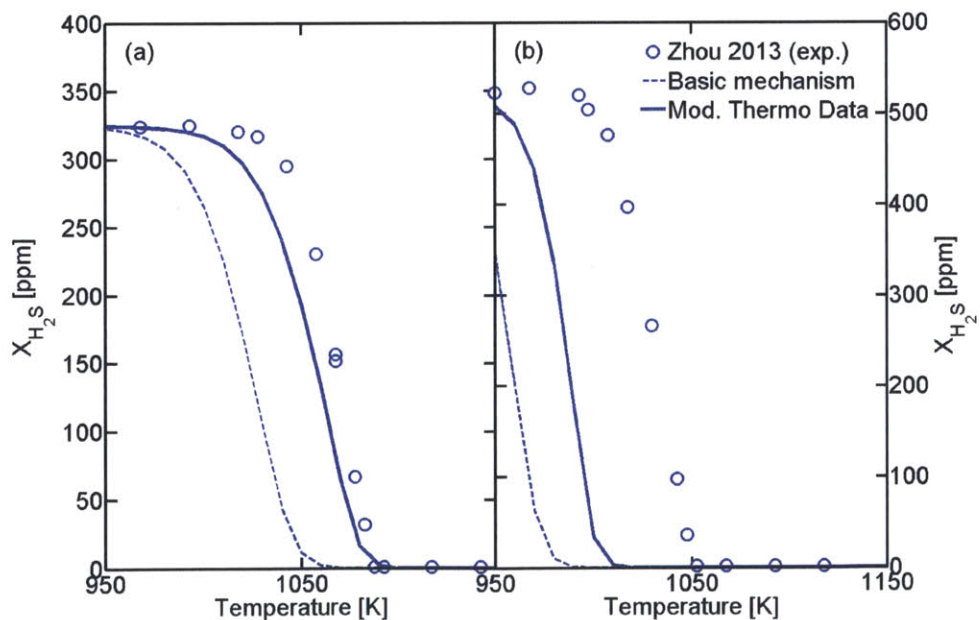


Figure 3-7: The modified thermodynamic data for SH leads to improved agreement with the flow reactor experiment of Zhou et al. [32]. Inlet: (a) $X_{\text{H}_2\text{S}} = 325$ ppm, $X_{\text{O}_2} = 600$ ppm, (b) $X_{\text{H}_2\text{S}} = 520$ ppm, $X_{\text{O}_2} = 1000$ ppm.

significant discrepancies between the modeling results and the experimental data were observed and which were thus chosen as optimization targets are:

- the laminar burning velocity of H₂S in air at atmospheric pressure [95–98]
- the ignition delay time of H₂S in air as measured by Frenklach et al. [100]
- the pyrolysis of H₂S in the experiment of Hawboldt et al. [119]
- the H₂S flow reactor experiment of Zhou et al. [32]

The exact points used, the corresponding target values, and the assigned weights are listed in Table 3.1. The weights were determined empirically to give good overall agreement. For the laminar burning velocity, a target range was chosen to account for the range of the data points from the different experiments. For the ignition delay time, target ranges were chosen because the selection of a single data point lead to arbitrarily different results. For the flow reactor experiment of Zhou et al. [32], we only consider the cases with $\Phi = 0.8$ because they are closer to the conditions around stoichiometry that we are interested in than the third case presented therein ($\Phi = 0.15$).

The objective function f used in the optimization was defined as the sum of the quadratic deviations of the modeling predictions (x_i) from the target values ($X_{i,\min}, X_{i,\max}$) normalized

Table 3.1: Targets used in the optimization of the combined mechanism.

No.	Case	Point	Target Value	Weight	Ref.
1	Burning Velocity	$\Phi = 1$	42 – 46 cm/s	40	[95–98]
2	Ignition Delay Time	Lean, $T = 950$ K	1000 – 1600 μ s	1	[100]
3		Lean, $T = 1200$ K	60 – 90 μ s	1	[100]
4		Rich, $T = 950$ K	1600 – 2500 μ s	1	[100]
5		Rich, $T = 1200$ K	100 – 160 μ s	1	[100]
6		Pyrolysis	$T = 1273$ K, $t = 0.64$ s	18.6% H ₂ S Loss	1
7	$T = 1423$ K, $t = 0.17$ s		45.1% H ₂ S Loss	1	[119]
8	Flow Reactor, 520 ppm	$T = 1000$ K	498 ppm H ₂ S	1	[32]
9		$T = 1050$ K	19 ppm H ₂ S	1	[32]
10	Flow Reactor, 325 ppm	$T = 1030$ K	314 ppm H ₂ S	1	[32]
11		$T = 1070$ K	132 ppm H ₂ S	1	[32]
12		$T = 1100$ K	0 ppm H ₂ S	5	[32]

by a characteristic value ($X_{i,\text{char}}$) multiplied by the respective weights (w_i) (cf. Table 3.1):

$$f = \sum_i w_i \cdot \frac{\frac{1}{4} [\text{sgn}(x_i - X_{i,\text{min}}) + \text{sgn}(x_i - X_{i,\text{max}})]^2 \cdot \min [(x_i - X_{i,\text{min}})^2, (x_i - X_{i,\text{max}})^2]}{X_{i,\text{char}}^2}$$

The sum did not necessarily include all targets listed in Table 3.1, but different subsets were used to obtain different optimized versions of the mechanism by only considering certain combinations of experiments. In the comprehensive model validation presented in the next section, three of these versions were investigated. In the following, they are referred to as 'Optimization 1–12', 'Optimization 1–7', and 'Optimization 8–12', where the numbers are the target numbers given in Table 3.1. These combinations correspond to an optimization with respect to all experiments mentioned above, all experiments except the H₂S flow reactor of Zhou et al. [32], and only the H₂S flow reactor, respectively.

The decision variables used in the optimization were the rate parameters of 10 reactions in the sulfur mechanism to which the results for the target cases were specifically sensitive. To identify these reactions, we conducted sensitivity analyses for targets 1–7. Sensitivity analyses for the flow reactor experiment (targets 8–12) were already conducted by Zhou et al. [32]. The results of some of these analyses are summarized in Figure 3-8. The reactions highlighted in boldface were chosen to be varied in the systematic optimization of the mechanism. Zhou et al. [32] found the same reactions to be most important in their flow reactor experiment. We confirmed this in a similar analysis for the present combined model. The reaction $\text{H} + \text{SO}_2 (+\text{M}) = \text{HOSO} (+\text{M})$ was not considered for variation in the optimization despite its high sensitivity coefficient for the laminar burning velocity, because it is also important for other cases for which good agreement is achieved with the basic combined model. Namely, it has a strong influence on the prediction of CO oxidation inhibition by SO₂ in the experiments of Giménez-López et al. [54] and Dagaut et al. [53].

The constraints on the variations of the rate parameters were determined from the uncertainties reported for the original experiments or calculations wherever possible, to make sure that the values for the rate parameters determined through the optimization are still in agreement with the more direct experimental or theoretical determinations. For the reaction

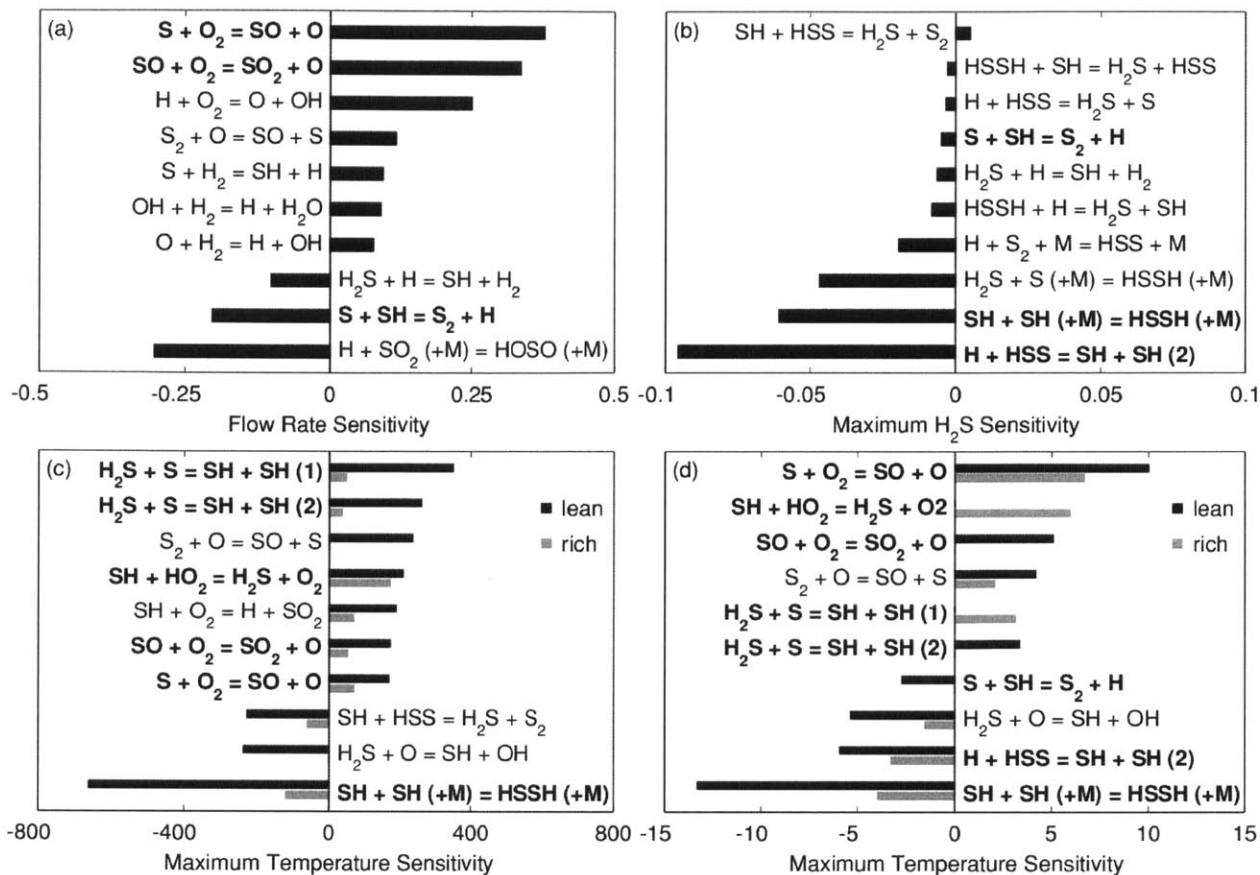


Figure 3-8: Sensitivity coefficients of the pre-exponential factor of different reactions. (a) Sensitivity with respect to the laminar burning velocity of H_2S in air at $p = 1$ atm, $\Phi = 1$; (b) Sensitivity with respect to the H_2S concentration in the pyrolysis experiment [119] at $T = 1273$ K; (c) Sensitivity with respect to temperature in the ignition delay measurement [100] for $T_0 = 950$ K; (d) Sensitivity with respect to temperature in the ignition delay measurement [100] for $T_0 = 1200$ K.

$S + O_2 = SO + O$, all three Arrhenius parameters were varied since explicit experimental uncertainties for them were reported [120]. For all other reactions, only the pre-exponential factor was varied in the optimization, leading to a total of 12 decision variables. For the reaction $SO + O_2 = SO_2 + O$, we reevaluated the fit to the experimental data of Grillo et al. [121], Black et al. [122], and Garland [123]. The uncertainty of the pre-exponential factor was determined to be about 10% by combining the higher and lower limits for the different rate constants considered in the fitting. For the reaction $H_2S + S = SH + SH$, two duplicate reactions corresponding to different reaction channels were defined in the original

sulfur mechanism [32]. We determined the uncertainties in the pre-exponential factors of each of these by varying them and comparing the resulting fit to the original data of Gao et al. [124] and Shiina et al. [125]. The limits on the variation of the pre-exponential factor that were chosen are +20%/-40% for the first of the two duplicate reactions and $\pm 25\%$ for the second reaction. The rates of the other reactions were obtained from high-level theoretical calculations so that an uncertainty of a factor of three was assumed [118, 126].

We implemented a simple coordinate descent method to solve the optimization problem described above. Coordinate descent methods are not particularly fast, but they have the advantage that no knowledge of the structure of the problem is required and the objective function can be treated as a black box. In a coordinate descent method, only one decision variable (i.e. one rate parameter) is varied at a time while keeping the others constant. This one dimensional line search problem was solved by the golden section method (see e.g. [127] for more information). Once the line search is solved, the next decision variable is varied. This procedure is repeated until convergence is reached (see Figure 3-9). The number of cycles over the 12 decision variables necessary to achieve convergence varied from about 5 to 30, depending on the combination of targets used. The order in which the decision variables are varied was found to have no influence on the result.

Within each line search, the objective function is evaluated several times by inserting the current values of the decision variables into the combined reaction mechanism, calling CHEMKIN to sequentially run all the target cases with the current mechanism, and extracting the relevant values from the CHEMKIN output files to insert them in the objective function. To allow easy processing of the output files, the programming language Perl was used to implement the optimization algorithm. The use of a relatively slow language like Perl seemed justified because the bulk of the runtime is used for running the models in CHEMKIN so that execution speed of the algorithm is not as important.

Optimization with respect to the three different combinations of targets ('Optimization 1-12', 'Optimization 1-7', and 'Optimization 8-12') resulted in different values for the rate parameters that were varied. The exact values for each of the three versions are listed in Appendix A.1. Furthermore, a complete version of the combined mechanism using the values

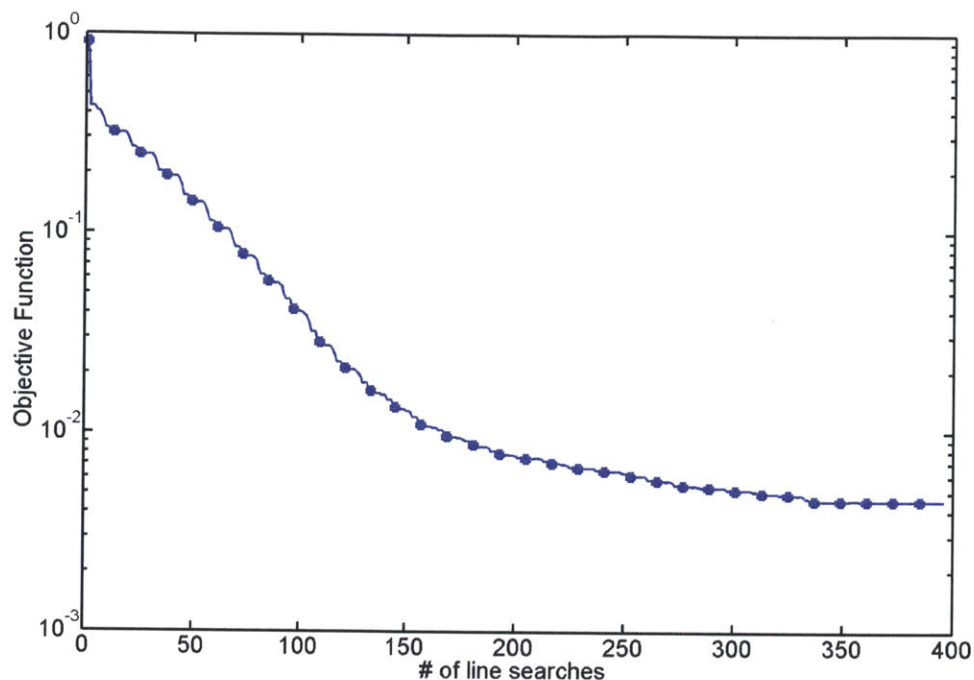


Figure 3-9: Example for the convergence behavior of the optimization (here for Optimization 8–12). The squares denote the beginning of a new cycle over the decision variables.

of 'Optimization 1–12' in CHEMKIN format is given in Appendix A.2 since this version was found to give the best overall agreement (cf. Section 3.3). For this 'Optimization 1 – 12' mechanism, the most significant changes relative to the initial mechanism are the following:

1. The reaction $S + O_2 = SO + O$ is made up to 25% slower at high temperatures, and so is the second of the two duplicate reactions $H_2S + S = SH + SH$.
2. The rate of $SH + SH(+M) = HSSH(+M)$ is reduced to one third of its original value.

While the first two reactions belong to a chain branching sequence, the third one initiates a chain termination sequence [32].

3.3 Model Validation

The basic combined mechanism and the three optimized combined mechanisms ('Optimization 1–12', 'Optimization 1–7', and 'Optimization 8–12') were validated against experimental data covering a wide range of phenomena and conditions, including but not limited to the

cases used as optimization targets. Where possible, emphasis was put on situations that are relevant to oxy-fuel combustion. All modeling calculations were again conducted using CHEMKIN-PRO [105]. Because of the special set of reactions that was varied in the optimization, only the predictions for experiments similar to the ones that were considered as targets (cf. Table 3.1) were affected noticeably by the resulting changes. For these cases, results obtained with all four mechanisms are shown. In all other cases, only the computation using the recommended version 'Optimization 1–12' is presented. The validation cases can be divided into cases relevant to oxy-fuel combustion of CH_4 , H_2S combustion, and interactions between carbon and sulfur species.

3.3.1 Oxy-Fuel Combustion of Methane

In the absence of sulfur species, the added sulfur reactions are inactive and the mechanism should behave exactly like the GRI-Mech 3.0. As mentioned in Chapter 2, the ability of the GRI-Mech 3.0 to predict the influence of CO_2 and H_2O dilution on burning velocity and ignition delay time of CH_4 has already been reported in the literature. However, it has not been shown yet to what extent it can capture the influence of CO_2 and H_2O on CO concentrations (cf. Section 2.1.2).

Our tests showed that the mechanism is able to reproduce the inhibiting effect of large CO_2 concentrations on CO oxidation observed by Abián et al. [28] both for lean and rich conditions (see Figure 3-10). The flow reactor was modeled using the plug flow model in CHEMKIN with a constant flow rate of 1 $\text{L}_{\text{STP}}/\text{min}$ and the measured temperature profiles presented in [54]. The degree of agreement achieved is similar to the modeling presented in the original publication using their own reaction mechanism.

The slightly enhancing effect of moderate concentrations of H_2O on CO oxidation in the presence of CO_2 in the same experiment is captured qualitatively by the mechanism (see Figure 3-11). The quantitative discrepancies are somewhat larger than for the modeling presented by Abián et al. [28].

The inhibiting effect of larger concentrations of H_2O on CO oxidation at very lean conditions ($\Phi \approx 0.04$) observed by Glarborg et al. [128] is captured better by the modeling results

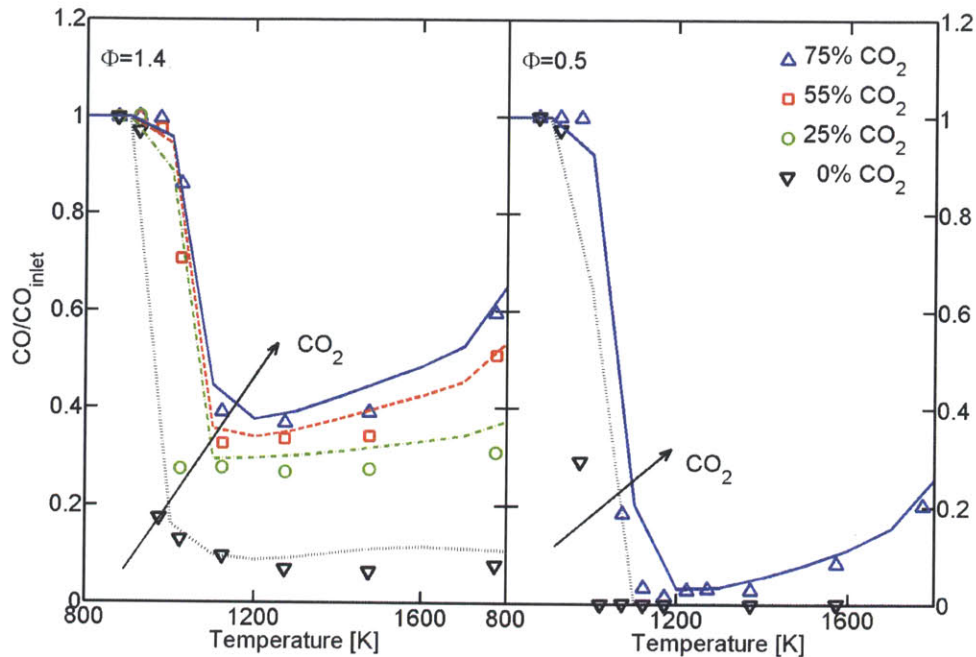


Figure 3-10: The modeling (lines) agrees with the experimental data (symbols) for the atmospheric CO/O₂/CO₂/H₂O/N₂ flow reactor of Abián et al. [28] on CO oxidation in the presence of CO₂. Inlet: $X_{CO} \approx 2000$ ppm, $X_{H_2O} = 0.6\%$, varying CO₂, balance N₂.

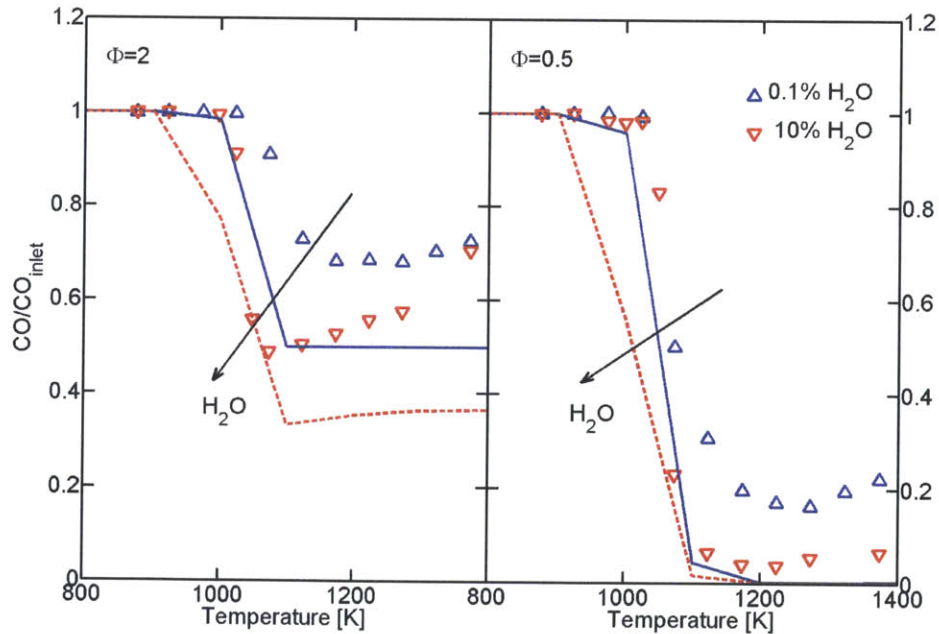


Figure 3-11: The modeling (lines) qualitatively predicts the trends in the experimental data (symbols) for the atmospheric CO/O₂/CO₂/H₂O/N₂ flow reactor of Abián et al. [28] on CO oxidation in the presence of H₂O and CO₂. Inlet: $X_{CO} \approx 5100$ ppm, $X_{CO_2} = 25\%$, varying H₂O, balance N₂.

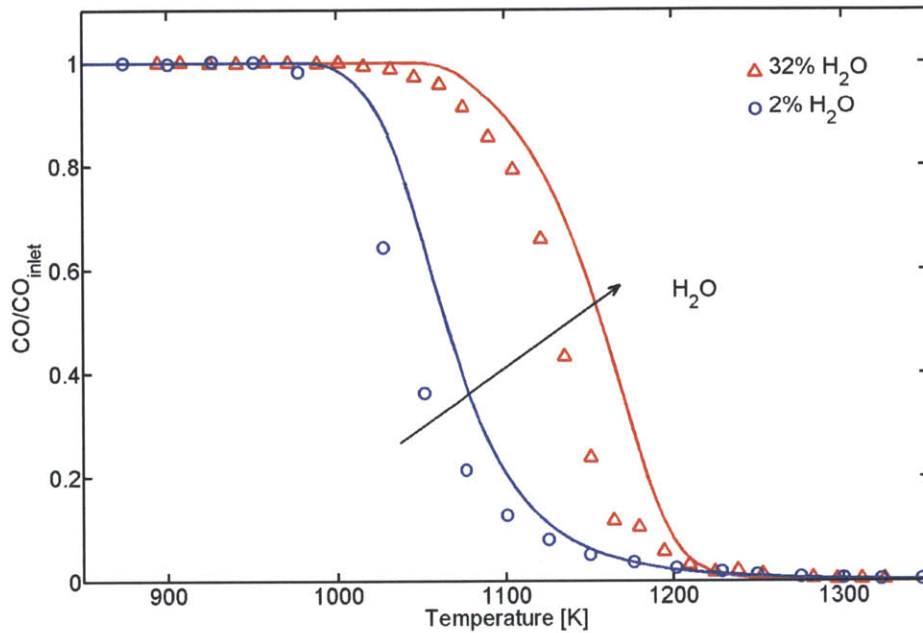


Figure 3-12: The modeling (lines) agrees with the experimental data (symbols) for the atmospheric $\text{CO}/\text{O}_2/\text{H}_2\text{O}/\text{N}_2$ flow reactor of Glarborg et al. [128] on CO oxidation in the presence of H_2O at $\Phi = 0.04$. Inlet: $X_{\text{CO}} \approx 1500/1630$ ppm, $X_{\text{O}_2} = 2.0\%$, varying H_2O , balance N_2 .

(see Figure 3-12). This experiment was also modeled with the plug flow model. In this case, no full experimental temperature profiles were available so that a fixed residence time of $\tau = 64/T$ s was assumed, where T is the constant reactor temperature in kelvin.

While the previous cases studied the impact of CO_2 and H_2O on CO oxidation, the model can also at least qualitatively predict the effect of CO_2 on CO concentrations in CH_4 oxidation in the experiment of Glarborg and Bentzen [16] (see Figure 3-13). The modeling was done assuming a fixed residence time of $\tau \approx 960/T$ s and constant temperature since the full temperature profile was not available. The prediction quality is similar to the modeling results of Glarborg and Bentzen [16] when using a fixed temperature equal to the maximum temperature measured in the reactor.

3.3.2 Hydrogen Sulfide Combustion

For the sulfur part of the mechanism, a new complete model validation was necessary because the combined mechanism uses the O-H reactions from the GRI-Mech 3.0 instead of the ones

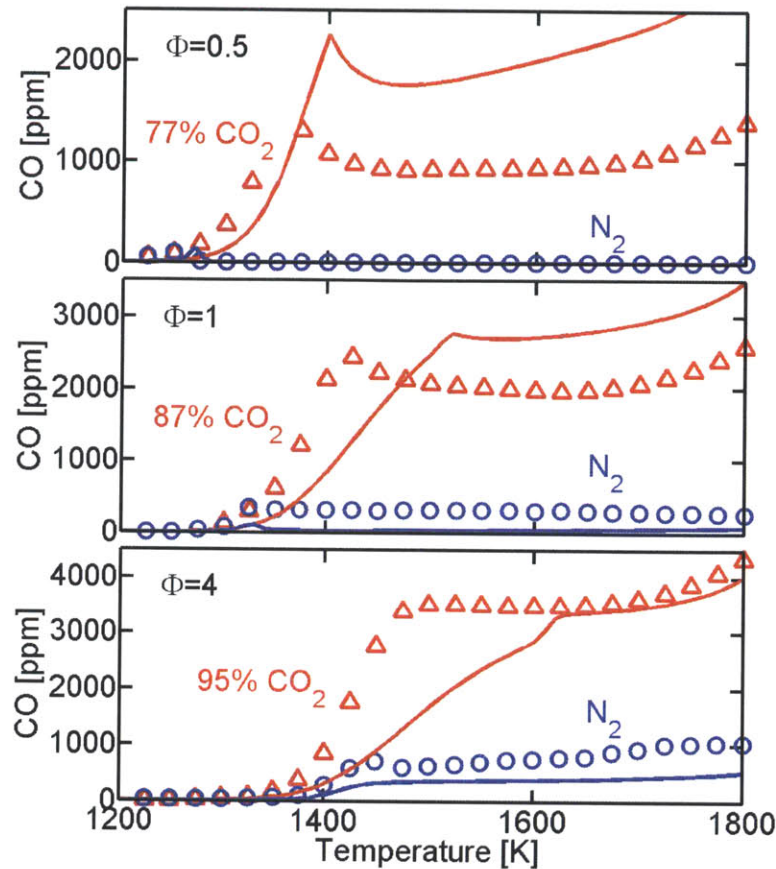


Figure 3-13: The modeling (lines) reproduces the qualitative trends of the experimental data (symbols) for the atmospheric $\text{CH}_4/\text{O}_2/\text{CO}_2/\text{N}_2$ flow reactor of Glarborg and Bentzen [16] on CO formation in CH_4 oxidation in the presence of CO_2 . Inlet: $X_{\text{CO}} \approx 1000$ ppm, varying CO_2 , balance N_2 .

used in the original sulfur mechanism of Zhou et al.

As mentioned in Section 2.2.2, the laminar burning velocity of H_2S in air has been measured in only four studies [95–98] and there is considerable scatter in the data. It was one of the targets chosen in the mechanism optimization (target 1). As shown in Figure 3-14, the prediction of the basic combined mechanism seems to be too high at stoichiometric conditions since most experiments suggest a value around 40 cm/s. We found that this discrepancy could be removed if the laminar burning velocity was considered in the optimization.

Merryman and Levy [129] measured the flame structures of premixed H_2S flames at low pressure. Figure 3-15 shows that the prediction of the major species for a lean flame using the combined mechanism is good while the hydrogen (H_2) concentration is somewhat

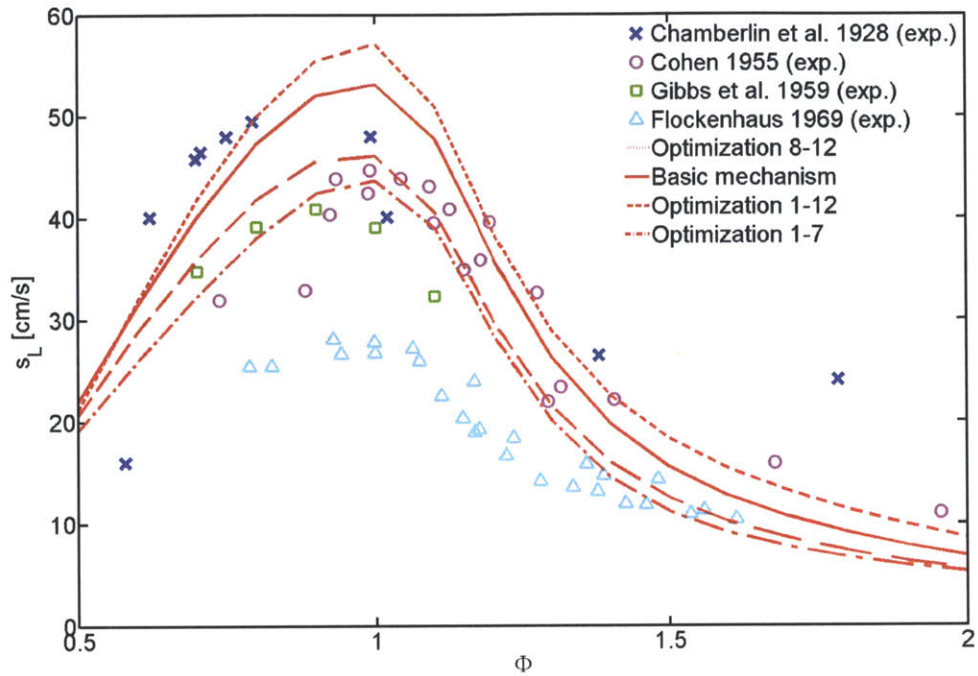


Figure 3-14: The modeling (lines) results for the laminar burning velocity of H_2S in air at atmospheric pressure agree better with the experimental data (symbols) of [95–98] if target 1 is included in the optimization.

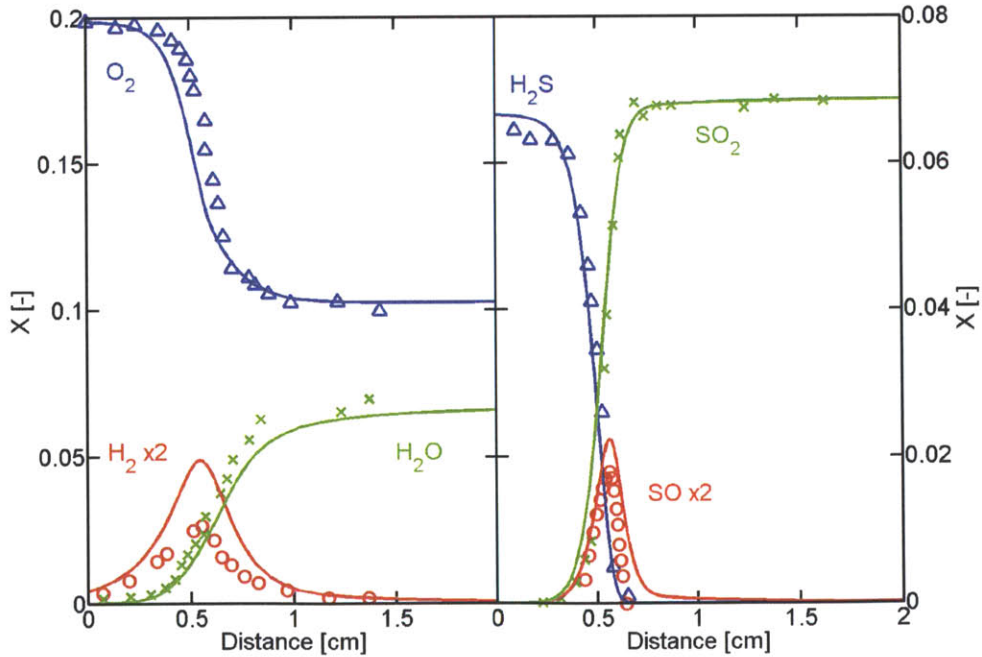


Figure 3-15: The modeling (lines) results agree well with the experimental data (symbols) of Merryman and Levy [129] for the major species profiles in a H_2S -air flame. $P = 0.1$ atm, $\Phi = 0.5$.

overpredicted. This is in agreement with the findings of Zhou et al [32]. The modeling used the experimental temperature profile and extrapolated upstream to 300 K.

Frenklach et al. [100] measured the ignition delay time of H_2S in air at 30 – 45 bar under fuel-lean and fuel-rich conditions. Their data also served as an optimization target (targets 2–5). Figure 3-16 shows that while the calculated order of magnitude is correct, the temperature dependence predicted by the basic mechanism is somewhat too strong. Again, improved agreement was achieved in the optimization, especially if targets 8–12 were not used. For our modeling, the ignition delay time was taken to be the time needed for a temperature rise of 600 K similar to [112]. The pressure was varied along with the initial temperature to keep the partial density of H_2S constant.

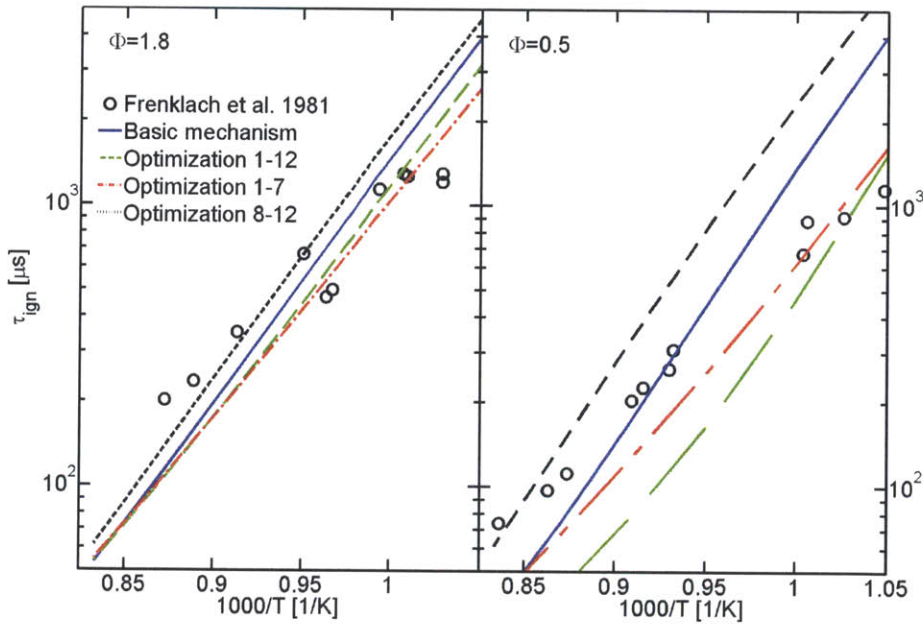


Figure 3-16: The agreement between modeling (lines) results and experimental data (symbols) of Frenklach et al. [100] for the ignition delay time of H_2S in air at $p = 30 - 45$ bar is improved if targets 8–12 are not considered.

The pyrolysis of H_2S has been the subject of a number of experimental (e.g. [119, 130]) and modeling (e.g. [125, 126]) studies. Compared to the experimental data of Hawboldt et al. [119] which was also used as optimization targets 6–7, the predicted H_2S conversion tends to be too slow for most temperatures (see Figures 3-17). The optimization was able to improve this slightly if targets 8–12 were not considered. Similar changes were observed

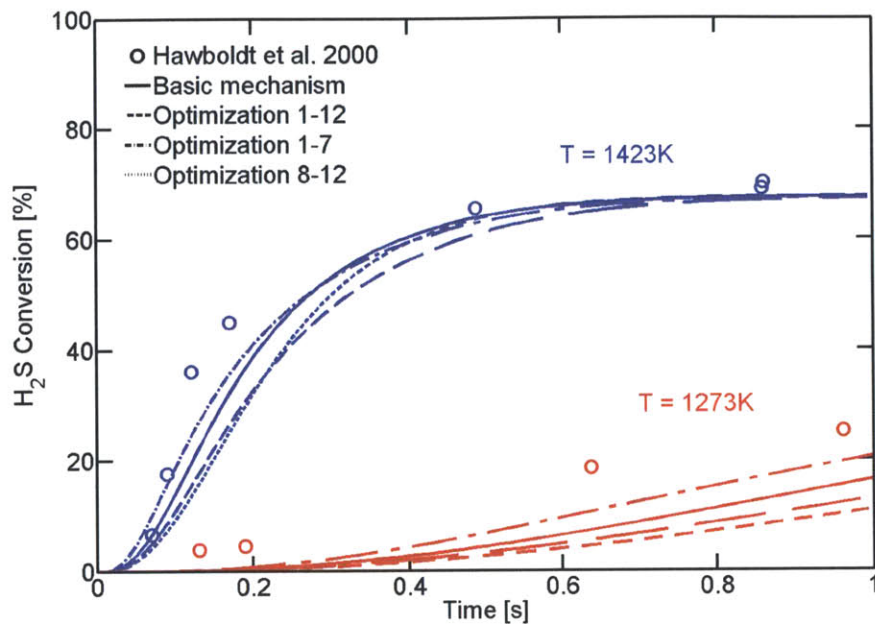


Figure 3-17: The agreement between modeling (lines) results and experimental data (symbols) of Hawboldt et al. [119] for the pyrolysis of H_2S at $p = 1$ atm is improved slightly if targets 8–12 are not considered. Initial conditions: $X_{\text{H}_2\text{S}} = 2.5\%$, balance N_2 .

for the experiment of Binoist et al. [130], which was not used as a target.

Zhou et al. [32] also presented data on lean H_2S oxidation in an atmospheric flow reactor. Since we are interested in oxy-fuel combustion which is likely to occur at stoichiometric conditions, we only consider the experiments with $\Phi \approx 0.8$. The H_2S profiles in this experiment also served as optimization targets 8–12. Figure 3-18 shows that while the trends of the prediction of the H_2S profiles are correct, the profiles are shifted to lower temperatures, which is in agreement with the original findings of Zhou et al. Significant improvements were only achieved in the optimization if none of the other experiments (targets 1–7) were considered. The prediction quality for sulfur dioxide (SO_2) is comparable to the H_2S profiles (see Figure 3-19). Hydrogen is again overpredicted (see Figure 3-20), similar to the H_2S flame results shown above. The modeling was again done assuming plug flow and temperature profiles similar to the one presented in [32].

As mentioned in Section 2.1.3, SO_3 formation is a major concern when using sulfur containing gases in power plants. Fleig et al. [34] recently investigated the formation of SO_3 in a flow reactor over a wide range of conditions. Figure 3-21 shows a comparison of the

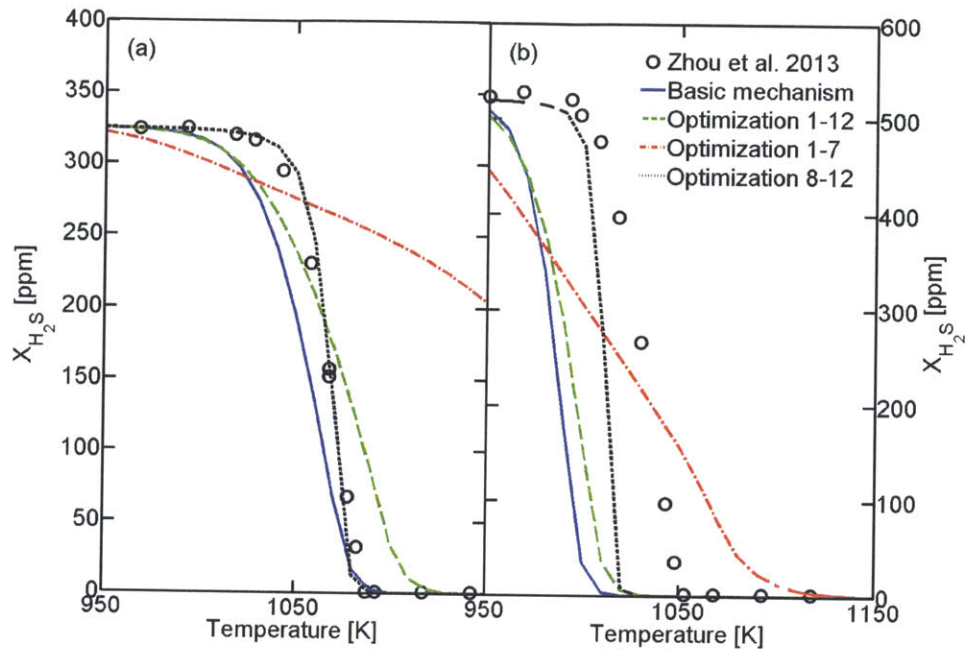


Figure 3-18: The agreement between modeling (lines) results and experimental data (symbols) of Zhou et al. [32] for H_2S oxidation in a flow reactor is improved if only targets 8–12 are considered. Inlet: (a) $X_{\text{H}_2\text{S}} = 325$ ppm, $X_{\text{O}_2} = 600$ ppm, (b) $X_{\text{H}_2\text{S}} = 520$ ppm, $X_{\text{O}_2} = 1000$ ppm.

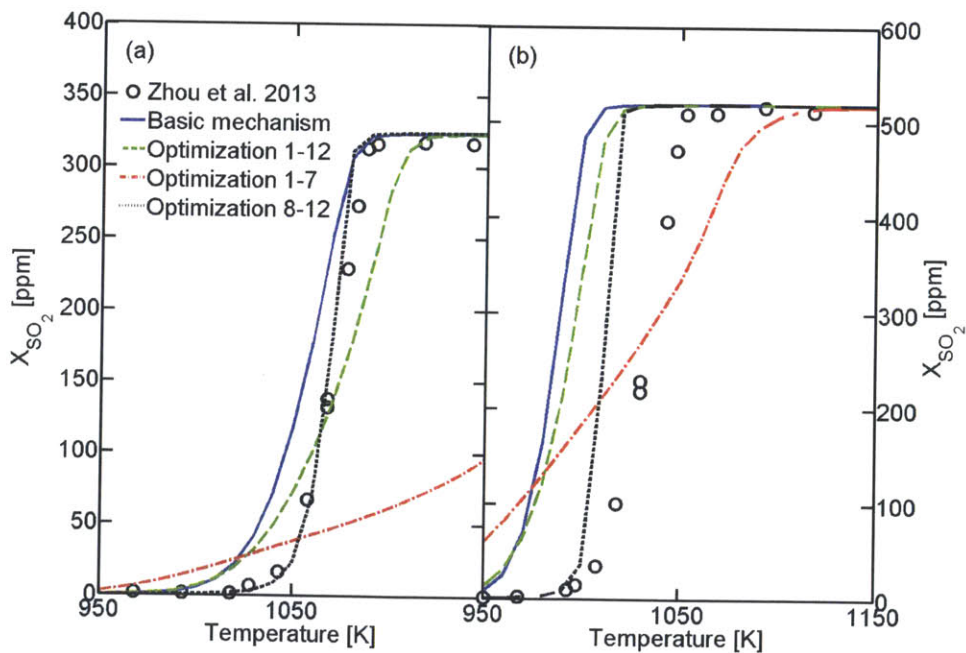


Figure 3-19: The agreement between modeling (lines) results and experimental data (symbols) of Zhou et al. [32] for SO_2 formation in a H_2S flow reactor is improved if only targets 8–12 are considered. The inlet conditions are the same as for Figure 3-18.

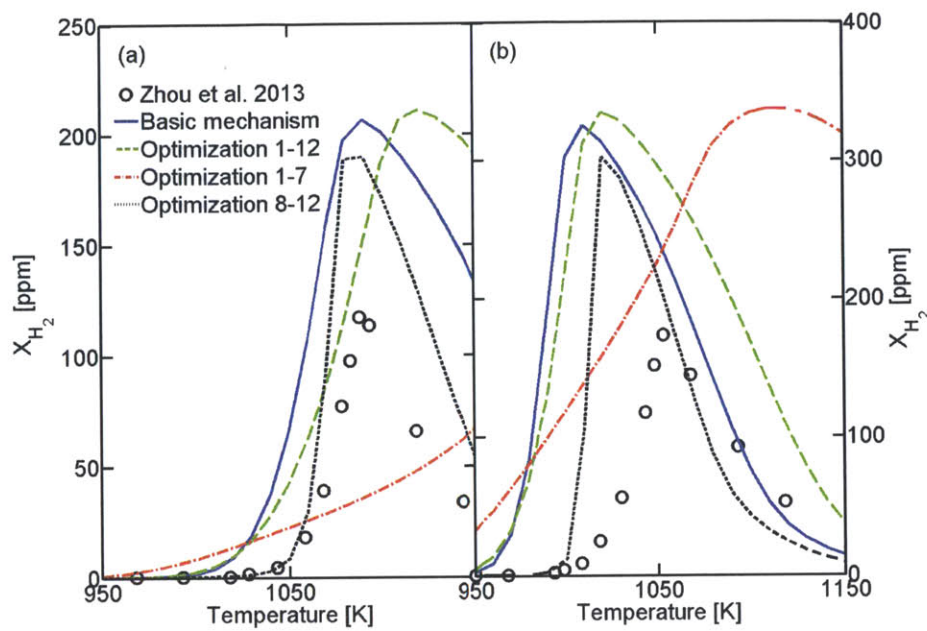


Figure 3-20: The modeling (lines) overpredicts the H_2 concentration in the flow reactor of Zhou et al. [32] compared to the experimental data (symbols). Inlet: (a) $X_{\text{H}_2\text{S}} = 325$ ppm, $X_{\text{O}_2} = 600$ ppm, (b) $X_{\text{H}_2\text{S}} = 520$ ppm, $X_{\text{O}_2} = 1000$ ppm.

modeling results with some of their experimental data. It can be seen that the mechanism can capture the qualitative changes with varying O_2 and SO_2 content, the influence of an environment with high CO_2 concentration, and the impact of H_2O . However, there remain some quantitative discrepancies, especially at higher temperatures. This was also observed by Fleig et al. [34] using the kinetic model from [54]. The modeling assumed plug flow with a constant volume flow rate of $1.011 \text{ L}_{\text{STP}}/\text{min}$, and the experimental temperature profiles.

3.3.3 Interaction

One known interaction between carbon and sulfur species is the inhibition of CO oxidation by SO_2 [30, 53, 54, 109]. The mechanism can capture the inhibiting effect of SO_2 on CO oxidation at stoichiometric conditions observed by Giménez-López et al. [54] both in an N_2 bath and with CO_2 (see Figure 3-22). Similar agreement is achieved for the CO/ H_2 flow reactor of Dagaut et al. [53] at stoichiometric and rich conditions (see Figure 3-23).

Chin et al. [101] measured the simultaneous oxidation of CH_4 and H_2S in a flow reactor

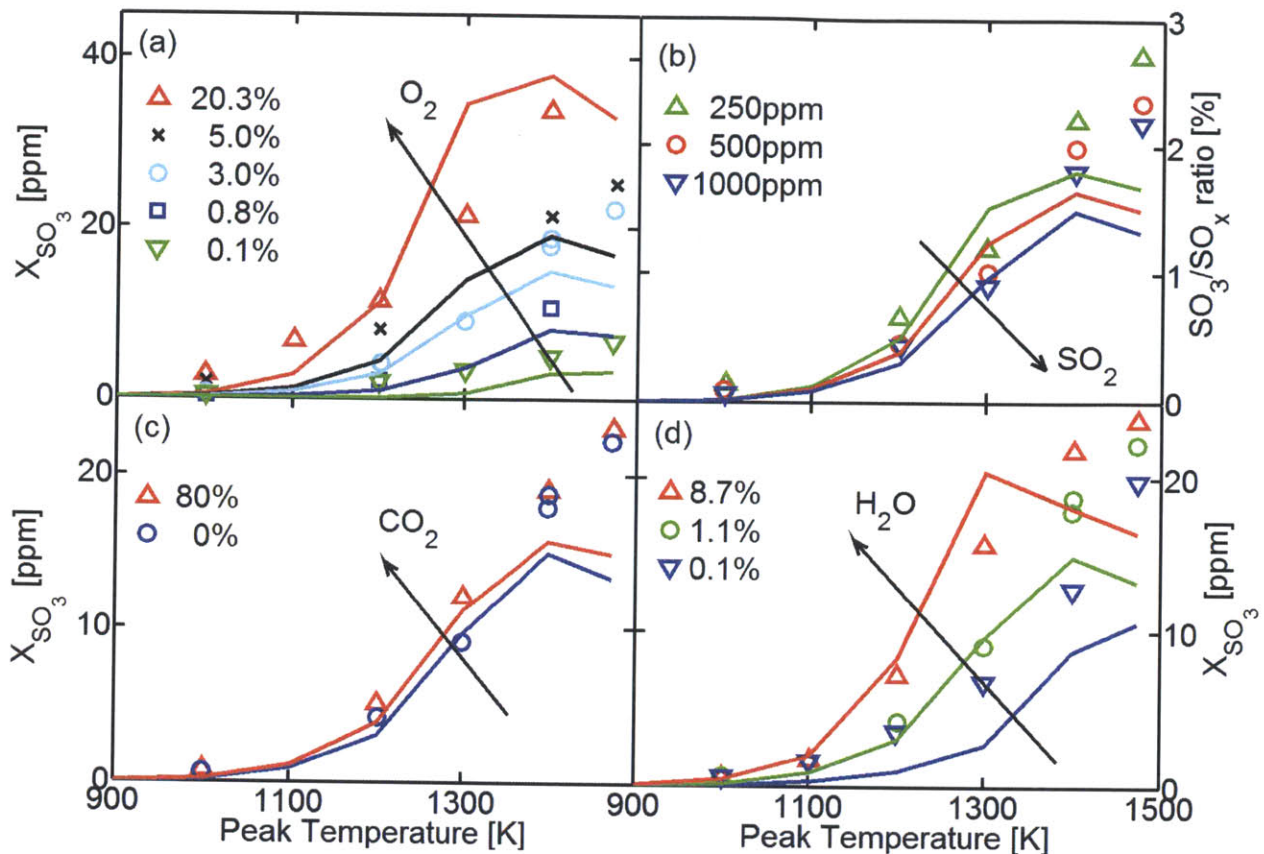


Figure 3-21: The modeling results (lines) capture all trends in the experimental data (symbols) for the atmospheric flow reactor of Fleig et al. [34]. Inlet conditions: (a) $X_{\text{SO}_2} = 1000$ ppm, $X_{\text{H}_2\text{O}} = 1.11\%$, varying O_2 ; (b) $X_{\text{O}_2} = 3\%$, $X_{\text{H}_2\text{O}} = 1.11\%$, varying SO_2 ; (c) $X_{\text{SO}_2} = 1000$ ppm, $X_{\text{O}_2} = 3\%$, $X_{\text{H}_2\text{O}} = 1.11\%$, varying CO_2 ; (d) $X_{\text{SO}_2} = 1000$ ppm, $X_{\text{O}_2} = 3\%$, varying H_2O . Balance N_2 in all cases.

under fuel-rich conditions. As can be seen from Fig. 3-24, the combined mechanism can predict the relative oxidation speed of the two fuels, although there are some quantitative discrepancies especially for methane.

Fleig et al. [34] also investigated the influence of CO and CH_4 on the oxidation of SO_2 to SO_3 . As shown in Fig. 3-25, the model qualitatively predicts the increased SO_3 formation at intermediate temperatures in the presence of combustibles. The slightly varying extent of this effect when comparing different amounts of CO/CH_4 is not captured correctly.

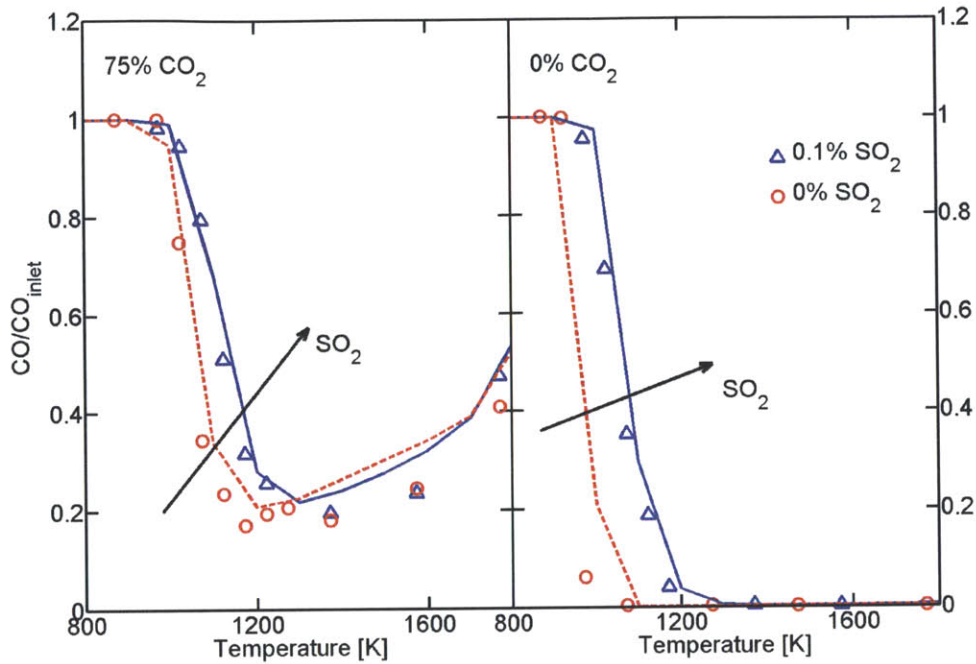


Figure 3-22: The modeling results (lines) agree well with the experimental data (symbols) for the atmospheric flow reactor of Giménez-López et al. [54]. Inlet conditions: $X_{\text{CO}} = 2000$ ppm, $X_{\text{O}_2} = 1000$ ppm, $X_{\text{H}_2\text{O}} = 0.6\%$, $X_{\text{CO}_2} = 75\%/0\%$, varying SO_2 , balance N_2 .

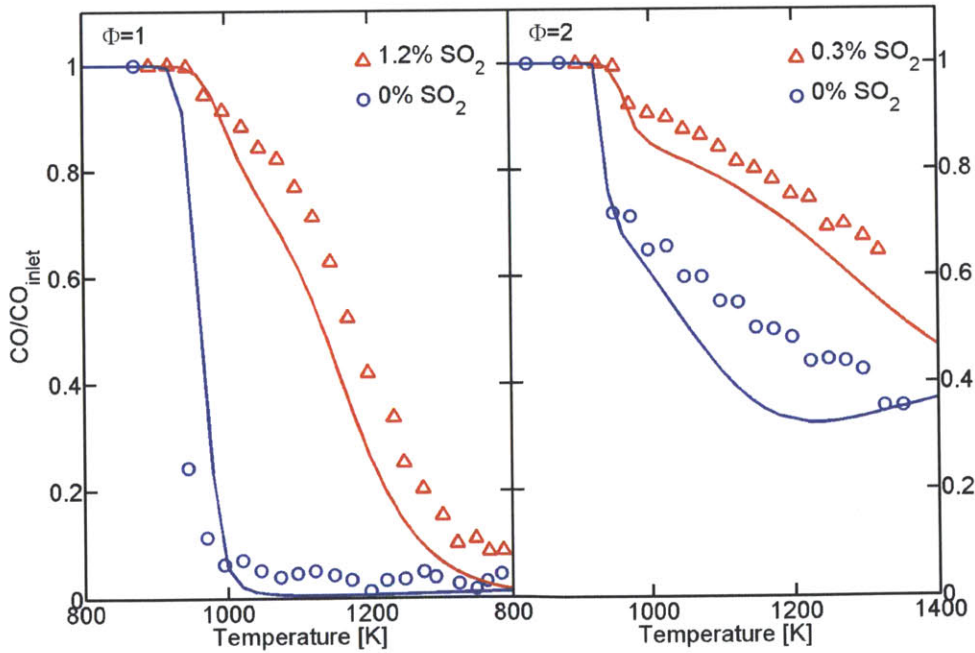


Figure 3-23: The modeling results (lines) agree well with the experimental data (symbols) for the atmospheric flow reactor of Dagaut et al. [53]. Inlet conditions: $X_{\text{CO}} = 1.0\%$, $X_{\text{H}_2} = 1.0\%$, $X_{\text{H}_2\text{O}} = 2.0\%$, varying SO_2 , balance N_2 .

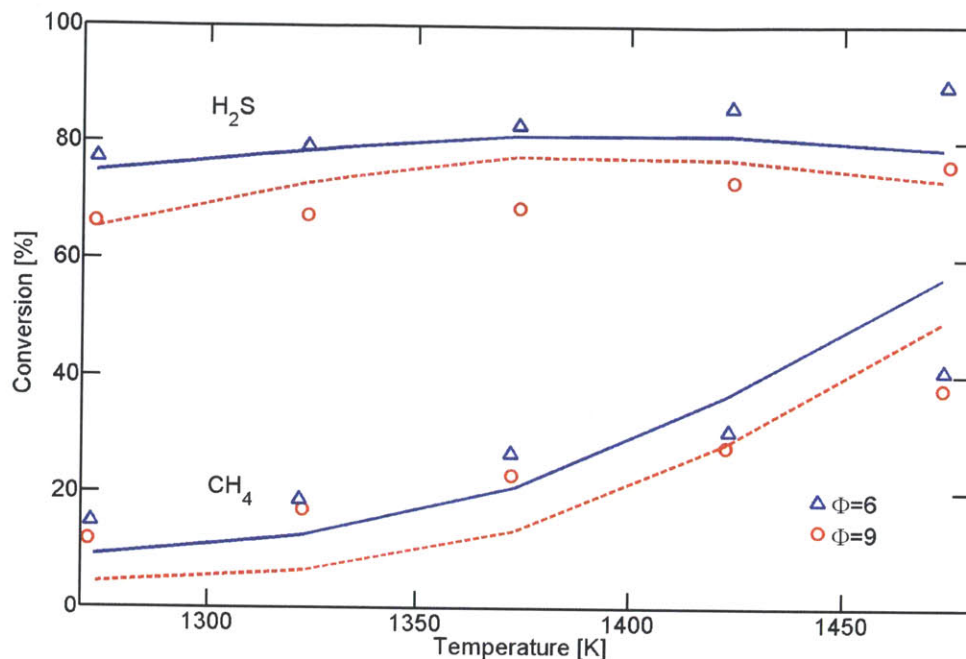


Figure 3-24: The modeling results (lines) capture the trends of the experimental data (symbols) for the flow reactor of Chin et al. [101]. $P = 1.1$ bar. Inlet conditions: $X_{\text{H}_2\text{S}} = 2.45\%$, $X_{\text{CH}_4} = 2.45\%$, varying O_2 , balance N_2 ; $\tau = 0.6$ s.

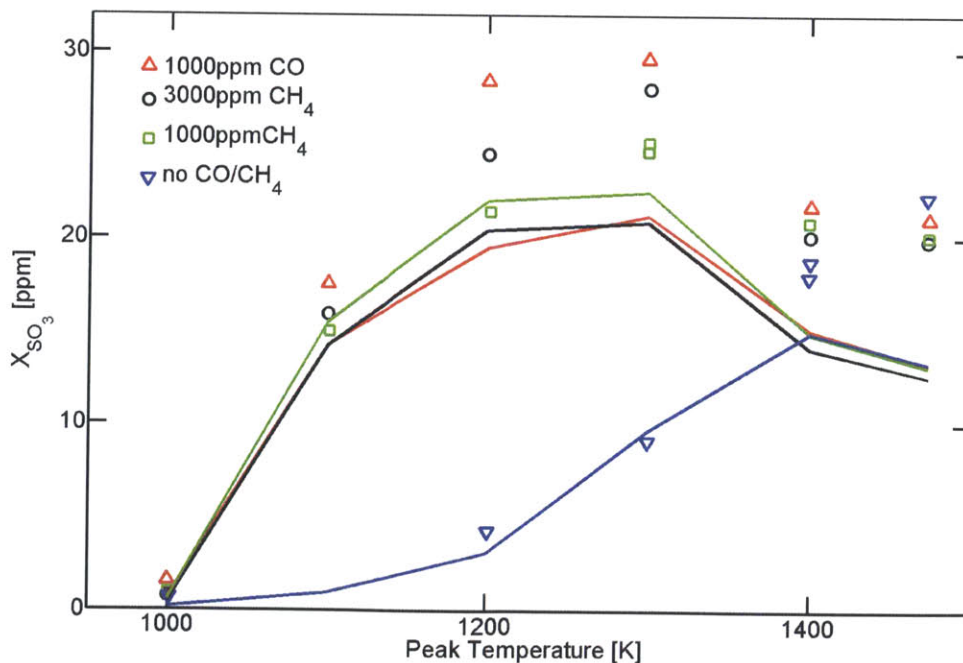


Figure 3-25: The modeling results (lines) capture the trends of the experimental data (symbols) for the atmospheric flow reactor of Fleig et al. [34]. Inlet conditions: $X_{\text{SO}_2} = 1000$ ppm, $X_{\text{O}_2} = 3\%$, $X_{\text{H}_2\text{O}} = 1.11\%$, varying CO and CH₄, balance N_2 .

3.4 Conclusion

A detailed chemical kinetic model has been developed for oxy-fuel combustion of sour gas by combining existing mechanisms for CH_4 and H_2S , revising the thermochemistry of the sulfur species, and optimizing the sulfur kinetics. The resulting mechanism largely fulfills the requirements stated at the beginning of this chapter:

1. The GRI Mech 3.0, which was used as the CH_4 sub-mechanism, was shown to give good agreement with the experiment for the impact of the typical oxy-fuel diluents on CO oxidation as well as reasonable agreement for CO formation in CH_4 oxidation in a CO_2 environment. Its ability of capturing the influence of CO_2 and H_2O on the laminar burning velocity and ignition delay time of CH_4 has been shown previously in the literature.
2. The sulfur part of the mechanism was optimized by varying the rate parameters of 10 reactions within the experimental or computational uncertainties. While it was possible to get good agreement for a combination of the laminar burning velocity, ignition delay time, and pyrolysis data or for the H_2S flow reactor data [32], the discrepancies were larger if a combination of those two groups was considered. For the recommended version ('Optimization 1–12'), overall agreement for the oxidation of H_2S and formation of SO_3 after optimization is reasonable. The main improvements over the original mechanism is the better prediction of the laminar burning velocity and the slightly improved agreement of the ignition delay time at low temperatures.
3. The mechanism can also predict phenomena related to the interaction between carbon and sulfur species and the predicted relative oxidation speed of CH_4 and H_2S is correct.
4. Some quantitative discrepancies remain that highlight the uncertainties that still exist in sulfur chemistry. One important shortcoming that could not be improved through a similar optimization attempt is the underprediction of SO_3 formation at high temperature (cf. Figures 3-21 and 3-25).

We also observe that the amount of experimental data on sulfur combustion chemistry that is available for validation is very limited. More reliable data on laminar burning velocities and flame structures for H_2S , especially at higher pressure, as well as data on $\text{CH}_4/\text{H}_2\text{S}$ flames under air and oxy-fuel conditions would be extremely valuable in this respect.

To further improve the accuracy of the mechanism, more fundamental research on sulfur chemistry is necessary. As mentioned before, especially the formation of SO_3 at high temperature does not seem to be explicable with the pathways currently included in the mechanism. Depending on the exact EOR requirements, it might also become necessary to include some species containing both carbon and sulfur species (e.g. COS or CS_2) if the concentrations of these have to be kept low.

Chapter 4

Characteristics of Sour Gas Combustion

Up to now, very little is known about the behavior of sour gas as a fuel. To address this issue, we performed several standard calculations using the reaction mechanism presented in Chapter 3, with the objective of identifying possible general advantages of one combustion mode (i.e. air combustion vs. CO₂ or H₂O diluted oxy-combustion) over another and to characterize the influence of varying fuel composition.

In the following sections, we present our results for the adiabatic flame temperature, the ignition delay time, the laminar burning velocity, and the structure of premixed laminar flames. The H₂S mole fraction in the fuel was varied between 0% and 30% to cover the range of common sour gas compositions. Carbon dioxide in the fuel was not considered, since its influence can be inferred from the calculations with CO₂ dilution. For oxy-fuel combustion, the equivalence ratio was fixed at $\Phi = 1$. In calculating the equivalence ratio, both CH₄ and H₂S were considered as fuel. All calculations were conducted using CHEMKIN-PRO [105].

4.1 Adiabatic Flame Temperature

The adiabatic flame temperature is an important parameter because it determines how much diluent has to be added to the primary flame zone of the combustor and in the dilution zone to achieve temperatures that are within the material limits of the combustor walls and the first turbine stages. It thus has to be considered as a constraint when designing a combustor.

In air combustion, the flame temperature can be varied by changing the equivalence

ratio. In oxy-combustion, it is controlled by the diluent mole fraction since the equivalence ratio is fixed at $\Phi \approx 1$ to avoid wasting energy for O_2 production. The adiabatic flame temperature also increases with both preheat temperature and pressure. For simplicity, we only considered atmospheric pressure without preheating ($p = 1 \text{ atm}$, $T_{in} = 300 \text{ K}$). For these calculations, we used the equilibrium model of CHEMKIN.

Regardless of the combustion mode, the flame temperature decreases by about 30 – 50 K when raising the H_2S content in the fuel from 0% to 30% (see Figure 4-1). This behavior is caused by the smaller lower heating value of H_2S , which according to calculations using the same thermochemical data is only 65% of the heating value of CH_4 ($LHV_{H_2S} = 518 \text{ kJ/mol}$ as compared to $LHV_{CH_4} = 803 \text{ kJ/mol}$).

To achieve the same adiabatic flame temperature, the diluent concentration has to be 5–10 percentage points higher for H_2O dilution than for CO_2 dilution. This can be explained with the higher isobaric heat capacity of CO_2 (e.g. $c_{p,CO_2} = 58.4 \text{ J/molK}$ at $T = 1500 \text{ K}$

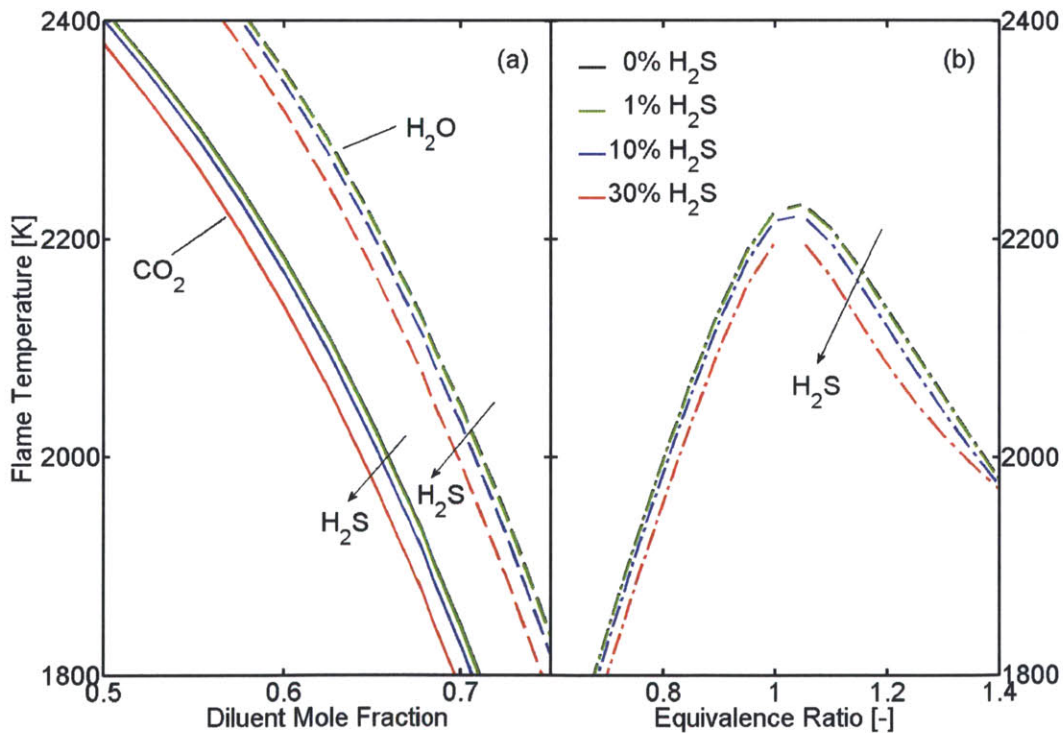


Figure 4-1: The adiabatic flame temperature of sour gas with varying H_2S content in the fuel: (a) Oxy-fuel combustion with CO_2 dilution (solid lines) and H_2O dilution (dashed lines), (b) Air combustion.

as compared to $c_{p,H_2O} = 47.1 \text{ J/molK}$ [60]). If the temperatures are to be limited to the maximum temperatures encountered in air combustion, the dilution percentage has to be greater than 58% for CO_2 or 64% for H_2O dilution.

4.2 Ignition Delay Time

The ignition delay time is a common metric for describing the oxidation characteristics of a fuel and can give some indications on flame stabilization behavior. For the present analysis, we used the closed homogeneous reactor model in CHEMKIN and defined the ignition delay time as the time needed for a temperature increase of $\Delta T = 600 \text{ K}$. We chose a constant pressure of $p = 40 \text{ atm}$ and an initial temperature of $T_0 = 800 - 1200 \text{ K}$, which is representative of the inlet conditions of gas turbine combustors [131].

First, we compared the ignition delay time for different H_2S mole fractions in the fuel for air combustion at $\Phi = 1$ and oxy-fuel combustion with CO_2 or H_2O mole fractions adjusted to give the same adiabatic flame temperature. For all three combustion modes, the ignition delay time decreases with increasing H_2S content in the fuel, indicating that the kinetics get faster (see Figure 4-2). One reason for this is that the direct reaction of H_2S with O_2 is faster than its CH_4 counterpart (e.g. 26 times faster at $T = 1200 \text{ K}$), which helps to build up a radical pool more quickly:



When comparing the different combustion modes, the ignition delay time is about a factor of 1.5 higher for air combustion than oxy-combustion and somewhat higher for CO_2 dilution than H_2O dilution. This behavior is caused by two effects which are highlighted in Figure 4-3. First, the different diluent mole fractions between the combustion modes lead to different concentrations of fuel and oxidizer (although all are at $\Phi = 1$). As we can see in Figure 4-3a, which shows the same calculation as Figure 4-2 but with inert versions of the

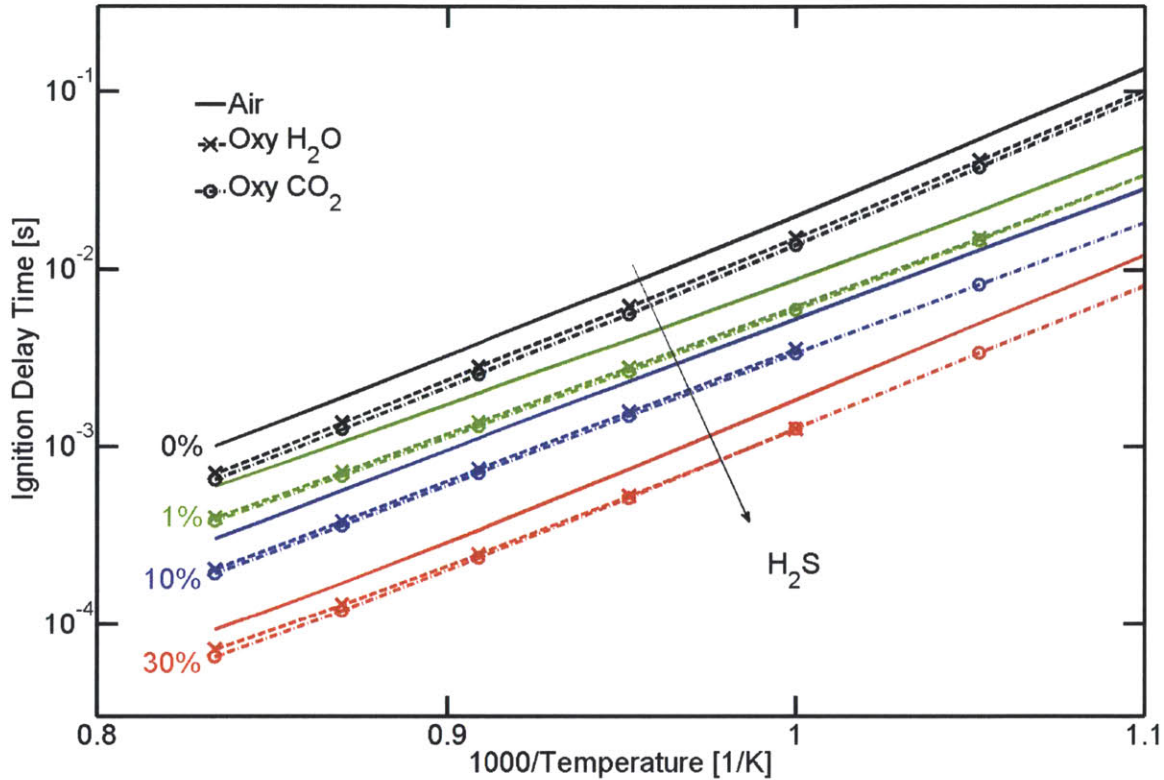


Figure 4-2: The ignition delay time of sour gas at $p = 40$ atm decreases with increasing H_2S mole fraction in the fuel. Here the diluent mole fractions in the oxy-fuel case are adjusted to match the flame temperature of the air case ($\Phi = 1$). This leads to lower ignition delay for the oxy-fuel cases.

diluents ($'\nu\text{N}_2'$, $'\nu\text{H}_2\text{O}'$, and $'\nu\text{CO}_2'$)¹, this leads to faster ignition for the modes that have lower diluent mole fractions, namely the oxy-fuel modes ($X_{\text{CO}_2} = 0.578$ and $X_{\text{H}_2\text{O}} = 0.646$ as compared to $X_{\text{N}_2} = 0.715$ for air). In addition to this, H_2O also has a chemical effect that tends to decrease the ignition delay time slightly. The chemistry of N_2 and CO_2 , on the other hand, has virtually no impact (see Figure 4-3b-d).

The chemical effect of H_2O can be explained by the influence of high H_2O concentrations on the radical pool. Both for CH_4 and H_2S oxidation, the main fuel consumption reaction under the present conditions is the reaction with the OH radical:

¹These fictitious molecules have the same thermodynamic and transport properties as N_2 , H_2O , and CO_2 , respectively, but do not participate in any reactions. This is analogous to the procedure used in [59].

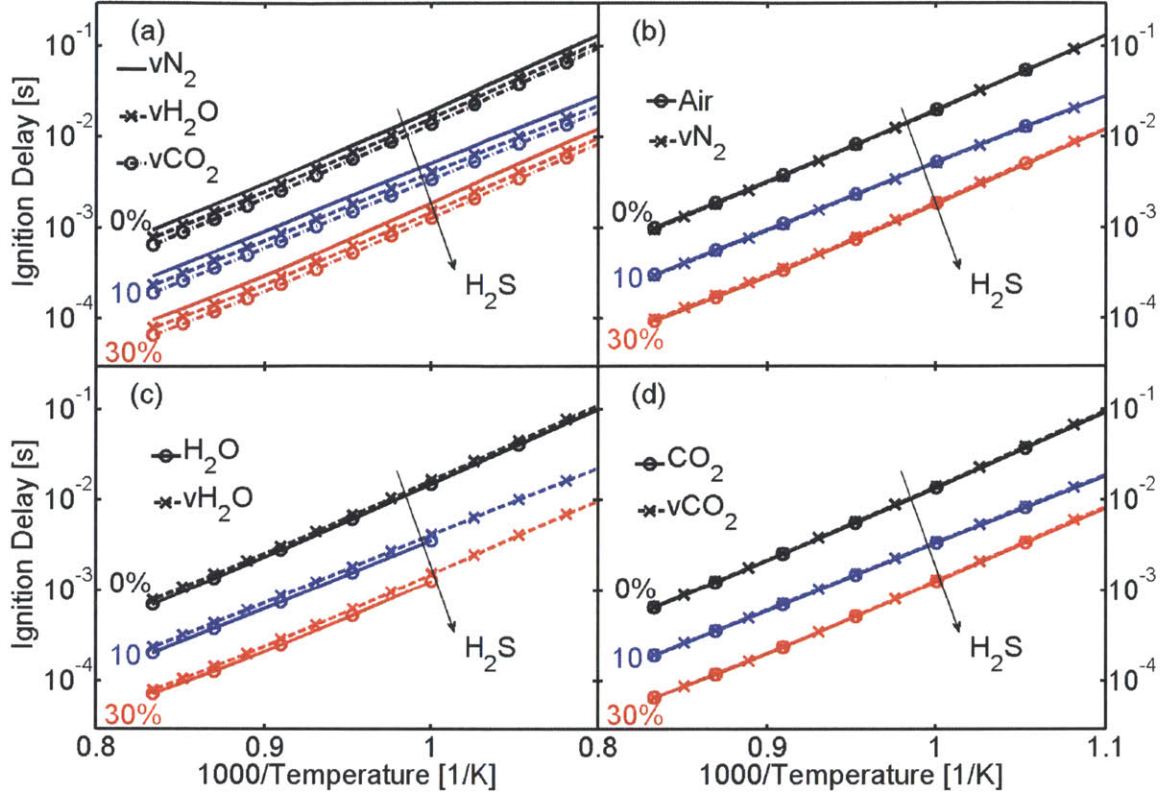


Figure 4-3: The ignition delay time of sour gas at $p = 40$ atm at $\Phi = 1$ is influenced by chemical and dilution effects when keeping the flame temperature constant among the combustion modes. (a) When chemical effects are removed, the ignition delay time is smallest for CO_2 dilution and largest in air, corresponding to the different fuel and oxidizer concentrations. (b) N_2 has no chemical effect. (c) The chemistry H_2O decreases the ignition delay slightly. (d) CO_2 has no chemical effect.



Especially for CH_4 , this reaction dominates the fuel consumption in the early stages leading to autoignition. High concentrations of H_2O tend to increase the OH mole fraction in these early stages (see Figure 4-4 for the case of pure CH_4) through the reaction



This in turn leads to enhanced fuel breakup via the reactions (4.2), which shortens the

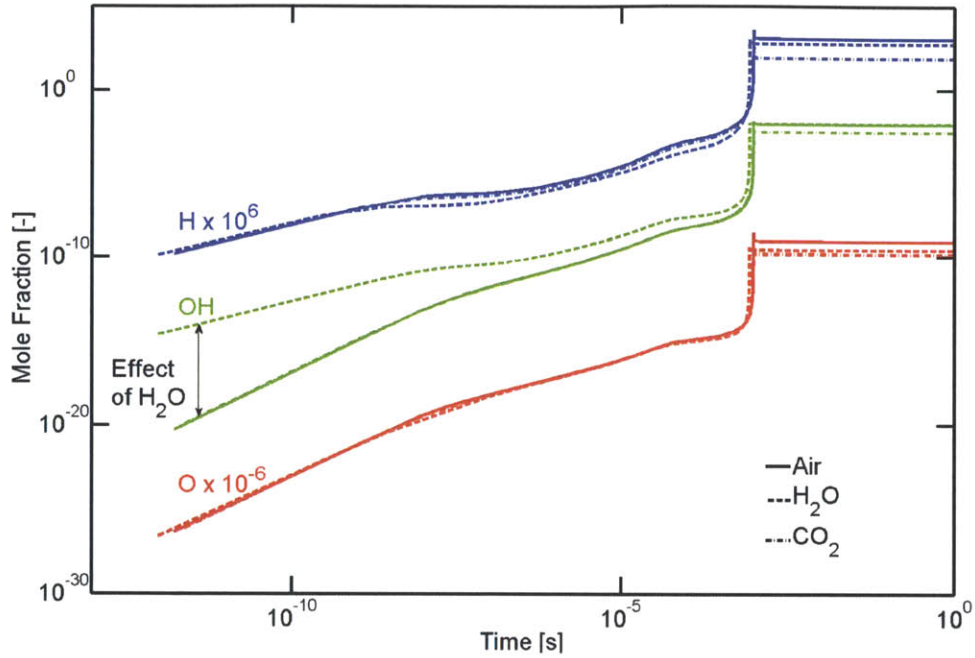


Figure 4-4: High H_2O contents lead to increased OH radical concentrations in the autoignition of CH_4 . The H and O profiles have been shifted for better visibility.

ignition delay time. The slight change of slope in the profiles around $t = 10^{-7}$ s marks the point where these reactions start to get important besides the direct reactions with O_2 (reactions (4.1)). The second change of slope around $t = 10^{-5}$ s occurs when the reactions of the H and O radicals with CH_4 start to get significant too.

If instead of adjusting the diluent mole fractions to keep the same flame temperature we use the same diluent mole fraction ($X_{\text{dil}} = 0.715$) for all three cases, the dilution effect explained above disappears. In this case, however, we get additional differences between the three combustion modes due to the different heat capacities of the diluents. Calculations with inert versions of the diluents show that this leads to air combustion (i.e. N_2 dilution) having a slightly lower ignition delay than oxy-combustion with H_2O and CO_2 dilution, in that order. The differences are almost constant at all conditions, so that on a logarithmic plot they appear bigger for cases with overall shorter ignition delay time. Superimposed with the chemical effects explained above, this leads to the behavior shown in Figure 4-5. For pure CH_4 , CO_2 diluted oxy-combustion shows almost the same behavior as air combustion, while H_2O dilution has an enhancing effect. As the H_2S mole fraction is increased, CO_2

dilution has an increasing inhibiting effect as compared to air combustion and H₂O dilution leads to a similar ignition delay as air combustion.

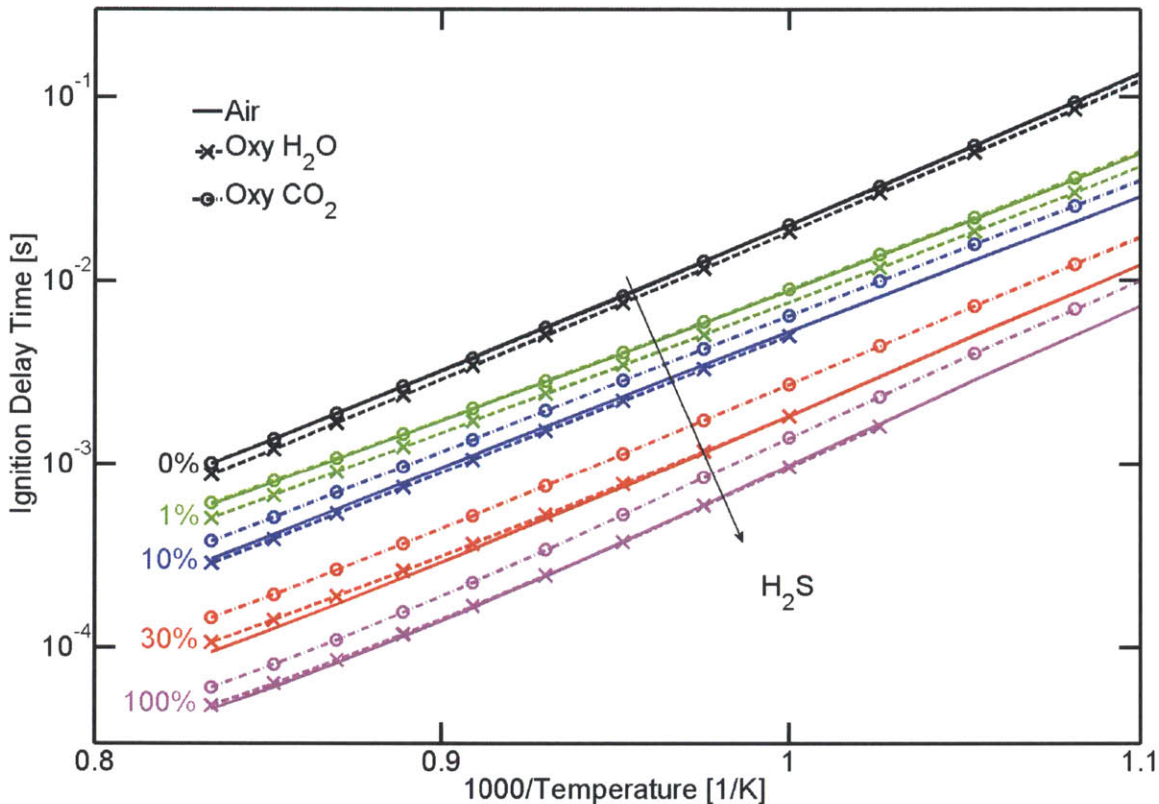


Figure 4-5: For a constant diluent mole fraction ($X_{dil} = 0.715$), the ignition delay time of sour gas at $p = 40$ atm shows different trends when changing the combustion mode depending on the H₂S mole fraction.

4.3 Laminar Burning Velocity

The laminar burning velocity can give valuable insight into flame stabilization characteristics because the local flow speed in the combustor should match the burning velocity to achieve stable combustion. As in Section 4.1, the degrees of freedom are the H₂S mole fraction in the fuel and the equivalence ratio for air combustion or the diluent mole fraction for oxy-fuel combustion. The calculations were done using the flame speed analyzer in CHEMKIN which simulates a freely propagating one dimensional laminar flame. Thermal diffusion of species (Soret effect) had to be considered.

4.3.1 Impact of the Combustion Mode

We investigated the influence of the different combustion modes (air vs. oxy-combustion with CO₂ or H₂O dilution) on the laminar burning velocity. In order to make a fair comparison, the burning velocities are plotted as a function of the adiabatic flame temperature.

For simplicity, we first consider pure CH₄ (see Figure 4-6d). For air combustion, there are two branches corresponding to the fuel-rich and fuel-lean side. Maximum burning velocity and flame temperature both occur around $\Phi = 1$. Since the burning velocity peaks at slightly higher values of Φ than the temperature while the burning velocity decays much faster on the rich side, there is a small loop in the curve.

For a given flame temperature, air combustion always gives the highest burning velocity, followed by oxy-fuel combustion with H₂O dilution, while CO₂ dilution gives the lowest values. At high flame temperatures ($T \approx 2200$ K), the H₂O diluted flames are almost as fast as the air flames, while at low temperatures ($T \approx 1800$ K) they are closer to the CO₂ diluted flames. To highlight what causes this behavior, we conducted several additional calculations.

First, we compared the burning velocity of CH₄/air flames with varying equivalence ratio to CH₄/O₂/N₂ flames at $\Phi = 1$ with varying N₂ mole fraction (labeled 'Oxy N₂'), as well as flames with a virtual molecule 'vN₂' that has the same properties as N₂ but does not participate in any reactions (see Figure 4-6a). The air flames are faster than the oxy flames because in cases where $\Phi \neq 1$ the 'diluent' consists not only of virtually inert N₂, but also either excess O₂ or fuel. It can be seen that N₂, which is usually considered to be inert, does have a very small chemical effect that tends to increase the burning velocity. At low temperatures, this is mainly caused by the participation of N₂ as a third body in the reaction that converts methylene from the singlet state (CH₂(s)) to the triplet state (CH₂)



which provides an additional pathway from methyl (CH₃) to formaldehyde (CH₂O) during the oxidation of CH₄ (see e.g. [8]). At high temperatures, direct reactions with nitrogen such as those responsible for NO_x formation become more important.

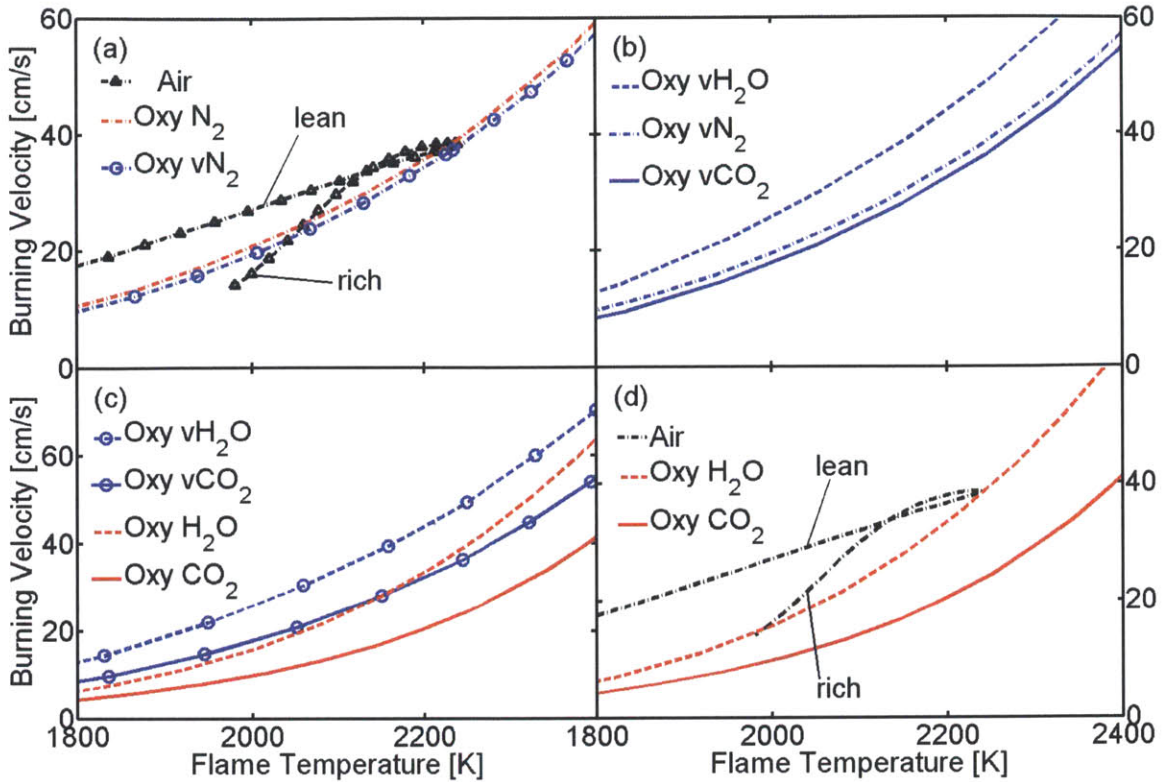


Figure 4-6: The influence of different effects on the laminar burning velocity of CH_4 at $p = 1$ atm. (a) Air combustion compared to combustion in O_2 and N_2 or O_2 and $v\text{N}_2$ (=inert N_2) with fixed $\Phi = 1$ and varying diluent concentration. (b) Oxy-fuel combustion using inert versions of N_2 , CO_2 , and H_2O as diluents, showing the influence of the transport properties. (c) Comparison of combustion using the inert and real diluents, showing the chemical effect of the diluents. (d) Comparison of the three relevant combustion modes.

Next, we compared the burning velocity of the oxy-fuel flames with the inert N_2 to similar flames using inert CO_2 ($v\text{CO}_2$) and H_2O ($v\text{H}_2\text{O}$) (see Figure 4-6b). Since the flame temperature is the same and the diluents do not participate in any reactions, the differences between the three cases are mainly due to the different transport properties. The transport properties of H_2O lead to an increase in the burning velocity relative to N_2 whereas the properties of CO_2 lead to a slight decrease. The relative change in the burning velocity corresponds roughly to the square root of the change in the diffusion coefficient for H radicals, which at $T = 2000$ K is increased by 27% in H_2O as compared to N_2 but decreased by 11% in CO_2 .

When comparing the cases with inert $v\text{CO}_2$ and $v\text{H}_2\text{O}$ to the ones with the normal

(reacting) diluents, we observe that both diluents have chemical effects that slow down the kinetics, with CO_2 leading to the stronger effect (see Figure 4-6c). This is in agreement with the results in the literature (cf. Section 2.2.1). The combination of all these effects finally leads to the differences in burning velocity for the relevant combustion modes (see Figure 4-6d).

We also conducted the same analysis for pure H_2S . The general trends are similar as for CH_4 in that air combustion leads to the highest burning velocity and CO_2 diluted oxy-combustion to the lowest (see Figure 4-7d). However, in this case the difference between H_2O and CO_2 dilution is much smaller than for CH_4 . Also, the curve for air combustion does not exhibit the loop found for CH_4 , because the burning velocity peaks at lower values of Φ than the flame temperature.

The observation that the burning velocity is almost equal for CO_2 and H_2O dilution can be explained by the fact that for H_2S combustion, H_2O has a significantly stronger inhibiting chemical effect than CO_2 (see Figure 4-7c). This balances the promoting effect of the transport properties of H_2O (see Figure 4-7b). For H_2S combustion, N_2 has virtually no chemical effect because reaction (4.4) is not relevant (see Figure 4-7a).

For CO_2 , sensitivity and reaction pathway analyses show that the inhibiting chemical effect on H_2S combustion is due to the reaction



which competes with the main chain branching reaction $\text{H} + \text{O}_2 = \text{OH} + \text{O}$. This is the same reaction that Liu et al. [59] found to be responsible for the inhibiting effect in CH_4 and H_2 combustion. Indeed, if this reaction is removed from the mechanism, the original burning velocity is recovered.

For H_2O , our analyses suggest that there are at least two pathways through which a chemical inhibition takes place. First, similar to what has been found for CH_4 combustion [84], H_2O acts as a very efficient third body in the reaction



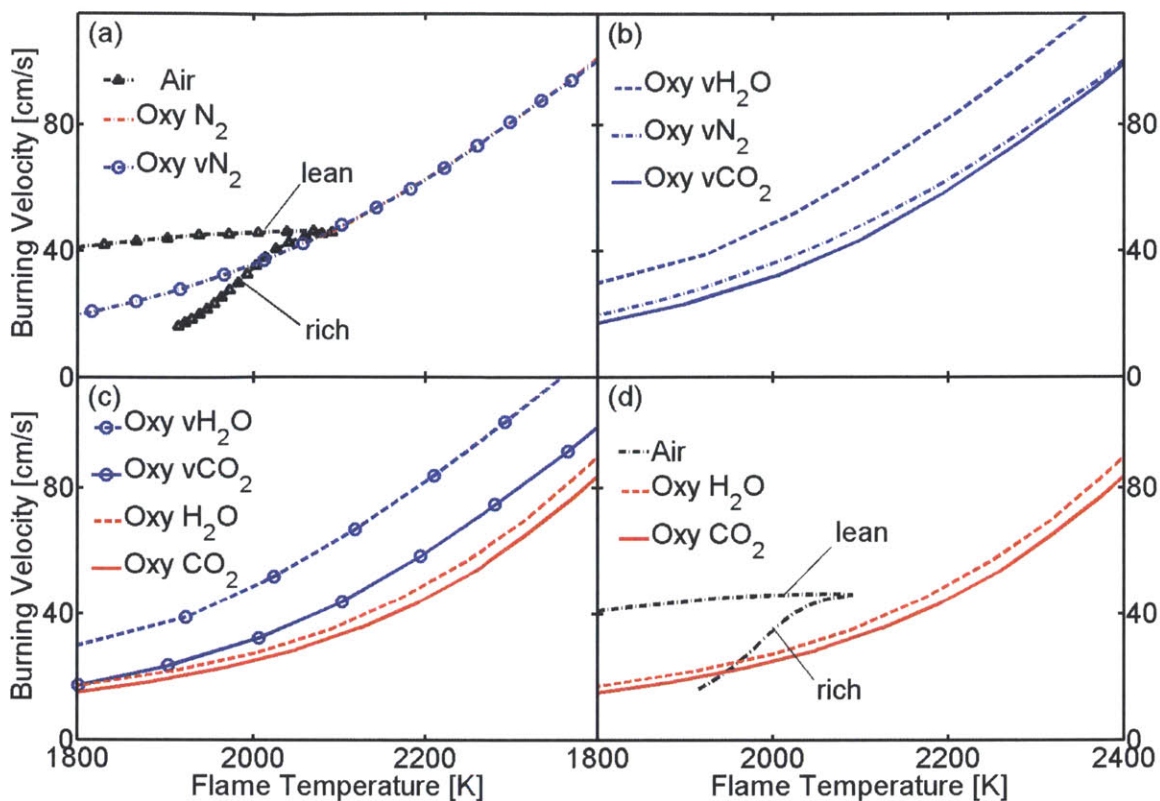
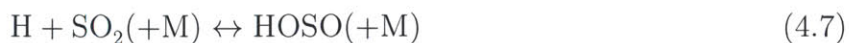


Figure 4-7: The influence of different effects on the laminar burning velocity of H₂S at p = 1 atm. (a) Air combustion compared to combustion in O₂ and N₂ or O₂ and vN₂ (=inert N₂) with fixed $\Phi = 1$ and varying diluent concentration. (b) Oxy-fuel combustion using inert versions of N₂, CO₂, and H₂O as diluents, showing the influence of the transport properties. (c) Comparison of combustion using the inert and real diluents, showing the chemical effect of the diluents. (d) Comparison of the three relevant combustion modes.

which also competes with the main chain branching reaction $H + O_2 = OH + O$. Second, H₂O promotes the removal of H radicals initiated by the reaction



by acting as an efficient third body (cf. Section 4.3.2). This effect accounts for about 20% of the reduction in the burning velocity and explains at least part of the stronger inhibition by H₂O as compared to CO₂.

4.3.2 Impact of the Fuel Composition

Next, we investigated the influence of varying H_2S mole fractions in the fuel. Again, comparison is first made at a constant temperature. From a design point of view, this corresponds to the case where the conditions are always adjusted to the fuel composition in order to achieve the same flame temperature.

For all combustion modes, addition of 1% H_2S leads to a very slight decrease in the burning velocity (see Figure 4-8). Addition of 10% H_2S results either in a slight increase or decrease, depending on the exact conditions. When the H_2S content is further increased to 30%, the burning velocity increases in all modes and at all flame temperatures by up to 6 cm/s compared to pure CH_4 . The inhibiting effect at low H_2S mole fractions with an increase of the burning velocity at higher mole fractions has been observed experimentally in similar form by Kurz for propane- H_2S -air flames [102]. This behavior is caused by two separate chemical effects.

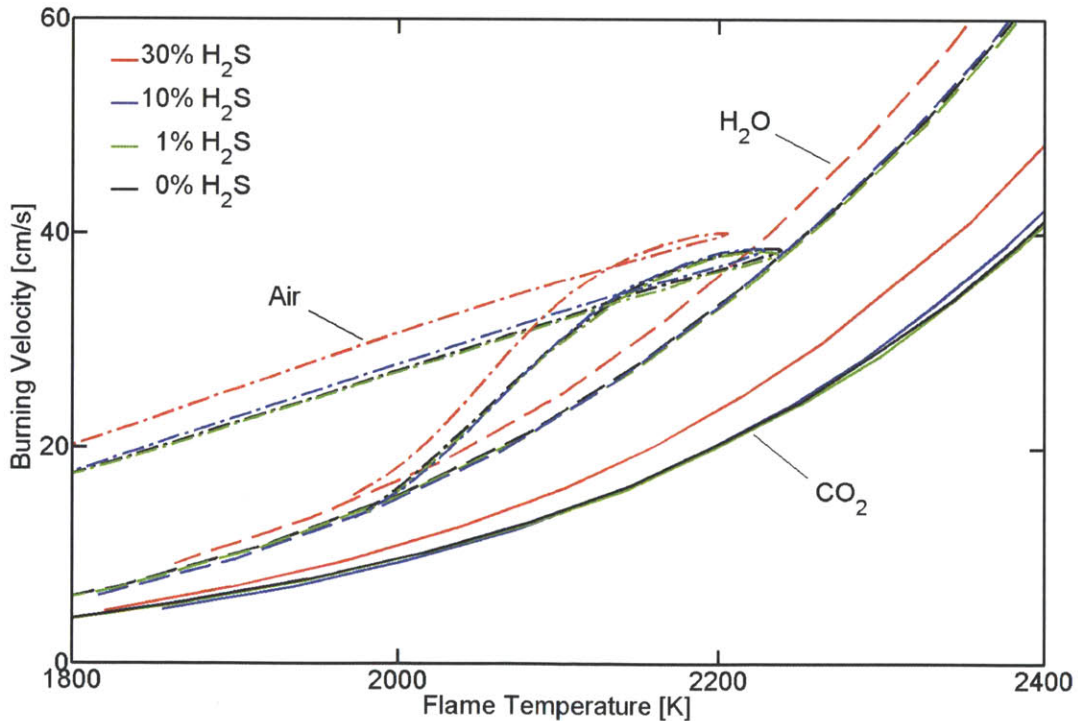
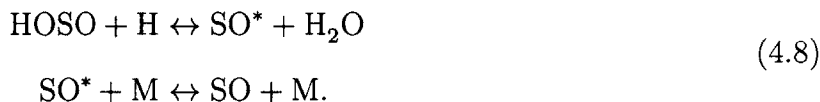


Figure 4-8: The laminar burning velocity of sour gas with varying H_2S content in the fuel at $p = 1$ atm for oxy-fuel combustion with CO_2 dilution (solid lines) and H_2O dilution (dashed lines), and air combustion (dash-dotted lines).

The slight decrease in the burning velocity when adding small amounts of H₂S is due to the fact that the SO₂ formed catalyzes H radical removal through reaction (4.7), which according to a reaction pathway analysis is mostly followed by



This corresponds to a net removal of H radicals similar to the mechanism described in Section 2.1.4. To demonstrate this effect, we compared H₂O diluted flames with 0% H₂S and 10% H₂S, while adjusting the H₂O mole fraction to get a flame temperature of $T_f = 1900$ K in both cases. The burning velocity with 10% H₂S is about 6% lower than without H₂S (see Table 4.1). When comparing the profiles of the H radical through the flame, we observe that the peak concentration is about 12% lower when adding H₂S (see Figure 4-9). When the same calculation (with 10% H₂S) is conducted with a version of the reaction mechanism from which reaction (4.7) has been removed, the peak H concentration and burning velocity are virtually the same as in the case without H₂S (cf. Figure 4-9 and Table 4.1), proving that it is indeed this reaction that is responsible for the observed effects.

When the H₂S mole fraction is increased further, the burning velocity increases as it approaches that of pure H₂S (e.g. for air combustion at $\Phi = 1$ we have $s_{L,\text{CH}_4} = 38$ cm/s and $s_{L,\text{H}_2\text{S}} = 46$ cm/s). The relative importance of these effects depends slightly on the exact conditions.

If, instead of keeping the flame temperature constant, we just fix the equivalence ratio and diluent mole fraction while varying the H₂S content in the fuel, the chemical effects are superimposed with the effect of the changing flame temperature (cf. Section 4.1). Because

Table 4.1: Reduction in the laminar burning velocity when adding H₂S to a H₂O diluted flame at $T_f = 1900$ K.

	Burning Velocity [cm/s]	Relative Change
0% H ₂ S	10.26	-
10% H ₂ S	9.68	-5.7%
10% H ₂ S, without reaction (4.7)	10.22	-0.4%

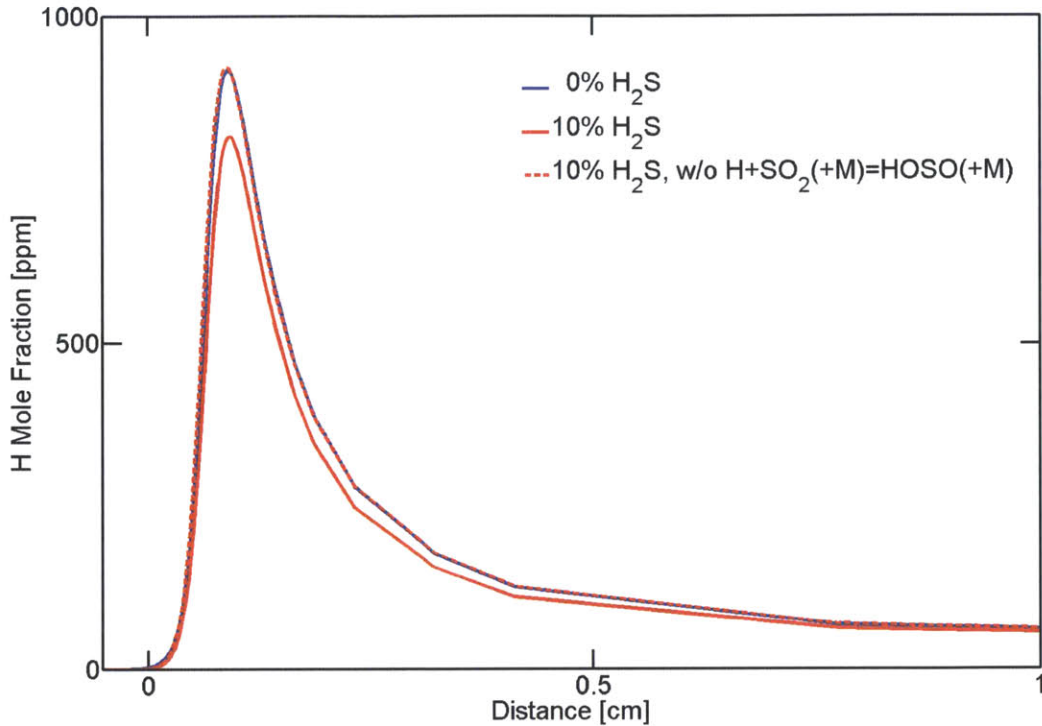


Figure 4-9: The peak H radical concentration is reduced when adding H_2S to a H_2O diluted CH_4 oxy-fuel flame at $T_f = 1900$ K through the reaction $\text{H} + \text{SO}_2(+\text{M}) = \text{HOSO}(+\text{M})$.

of the different heat capacities of the diluents and the slightly varying extent of the chemical effects under different conditions, this leads to a differing behavior between the combustion modes (see Figure 4-10). For air combustion and CO_2 diluted oxy-fuel combustion, the burning velocity decreases slightly for small H_2S mole fraction and increases over the initial value for larger H_2S mole fractions. For H_2O diluted oxy-combustion, there is a continuing decrease in the burning velocity up to high H_2S mole fractions because the effect of decreasing flame temperature is strongest and there is an increasing chemical effect (cf. Section 4.3.1).

4.3.3 Influence of Pressure

To investigate the influence of pressure, we calculated burning velocities for a fixed equivalence ratio of $\Phi = 1$ for air combustion and a fixed diluent mole fraction for oxy-combustion that leads to the same flame temperature as air at $\Phi = 1$ for pure CH_4 ($X_{\text{CO}_2} = 0.578$ for CO_2 dilution and $X_{\text{H}_2\text{O}} = 0.646$ for H_2O dilution) and a H_2S mole fraction of 0% and 30%

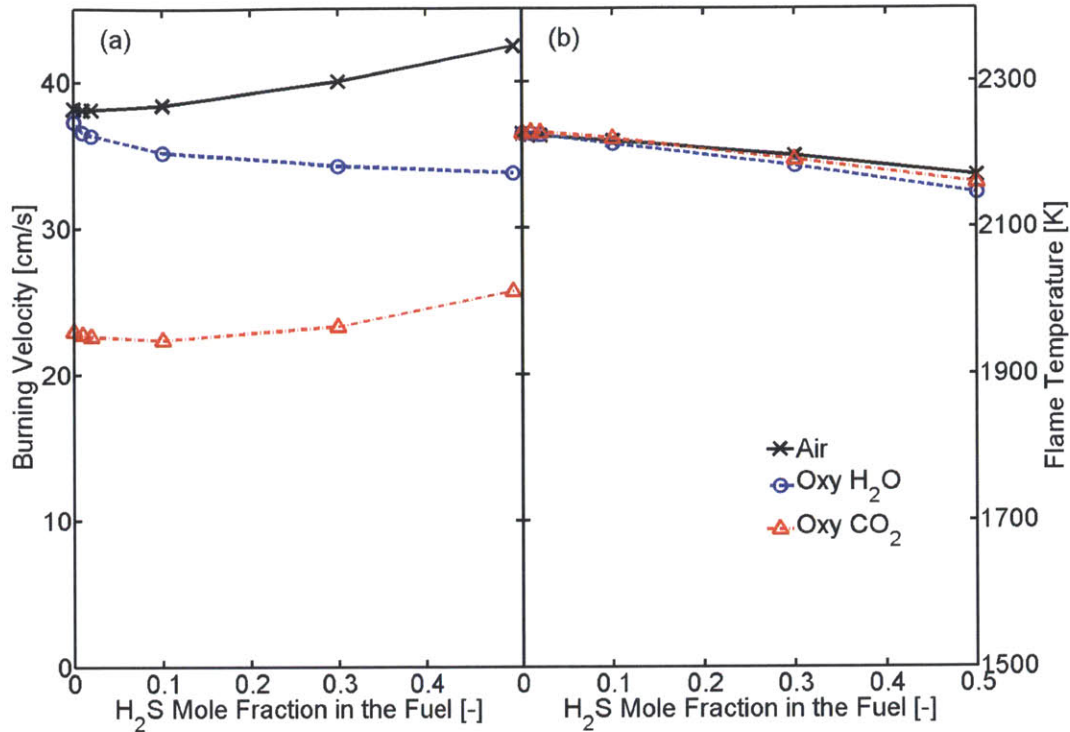


Figure 4-10: For a fixed equivalence ratio of $\Phi = 1$ and diluent mole fraction ($X_{\text{CO}_2} = 0.578$ for CO_2 dilution and $X_{\text{H}_2\text{O}} = 0.646$ for H_2O dilution), the burning velocity shows a different behavior with changing H_2S content for the different combustion modes (a). This is in part caused by the different heat capacities, which lead to different flame temperatures (b).

for pressures between 1 atm and 40 atm. For all fuel compositions and combustion modes, the burning velocity decreases significantly when raising the pressure from 1 atm to 20 atm and changes only relatively little with further increases in pressure (see Figure 4-11). For low pressure ($p \lesssim 10 - 20$ atm), the decrease corresponds roughly to the expected power law $s_L \propto p^{(n-2)/2}$ (see e.g. [8]), where s_L is the laminar burning velocity and n is the overall reaction order. At higher pressures, the effect of pressure is weaker than predicted by the power law.

The pressure dependence is stronger for air combustion than for oxy-combustion. As a consequence, at elevated pressures H_2O diluted oxy-combustion leads to the highest burning velocities while air combustion and CO_2 diluted oxy-combustion give similar values that are substantially lower. The decreases in the burning velocity when increasing the pressure to 40 atm can be recovered if the mixture is preheated to 600 – 750 K for air com-

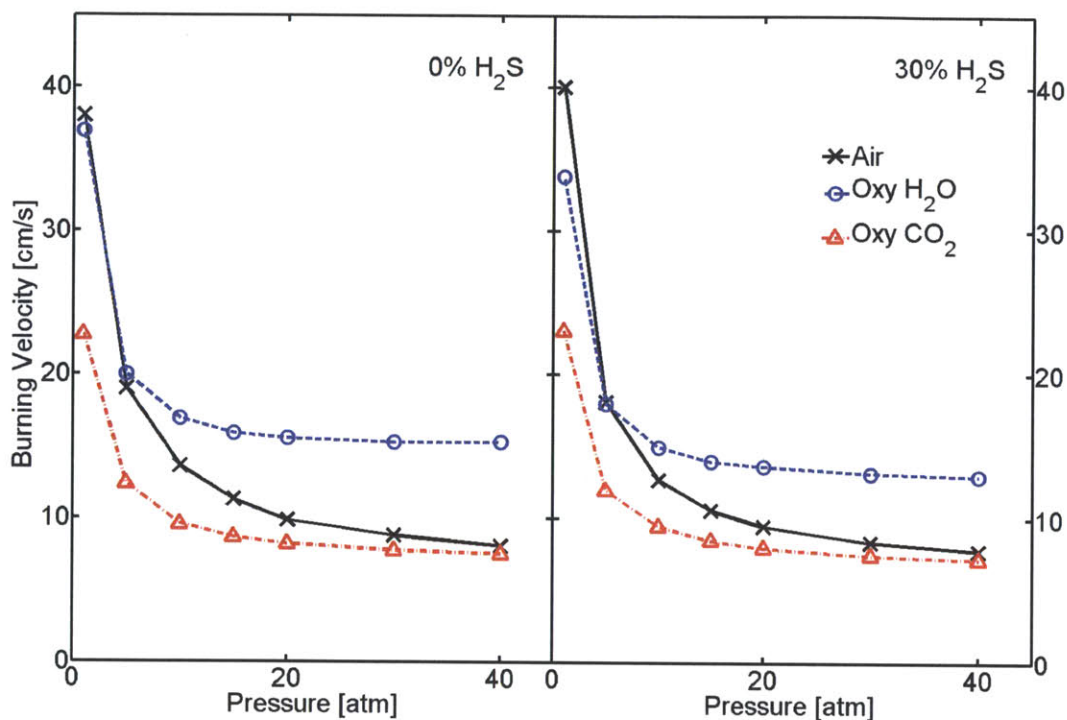


Figure 4-11: The burning velocity of CH_4 decreases faster with pressure for air combustion at $\Phi = 1$ than for oxy-combustion at $\Phi = 1$ with CO_2 dilution ($X_{\text{CO}_2} = 0.578$) or H_2O dilution ($X_{\text{H}_2\text{O}} = 0.646$).

bustion, 550 – 650 K for CO_2 diluted oxy-combustion, and 500 – 550 K for H_2O diluted oxy-combustion.

The pressure dependence of the laminar burning velocity is somewhat stronger for the case with 30% H_2S in the fuel. Accordingly, the overall reaction order is about $n = 1.0$ for air combustion and $n = 1.2$ for oxy-combustion, as compared to $n = 1.1$ and $n = 1.3$ for pure CH_4 . The lower reaction orders are consistent with the fact that less O_2 is needed for the complete oxidation of H_2S than for CH_4 :



Because of the stronger decrease in the burning velocity of H_2S as the pressure is increased, the behavior with varying fuel composition is slightly different at high pressure than what we described for atmospheric pressure. The inhibiting effect due to H radical re-

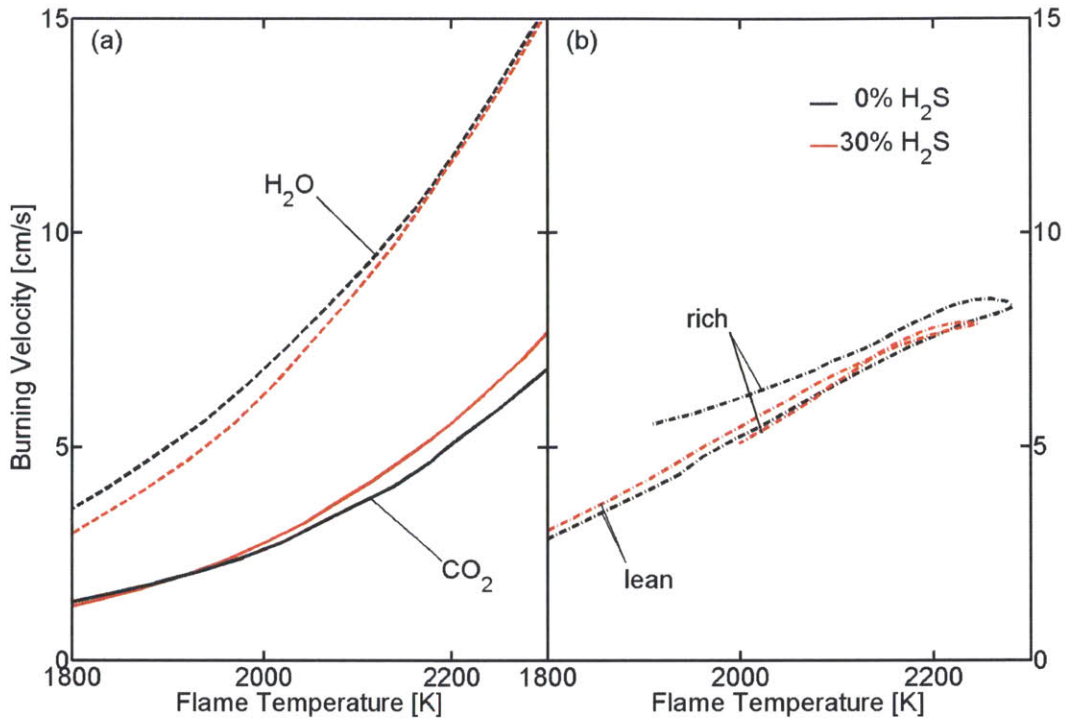


Figure 4-12: The laminar burning velocity of sour gas with varying H₂S content in the fuel at $p = 40$ atm: (a) Oxy-fuel combustion with CO₂ dilution (solid lines) and H₂O dilution (dashed lines), (b) Air combustion.

combination catalyzed by SO₂ is still present at high pressure, and its relative importance is greater than at atmospheric conditions. Therefore, at $p = 40$ atm small H₂S mole fractions in the fuel still lead to a smaller burning velocity than pure CH₄, and even for 30% H₂S in the fuel it depends on the exact conditions whether the burning velocity is increased or decreased compared to pure CH₄ (see Figure 4-12).

However, when interpreting these results we have to keep in mind that there is increased uncertainty in the reaction mechanisms at elevated pressure. The prediction quality of the GRI-Mech 3.0 for the burning velocity of CH₄ in O₂/He mixtures has been found to decrease above pressures of 20 – 40 atm [132]. For H₂S, data on the burning velocity at increased pressure is lacking altogether and the mechanism was only validated at atmospheric pressure (cf. Section 3.3.2). Thus, the present results should only be seen as qualitative trends.

4.4 Premixed Flame Structure

To gain further insight into the general combustion behavior, it is useful to investigate not only the burning velocity but also the structure of laminar premixed flames. For this analysis, the same model of a freely propagating one dimensional flame in CHEMKIN was used as for the laminar burning velocity in the previous section.

4.4.1 General Structure

To show what the general structure of a sour gas flame (i.e. a flame in which CH_4 and H_2S are oxidized simultaneously) looks like, we simulated an air flame with a fuel consisting of 70% CH_4 and 30% H_2S at $\Phi = 0.87$ and atmospheric pressure (see Figure 4-13).

The oxidation of the two fuels starts almost simultaneously, but the consumption of H_2S is completed at a point where about 20% of the CH_4 is still present. Similarly, while the

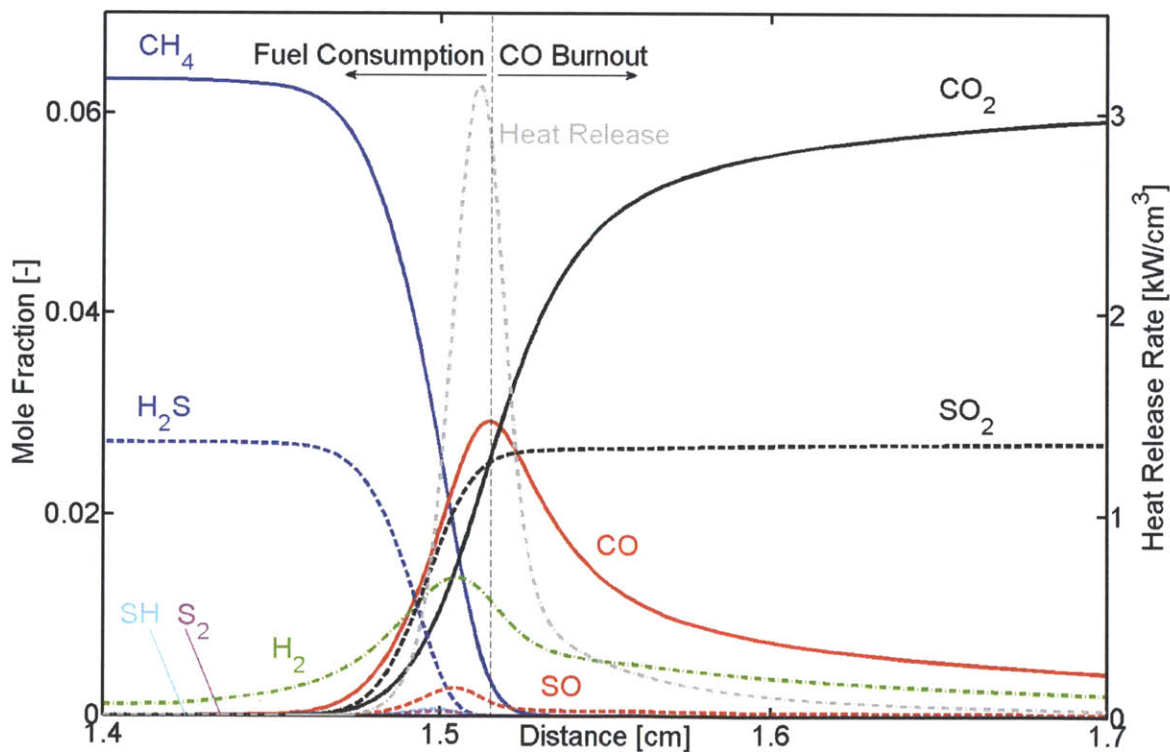


Figure 4-13: The flame structure of a premixed sour gas-air flame with 30% H_2S in the fuel at $\Phi = 0.87$ and $p = 1$ atm can be divided into two zones (vertical dashed line).

first appearance of the final combustion products CO_2 and SO_2 is approximately at the same point, the SO_2 profile is steeper and approaches its final concentration much faster than the CO_2 profile. Accordingly, the concentrations of SO as the last intermediate product of H_2S combustion is much lower (even in relation to the initial mole fraction of H_2S) and its peak occurs earlier than for CO, the corresponding carbon species. The peak mole fractions of the only other sulfur compounds occurring in significant amounts, SH and S_2 , are another order of magnitude lower and occur slightly before the SO peak, corresponding to their position in the oxidation sequence of H_2S (cf. Figure 3-5). Hydrogen, which appears as an intermediate product of the oxidation of both fuels, has a peak that coincides roughly with the SO peak. The overall heat release rate peaks close to the point where the CH_4 consumption is complete.

In total, we can identify a two-zone structure similar to the one commonly observed in premixed CH_4 -air flames [8]: In the first zone (labeled 'Fuel Consumption' in Figure 4-13), both CH_4 and H_2S are consumed almost entirely. The H_2S is converted virtually completely to SO_2 , while the CH_4 forms significant amounts of CO (only about 35% of the carbon are in the form of CO_2 at the end of this zone). While some hydrogen is still in the form of H_2 , the majority (80%) of the H_2O produced in the process is already present. In the second zone (labeled 'CO Burnout' in Figure 4-13), the main reaction occurring is the oxidation of CO to CO_2 . Simultaneously, the remaining H_2 is converted to H_2O .

Given the importance of SO_3 due to its role in different corrosion mechanisms (cf. Section 2.1.3) we also looked at the SO_3 profiles, although we expect most of the SO_3 formation in a power plant to occur during the cooling of the flue gas and not in the combustor. Some SO_3 is formed in the flame, corresponding to the equilibrium values at the flame temperature. For all fuel compositions and combustion modes, roughly 0.05% of the total sulfur gets converted to SO_3 (as compared to $\mathcal{O}(1\%)$ after cooling in power plants [37]), leading to a maximum concentration of about 20 ppm at the end of the domain for the cases that were considered (occurring for 30% H_2S in the fuel and air combustion).

Virtually all of the SO_3 is formed in the 'CO Burnout' zone (cf. Figure 4-13) and the time required to approach the equilibrium concentration is always shorter than the time required for CO oxidation. Only for the highest SO_3 content of 30%, the two times are

almost equal (see Figure 4-14). For modeling purposes, this means that as soon as we assume equilibrium CO at the end of a combustion process, it is a good approximation to also assume equilibrium SO_3 . From a practical point of view, it means that quenching of SO_3 formation in the combustor can only be achieved at the expense of quenching CO oxidation as well because they happen on the same time scale and they both virtually stop once the temperature drops below $T = 1000$ K [28, 34].

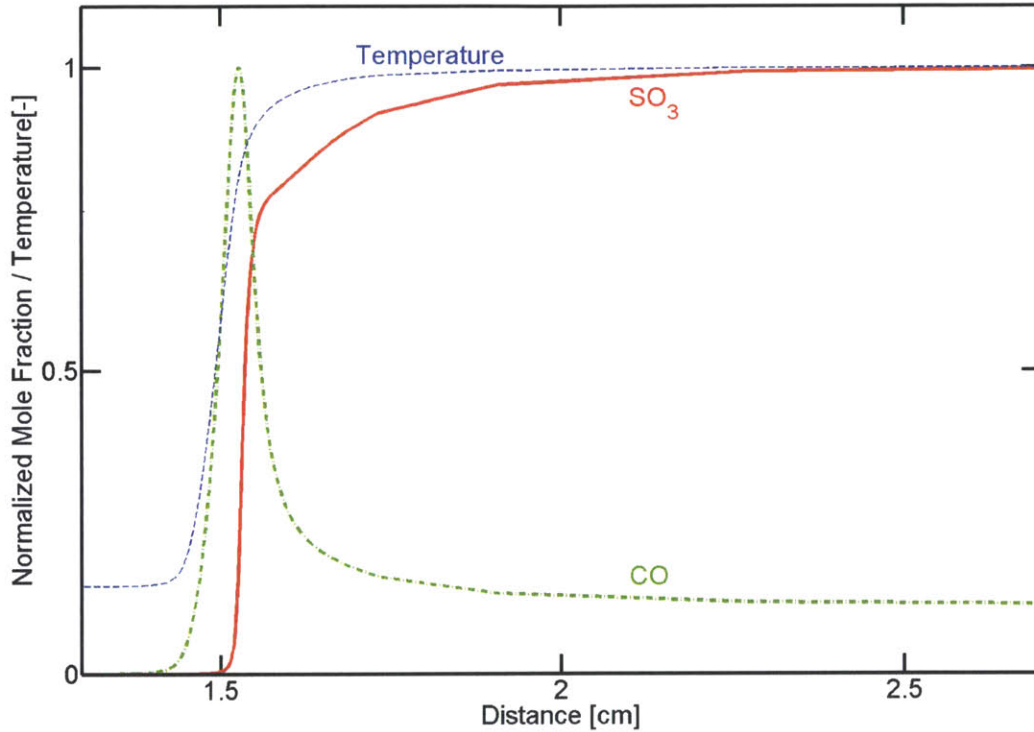


Figure 4-14: The formation of SO_3 in a H_2O diluted sour gas oxy-fuel flame occurs on the same time scale as the oxidation of CO. The calculations shown are for 30% H_2S in the fuel and combustion at $\Phi = 1$ with $X_{\text{H}_2\text{O}} = 0.678$, leading to a flame temperature of $T_f = 2073$ K. The mole fractions and the temperature are normalized by their respective maximum value.

4.4.2 Impact of the Combustion Mode

To investigate possible changes in the flame structure for oxy-fuel combustion with different diluents as compared to air combustion, we conducted similar calculations for CO_2 and H_2O diluted oxy-fuel combustion at $\Phi = 1$, in each case adjusting the diluent mole fraction to get the same flame temperature. Because of the different heat capacities of CO_2 and H_2O as

compared to N_2 the concentrations of the fuels in the mixtures thus differ between the three cases (see Figure 4-15). The consumption profiles of CH_4 and H_2S also have different slopes for the different combustion modes, corresponding to the differences in burning velocity discussed in Section 4.3.

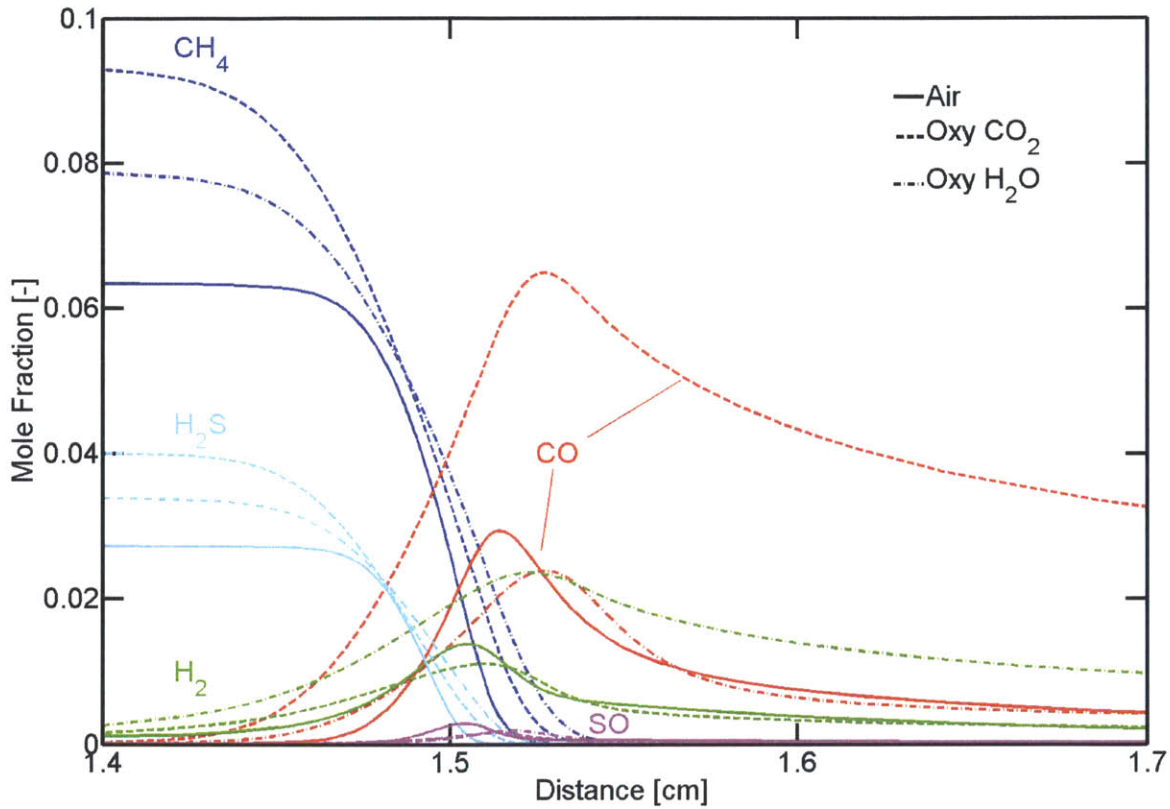


Figure 4-15: The flame structure of a premixed sour gas-air flame at $\Phi = 0.87$ as compared to CO_2 and H_2O diluted oxy-fuel flames at $\Phi = 1$ and $p = 1$ atm. The diluent mole fractions in the oxy-fuel flames are adjusted to give a flame temperature of $T = 2073$ K in all three cases ($X_{CO_2} = 0.619$ and $X_{H_2O} = 0.678$).

In case of CO_2 diluted oxy-combustion, the CO peak is a lot higher than in the other two cases. This is in agreement with the experimental findings for premixed CH_4 oxidation in flow reactors [16] and calculations for CH_4 diffusion flames [133] and as was shown in the cited articles it can be explained through inhibited CO oxidation or even promoted CO formation through reaction (4.5). On the other hand, the peak concentration of H_2 is slightly reduced compared to the values for air combustion. This reduction has also been predicted for diffusion flames [133] and can be attributed to the increased ratio of OH and H radical

concentrations (see Figure 4-16) due to reaction (4.5), which in turn enhances the main H_2 consumption reaction



For H_2O dilution, the changes in the CO and H_2 peaks are opposite to CO_2 dilution: the H_2 peak is higher than in the other cases while the CO peak is slightly lower. This can be explained by an inhibition of the main H_2 consumption reaction (4.10) because of the high H_2O concentration. The slight decrease in the CO concentration is likely to be caused by the change in the radical pool with higher OH concentrations (+15-60%, cf. Figure 4-16) due to the inhibition of reaction (4.10) and the reaction $O+H_2O=OH+OH$ [28].

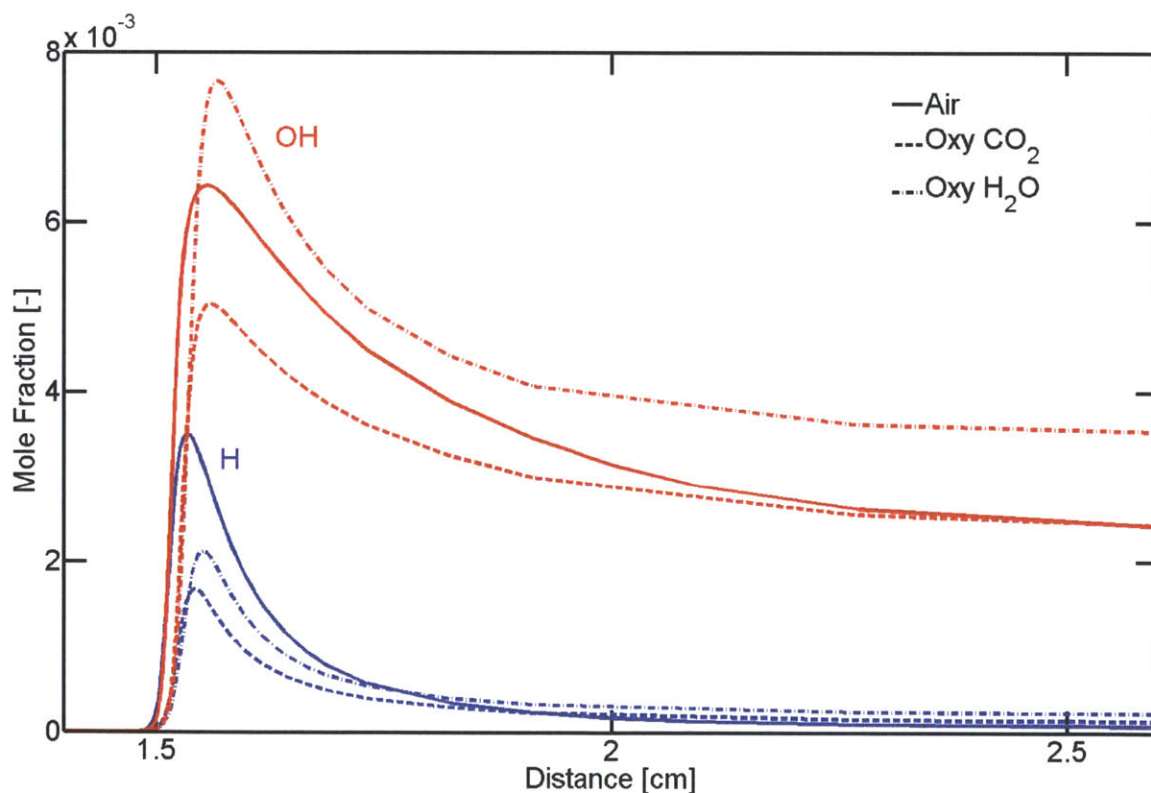


Figure 4-16: The radical concentrations in a sour gas-air flame change with the combustion mode. For CO_2 dilution, the H concentration is decreased more than the OH concentration. Water dilution leads to increased OH concentrations and decreased H concentrations. The conditions are the same as for Figure 4-15.

4.4.3 Impact of the Fuel Composition

The general flame structure does not change when the H₂S mole fraction in the fuel is varied (see Figure 4-17). When the amount of H₂S in the fuel is increased, the concentrations of the sulfur species increases while the concentrations of the carbon species decreases accordingly. The shape of the profiles and the locations of the peaks stay the same except for H₂. With increasing H₂S content, the H₂ peak gets higher and tends to occur slightly earlier.

From the rates of production of H₂ we can see that there is additional H₂ formation mainly through the following reactions:



These occur slightly earlier than the main H₂ formation reactions due to CH₄ oxidation:

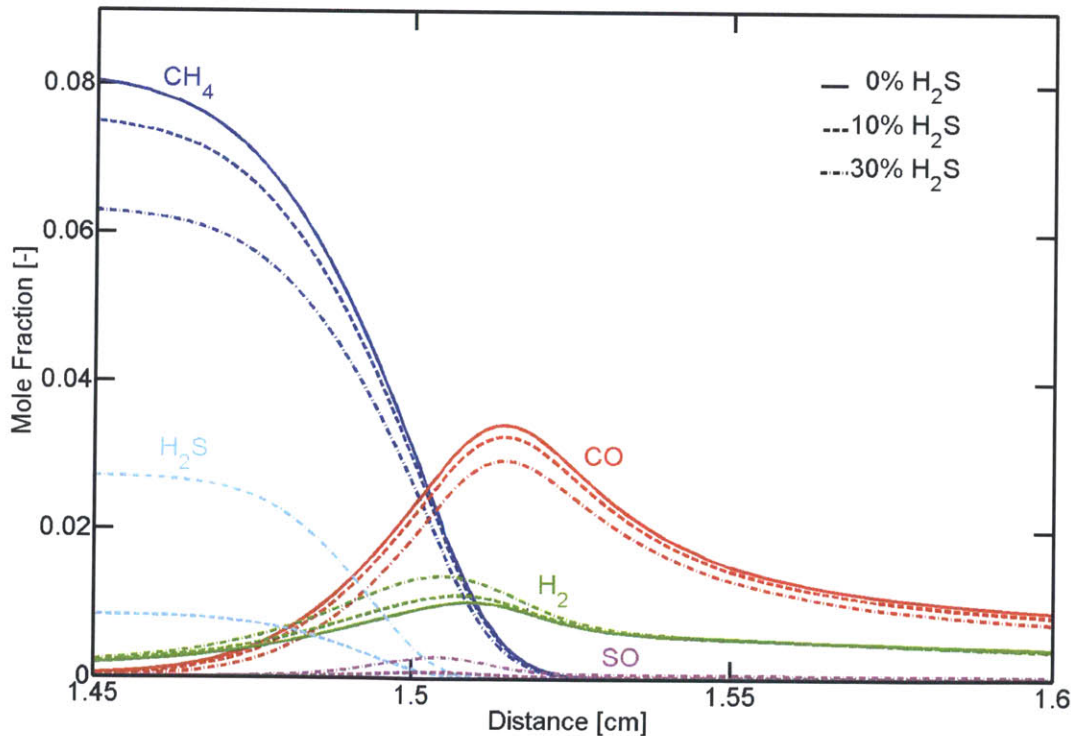


Figure 4-17: The general flame structure of a premixed sour gas-air flame at $p = 1$ atm does not change with varying H₂S content except for the location of the H₂ peak. The equivalence ratio was adjusted to always give $T_f = 2073$ K



In all cases the consumption of H_2 is dominated mainly by reaction (4.10).

4.4.4 Flame Thickness

Changes in flame thickness of sour gas flames can most easily be observed in the heat release profiles. In general, the flame thickness δ is expected to scale as

$$\delta \propto \sqrt{\alpha\tau_r}, \tag{4.13}$$

where α is a diffusivity and τ_r is a chemical time scale [8].

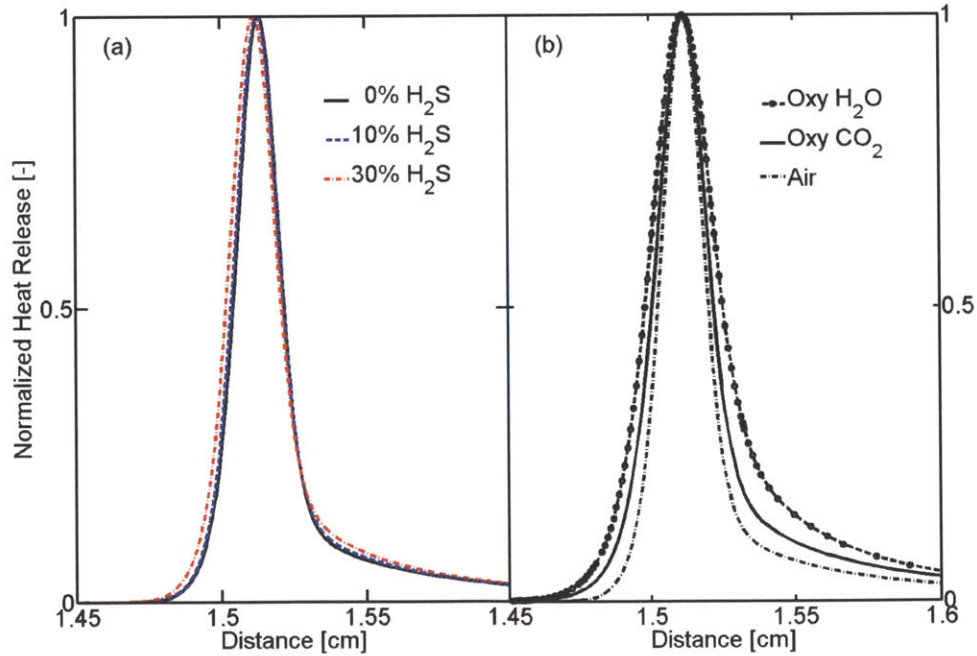


Figure 4-18: The normalized heat release rate shows the changes in flame thickness of pre-mixed sour gas flames at $p = 1$ atm. a) Air combustion at $\Phi = 0.87$ with varying H_2S mole fractions in the fuel. b) Combustion of pure CH_4 in air at $\Phi = 0.87$ and CO_2 and H_2O diluted oxygen at $\Phi = 1$ where diluent mole fractions are adjusted to give the same flame temperature.

For each combustion mode, the flame thickness changes only marginally when varying the H₂S mole fraction (see Figure 4-18a). Presumably, this is due to the opposing effects of the faster H₂S kinetics and the fact that the two fuels are not oxidized exactly simultaneously (cf. Figure 4-13).

For a constant H₂S mole fraction, the flame thickness is largest for H₂O dilution and smallest for air combustion (see Figure 4-18b). This can be explained by the slower kinetics of H₂O and CO₂ diluted oxy-combustion as compared to air combustion on the one hand and the higher diffusivity (e.g. of H radicals) in H₂O than in N₂ and CO₂ on the other hand (cf. Section 4.3).

4.5 Conclusion

Both the fuel composition (i.e. the H₂S mole fraction) and the combustion mode (i.e. air combustion vs. oxy-combustion with CO₂ or H₂O dilution) have a significant impact on the basic combustion properties of sour gas:

1. Increasing H₂S content in the fuel leads to a decrease in the adiabatic flame temperature due to its lower heating value. At the same time, the faster kinetics of H₂S oxidation as compared to CH₄ oxidation lead to a decrease in the ignition delay time. The laminar burning velocity (at constant flame temperature) decreases slightly when adding small amounts ($\mathcal{O}(1\%)$) of H₂S to CH₄ because the SO₂ formed catalyzes H radical removal. Larger mole fractions of H₂S ($\mathcal{O}(30\%)$) either lead to a small increase or a decrease in the burning velocity, depending on the conditions.
2. Mixed CH₄ and H₂S flames exhibit a two-zone structure similar to the one found in pure CH₄ flames. The oxidation of H₂S to SO₂ occurs in the same zone as the partial oxidation of CH₄ to CO. With increasing amounts of H₂S in the fuel, the H₂ peak which occurs close to the end of this zone gets higher and moves slightly upstream. In a second zone, CO is converted to CO₂ and simultaneously some SO₂ is further oxidized to SO₃. The amount of SO₃ formed in the flame is on the order of 1 – 10 ppm and the equilibrium value is reached on the same time scale as the CO burnout.

3. The ignition delay time changes slightly between the combustion modes, depending on whether the same diluent mole fraction is used or the same flame temperature. For a given flame temperature, the laminar burning velocity at atmospheric conditions is highest for (lean) air combustion and smallest for CO_2 diluted oxy-combustion. At elevated pressures ($\gtrsim 10$ atm), H_2O diluted oxy-combustion gives the highest burning velocity while air combustion approaches the values for CO_2 dilution. The only significant changes in the flame structure are an increase in the CO concentrations for CO_2 dilution and an increased H_2 mole fraction for H_2O dilution.

We thus draw the following conclusions for the design of combustors handling sour gas:

1. Static flame stability (i.e. blowoff prevention) should tend to improve slightly when adding H_2S to the fuel. Resulting changes in either the flame temperature or the burning velocity can be compensated by relatively minor adjustments to the diluent mole fraction (for oxy-combustion) or the equivalence ratio (for air combustion). It thus appears feasible to handle fuels of varying composition in a given combustor.
2. The oxidation of H_2S can be expected to always go to completion (i.e. no significant amounts of H_2S or intermediate species are expected in the post-flame zone). The formation of SO_3 in the post-flame zone can be quenched only at the expense of quenching CO oxidation too.
3. Oxy-fuel combustion with H_2O dilution seems to be the most promising of the three combustion modes considered here for achieving static stability (highest burning velocity at relevant pressures) and low CO concentrations.

Chapter 5

Kinetic Modeling of a Sour Gas Power Cycle

So far, no studies have been reported on the formation and destruction of undesired species (mainly CO, O₂, and SO₃) in sour gas combustion in an oxy-fuel power cycle with EOR. The only work on a related topic that we are aware of are analyses of oxy-fuel combustion of pure CH₄ using CO₂ and H₂O dilution. Richards et al. [24] showed that CO₂ dilution leads to higher equilibrium CO concentrations and requires longer residence times to reach equilibrium than H₂O dilution, although they state that the values were not unreasonably high for either diluent. They also report good combustion efficiency in a 1 MW H₂O diluted combustor operating with low levels of excess O₂. In a previous study [26, 27], they had modeled the reheat combustor for the CES power cycle [25] using a simple reactor network model and again found CO₂ to lead to higher CO concentrations than H₂O, although both achieved acceptable levels in reasonable residence times. However, since this work was not explicitly focused on EOR, it does not consider O₂ concentrations in the products and considers different performance measures (see Section 5.1.2).

It is thus still unclear which combustion mode (i.e. air combustion vs. CO₂ or H₂O diluted oxy-combustion) is best suited to handle a fuel containing large amounts of H₂S, whether the integration of a sour gas oxy-combustion cycle with EOR is feasible with or without expensive gas cleanup processes, or how a combustor for handling sour gas should be designed.

In this chapter, we aim at closing this gap by conducting chemical kinetics calculations with the detailed reaction mechanism presented in Chapter 3. First, we describe the de-

velopment of a reactor network model that is representative for the relevant part of a gas turbine power cycle for EOR, from the combustor to the CO₂ extraction point. Next, we investigate the behavior and design possibilities for the flame zone of the combustor. Finally, the dilution of the hot gases between the flame zone and the turbine inlet and the subsequent cooling through expansion in the gas turbine is investigated for a given flame zone design to give a complete picture all the way to the CO₂ extraction point. The effect of running the entire process slightly fuel-rich or fuel-lean is also discussed briefly.

As in the previous chapters, the H₂S mole fraction in the fuel is varied between 0% and 30% to cover the range of common sour gas compositions. Unless otherwise noted, the equivalence ratio is fixed at $\Phi = 1$ for the oxy-fuel cases. All calculations were conducted using CHEMKIN-PRO [105].

5.1 Model Development

In order to gain some insight into the emission behavior of sour gas combustion under different conditions and to compare the different combustion modes, we developed a model of a generic power cycle for both CO₂ and H₂O diluted oxy-fuel combustion for EOR. An open version of the cycle using air combustion was also included for comparison. For all three combustion modes, we used the same fixed boundary conditions and the same model setup.

5.1.1 Power Cycle and Boundary Conditions

The three versions of the generic gas turbine power cycle that we chose for our analysis are similar to the oxy-fuel combined cycle analyzed by Kvamsdal et al. [55] and Sanz et al. [134] (see Figure 5-1). Air or a diluent (either CO₂ or H₂O) are compressed to the combustor pressure of $p_{\text{comb}} = 40$ atm. In the combustor, the sour gas and in the oxy-fuel cases also O₂ is added to raise temperature to the turbine inlet temperature of $T_{\text{ti}} = 1500$ K. The gas is then expanded in a gas turbine down to $p_{\text{end}} = 1$ atm and $T_{\text{out}} = 750$ K and further cooled in a heat recovery steam generator (HRSG) which is powering a steam turbine. In the oxy-fuel

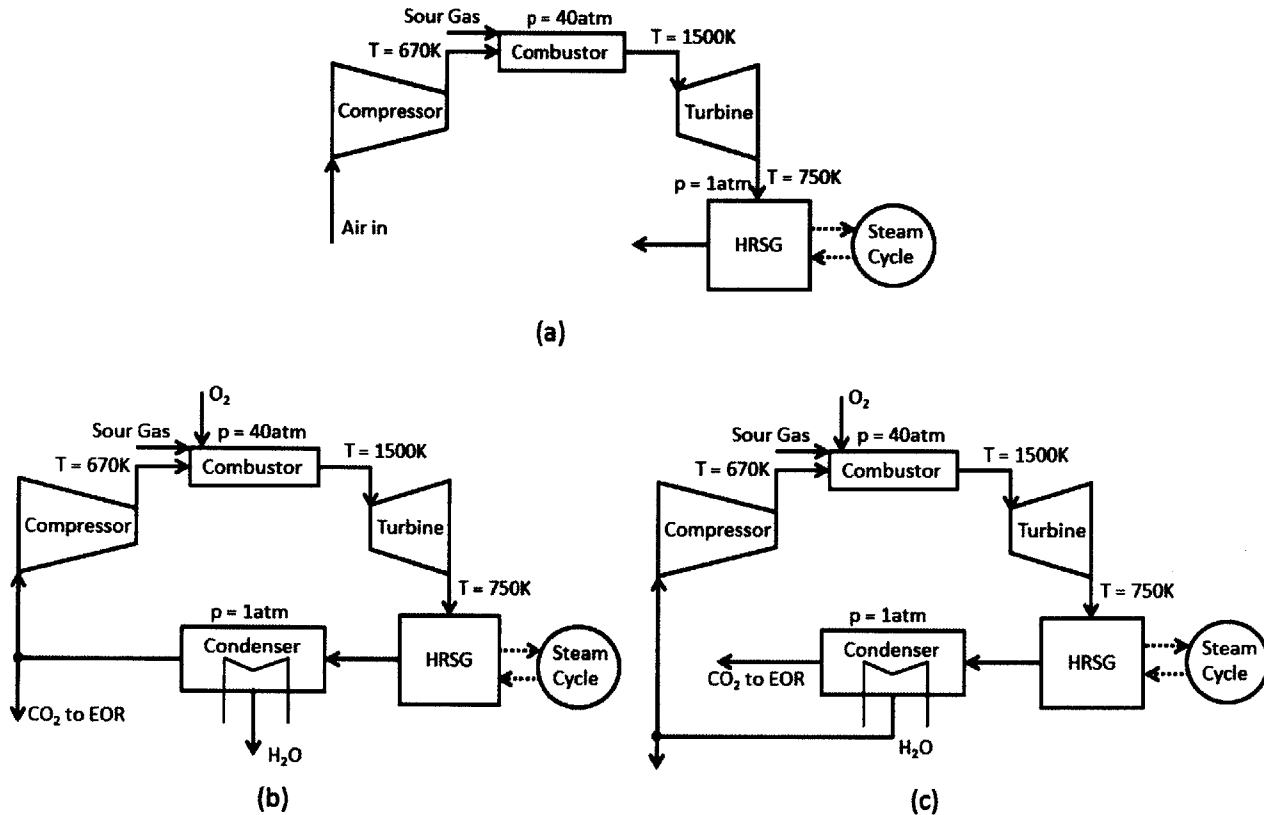


Figure 5-1: The generic gas turbine cycles used for the analysis based on the oxy-fuel combined cycle in [55, 134]. (a) Air combustion. (b) Oxy-fuel combustion with CO_2 dilution. (c) Oxy-fuel combustion with H_2O dilution.

cases, the flue gas then enters a condenser where all the H_2O in the gas is condensed out leaving a stream of CO_2 with other non-condensable species that is to be used in EOR. Part of either the H_2O or the CO_2 is recycled to the combustor.

As commonly encountered in gas turbines, the combustor is assumed to consist of two main zones [131, 135] (see Figure 5-2). In the flame zone, the fuel is burned with a level of diluent or air addition adjusted to guarantee stable combustion and quick burnout. In the dilution zone, the remaining diluent or air is added to lower the gas temperature to the turbine inlet temperature of $T_{ti} = 1500 \text{ K}$.

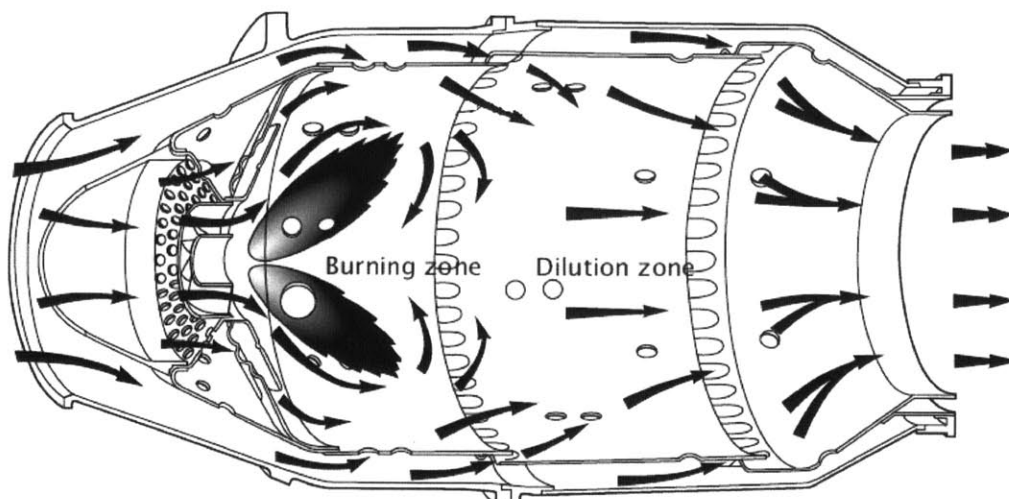


Figure 5-2: A typical can-type gas turbine combustor consisting of a flame zone (labeled 'Burning zone') and a dilution zone. Adopted from [131], modified.

5.1.2 Performance Measures

Based on the literature review presented in Section 2.1, we can identify three main performance measures with respect to the combustion products for a sour gas oxy-fuel power cycle with EOR.

First, both CO and O₂ at the combustor outlet should be low for good combustion efficiency. Excessive CO signifies a waste of fuel and excess O₂ a waste of energy for air separation. The cryogenic air separation processes that are the industry standard consume on the order of 0.2 kWh/kg O₂, mostly in the form of compression work [136]. Assuming a thermal efficiency for the generation of this work of 33%, this corresponds to an energy penalty of about 70 kJ/mol O₂ in the exhaust gas. Comparing this to the heating value of CO of roughly 280 kJ/mol, we can see that CO is about four times more important for the combustion efficiency than O₂.

Second, the concentrations of CO and O₂ in the CO₂ stream to be used in EOR are also restricted (cf. Section 2.1.1). The concentrations in the EOR stream differ considerably from the ones in the exhaust gas because the water is condensed out (cf. Figure 5-1), which, depending on the conditions, can lead to a significant change in the total molar flow rate. They

thus correspond to the concentrations in the *dry* products. Carbon monoxide is restricted because it increases the so called Minimum Miscibility Pressure (MMP) required for injecting the products into the oil well, and because of safety concerns for pipeline transportation of the products. Oxygen also increases the MMP, but more importantly can also cause local overheating and increased viscosity in the oil well due to oxidation and enhance bacterial growth [14]. For our analysis, we refer to the requirements specified for the Weyburn EOR project [13, 14], which imposes a limit on the CO and O₂ concentrations of 1000 ppm and 50 ppm, respectively. However, it should be kept in mind that the limits on these species vary between different EOR projects and there is no uniform industry standard yet.

Third, the concentration of SO₃ has to be kept as low as possible in the entire cycle because of the role of SO₃ in low temperature hot corrosion and cold end corrosion (cf. Section 2.1.3). The former commonly occurs in gas turbines at temperatures of 925 – 1075 K [49] and hence depends on the SO₃ mole fraction from the combustor outlet to the turbine outlet. For the latter, the concentrations of both SO₃ and H₂O at the cold end of the cycle are most important because sulfuric acid only starts to condense and cause damage at around $T \lesssim 500$ K. There is no specific threshold of SO₃ below which sulfuric acid corrosion does not occur, and severe corrosion problems have been experienced with concentrations as low as 20 ppm [37]. However, the lower the SO₃ mole fraction, the lower is the sulfuric acid dew point, meaning that the gas can be cooled down further to extract more energy before the acid starts to condense. Since in an oxy-fuel cycle the working fluid has to condense at some point, this determines from which point in the cycle expensive acid resistant materials have to be used or where a flue gas desulfurization unit should be installed. This has important implications for both the efficiency and the economics of the cycle [137].

Nitrogen oxides (NO_x) are not considered because they are not particularly problematic in oxy-fuel combustion of gaseous fuels thanks to the very low concentrations of N₂ in the oxidizer (at most a few percent due to imperfect air separation). Unlike for coal power plants that operate at atmospheric pressure, N₂ from air ingress is not a problem in gas turbine combustors. Indeed, previous studies have found NO_x formation to be negligible in oxy-fuel combustion with realistic O₂ purities [18, 24, 26].

5.1.3 Reactor Network Model

The parts of the cycle that are strongly influenced by chemistry are the combustor and possibly the turbine. Since the kinetics of both CO oxidation and SO₃ formation essentially freeze at temperatures below $T = 1000$ K [28, 34], we do not expect further reactions to occur in the HRSG and the condenser. To model the chemistry in the relevant part of the cycle, we set up the reactor network model that is shown in Figure 5-3.

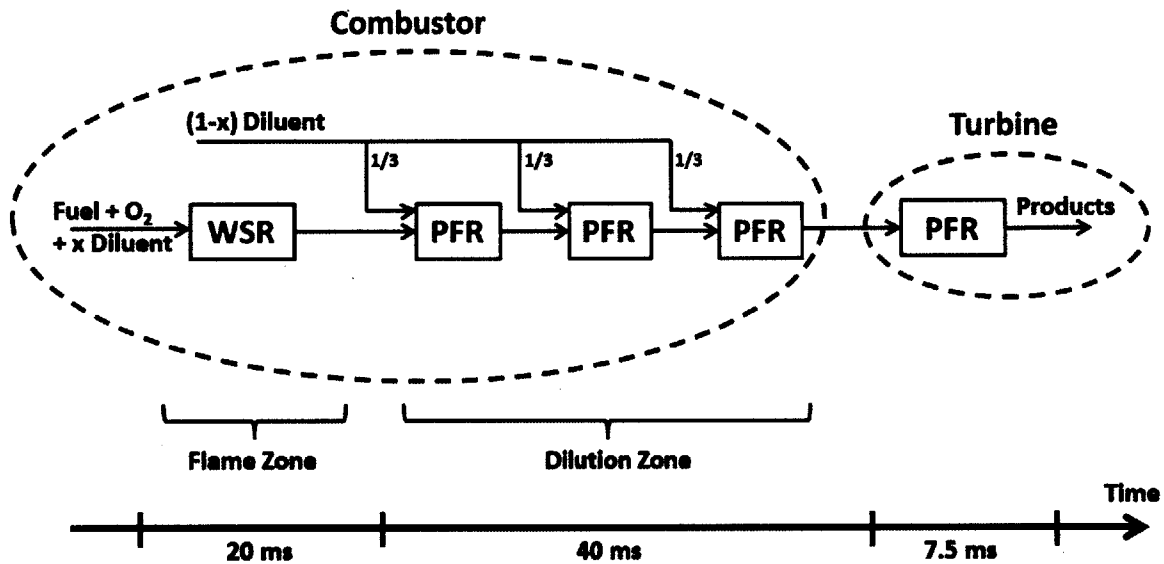


Figure 5-3: The reactor network model used in this chapter. The diluent stream added in the dilution stream is split equally between the three PFRs of equal residence time. For all reactors in the combustor the energy equation is solved without heat losses. For the PFR representing the cooling in the turbine and heat exchangers, a linear temperature and pressure profile is prescribed.

The fuel, oxidizer, and possibly diluent enter the flame zone perfectly mixed at a temperature of $T_{in} = 670$ K and a pressure of $p = 40$ atm. For the oxy-fuel cases, the oxygen purity is taken to be 100% for simplicity. Heat losses to the environment or to the dilution streams are not considered, since they are usually small [138]. The choice of the residence times will be discussed in the following sections.

The flame zone of the combustor is represented by a single well-stirred reactor (WSR) to model the recirculation zone with intense mixing that occurs behind the swirler (cf. Figure 5-2). The approach of using a single WSR for the flame zone followed by one or more plug flow

reactors (PFR) is based on the work by Bragg [139] and Beér and Lee [9] and is widely used for modeling combustion in different systems. Many variations and refinements of this model have been proposed. One of the most common of these extensions is the introduction of a reactor accounting for macroscopic flow recycling through the inner or outer recirculation zones found in many swirl-stabilized combustors [140]. The introduction of such a reactor has advantages for predicting blowout phenomena [141–144], and NO_x formation in pulverized coal combustion [10, 145, 146]. However, simple models without a recycling reactor have been shown to give good results for predicting both CO and NO_x emissions from the combustion of gaseous fuels in gas turbine combustors [147–153]. Since the focus of the present study is on giving general trends for CO, O₂, and SO₃ concentrations and we are not aiming at predicting NO_x formation or blowout accurately, the choice of this simplistic models seems justified.

The dilution zone of the combustor is modeled by three PFRs of equal residence time in series. The additional diluent or air is added to these three reactor in equal parts. The importance of modeling the dilution zone for predicting CO concentrations from realistic gas turbine combustors is well established [138, 142, 147, 154]. Three PFRs with addition of diluent at the beginning of each reactor have been found to be the most effective way of modeling this zone [155]. The added streams account for both dedicated dilution jets and entrainment of cooling air from the combustor walls.

After the combustor, the flue gas is quenched rapidly during the expansion in the turbine. This is modeled by a plug flow reactor in which the temperature and pressure is decreased linearly with time. The following calculation was used to roughly estimate the cooling rate in the gas turbine: Typically, in the turbine the temperature of the gas drops by about $\Delta T = 750$ K from $T_{\text{ti}} = 1500$ K to around $T_{\text{out}} = 750$ K. The average residence time of the gas in the turbine can be estimated by dividing the approximate turbine length, which is on the order of $L = 1.5$ m, by the axial velocity. The axial velocity is typically roughly constant along the flow path and corresponds to a Mach number of 0.3 at the turbine outlet:

$$v_{\text{ax}} \approx 0.3 \cdot c_{\text{out}} = 0.3 \cdot \sqrt{\gamma RT_{\text{out}}} \approx 165 \text{ m/s}, \quad (5.1)$$

where c_{out} is the speed of sound at the outlet, $\gamma \approx 1.4$ is the heat capacity ratio, and $R \approx 287 \text{ J/kgK}$ is the gas constant. This leads to an estimate for the cooling rate on the order of

$$\frac{\Delta T}{\tau_{\text{res}}} \approx 82,500 \text{ K/s.} \quad (5.2)$$

For simplicity, we assume cooling at a constant rate of $100,000 \text{ K/s}$ down to $T_{\text{out}} = 750 \text{ K}$.

From a design point of view, the parameters that can be varied are the fraction x of the diluent or combustion air that is added to the flame zone to control the flame temperature (cf. Figure 5-3), the residence time of the flame zone WSR, and the residence time in the dilution zone. The total amount of diluent added or the overall equivalence ratio (for air combustion) is constrained by the requirement to meet a fixed turbine inlet temperature. In order to avoid excessively large combustor designs, the sum of the residence times in the flame zone and the dilution zone should be on the order of 50 ms , which is similar to current gas turbine combustors.

5.2 Flame Zone Design

As mentioned previously, the purpose of the flame zone is to stabilize a flame and provide the necessary conditions to allow for fast burnout of the fuel [135]. Also, if the concentrations of the undesired species CO and O_2 in this zone get too large, poor mixing could result in high emissions because of insufficient burnout in the dilution zone. There are two design parameters for achieving these goals, namely the flame temperature and the residence time of the WSR.

Increasing the flame temperature by adding less diluent or air to the flame zone leads to a higher burning velocity, which means easier flame stabilization [8]. Typical flame temperatures in gas turbines range from 1700 K for lean premixed systems to 2200 K in diffusion burners [131]. Since there is no established strategy for oxy-fuel combustion yet [154], we consider this complete range of flame temperatures. To get an unbiased comparison, we have to keep in mind that depending on the flame temperature different amounts of diluent have to be added in the dilution zone to achieve the specified turbine inlet temperature, which

lowers the concentrations of all other species. We therefore have to correct the concentrations in the flame zone via

$$X_{i,\text{diluted}} = X_i \cdot \frac{1}{1 + \dot{n}_{\text{dilution}}/\dot{n}_{\text{flame}}}, \quad (5.3)$$

where X_i denotes the concentrations at the end of the flame zone, $X_{i,\text{diluted}}$ the concentrations after addition of the diluent, and $\dot{n}_{\text{dilution}}/\dot{n}_{\text{flame}}$ the ratio of the molar flow rates of the added diluent and in the flame zone.

5.2.1 Equilibrium Trends

For evaluating the emissions of the species of interest (CO, O₂, and SO₃), we first calculate the concentrations at thermodynamic equilibrium. This corresponds to the case where the combustor is designed so that the residence time in the flame zone is sufficient for CO burnout and SO₃ formation to go to completion. Although it is unlikely that this will be achieved in an actual combustor (except maybe at very high flame temperatures), this analysis does provide some insight into the underlying trends.

At chemical equilibrium, CO₂ dilution leads to CO concentrations that are one order of magnitude larger than for H₂O dilution and O₂ concentrations that are about twice as large (see Figures 5-4 and 5-5). The concentrations of both species increase with temperature because of increased dissociation of CO₂. Fuel-lean air combustion is shown for comparison and leads to much lower CO and much higher O₂ concentrations due to the large amount of excess O₂ available at the low equivalence ratios required for achieving these temperatures.

For SO₃, the H₂S content in the fuel has the strongest influence on the results (see Figure 5-6). For both H₂O and CO₂ diluted oxy-combustion, the SO₃ concentration after addition of the diluent shows almost no dependence on the temperature. Water dilution leads to slightly lower values than H₂O dilution. Lean air combustion, which is again shown for comparison, leads to SO₃ concentrations that can be more than an order of magnitude higher and decrease with increasing flame temperature. The behavior of the SO₃ concentration at equilibrium is caused by the combined effect of temperature and O₂ concentration, with lower temperatures and higher O₂ content leading to higher SO₃ concentrations [29].

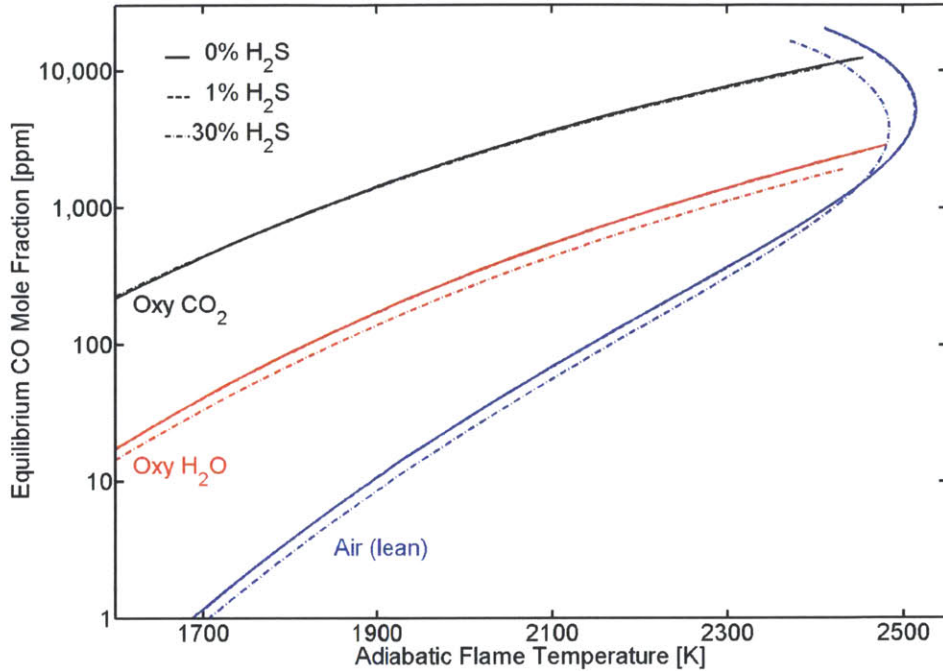


Figure 5-4: The equilibrium concentration of CO at the end of the flame zone is much larger for CO₂ dilution than for H₂O dilution and increases with the flame zone temperature. Equilibrium at constant pressure and enthalpy for $T_{in} = 670$ K and $p = 40$ atm.

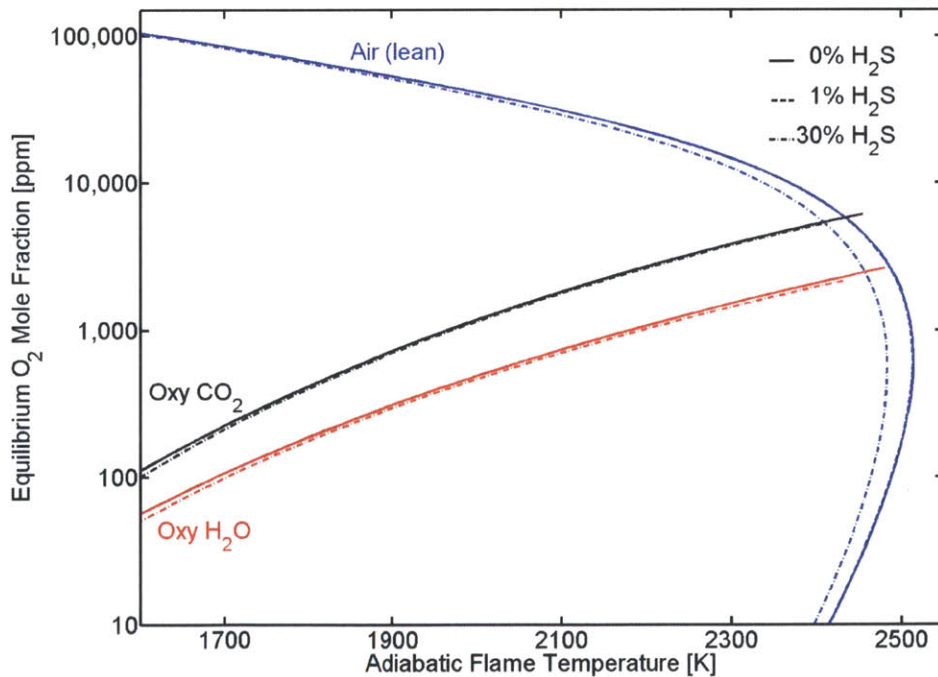


Figure 5-5: The equilibrium concentration of O₂ at the end of the flame zone is larger for CO₂ dilution than for H₂O dilution and increases with the flame zone temperature. Equilibrium at constant pressure and enthalpy for $T_{in} = 670$ K and $p = 40$ atm.

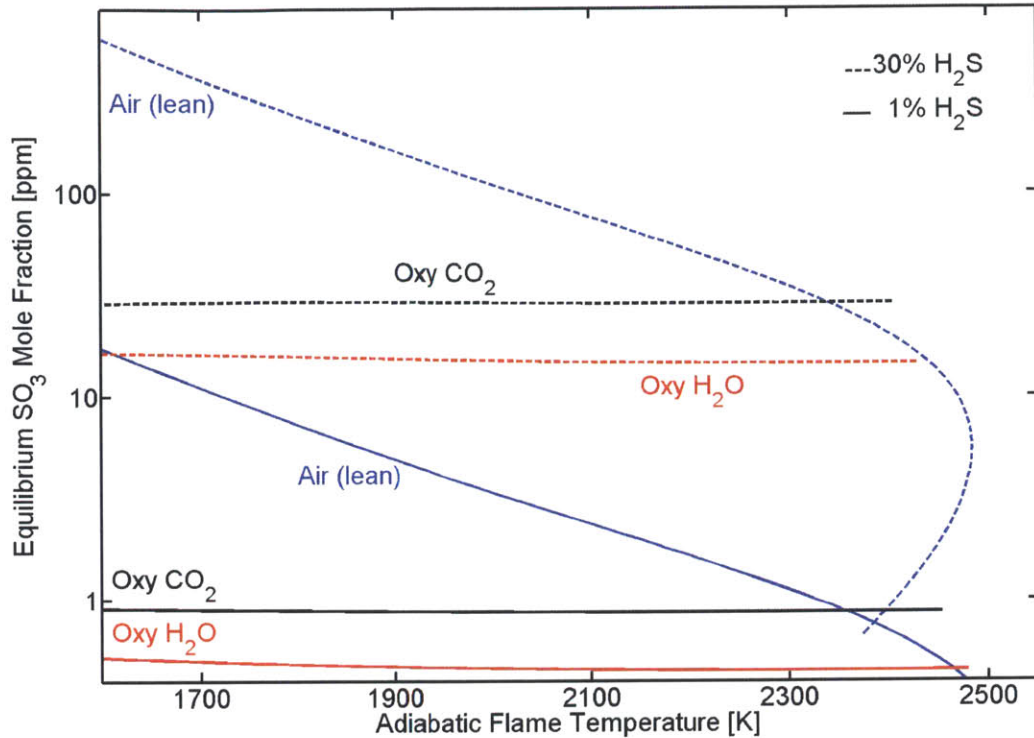


Figure 5-6: The flame zone equilibrium concentration of SO_3 corrected for dilution to the turbine inlet temperature is somewhat larger for CO_2 dilution than for H_2O dilution and is almost independent of the flame temperature. Air combustion leads to much higher concentrations.

5.2.2 Chemical Time Scales

Since both CO oxidation and SO_3 formation are usually limited by chemical kinetics and equilibrium will likely not be achieved in the flame zone, we investigated the effect of varying the residence times of the flame zone WSR. The residence time in the WSR ($\tau_{\text{res,WSR}}$) represents the size of the recirculation zone in a typical swirl stabilized combustor [140]. If it is too small, blowout may occur because the reactants do not have enough time to get mixed with hot products and ignite. At the same time, the residence time should not be too large in order to allow for sufficient residence time in the rest of the combustor, namely the dilution zone.

Higher residence times lead to lower CO and O_2 concentrations in the WSR because there is more time for CO burnout (see Figures 5-7a and 5-8a). For a fixed residence time, there is always an intermediate temperature (around 1900 K) for which the CO and

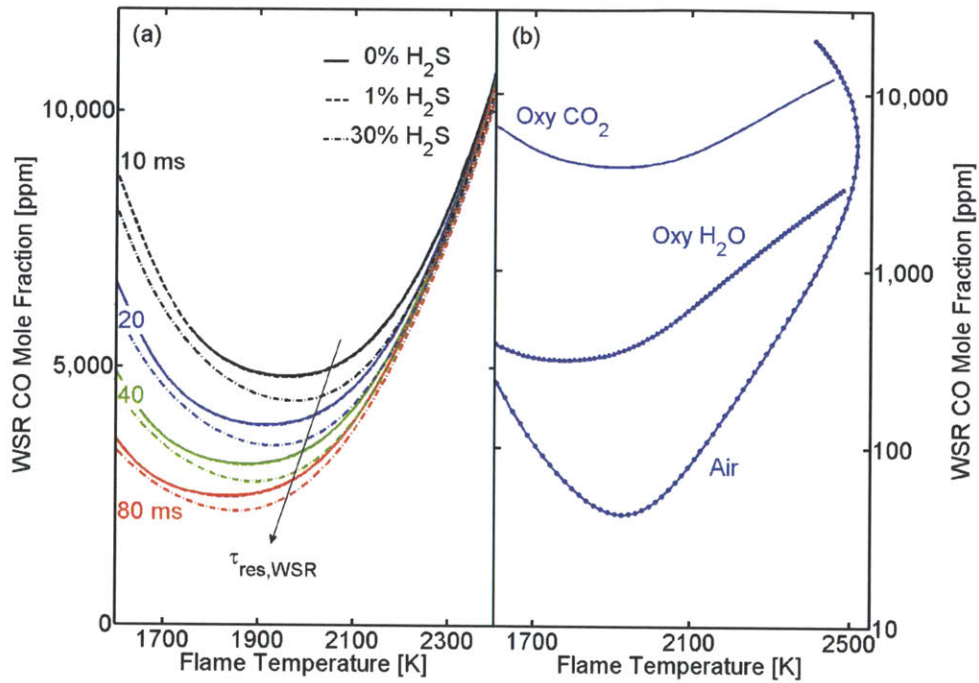


Figure 5-7: The CO concentration in the flame zone as a function of flame temperature: (a) CO₂ diluted oxy-combustion at different residence times and H₂S contents in the fuel. (b) Different combustion modes at $\tau_{res,WSR} = 20$ ms and 0% H₂S in the fuel.

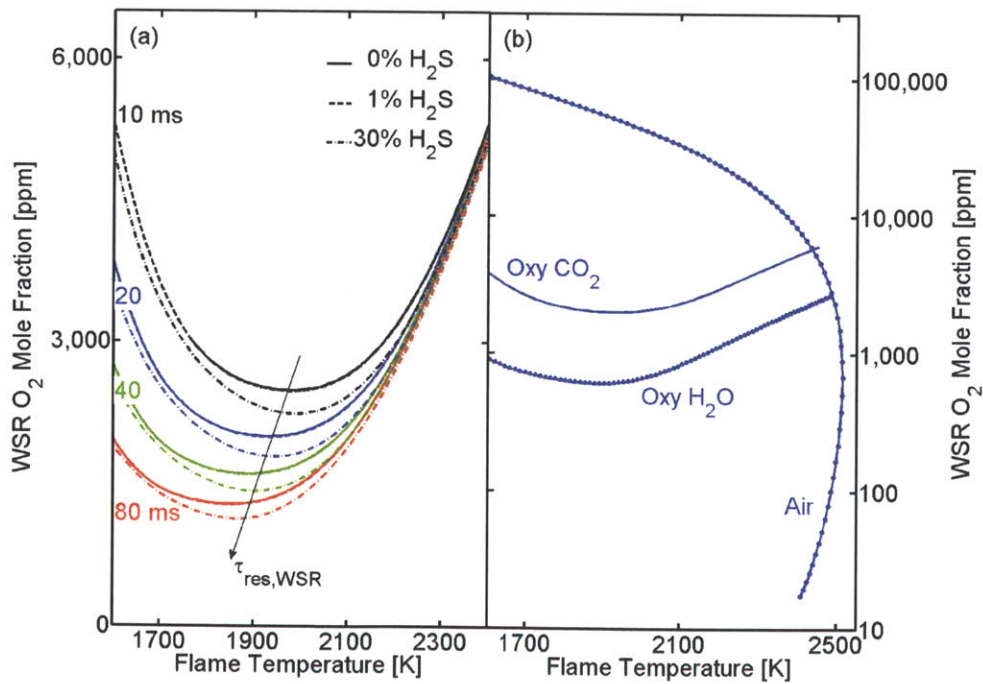


Figure 5-8: The O₂ concentration in the flame zone as a function of flame temperature: (a) CO₂ diluted oxy-combustion at different residence times and H₂S contents in the fuel. (b) Different combustion modes at $\tau_{res,WSR} = 20$ ms and 0% H₂S in the fuel.

O₂ concentrations are minimal. At high temperatures, the concentrations increase because of the increasing equilibrium values, while at low temperatures they increase because the kinetics get slower and do not allow sufficient burnout within the residence time.

Increasing H₂S content in the fuel leads to lower CO and O₂ concentrations, corresponding to the lower carbon content in the fuel and the lower amount of O₂ needed for oxidation (cf. Reaction (4.9)).

Carbon dioxide dilution leads to CO concentrations that are an order of magnitude higher than for H₂O dilution and O₂ concentrations that are about twice as high (see Figures 5-7b and 5-8b). Fuel-lean air combustion, which is shown for comparison, leads to much lower CO and much higher O₂ concentrations for a given flame temperature due to the availability of excess O₂. The increased CO concentrations for CO₂ dilution have been reported in the previous studies on oxy-fuel combustion of CH₄ [21, 24, 26, 27] and are consistent with the findings for CH₄ oxy-fuel diffusion flames [133]. They can be explained by increased dissociation of CO₂ and slower kinetics of CO burnout.

For oxy-combustion at high temperature, the SO₃ mole fraction in the WSR is independent of the residence time and flame temperature, corresponding to the equilibrium trend (see Figure 5-9a). At low temperature, the kinetics get too slow and less SO₃ is formed. Carbon dioxide dilution leads to higher SO₃ concentrations corresponding to the higher O₂ values. Fuel-lean air combustion, which is again shown for comparison, leads to SO₃ concentrations that can be more than an order of magnitude higher and decrease with increasing flame temperature.

5.3 Dilution Zone Design

To investigate the influence of the cooling rate in the dilution zone, we fixed the residence times in the flame zone WSR at $\tau_{\text{res,WSR}} = 20$ ms similar to [26, 27] to balance the requirements of low CO and O₂ and blowout safety on the one hand and allowing enough time for the dilution zone on the other hand. We considered flame temperatures in the WSR of 1700 K, 1900 K, 2100 K, and 2300 K.

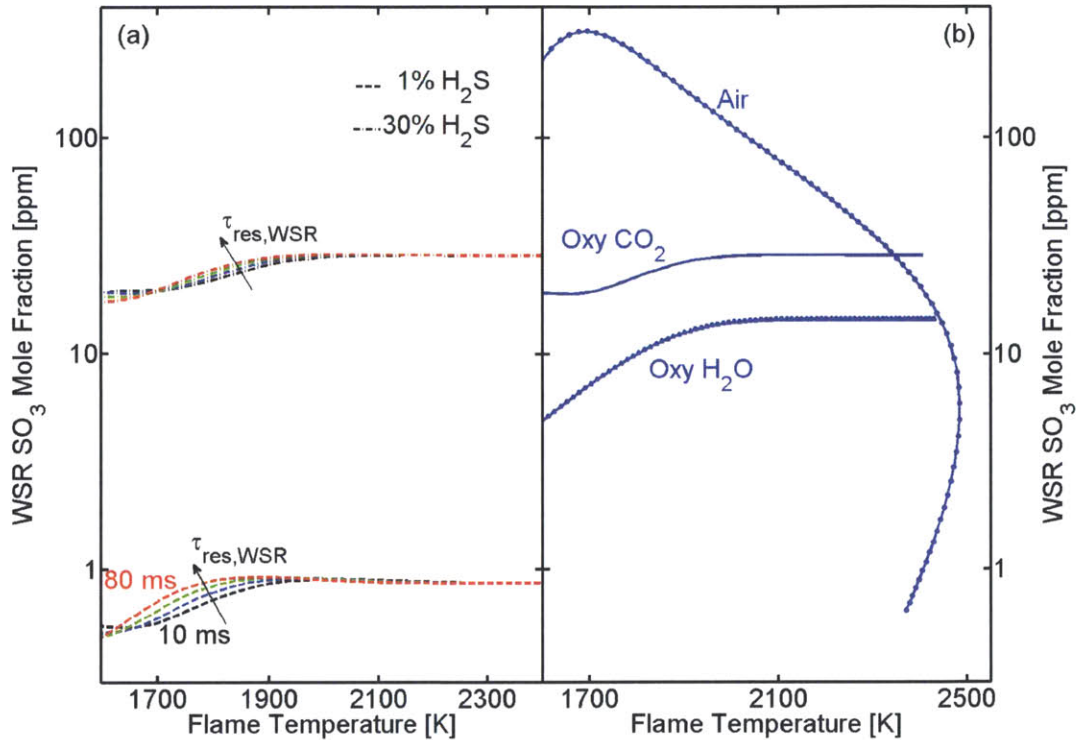


Figure 5-9: The SO₃ concentration in the flame zone as a function of flame temperature: (a) CO₂ diluted oxy-combustion at different residence times and H₂S contents in the fuel. (b) Different combustion modes at $\tau_{res,WSR} = 20$ ms and 0% H₂S in the fuel.

5.3.1 Dilution Cooling Rate

The cooling rate in the dilution zone is varied by changing the residence time in this zone ($\tau_{res,dil}$), which is equally distributed between the three PFRs (cf. Figure 5-3). The cooling rate in the turbine is not expected to be a design variable and remains fixed at 100,000 K/s.

Increasing the residence time in the dilution zone (i.e. slower cooling) generally leads to lower CO and O₂ concentrations since more time for CO oxidation is available (see Figures 5-10a and 5-11a). This effect is most pronounced for lower flame temperatures. The higher the flame temperature, the faster equilibrium is achieved in the first PFR of the dilution zone. After this point, increasing the residence time further does not lead to more CO burnout in this reactor.

Because of the faster kinetics, H₂O dilution compares even more favorably to CO₂ than it does for the flame zone WSR, indicating a better combustion efficiency (see Figures 5-10b

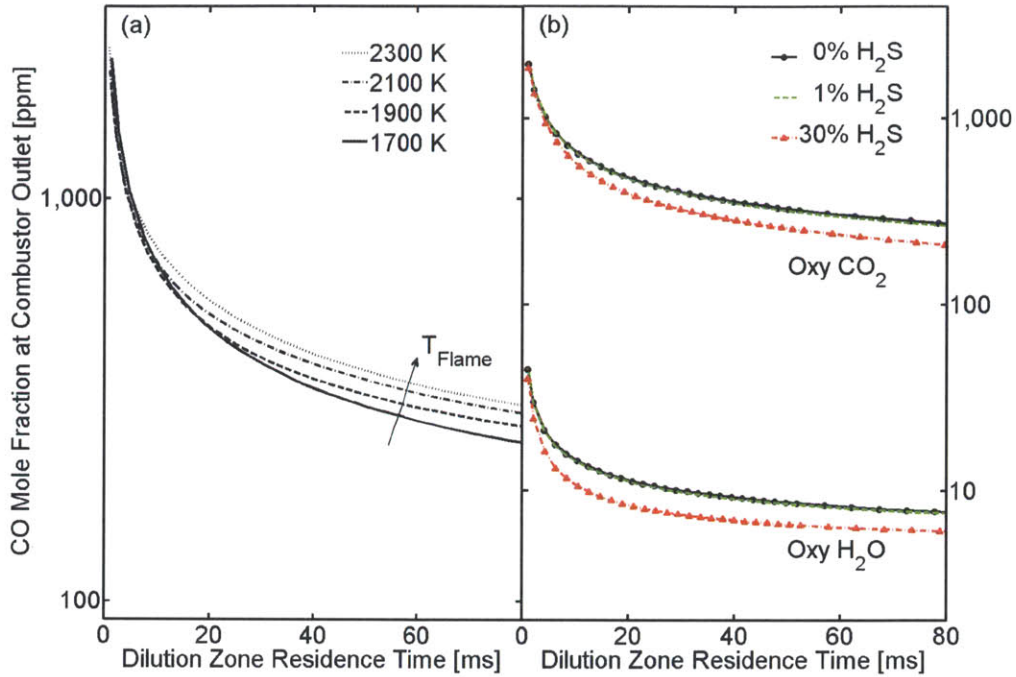


Figure 5-10: The CO concentration at the combustor outlet as a function of the residence time in the dilution zone: (a) CO₂ diluted oxy-combustion of CH₄ at different flame temperatures. (b) Different combustion modes and H₂S contents in the fuel at $T_{\text{Flame}} = 1900$ K.

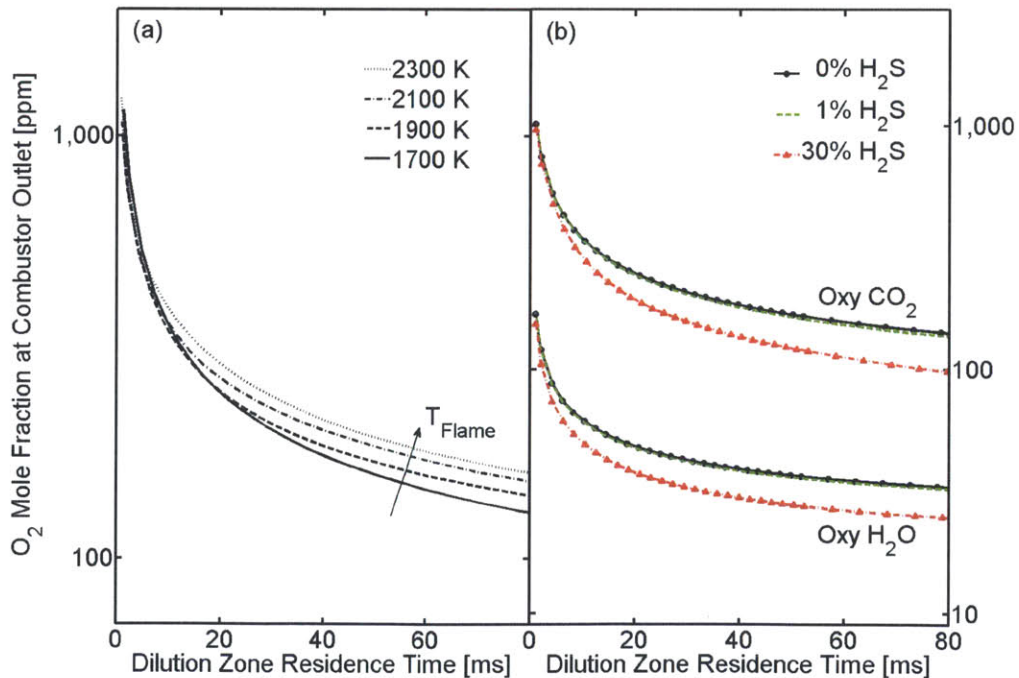


Figure 5-11: The O₂ concentration at the combustor outlet as a function of the residence time in the dilution zone: (a) CO₂ diluted oxy-combustion of CH₄ at different flame temperatures. (b) Different combustion modes and H₂S contents in the fuel at $T_{\text{Flame}} = 1900$ K.

and 5-11b). Increasing H_2S content in the fuel again leads to lower CO and O_2 values.

However, as mentioned in Section 5.1.2, CO and O_2 are not only measures for the combustion efficiency but their concentrations are also restricted for EOR. In the CO_2 stream for EOR (i.e. in the dry products), the comparison between H_2O and CO_2 dilution gives a different result than for the combustion efficiency. For H_2O dilution, about 90% of the exhaust gas is steam so that the condensation process leads to a strong enrichment of CO and O_2 in the gas phase. Therefore, in the EOR stream the CO concentrations are only two to four times lower for H_2O dilution than for CO_2 dilution, while the O_2 concentrations are *higher* (see Figure 5-12). Comparison with the limits specified for the Weyburn EOR [13, 14] (dashed lines) shows that the CO concentrations are within the allowable range for both diluents (for residence times in the dilution zone of more than 5 ms), while the O_2 concentrations exceed the allowable values in either case.

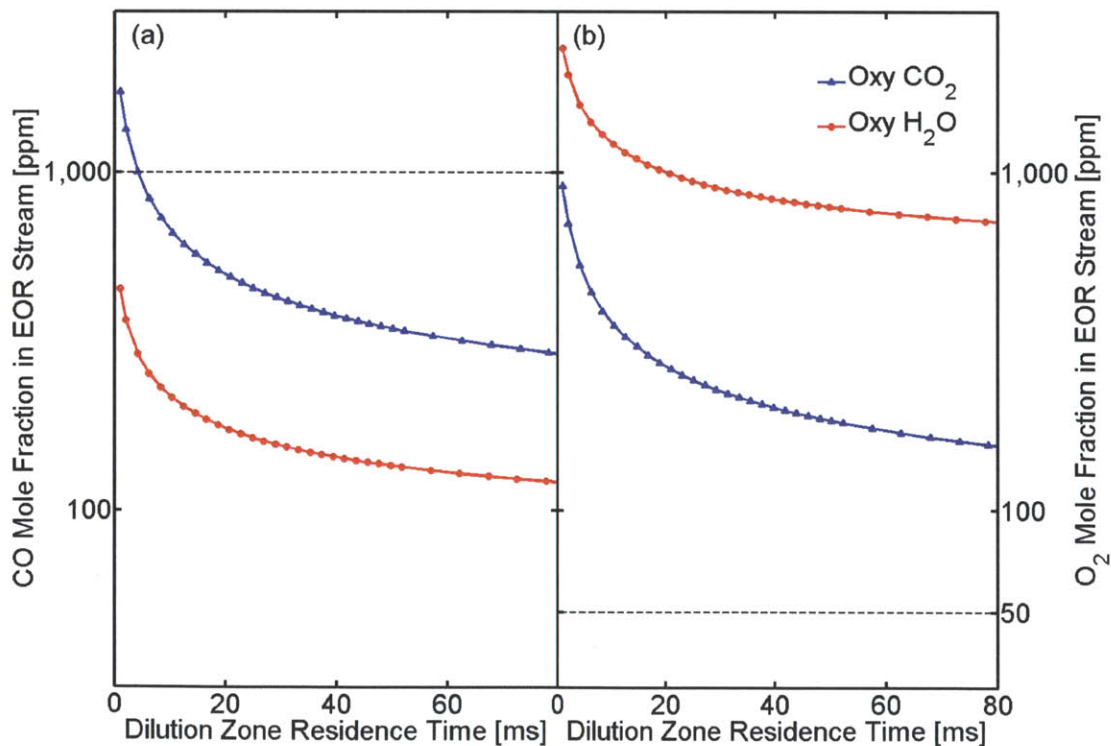


Figure 5-12: The concentrations in the CO_2 stream for use in EOR for oxy-fuel combustion of pure CH_4 at $T_{\text{Flame}} = 1900$ K. (a) CO mole fraction, (b) O_2 mole fraction. The horizontal dashed lines represents the limits specified for the Weyburn EOR [13, 14]

The concentration of SO_3 at the combustor outlet is up to two orders of magnitude higher for air combustion than for oxy-fuel combustion (see Figure 5-13). Carbon dioxide dilution produces about 50% more SO_3 than H_2O dilution, corresponding to the higher O_2 concentrations which favor SO_3 formation [34]. The dependence on the flame temperature and the dilution time is more complex and not as strong as for CO or O_2 .

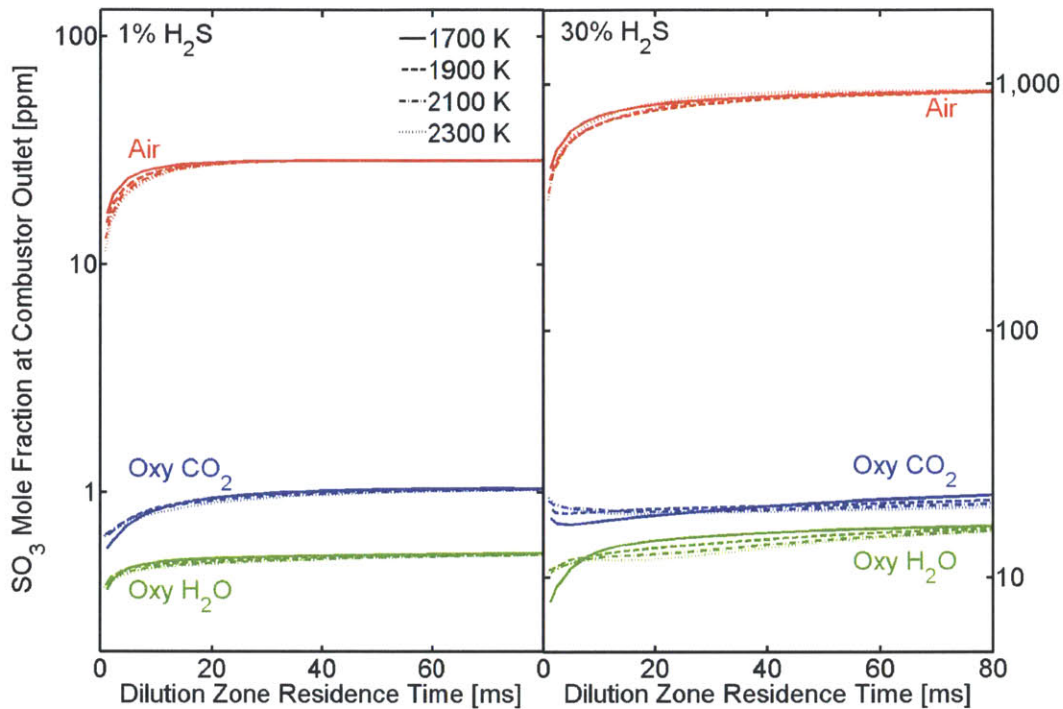


Figure 5-13: The SO_3 concentration at the combustor outlet as a function of the residence time in the dilution zone for different flame temperatures for 1% and 30% H_2S in the fuel.

While the SO_3 concentration at the combustor outlet is important for hot corrosion in the gas turbine, sulfuric acid corrosion is determined by the SO_3 and H_2O concentrations after the turbine. For oxy-fuel combustion, we observe that the SO_3 concentration *decreases* during the expansion of the gas in the turbine (see Figure 5-14). For air combustion, the concentration *increases* during the expansion, which is similar to what is commonly encountered in power plants and oil boilers, where most of the SO_3 is formed during the cooling of the flue gas [29, 37].

In fact, if we compare the SO_3 profiles along the flow path of the gas for air combustion and oxy-fuel combustion, we observe that the behavior differs widely between the two

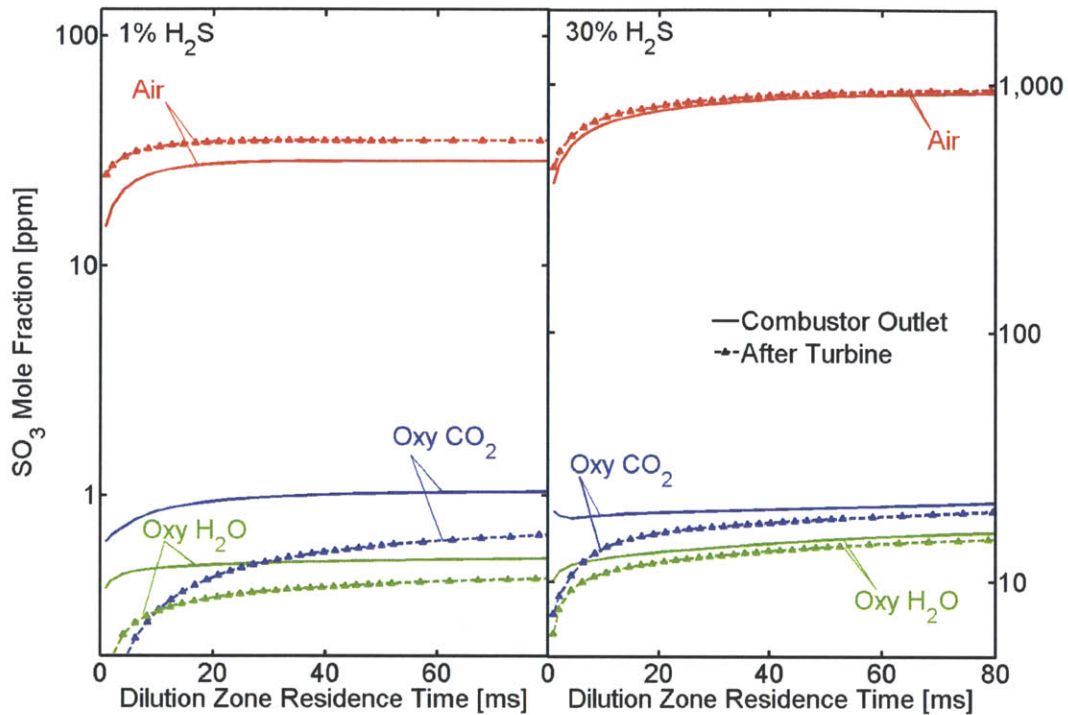


Figure 5-14: The SO_3 concentration at the combustor outlet and after the turbine as a function of the residence time in the dilution zone for $T_{\text{Flame}} = 1900 \text{ K}$ and 1% and 30% H_2S in the fuel.

combustion modes. For air combustion, more SO_3 is formed in each zone as the temperature drops and more O_2 is added (see Figure 5-15). For CO_2 diluted oxy-combustion, the behavior is more complex and SO_3 is either produced or consumed in the different reactors representing the dilution zone and the turbine (see Figure 5-16). Together with the increasing dilution of the mixture, this leads to a significant decrease in the SO_3 mole fraction from the flame zone (even here the values are already much lower than for air) to the end of the turbine.

This clearly shows the advantage of handling sulfur containing gaseous fuels in an oxy-fuel process rather than through air combustion. This is opposite to what is generally reported for oxy-fuel combustion of coal, where SO_3 concentrations are expected to be *higher* than in air combustion [15, 29, 35]. The main difference is that coal power plants cannot operate as close to stoichiometric conditions as gas fired plants because of the heterogeneous reactions that generally require a few percent of excess O_2 [6]. Also, Fleig et al. [29] attribute most of

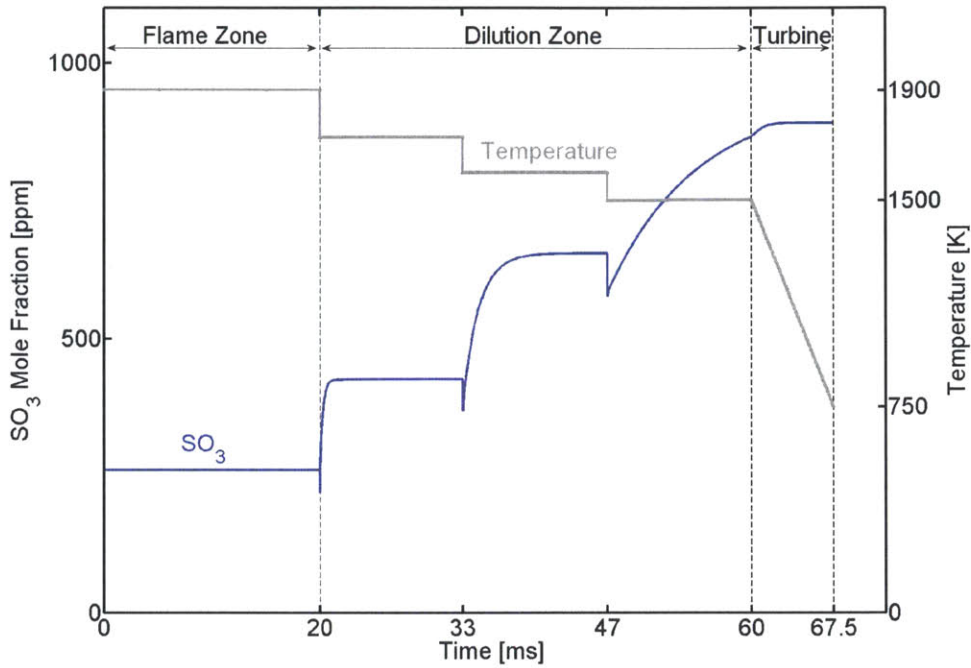


Figure 5-15: For air combustion, the SO_3 mole fraction increases from the flame zone to the turbine outlet. The calculations shown are for 30% H_2S in the fuel, $T_{\text{Flame}} = 1900$ K and a dilution zone residence time of 40 ms.

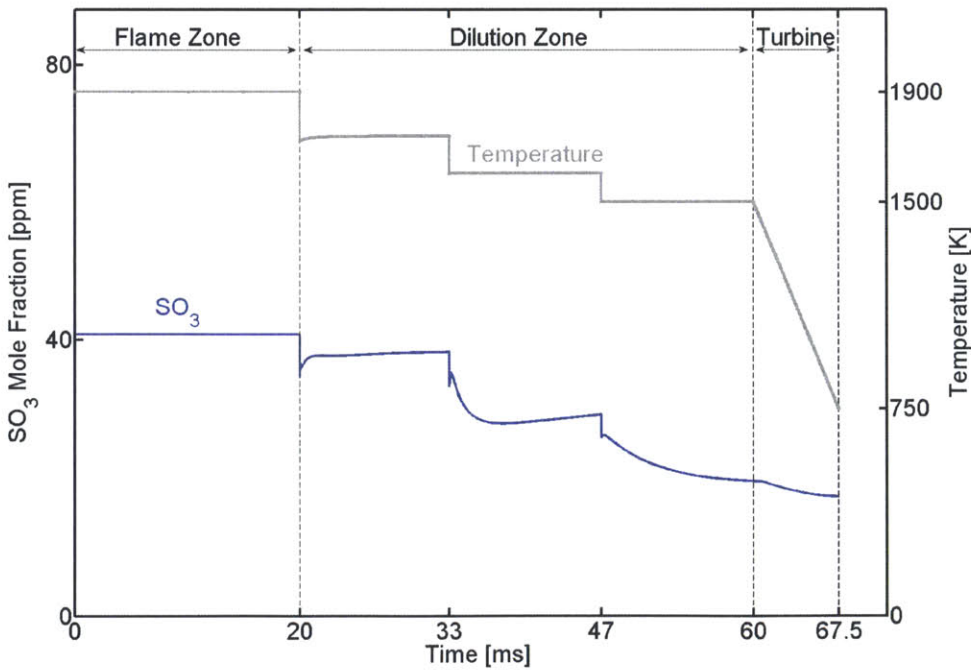


Figure 5-16: For oxy-combustion with CO_2 dilution, the SO_3 mole fraction decreases from the flame zone to the turbine outlet. The calculations shown are for 30% H_2S in the fuel, $T_{\text{Flame}} = 1900$ K and a dilution zone residence time of 40 ms.

the increase in SO_3 for oxy-combustion as compared to air combustion to the recirculation of flue gas containing SO_2 . In our calculation, we did not consider SO_2 in the diluent, which corresponds to the case where a flue gas desulfurization unit is installed in the cycle. This has been found to be the most economical way of handling the sulfur combustion products [137]. Preliminary calculations show that considering SO_2 in the diluent does increase the SO_3 mole fraction by a factor of five to ten, but even in this case it is still much lower than for air combustion.

5.3.2 Formation of Sulfur Trioxide During Cooling

The differences between air combustion and oxy-combustion with respect to SO_3 formation can be explained by the fact that SO_3 formation depends strongly on both temperature and O_2 concentration, with lower temperatures and higher O_2 content leading to higher SO_3 concentrations [29, 34]. To demonstrate the thermodynamic and chemical effects that determine the observed behavior, we conducted calculations for the simplified situation of a homogeneous mixture of 1% SO_2 , 1% CO , 1% H_2O , and varying amounts of O_2 in an argon (Ar) bath. The mixture is initially at equilibrium at $T = 1700$ K and is cooled down to $T = 300$ K at different cooling rates.

If there is ample excess O_2 (1% O_2 , which corresponds to $\Phi = 0.5$), at chemical equilibrium (i.e. infinitely slow cooling) all SO_2 gets converted to SO_3 as the temperature is decreased, because its formation is thermodynamically favored (see Figure 5-17). In this case, higher cooling rates lead to less SO_3 because its formation gets quenched as the temperature drops, but still SO_3 is only formed and never consumed during the cooling process. This is similar to the case of fuel-lean air-combustion (cf. Figure 5-15).

At stoichiometric conditions (0.5% O_2), the situation gets more complex because SO_3 formation has to compete for O_2 with the oxidation of CO . At equilibrium (i.e. infinitely slow cooling), virtually all CO gets oxidized as the temperature is decreased, consuming all the O_2 (see thick blue line in Figure 5-18). Accordingly, SO_3 (which is already low at $T = 1700$ K) gets *consumed* as the temperature is decreased (see thick blue line in Figure 5-19). This shows that thermodynamically CO oxidation is favored over SO_3 formation.

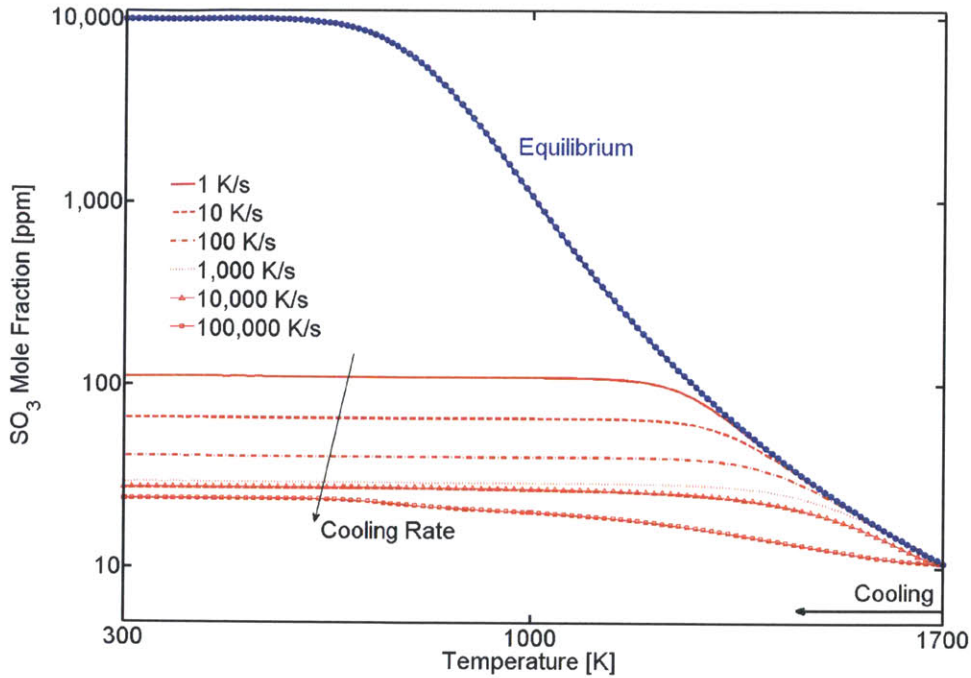


Figure 5-17: In the presence of excess O_2 , the SO_3 concentration increases with decreasing temperature. Higher cooling rates lead to quenching of SO_3 formation. Initial conditions: equilibrium of 1% SO_2 , 1% CO , 1% H_2O and 1% O_2 in Ar at $T = 1700$ K and $p = 1$ atm.

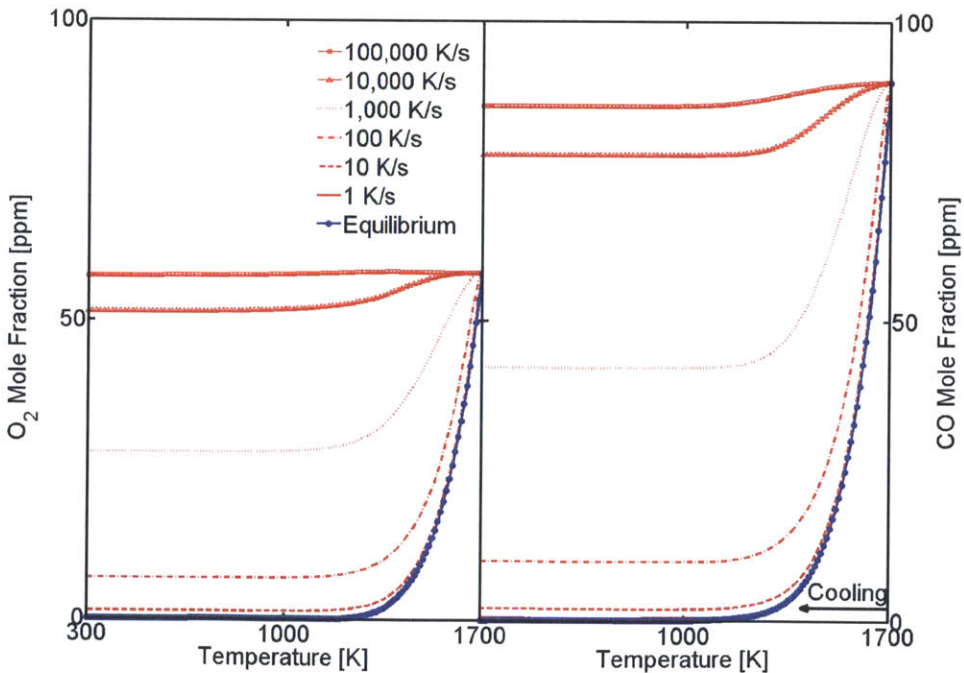


Figure 5-18: At stoichiometric conditions, higher cooling rates lead to quenching of CO oxidation. Initial conditions: equilibrium of 1% SO_2 , 1% CO , 1% H_2O and 1% O_2 in Ar at $T = 1700$ K and $p = 1$ atm.

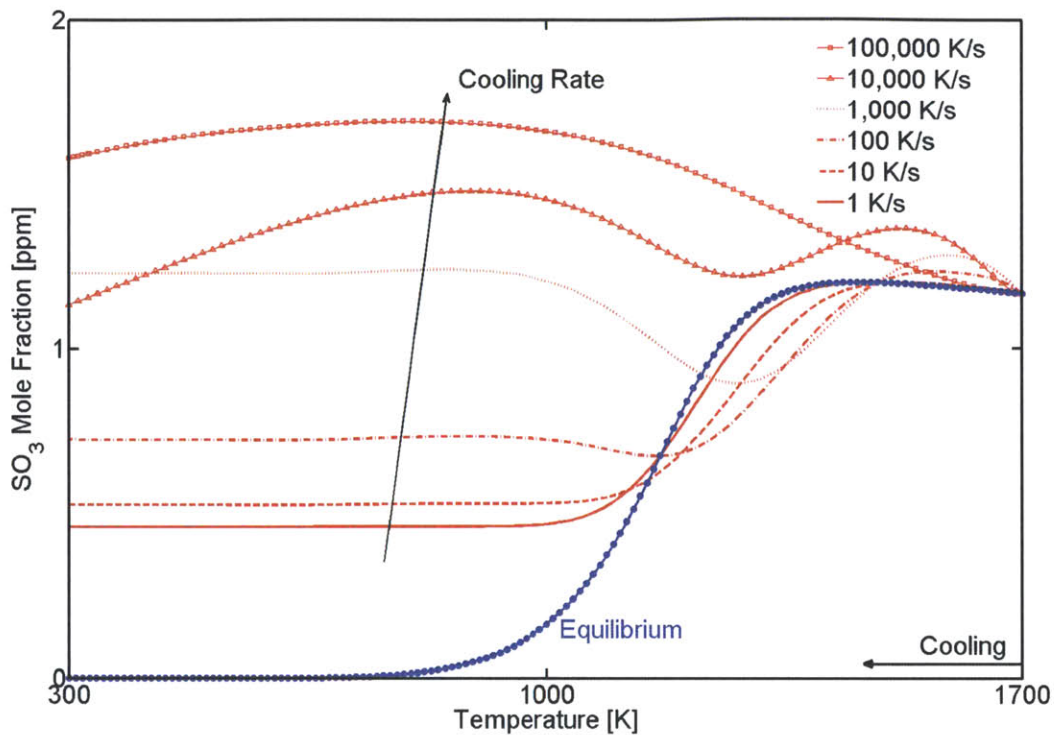


Figure 5-19: At stoichiometric conditions, SO_3 is either formed or consumed during cooling, depending on the cooling rate. Initial conditions: equilibrium of 1% SO_2 , 1% CO , 1% H_2O and 1% O_2 in Ar at $T = 1700$ K and $p = 1$ atm.

On the other hand, the kinetics of SO_3 formation are faster than those of CO oxidation, meaning that it takes longer for CO burnout to go to completion than for SO_3 formation (see Figure 5-20). The combination of these two effects leads to the complex dependence of SO_3 formation on the cooling rate seen in Figure 5-19.

As the cooling rate is increased, CO formation is being increasingly quenched and more and more O_2 is left (see Figure 5-18). Therefore, with increasing cooling rate more SO_3 is formed initially because the temperature drops while O_2 is still relatively high (CO oxidation has not started yet). As O_2 starts to drop due to CO oxidation, SO_3 is being consumed again. Once CO oxidation stops at around $T = 1200$ K, SO_3 rises again because O_2 remains constant and the temperature rises. Around $T = 1000$ K, SO_3 formation freezes as well. The consumption of SO_3 at low temperatures observed for cooling rates of 10,000 – 100,000 K/s is probably unphysical because it is caused by the reaction $\text{SO}_3 + \text{S}_2 = \text{S}_2\text{O} + \text{SO}_2$, the rate of which is based on an estimate [32].

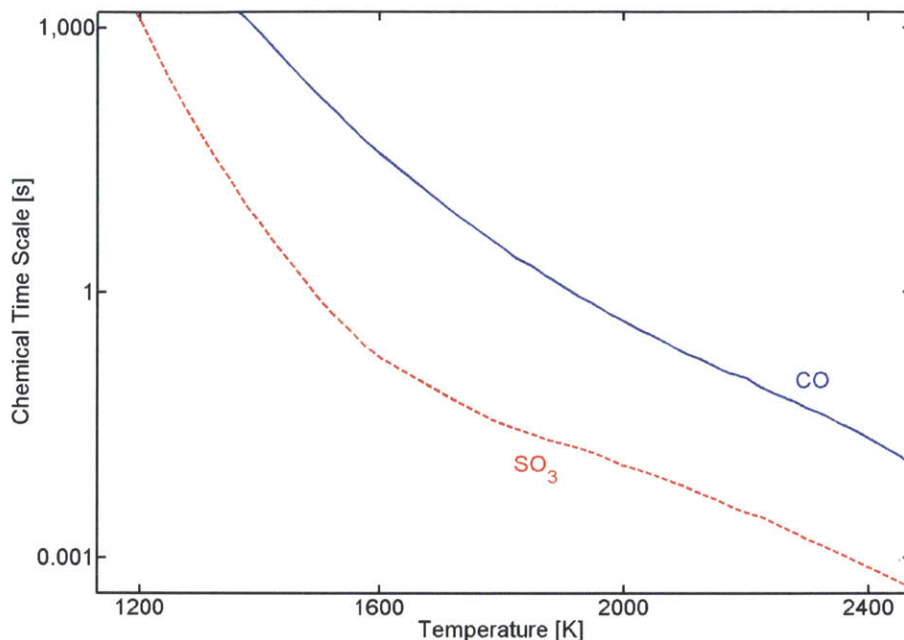


Figure 5-20: The chemical time scale for SO_3 formation is much smaller than that of CO formation. We define it as the time to reach 90% of equilibrium SO_3 or 110% of equilibrium CO, respectively. Initial conditions: 1% O_2 , 1% H_2O , and either 1% CO or 1% SO_2 in Ar.

In total, at stoichiometric conditions SO_3 is thus either produced or consumed during cooling, depending on the cooling rate. This is similar to the case of CO_2 diluted oxy-combustion (cf. Figure 5-16). Under the present conditions, increasing cooling rate leads to more SO_3 , not less. This shows the strong influence of both the equivalence ratio and the time-temperature history for the formation of SO_3 .

5.4 Influence of the Equivalence Ratio

As shown in the previous section, it may not be possible to reach the low O_2 concentrations required for EOR with either diluent at stoichiometric conditions. However, since the CO concentrations are well below the allowable limits, it seems promising to operate the cycle slightly rich instead of stoichiometric to achieve lower O_2 concentrations. To assess whether this approach is feasible, we conducted similar calculations to the ones presented in the previous section for CO_2 and H_2O dilution with 30% H_2S in the fuel for different equivalence ratios close to stoichiometry.

Both CO and O₂ mole fractions are highly sensitive to the equivalence ratio, especially for H₂O dilution (see Figure 5-21). Operating slightly fuel-rich can lead to significantly lower O₂ concentrations, but at the expense of higher CO and thus a lower combustion efficiency. In fact, there is a very narrow window of the equivalence ratio around $\Phi = 1.0025$ within which we can satisfy the EOR requirements for both CO and O₂ concentrations. However, in order to meet this point the equivalence ratio would have to be controlled within 0.15%. The system would thus be highly vulnerable to the influence of poor mixing.

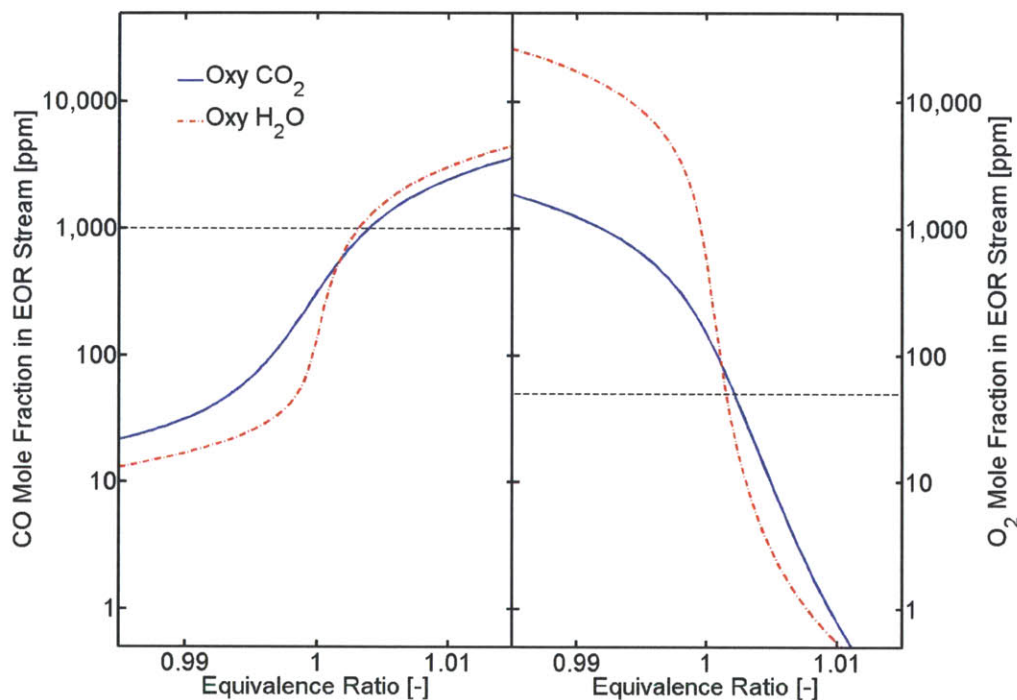


Figure 5-21: The CO and O₂ mole fractions in the dry products for CO₂ and H₂O diluted oxy-combustion with 30% H₂S at $T_{\text{Flame}} = 1900$ K and a dilution zone residence time of 40 ms. At an equivalence ratio around $\Phi = 1.0025$, both the CO and O₂ concentrations are below the limits for the Weyburn EOR (horizontal dashed lines).

Operating fuel-rich also has the added benefit of further reducing SO₃ formation because of the lower O₂ concentrations (see Figure 5-22). At $\Phi = 1.0025$, the SO₃ concentration is reduced by a factor of three to six compared to the stoichiometric case.

If the equivalence ratio gets too high, formation of solid sulfur may occur [31, 94, 156]. However, in the range considered here the concentrations of the disulfur molecule (S₂), which is considered the first precursor of solid sulfur formation, remains well below 1 ppm.

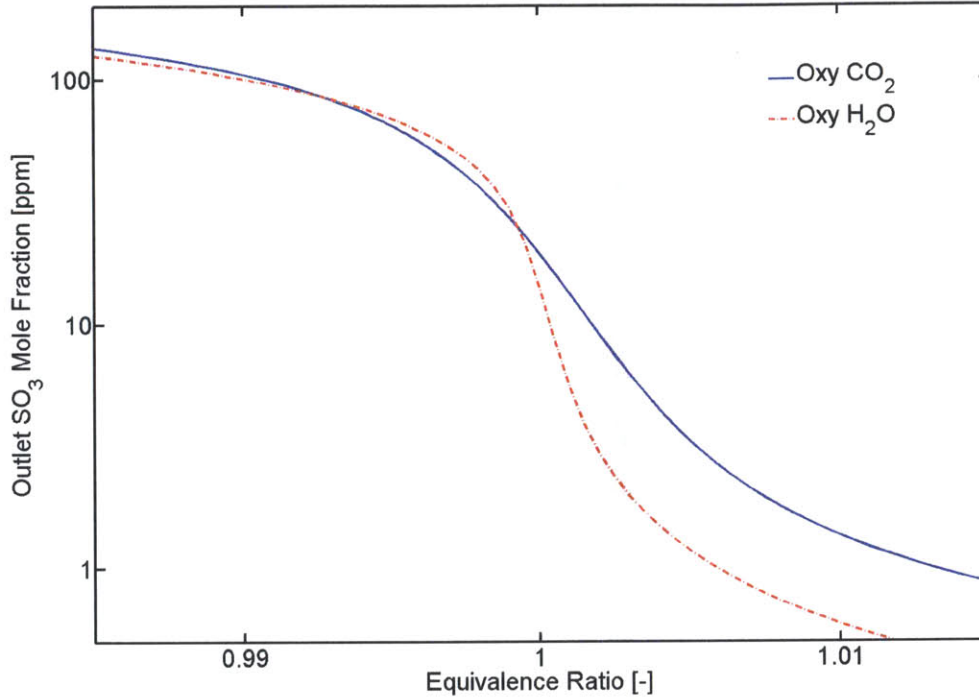


Figure 5-22: The SO_3 mole fraction at the turbine outlet for CO_2 and H_2O diluted oxy-combustion with 30% H_2S at $T_{\text{Flame}} = 1900$ K and a dilution zone residence time of 40 ms. The shaded area is the range in which the EOR requirements for CO and O_2 are met.

5.5 Conclusion

A reactor network model has been applied to study oxy-fuel combustion of sour gas in a gas turbine power cycle with carbon capture for EOR. Several calculations have been conducted to compare CO and O_2 concentrations in the EOR stream and SO_3 concentrations throughout the cycle for CO_2 and H_2O dilution and to identify promising combustor design strategies. From the results, we can draw the following conclusions:

1. The combustion efficiency, measured by the concentrations of CO and O_2 in the exhaust gas, is higher for H_2O dilution than for CO_2 dilution. On the other hand, CO_2 dilution seems more promising for keeping CO and O_2 concentrations in the CO_2 stream within the allowable limits for EOR than H_2O dilution. This is mainly due to the large change in concentrations in the gas stream for H_2O dilution as water is condensed before sequestration.

2. For either diluent, it may not be possible to reach the required O_2 concentration of less than 50 ppm when operating the cycle at stoichiometric conditions. However, since the CO limit of 1000 ppm is much less strict, it may be beneficial to operate the cycle slightly rich. This also significantly decreases SO_3 formation, but at the expense of a decreased combustion efficiency.
3. In terms of hot corrosion and cold-end corrosion, oxy-fuel combustion is much more promising than air combustion for handling gas with a large H_2S content. The absence of excess O_2 in the oxy-fuel cases leads to SO_3 concentrations that are one to two orders of magnitude lower than for fuel-lean air combustion. Unlike for air combustion, the concentration of SO_3 changes very little in the dilution zone and decreases as the flue gas is cooled in the turbine as the oxidation of CO consumes more O_2 . The exact behavior depends strongly on the equivalence ratio and the time-temperature history.
4. Carbon dioxide and H_2O dilution are likely to be comparable in terms of cold-end corrosion. While the SO_3 concentrations are up to 50% higher for CO_2 dilution, the higher H_2O content of the gas when using H_2O dilution will increase the sulfuric acid dew point as well. However, it has to be kept in mind that the existing correlations for predicting the sulfuric acid dew point may not be valid for the conditions encountered in oxy-fuel combustion.
5. The temperature in the flame zone of the combustor has almost no impact on SO_3 formation. For good CO and O_2 burnout, it should be relatively low (1700 – 1900 K). However, this might make flame stabilization more challenging.
6. In the dilution zone of the combustor, slower cooling leads to better CO and O_2 burnout, but also increases SO_3 formation under most conditions.

It should be kept in mind that the limits on CO and O_2 concentrations used in this study represent the values for only one specific project and to this date no universal standard for CO_2 purity requirements for EOR has been developed [14].

A caveat regarding the comparison of CO₂ and H₂O dilution presented here is that they were compared for the same cycle design. In practice, a H₂O diluted cycle would likely be designed slightly differently to maximize thermodynamic efficiency, meaning mostly at different temperatures and pressures. For a more realistic comparison, it might be useful to model the cycle for each diluent according to the designs that have been developed from a thermodynamic point of view [55].

At that point, one should also take into account the recycling stream in more detail. While in this study we treated the recycling stream as either pure H₂O or pure CO₂, in reality it will contain traces of the other species due to imperfect separation, some CO and O₂, and possibly SO₂ and SO₃ depending on whether or not there is a flue gas desulfurization unit and at which point in the cycle it will be installed [137].

Finally, a more thorough design study could show how well cycles can be adapted to comply with the specified CO and O₂ requirements. If it seems unrealistic that such a design point can be found, the cycle will have to be combined with some sort of after-treatment process like a gas separation process for removing O₂ or a post-combustion process to simultaneously remove O₂ and combustibles [157].

Chapter 6

Conclusions

6.1 Summary

In this thesis, a detailed chemical reaction mechanism for sour gas combustion was developed with a focus on oxy-fuel combustion. The mechanism was constructed by combining existing literature mechanisms and optimizing the rate parameters of ten sulfur reactions. The reaction mechanism is able to predict with reasonable accuracy the influence of the oxy-fuel diluents CO_2 and H_2O on the flame stabilization and emission behavior of CH_4 combustion. The mechanism can predict the laminar burning velocity and ignition delay time of H_2S in air, H_2S flame structures, and the rate of SO_3 formation under different conditions, capturing all important trends, although some quantitative discrepancies remain. The main interactions between carbon and sulfur species are also captured correctly.

The reaction mechanism was used for predicting the general combustion behavior of sour gas both in air combustion and under oxy-fuel conditions, and for studying emissions in a reactor network model representing the combustor, turbine, and heat recovery steam generator of a gas turbine power cycle for use with EOR.

Higher H_2S contents lead to lower flame temperatures, while significantly decreasing the ignition delay time. Depending on the conditions, the laminar burning velocity is either slightly increased or decreased. If desired, the changes in either burning velocity or flame temperature resulting from a changing fuel composition can be compensated by small changes in the diluent mole fraction or equivalence ratio.

Water diluted oxy-fuel combustion offers the easiest flame stabilization at gas turbine

conditions. For pressures greater than 10 atm it has a higher laminar burning velocity than air combustion or CO₂ diluted oxy-fuel combustion. It also leads to a better combustion efficiency than CO₂ dilution due to the lower equilibrium CO values and faster kinetics.

The most important requirements for the intended use of the combustion products in EOR are the concentrations of CO and especially O₂. The relevant quantities in this respect are the concentrations in the dry products. Carbon dioxide dilution is more promising than H₂O dilution for complying with these CO and O₂ concentration limits. To meet the limits simultaneously, it could be beneficial to operate the cycle slightly fuel-rich.

A major concern related to the sulfur content of the fuel is the formation of SO₃, which upon cooling forms sulfuric acid that condenses at temperatures around 500 K and causes severe corrosion problems. Oxy-fuel combustion was shown to be much better suited for avoiding sulfuric acid corrosion than air combustion. The concentrations of SO₃ are one to two orders of magnitude lower due to the lack of excess O₂. This is further improved by operating the cycle slightly fuel-rich. Unlike in air combustion, SO₃ is not formed but consumed during the dilution and cooling of the flue gas as the O₂ concentration decreases because of CO burnout.

For oxy-fuel combustion, most of the SO₃ is thus produced in the flame zone of the combustor. In this zone, SO₃ formation happens on the same time scale as the oxidation of CO. Therefore, further reduction of SO₃ through quenching can only be achieved at the expense of increased CO emissions.

6.2 Suggested Future Work

To further improve the fidelity of the chemical reaction mechanism, more fundamental research on sulfur chemistry is needed. This includes both fundamental studies on the kinetics of sulfur reactions and experiments that can be used for validation and optimization of the mechanism. In the latter group, data which would be particularly useful include more accurate measurements of the laminar burning velocity of H₂S, both in air and under oxy-fuel conditions, and at elevated pressure. Also, data on burning velocities and flame structures

of flames containing both CH_4 and H_2S , as well as more experiments on the formation of SO_3 at high temperatures and pressures would be extremely valuable.

The reactor network modeling presented in this work could be extended by building a more comprehensive model of the whole cycle, including recycling streams and flue gas desulfurization. However, this is not feasible with the standard models included in CHEMKIN. Therefore, one would either have to use a different software such as Cantera [158], or program new components for CHEMKIN using user defined functions. Also, while we deliberately chose to compare CO_2 and H_2O dilution at similar conditions, it would be helpful to investigate the case of H_2O dilution in the context of the cycle that is being proposed based on thermodynamic considerations [55]. Furthermore, the reactor network model should be used in a more comprehensive design study or optimization to determine the optimal operating conditions for different fuel compositions and combustion modes. This will also determine whether or not such a cycle could be combined with EOR without requiring further after-treatment processes. If this is not the case, more research would have to go into the selection of an appropriate technology for reducing the O_2 and CO concentrations to the required levels.

Finally, the reaction mechanism could serve as a basis for developing a mechanism that is suitable for use in multi-dimensional CFD simulations. This could be done either by postulating a global mechanism based on the main reaction pathways shown by the detailed mechanism, or reducing the detailed mechanism by eliminating unimportant reactions and species and applying steady-state and partial equilibrium assumptions. Due to the size of the detailed mechanism, the second approach would have to be supported by a specialized software package such as, for example, KINALC [159]. Such a reduced mechanism could be used to conduct CFD simulations of sour gas combustion in more realistic geometries to aid the design of gas turbine combustors suited for handling a sulfur containing fuel in the desired combustion environment.

References

- [1] International Energy Agency. World Energy Outlook 2013, available at <http://www.worldenergyoutlook.org/>, 2013.
- [2] G. Hammer, T. Lübcke, R. Kettner, M.R. Pillarella, H. Recknagel, A. Commichau, H.-J. Neumann, and B. Paczynska-Lahme. Natural Gas. In *Ullmann's Encyclopedia of Industrial Chemistry*. Wiley, 2012.
- [3] W.F.J. Burgers, P.S. Northrop, H.S. Kheshgi, and J.A. Valencia. Worldwide development potential for sour gas. *Energy Procedia*, 4:2178–2184, 2011.
- [4] A.F. Ghoniem. Needs, resources and climate change: Clean and efficient conversion technologies. *Progress in Energy and Combustion Science*, 37:15–51, 2011.
- [5] L. Chen, S. Zheng Yong, and A.F. Ghoniem. Oxy-fuel combustion of pulverized coal: Characterization, fundamentals, stabilization and CFD modeling. *Progress in Energy and Combustion Science*, 38:156–214, 2012.
- [6] M.B. Toftegaard, J. Brix, P.A. Jensen, P. Glarborg, and A.D. Jensen. Oxy-fuel combustion of solid fuels. *Progress in Energy and Combustion Science*, 36:581–625, 2010.
- [7] J. Davison. Performance and costs of power plants with capture and storage of CO₂. *Energy*, 32:1163–1176, 2007.
- [8] S.R. Turns. *An Introduction to Combustion*. McGraw-Hill Higher Education, 2000.
- [9] J.M. Beér and K.B. Lee. The effect of the residence time distribution on the performance and efficiency of combustors. *Proceedings of the Combustion Institute*, 10: 1187–1202, 1965.
- [10] L.S. Pedersen, P. Glarborg, K. Dam-Johansen, P.W. Hepburn, and G. Hesselmann. A chemical engineering model for predicting NO emissions and burnout from pulverized coal flames. *Combustion Science and Technology*, 132(1-6):251–314, 1998.
- [11] R.F.D. Monaghan, R. Tâhir, A. Cuoci, G. Bourque, M. Fûri, R.L. Gordon, T. Faravelli, A. Frassoldati, and H.J. Curran. Detailed multi-dimensional study of pollutant formation in a methane diffusion flame. *Energy & Fuels*, 26:1598–1611, 2012.
- [12] J. Park, T.H. Nguyen, D. Joung, K.Y. Huh, and M.C. Lee. Prediction of NO_x and CO emissions from an industrial lean-premixed gas-turbine combustor using a chemical reactor network model. *Energy & Fuels*, 27:1643–1651, 2013.

- [13] E. de Visser, C. Hendriks, M. Barrio, M.J. Molnvik, G. de Koeijer, S. Lijemark, and Y. LeGallo. Dynamis CO₂ quality recommendations. *International Journal of Greenhouse Gas Control*, 2:478–484, 2008.
- [14] G. Pipitone and O. Bolland. Power generation with CO₂ capture: Technology for CO₂ purification. *International Journal for Greenhouse Gas Control*, 3:528–534, 2009.
- [15] R. Stanger and T. Wall. Sulphur impacts during pulverised coal combustion in oxy-fuel technology for carbon capture and storage. *Progress in Energy and Combustion Science*, 37:69–88, 2011.
- [16] P. Glarborg and L.L.B. Bentzen. Chemical effects of a high CO₂ concentration in oxy-fuel combustion of methane. *Energy & Fuels*, 22:291–296, 2008.
- [17] P. Heil, D. Toporov, M. Förster, and R. Kneer. Experimental investigation on the effect of O₂ and CO₂ on burning rates during oxyfuel combustion of methane. *Proceedings of the Combustion Institute*, 33:3407–3413, 2011.
- [18] T.C. Williams, C.R. Shaddix, and R.W. Schefer. Effect of syngas composition and CO₂-diluted oxygen on performance of a premixed swirl-stabilized combustor. *Combustion Science and Technology*, 180:64–88, 2008.
- [19] G. Li, H. Zhou, and K. Cen. Emission characteristics and combustion instabilities in an oxy-fuel swirl-stabilized combustor. *Journal of Zhejiang University. Science. A*, 9: 1582–1589, 2008.
- [20] A. Amato, R. Hudak, D.R. Noble, D. Scarborough, P.A. D’Carlo, J.M. Seitzmen, and T.C. Liewuen. Methane oxy-combustion for low CO₂ cycles: measurement and modeling of CO and O₂ emissions. In *Proceedings of ASME Turbo Expo 2010: Power for Land, Sea and Air*, 2010.
- [21] A. Amato, B. Hudak, P. D’Souza, P. D’Carlo, D. Noble, D. Scarborough, J. Seitzman, and T. Lieuwen. Measurement and analysis of CO and O₂ emissions in CH₄/CO₂/O₂ flames. *Proceedings of the Combustion Institute*, 33:3399–3405, 2011.
- [22] A. Bhargava, M. Colket, W. Sowa, K. Casleton, and D. Maloney. An experimental and modeling study of humid air premixed flames. *Journal of Engineering for Gas Turbines and Power*, 122:405–411, 2000.
- [23] B. Chorpening, G.A. Richards, K.H. Casleton, M. Woike, B. Willis, and L. Hoffmann. Demonstration of a reheat combustor for power production with CO₂ sequestration. *Transactions of the ASME*, 127:740–747, 2005.
- [24] G.A. Richards, K.H. Casleton, and B.T. Chorpening. CO₂ and H₂O diluted oxy-fuel combustion for zero-emission power. *Proceedings of the Institution of Mechanical Engineers. Part A (Journal of Power and Energy)*, 219:121–126, 2005.

- [25] R. Anderson, H. Brandt, H. Mueggenburg, J. Taylor, and F. Viteri. A power plant concept which minimizes the cost of carbon dioxide sequestration and eliminates the emission of atmospheric pollutants. In *Fourth International Conference on Greenhouse Gas Control Technologies, Interlaken, Switzerland*, 1998.
- [26] R.E. Lewis, K.H. Caselton, G.A. Richards, D.L. Straub, and W.A. Rogers. A comparison of turbine combustion concepts suitable for integration with CO₂ sequestration. In *2001 Joint International Combustion Symposium, Kauai, HI*, 2001.
- [27] G.A. Richards, K.H. Caselton, R.E. Lewis, W.A. Rogers, M.R. Woike, and B.P. Willis. Advanced Steam Generators. Technical report, National Energy Technology Lab., Pittsburgh, PA, and Morgantown, WV; NASA Glenn Research Center (US), 2001.
- [28] M. Abián, J. Giménez-López, R. Bilbao, and M.U. Alzueta. Effect of different concentration levels of CO₂ and H₂O on the oxidation of CO: Experiments and modeling. *Proceedings of the Combustion Institute*, 33:317–323, 2011.
- [29] D. Fleig, F. Normann, K. Andersson, F. Johnsson, and B. Leckner. The fate of sulphur during oxy-fuel combustion of lignite. *Energy Procedia*, 1:383–390, 2009.
- [30] P. Glarborg, D. Kubel, K. Dam-Johansen, H.-M. Chiang, and J.W. Bozzelli. Impact of SO₂ and NO on CO oxidation under post-flame conditions. *International Journal of Chemical Kinetics*, 28:773–790, 1996.
- [31] H. Selim, A. Al Shoaibi, and A.K. Gupta. Effect of H₂S in methane/air flames on sulfur chemistry and products speciation. *Applied Energy*, 88:2593–2600, 2011.
- [32] C. Zhou, K. Sendt, and B.S. Haynes. Experimental and kinetic modelling study of H₂S oxidation. *Proceedings of the Combustion Institute*, 34:625–632, 2013.
- [33] D. Fleig, K. Andersson, F. Normann, and F. Johnsson. SO₃ formation under oxyfuel combustion conditions. *Industrial & Engineering Chemistry Research*, 50:8505–8514, 2011.
- [34] D. Fleig, M.U. Alzueta, F. Normann, M. Abian, K. Andersson, and F. Johnsson. Measurement and modeling of sulfur trioxide formation in a flow reactor under post-flame conditions. *Combustion and Flame*, 160:1142–1151, 2013.
- [35] D. Fleig, K. Andersson, and F. Johnsson. Influence of operating conditions on SO₃ formation during air and oxy-fuel combustion. *Industrial & Engineering Chemistry Research*, 51:9482–9491, 2012.
- [36] T.L. Jørgensen, H. Livbjerg, and P. Glarborg. Homogeneous and heterogeneously catalyzed oxidation of SO₂. *Chemical Engineering Science*, 62:4496–4499, 2007.
- [37] G. Blythe and K. Dombrowski. SO₃ mitigation guide update. Technical Report 1004168, EPRI, Palo Alto, CA, 2004.

- [38] Z. Faragó. Fuel sulfur content, sulfur-oxide emission and corrosion in oil heating plants. *Combustion Science and Technology*, 79:73–96, 1991.
- [39] R.K. Srivastava, C.A. Miller, C. Erickson, and R. Jambhekar. Emissions of sulfur trioxide from coal-fired power plants. *Journal of the Air and Waste Management Association*, 54:750–562, 2004.
- [40] Philip A. Schweitzer. *Fundamentals of Metallic Corrosion: Atmospheric and Media Corrosion of Metals*. CRC Press, 2006.
- [41] V. Ganapathy. Cold end corrosion: causes and cures. *Hydrocarbon Processing*, January: 57–59, 1989.
- [42] F.H. Verhoff and J.T. Banchemo. Predicting dew points of flue gases. *Chemical Engineering Progress*, 70:8:71–72, 1974.
- [43] A.G. Okkes. Get acid dewpoint of flue gases. *Hydrocarbon Processing*, 66:7:53–55, 1987.
- [44] B. ZareNezhad. New correlation predicts flue gas sulfuric acid dewpoint. *Oil & Gas Journal*, 107(35), 2009.
- [45] B. ZareNezhad. New correlation predicts dewpoints of acidic combustion gases. *Oil & Gas Journal*, 108(7), 2010.
- [46] J.F.P. Gomes. Avoid sulfuric acid corrosion in metallic stacks. *Hydrocarbon Processing*, March:1–2, 2005.
- [47] P.R. Roberge. *Handbook of Corrosion Engineering*. McGraw-Hill, 2000.
- [48] G.Y. Lai, editor. *High-Temperature Corrosion And Material Applications*. ASM International, 2007.
- [49] N. Eliaz, G. Shemesh, and R.M. Latanision. Hot corrosion in gas turbine components. *Engineering Failure Analysis*, 9:31–43, 2002.
- [50] M. Steinberg and K. Schofield. The chemistry of sodium with sulfur in flames. *Progress in Energy and Combustion Science*, 16:311–317, 1990.
- [51] M. Steinberg and K. Schofield. The controlling chemistry in flame generated surface deposition of Na_2SO_4 and the effects of chlorine. In *Twenty-Sixth Symposium (International) on Combustion/The Combustion Institute*, 1996.
- [52] P. Glarborg and P. Marshall. Mechanism and modeling of the formation of gaseous alkali sulfates. *Combustion and Flame*, 141:22–39, 2005.
- [53] P. Dagaut, F. Lecomte, J. Mieritz, and P. Glarborg. Experimental and kinetic modeling study of the effect of NO and SO_2 on the oxidation of CO- H_2 mixtures. *International Journal of Chemical Kinetics*, 35:564–575, 2003.

- [54] J. Giménez-López, M. Martínez, A. Mileera, R. Bilbao, and M.U. Alzueta. SO₂ effects on CO oxidation in a CO₂ atmosphere, characteristic of oxy-fuel conditions. *Combustion and Flame*, 158:48–56, 2011.
- [55] H.M. Kvamsdal, K. Jordal, and O. Bolland. A quantitative comparison of gas turbine cycles with CO₂ capture. *Energy*, 32:10–24, 2007.
- [56] R.E. Anderson, S. MacAdam, F. Viteri, D.O. Davies, J.P. Downs, and A. Paliszewski. Adapting gas turbines to zero emission oxy-fuel power plants. In *Proceedings of ASME Turbo Expo 2008: Power for Land, Sea and Air. Berlin, Germany*, 2008.
- [57] D.L. Zhu, F.N. Egolfopoulos, and C.K. Law. Experimental and numerical determination of laminar flame speeds of methane/(Ar, N₂, CO₂)-air mixtures as function of stoichiometry, pressure, and flame temperature. In *Twenty-Second Symposium (International) on Combustion/The Combustion Institute*, 1988.
- [58] A. Amato, B. Hudak, P. D’Carlo, D. Noble, D. Scarborough, J. Seitzman, and T. Lieuwen. Methane oxycombustion for low CO₂ cycles: Blowoff measurements and analysis. *Journal of Engineering for Gas Turbines and Power*, 133:061503, 2011.
- [59] F. Liu, H. Guo, and G.J. Smallwood. The chemical effect of CO₂ replacement of N₂ in air on the burning velocity of CH₄ and H₂ premixed flames. *Combustion and Flame*, 133:495–497, 2003.
- [60] NIST. NIST Chemistry WebBook: thermophysical properties of fluid systems, available at <http://webbook.nist.gov/chemistry/>, 2013.
- [61] V.R. Kishore, N. Duhan, M.R. Ravi, and A. Ray. Measurement of adiabatic burning velocity in natural gas-like mixtures. *Experimental Thermal and Fluid Science*, 33: 10–16, 2008.
- [62] F. Halter, F. Foucher, L. Landry, and C. Mounaim-Rousselle. Effect of dilution by nitrogen and/or carbon dioxide on methane and iso-octane air flames. *Combustion Science and Technology*, 181:813–827, 2009.
- [63] H. Guo, Y. Ju, K. Maruta, T. Niioka, and F. Liu. Numerical investigation of CH₄/CO₂/Air and CH₄/CO₂/O₂ counterflow premixed flames with radiation reabsorption. *Combustion Science and Technology*, 135:49–64, 1998.
- [64] K. Maruta, K. Abe, S. Hasegawa, S. Maruyama, and J. Sato. Extinction characteristics of CH₄/CO₂ versus O₂/CO₂ counterflow non-premixed flames at elevated pressures up to 0.7 mpa. *Proceedings of the Combustion Institute*, 31:1223–1230, 2007.
- [65] J. Ruan, H. Kobayashi, T. Niioka, and Y. Ju. Combined effects of nongray radiation and pressure on premixed CH₄/O₂/CO₂ flames. *Combustion and Flame*, 124:225–230, 2001.

- [66] Y. Levy, E. Olchanski, V. Sherbaum, V. Erenburg, and A. Burcat. Shock-tube ignition study of methane in air and recirculating gases mixtures. *Journal of Propulsion and Power*, 22-3:669–676, 2006.
- [67] S. Thiessen, G. Karim, and F. Seyedeyn-Azad. Consant volume autoignition of pre-mixed methane-carbon dioxide mixtures. *International Journal of Green Energy*, 4: 535–547, 2007.
- [68] D. Yossefi, S.J. Ashcroft, J. Hacoheh, M.R. Belmont, and I. Thorpe. Combustion of methane and ethane with CO₂ replacing N₂ as a diluent. *Fuel*, 74/7:1061–1071, 1995.
- [69] T.C. Williams, R.W. Schefer, J.C. Oefelein, and C.R. Shaddix. Idealized gas turbine combustor for performance research and validation of large eddy simulation. *Review of Scientific Instruments*, 78:0035114, 2007.
- [70] A.P. Shroll. Dynamic stability, blowoff, and flame characteristics of oxy-fuel combustion. Master's thesis, Massachusetts Institute of Technology, 2011.
- [71] P. Kutne, B.K. Kapadia, W. Meier, and M. Aigner. Experimental analysis of the combustion behaviour of oxyfuel flames in a gas turbine model combustor. *Proceedings of the Combustion Institute*, 33:3383–3390, 2011.
- [72] S. Seepana and S. Jayanti. Experimental studies of flame extinction in a swirl-stabilized oxy-fuel burner. *Fuel*, 93:75–81, 2012.
- [73] A.P. Shroll, S.J. Shanbhogue, and A.F. Ghoniem. Dynamic-stability characteristics of premixed methane oxy-combustion. *Journal of Engineering for Gas Turbines and Power*, 134:051504, 2012.
- [74] M. Ditaranto and J. Hals. Combustion instabilities in sudden expansion oxy-fuel flames. *Combustion and Flame*, 146:493–512, 2006.
- [75] P. Heil. *Investigation of the Flameless Combustion of Methane in an Oxyfuel Atmosphere*. PhD thesis, RWTH Aachen University, 2010.
- [76] S. Chen and C. Zheng. Counterflow diffusion flame of hydrogen-enriched biogas under mild oxy-fuel condition. *International Journal of Hydrogen Energy*, 36:15403–15413, 2011.
- [77] A.N. Mazas, B. Fiorina, D.A. Lacoste, and T. Schuller. Effects of water vapor addition on the laminar burning velocity of oxygen-enriched methane flames. *Combustion and Flame*, 158:2428–2440, 2011.
- [78] T. Boushaki, Y. Dhué, L. Selle, B. Ferret, and T. Poinsot. Effects of hydrogen and steam addition on laminar burning velocity of methane-air premixed flame: Experimental and numerical analysis. *International Journal of Hydrogen Energy*, 37:9412–9422, 2012.

- [79] T. LeCong and P. Dagaut. Experimental and detailed modeling study of the effect of water vapor on the kinetics of combustion of hydrogen and natural gas, impact on NO_x . *Energy & Fuels*, 23:725–734, 2009.
- [80] V.S. Babkin and A.V. V'yun. Effect of water vapor on the normal burning velocity of a methane-air mixture at high pressures. *Combustion, Explosion, and Shock Waves*, 7:339–341, 1971.
- [81] R. Anderson, F. Viteri, R. Hollis, A. Keating, J. Shipper, G. Merrill, C. Schillig, S. Shinde, J. Downs, D. Davies, and M. Harris. Oxy-fuel gas turbine, gas generator and reheat combustor technology development and demonstration. In *Proceedings of ASME Turbo Expo 2010: Power for Land, Sea and Air*, 2010.
- [82] H. H. Mueggenburg. "Steam Generator Injector." U.S. Patent 6,206,684, 2001.
- [83] Clean Energy Systems, Inc. CES Gas Generator - GG12, available at <http://www.cleanenergysystems.com/index.php/products>, 2013.
- [84] T. LeCong and P. Dagaut. Effect of water vapor on the kinetics of combustion of hydrogen and natural gas: Experimental and detailed modeling study. In *Proceedings of ASME Turbo Expo 2008: Power for Land, Sea and Air*, 2008.
- [85] T. Iijima and T. Takeno. Effects of temperature and pressure on burning velocity. *Combustion and Flame*, 65:35–43, 1986.
- [86] H. Eberius and T. Kick. Stabilization of premixed, conical methane flames at high pressures. *Berichte der Bunsengesellschaft für Physikalisch Chemie*, 96:1416–1419, 1992.
- [87] J. Lux and O. Haidn. Flame stabilization in high-pressure liquid oxygen/methane rocket engine combustion. *Journal of Propulsion and Power*, 25(1):15–24, 2009.
- [88] S. Candel, M. Juniper, G. Singla, P. Scouffaire, and C. Rolon. Structure and dynamics of cyogenic flames at supercritical pressure. *Combustion Science and Technology*, 178: 161–192, 2006.
- [89] H.I. Joo and Ö.L. Gülder. Structure of laminar methane-oxygen diffusion flames at high pressures. In *48th AIAA Aerospace Sciences Meeting Including the New Horizons Forum and Aerospace Exposition*, 2010.
- [90] D. Salgues, A.-G. Mouis, S.-Y. Lee, D. Kalitan, S. Pal, and R. Santoro. Shear and swirl coaxial injector studies of LOX/GCH₄ rocket combustion using non-intrusive laser diagnostics. In *44th AIAA Aerospace Sciences Meeting and Exhibit*, 2006.
- [91] G.P. Sutton and O. Biblarz. *Rocket Propulsion Elements*. John Wiley & Sons, Inc., 2010.

- [92] G.S. Gill and W.H. Nurick. Liquid rocket engine injectors. Technical report, NASA Glenn Research Center, 1976.
- [93] M.G. Zabetakis. Flammability characteristics of combustible gases and vapors. Technical report, U.S. Bureau of Mines, Bulletin No. 627 (7), 1965.
- [94] L. Vervisch, B. Labegorre, and J. Réveillon. Hydrogen-sulphur oxy-flame analysis and single-step flame tabulated chemistry. *Fuel*, 83:605–614, 2004.
- [95] D.S. Chamberlin and D.R. Clarke. Flame speed of hydrogen sulfide. *Industrial & Engineering Chemistry*, 20(10):1016–1019, 1928.
- [96] L. Cohen. Burning velocities of hydrogen sulfide in air and in oxygen. *Fuel*, 34:S119–S122, 1955.
- [97] G.J. Gibbs and H.F. Calcote. Effect of molecular structure on burning velocity. *Journal of chemical & engineering data*, 4:226–237, 1959.
- [98] C. Flockenhaus. Flammengeschwindigkeit v. Schwefelwasserstoff-Luft-Gemischen. *Gas Wärme international*, 18/4:153–156, 1969.
- [99] J.N. Bradley and D.C. Dobson. Oxidation of hydrogen sulfide in shock waves. I. absorption studies of OH and SO₂ in H₂S-O₂-Ar mixtures. *The Journal of Chemical Physics*, 46(8):2865–2871, 1967.
- [100] M. Frenklach, J.H. Lee, J.N. White, and W.C. Gardiner, Jr. Oxidation of hydrogen sulfide. *Combustion and Flame*, 41:1–16, 1981.
- [101] H.S.F. Chin, K. Karan, A.K. Mehrotra, and L.A. Behie. The fate of methane in a claus plant reaction furnace. *The Canadian Journal of Chemical Engineering*, 79:482–490, 2001.
- [102] P.F. Kurz. Influence of hydrogen sulfide on flame speed of propane-air mixtures. *Industrial and Engineering Chemistry*, 45(10):2361–2366, 1953.
- [103] P.F. Kurz. Flame-stability studies with mixed fuels: Hydrocarbons, hydrogen, and hydrogen sulfide. *Industrial and Engineering Chemistry*, 45(9):2072–2078, 1953.
- [104] P.F. Kurz. Influence of hydrogen sulphide on blow-off limits of hydrocarbon flames. *Fuel*, 34:463–470, 1955.
- [105] R.J. Kee, F.M. Rupley, and J.A. Miller et al. *CHEMKIN-PRO 15112*. Reaction Design, San Diego, CA, 2011.
- [106] G.P. Smith, D.M. Golden, M. Frenklach, N.W. Moriarty, B. Eiteneer, M. Goldenberg, C.T. Bowman, R.K. Hanson, S. Song, W.C. Gardiner Jr., V.V. Lissianski, and Z. Qin. GRI-Mech 3.0, available at http://www.me.berkeley.edu/gri_mech/.

- [107] T. LeCong, P. Dagaut, and G. Dayma. Oxidation of natural gas, natural gas/syngas mixtures, and effect of burnt gas recirculation: Experimental and detailed kinetic modeling. *Journal of Engineering for Gas Turbines and Power*, 130:041502, 2008.
- [108] K. Tsuchiya, K. Kamiya, and H. Matsui. Studies on the oxidation mechanism of H₂S based on direct examination of the key reactions. *International Journal of Chemical Kinetics*, 29:57–66, 1997.
- [109] M. Alzueta, R. Bilbao, and P. Glarborg. Inhibition and sensitization of fuel oxidation by SO₂. *Combustion and Flame*, 127:2234–2251, 2001.
- [110] K.J. Hughes and A.S. Tomlin. The SO_x mechanism extension to the Leeds Methane Oxidation Mechanism, available at <http://garfield.chem.elte.hu/Combustion/sox.htm>.
- [111] F.G. Cerru, A. Kronenburg, and R.P. Lindstedt. A systematically reduced reaction mechanism for sulphur oxidation. *Proceedings of the Combustion Institute*, 30(1):1227–1235, 2005.
- [112] F.G. Cerru, A. Kronenburg, and R.P. Lindstedt. Systematically reduced chemical mechanisms for sulfur oxidation and pyrolysis. *Combustion and Flame*, 146:437–455, 2006.
- [113] A.J. Hynes and P.H. Wine. Kinetics and mechanisms of the oxidation of gaseous sulfur compounds. In W.C. Gardiner, Jr., editor, *Gas-Phase Combustion Chemistry*, pages 343–388. Springer, 2000.
- [114] E. Goos, A. Burcat, and B. Ruscic. Third Millennium Ideal Gas and Condensed Phase Thermochemical Database for Combustion, available at <ftp://ftp.technion.ac.il/pub/supported/aetdd/thermodynamics>, 2013.
- [115] R.C. Shiell, X.K. Hu, Q.J. Hu, and J.W. Hepburn. A determination of the bond dissociation energy (D₀(H-SH)): Threshold ion-pair production spectroscopy (TIPPS) of a triatomic molecule. *The Journal of Physical Chemistry A*, 104:4339–4342, 2000.
- [116] P.A. Denis. Thermochemistry of 35 selected sulfur compounds, a comparison between experiment and theory. *Journal of Sulfur Chemistry*, 29:327–352, 2008.
- [117] A.G. Császár, M.L. Leininger, and A. Burcat. Enthalpy of formation of ²Π_{3/2} SH. *Journal of Physical Chemistry A*, 107:2061–2065, 2003.
- [118] C. Zhou, K. Sendt, and B.S. Haynes. Theoretical study of reactions in the multiple well H₂/S₂ system. *Journal of Physical Chemistry A*, 113:8299–8306, 2009.
- [119] K.A. Hawboldt, W.D. Monnery, and W.Y. Svrcek. New experimental data and kinetic rate expression for H₂S pyrolysis and re-association. *Chemical Engineering Science*, 55:957–966, 2000.

- [120] C.-W. Lu, Y.-J. Wu, Y.-P. Lee, R.S. Zhu, and M.C. Lin. Experimental and theoretical investigations of rate coefficients of the reaction $S(^3P)+O_2$ in the temperature range 298–878 K. *Journal of Chemical Physics*, 121(17):8271–8278, 2004.
- [121] A. Grillo, R. Reed, and M.W. Slack. Thermal decomposition of SO_2 monitored by ir emission. In *Proceedings of the 12th International Symposium on Shock Tubes and Waves, Jerusalem, July 12-19, 1979*, pages 486–494, 1980.
- [122] G. Black, R.L. Sharpless, and T.G. Slanger. Rate coefficients for SO reactions with O_2 and O_3 over the temperature range 230 to 420 K. *Chemical Physics Letters*, 93(6): 598–602, 1982.
- [123] N.L. Garland. Temperature dependence of the reaction: $SO + O_2$. *Chemical Physics Letters*, 290:385–390, 1998.
- [124] Y. Gao, C. Zhou, K. Sendt, B.S. Haynes, and P. Marshall. Kinetic and modeling studies of the reaction $S + H_2S$. *Proceedings of the Combustion Institute*, 33:459–465, 2011.
- [125] H. Shiina, M. Oya, K. Yamashita, A. Miyoshi, and H. Matsui. Kinetic studies of the pyrolysis of H_2S . *The Journal of Physical Chemistry*, 100(6):2136–2140, 1996.
- [126] K. Sendt, M. Jazbec, and B.S. Haynes. Chemical kinetic modeling of the H/S system: H_2S thermolysis and H_2 sulfidation. *Proceedings of the Combustion Institute*, 29:2439–2446, 2002.
- [127] D.P. Bertsekas. *Nonlinear Programming*. Athena Scientific, 2nd edition, 1999.
- [128] P. Glarborg, D. Kubel, P.G. Kristensen, J. Hansen, and K. Dam-Johansen. Interactions of CO , NO_x and H_2O under post-flame conditions. *Combustion Science and Technology*, 111:461–485, 1995.
- [129] E.L. Merryman and A. Levy. Kinetics of sulfur-oxide formation in flames: II. low pressure H_2S flames. *Journal of the Air Pollution Control Association*, 17(12):800–806, 1967.
- [130] M. Binoist, B. Labegorre, F. Monnet, P.D. Clark, N.I. Dowling, M. Huang, D. Archambault, E. Plasari, and P.-M. Marquaire. Kinetic study of the pyrolysis of H_2S . *Industrial & Engineering Chemistry Research*, 42:3943–3951, 2003.
- [131] M.P. Boyce. *Gas Turbine Engineering Handbook*. Butterworth-Heinemann, fourth edition, 2012.
- [132] G. Rozenchan, D.L. Zhu, C.K. Law, and S.D. Tse. Outward propagation, burning velocities, and chemical effects of methane flames up to 60 atm. *Proceedings of the Combustion Institute*, 29:1461–1469, 2002.

- [133] L. Chen and A.F. Ghoniem. Modeling CO₂ chemical effects on CO formation in oxy-fuel diffusion flames using detailed, quasi-global and global reaction mechanisms. *Combustion Science and Technology*, in press, 2014. doi: 10.1080/00102202.2014.883384.
- [134] W. Sanz, H. Jericha, B. Bauer, and E. Göttlich. Qualitative and quantitative comparison of two promising oxy-fuel power cycles for CO₂ capture. *Journal of Engineering for Gas Turbines and Power*, 130:031702, 2008.
- [135] A.H. Lefebvre. *Gas Turbine Combustion*. Taylor & Francis, 1999.
- [136] I. Pfaff and A. Kather. Comparative thermodynamic analysis and integration issues of CCS steam power plants based on oxy-combustion with cryogenic or membrane based air separation. *Energy Procedia*, 1:495–502, 2009.
- [137] N.W. Chakroun. Sour gas oxy-combustion power cycles for carbon capture and sequestration. Master’s thesis, Massachusetts Institute of Technology, 2014.
- [138] D.C. Hammond, Jr. and A.M. Mellor. Analytical predictions of emissions from and within an allison J-33 combustor. *Combustion Science and Technology*, 6 (5):279–286, 1973.
- [139] S.L. Bragg. Application of reaction rate theory to combustion chamber analysis. Technical Report Aeronautical Research Council Pub. ARC 16170, Ministry of Defense, London, England, 1953.
- [140] J.M. Beér and N.A. Chigier. *Combustion Aerodynamics*. Robert E. Krieger Publishing Company, 1983.
- [141] H.C. Hottel, G.C. Williams, and A.H. Bonnell. Application of well-stirred reactor theory to the prediction of combustor performance. *Combustion and Flame*, 2 (1): 13–34, 1958.
- [142] D.C. Hammond, Jr. and A.M. Mellor. A preliminary investigation of gas turbine combustor modelling. *Combustion Science and Technology*, 2 (2-3):67–80, 1970.
- [143] J. Swithenbank, I. Poll, and M.W. Vincent. Combustion design fundamentals. In *Fourteenth Symposium (International) on Combustion*. Pittsburgh, PA: The Combustion Institute, 1973.
- [144] G.J. Sturgess. Combustor LBO design model evaluation. Technical Report WL-TR-95-2089, United Technologies Corp. Pratt & Whitney, Government Engines & Space Propulsion, West Palm Beach, Florida, 1995.
- [145] M.P. Heap, T.M. Lowes, and R. Walmsley. Emission of nitric oxide from large turbulent diffusion flames. *Symposium (International) on Combustion*, 14 (1):883–895, 1973.
- [146] R.P. van der Lans, P. Glarborg, K. Dam-Johansen, and P.S. Larsen. Residence time distributions in a cold, confined swirl flow: Implications for chemical engineering combustion modelling. *Chemical Engineering Science*, 52 (16):2743–2756, 1997.

- [147] A.R. Morr, J.B. Heywood, and A.H. Fitch. Measurements and predictions of carbon monoxide emissions from an industrial gas turbine. *Combustion Science and Technology*, 11 (3-4):97–109, 1975.
- [148] M.G. Michaud, P.R. Westmoreland, and A.S. Feitelberg. Chemical mechanisms of NO_x formation for gas turbine conditions. *Symposium (International) on Combustion*, 24:879–887, 1992.
- [149] A.S. Feitelberg and M.A. Lacey. The GE rich-quench-lean gas turbine combustor. *Journal of Engineering for Gas Turbines and Power*, 120:502–508, 1998.
- [150] D.L. Straub, K.H. Casleton, R.E. Lewis, T.G. Sidwell, D.J. Maloney, and G.A. Richards. Assessment of rich-burn, quick-mix, lean-burn trapped vortex combustor for stationary gas turbines. *Journal of Engineering for Gas Turbines and Power*, 127:36–41, 2005.
- [151] P. Gokulakrishnan, C.C. Fuller, R.G. Joklik, and M.S. Klassen. Chemical kinetic modeling of ignition and emissions from natural gas and LNG fueled gas turbines. In *Proceedings of the ASME Turbo Expo 2012, GT2012, Copenhagen, Denmark, 2012*.
- [152] S. Göke and C.O. Paschereit. Influence of steam dilution on NO_x formation in premixed natural gas and hydrogen flames. In *50th AIAA Aerospace Sciences Meeting including the New Horizons Forum and Aerospace Exposition, Nashville, Tennessee*, pages AIAA 2012–1272, 2012.
- [153] S. Göke, S. Schimek, S. Terhaar, T. Reichel, K. Göckeler, O. Krüger, J. Fleck, P. Griebel, and C.O. Paschereit. Influence of pressure and steam dilution on NO_x and CO emissions in a premixed natural gas flame. In *Proceedings of ASME Turbo Expo 2013: Turbine Technical Conference and Exposition*, pages GT2013–94782, 2013.
- [154] T.C. Lieuwen and V. Yang, editors. *Gas Turbine Emissions*. Cambridge University Press, 2013.
- [155] D.L. Allaire, I.A. Waitz, and K.E. Willcox. A comparison of two methods for predicting emissions from aircraft gas turbine combustors. In *Proceedings of GT2007, ASME Turbo Expo 2007: Power for Land, Sea and Air, Montreal, Canada*, pages GT2007–28346, 2007.
- [156] W. Nehb and K. Vydra. Sulfur. In *Ullmann's Encyclopedia of Industrial Chemistry*. Wiley-VCH, 2006.
- [157] M. de Joannon, A. Chinnici, P. Sabia, and R. Ragucci. Optimal post-combustion conditions for the purification of CO₂-rich exhaust streams from non-condensable reactive species. *Chemical Engineering Journal*, 211-212:318–326, 2012.
- [158] D.G. Goodwin. Cantera: An object-oriented software toolkit for chemical kinetics, thermodynamics, and transport processes, available at <http://code.google.com/p/cantera/>, 2012.

- [159] T. Turányi, K.J. Hughes, M.J. Pilling, and A.S. Tomlin. KINALC, available at <http://garfield.chem.elte.hu/Combustion/kinalc.htm>, 2005.

Appendix A

Reaction Mechanism

A.1 Optimized Sulfur Reactions

The reaction numbers correspond to the numbering used in [32]. The rate parameters that were varied in the optimization are highlighted in boldface.

Table A.1: Rate parameters for $k = AT^n \exp(-E_a/[RT])$ for the relevant reactions optimized with respect to targets 1-12.

No.	Reaction	A [cm, mol, s, K]	n	E_a [cal/mol]
3	$\text{H}_2\text{S} + \text{S}=\text{SH} + \text{SH}$ (1)	8.47E+06	2.3	9007.0
4	$\text{H}_2\text{S} + \text{S}=\text{SH} + \text{SH}$ (2)	8.85E+17	-1.7	5975.0
6	$\text{S} + \text{SH}=\text{S}_2 + \text{H}$	3.20E+12	0.5	-29.0
8	$\text{H} + \text{HSS}=\text{SH} + \text{SH}$ (1)	2.72E+08	1.6	-1030.0
9	$\text{H} + \text{HSS}=\text{SH} + \text{SH}$ (2)	1.81E+18	-1.0	261.0
10	$\text{SH} + \text{SH} (+\text{M}) = \text{HSSH}$	6.34E+11	0.23	-829.3
	Low pressure limit	8.59E+30	-4.94	19980.0
25	$\text{SH} + \text{HO}_2=\text{H}_2\text{S} + \text{O}_2$	3.31E+04	2.8	-1529.5
59	$\text{S} + \text{O}_2=\text{SO} + \text{O}$	5.39E+05	2.06	-1593.9
116	$\text{SO} + \text{O}_2=\text{SO}_2 + \text{O}$	6.56E+06	1.42	3629.0

Table A.2: Rate parameters for $k = AT^n \exp(-E_a/[RT])$ for the relevant reactions optimized with respect to targets 1–7.

No.	Reaction	A [cm, mol, s, K]	n	E_a [cal/mol]
3	$H_2S + S=SH + SH$ (1)	8.87E+06	2.3	9007.0
4	$H_2S + S=SH + SH$ (2)	1.48E+18	-1.7	5975.0
6	$S + SH=S_2 + H$	9.96E+12	0.5	-29.0
8	$H + HSS=SH + SH$ (1)	1.78E+08	1.6	-1030.0
9	$H + HSS=SH + SH$ (2)	4.26E+18	-1.0	261.0
10	$SH + SH (+M) = HSSH$	5.95E+11	0.23	-829.3
	Low pressure limit	9.09E+30	-4.94	19980.0
25	$SH + HO_2=H_2S + O_2$	5.49E+04	2.8	-1529.5
59	$S + O_2=SO + O$	5.27E+05	2.08	-1690.7
116	$SO + O_2=SO_2 + O$	7.79E+06	1.42	3629.0

Table A.3: Rate parameters for $k = AT^n \exp(-E_a/[RT])$ for the relevant reactions optimized with respect to targets 8–12.

No.	Reaction	A [cm, mol, s, K]	n	E_a [cal/mol]
3	$H_2S + S=SH + SH$ (1)	6.62E+06	2.3	9007.0
4	$H_2S + S=SH + SH$ (2)	8.85E+17	-1.7	5975.0
6	$S + SH=S_2 + H$	1.11E+12	0.5	-29.0
8	$H + HSS=SH + SH$ (1)	3.32E+07	1.6	-1030.0
9	$H + HSS=SH + SH$ (2)	6.27E+17	-1.0	261.0
10	$SH + SH (+M) = HSSH$	5.36E+12	0.23	-829.3
	Low pressure limit	4.54E+31	-4.94	19980.0
25	$SH + HO_2=H_2S + O_2$	4.44E+04	2.8	-1529.5
59	$S + O_2=SO + O$	5.51E+05	2.06	-1324.0
116	$SO + O_2=SO_2 + O$	7.92E+06	1.42	3629.0

A.2 Recommended Sour Gas Mechanism

A.2.1 Thermodynamic Data

The thermodynamic data is given in the 7-term NASA polynomial format and can be used directly as an input file for CHEMKIN.

```
THERMO
  300.000  1000.000  5000.000
! Thermodynamic data for the Sour Gas Mechanism
!   assembled on 8/5/2013 by Dominik Bongartz (dominikb@mit.edu)
!   based on:
!   1. The thermo data used by GRI-Mech 3.0
!   2. The thermo data of the sulfur species used by Zhou et al.
!       (C. Zhou, K. Sendt, B.S. Haynes, Proc.Combust.Inst. 34(2013) 625-632 )
!   3. Because of its impact on the laminar flame speed of H2S, the heat of
!       formation of SH has been taken from Denis 2008 (H298=34.0pm0.3kcal/mol)
!       and Burcat/Goos 2013 (based on Csaszar 2003) (H298=33.9pm0.1kcal/mol)
!       and shifted to the lowest possible value considering the uncertainty
!       (33.8kcal/mol).
!
! NASA Polynomial format for CHEMKIN-II
O          L 1/900   1          G  200.000  3500.000  1000.000   1
  2.56942078E+00-8.59741137E-05 4.19484589E-08-1.00177799E-11 1.22833691E-15   2
  2.92175791E+04 4.78433864E+00 3.16826710E+00-3.27931884E-03 6.64306396E-06   3
-6.12806624E-09 2.11265971E-12 2.91222592E+04 2.05193346E+00                   4
O2         TPIS890   2          G  200.000  3500.000  1000.000   1
  3.28253784E+00 1.48308754E-03-7.57966669E-07 2.09470555E-10-2.16717794E-14   2
-1.08845772E+03 5.45323129E+00 3.78245636E+00-2.99673416E-03 9.84730201E-06   3
-9.68129509E-09 3.24372837E-12-1.06394356E+03 3.65767573E+00                   4
H          L 7/88H   1          G  200.000  3500.000  1000.000   1
  2.50000001E+00-2.30842973E-11 1.61561948E-14-4.73515235E-18 4.98197357E-22   2
  2.54736599E+04-4.46682914E-01 2.50000000E+00 7.05332819E-13-1.99591964E-15   3
  2.30081632E-18-9.27732332E-22 2.54736599E+04-4.46682853E-01                   4
H2         TPIS78H   2          G  200.000  3500.000  1000.000   1
  3.33727920E+00-4.94024731E-05 4.99456778E-07-1.79566394E-10 2.00255376E-14   2
```

-9.50158922E+02-3.20502331E+00	2.34433112E+00	7.98052075E-03-1.94781510E-05	3
2.01572094E-08-7.37611761E-12-9.17935173E+02	6.83010238E-01		4
OH	RUS 780	1H 1 G 200.000 3500.000 1000.000	1
3.09288767E+00	5.48429716E-04	1.26505228E-07-8.79461556E-11	2
3.85865700E+03	4.47669610E+00	3.99201543E+00-2.40131752E-03	3
4.61793841E-06			3
-3.88113333E-09	1.36411470E-12	3.61508056E+03-1.03925458E-01	4
H20	L 8/89H	20 1 G 200.000 3500.000 1000.000	1
3.03399249E+00	2.17691804E-03-1.64072518E-07-9.70419870E-11	1.68200992E-14	2
-3.00042971E+04	4.96677010E+00	4.19864056E+00-2.03643410E-03	3
6.52040211E-06			3
-5.48797062E-09	1.77197817E-12-3.02937267E+04-8.49032208E-01		4
H02	L 5/89H	10 2 G 200.000 3500.000 1000.000	1
4.01721090E+00	2.23982013E-03-6.33658150E-07	1.14246370E-10-1.07908535E-14	2
1.11856713E+02	3.78510215E+00	4.30179801E+00-4.74912051E-03	3
2.11582891E-05			3
-2.42763894E-08	9.29225124E-12	2.94808040E+02	4
3.71666245E+00			4
H202	L 7/88H	20 2 G 200.000 3500.000 1000.000	1
4.16500285E+00	4.90831694E-03-1.90139225E-06	3.71185986E-10-2.87908305E-14	2
-1.78617877E+04	2.91615662E+00	4.27611269E+00-5.42822417E-04	3
1.67335701E-05			3
-2.15770813E-08	8.62454363E-12-1.77025821E+04	3.43505074E+00	4
C	L11/88C	1 G 200.000 3500.000 1000.000	1
2.49266888E+00	4.79889284E-05-7.24335020E-08	3.74291029E-11-4.87277893E-15	2
8.54512953E+04	4.80150373E+00	2.55423955E+00-3.21537724E-04	3
7.33792245E-07			3
-7.32234889E-10	2.66521446E-13	8.54438832E+04	4
4.53130848E+00			4
CH	TPIS79C	1H 1 G 200.000 3500.000 1000.000	1
2.87846473E+00	9.70913681E-04	1.44445655E-07-1.30687849E-10	2
1.76079383E-14			2
7.10124364E+04	5.48497999E+00	3.48981665E+00	3
3.23835541E-04-1.68899065E-06			3
3.16217327E-09-1.40609067E-12	7.07972934E+04	2.08401108E+00	4
CH2	L S/93C	1H 2 G 200.000 3500.000 1000.000	1
2.87410113E+00	3.65639292E-03-1.40894597E-06	2.60179549E-10-1.87727567E-14	2
4.62636040E+04	6.17119324E+00	3.76267867E+00	3
9.68872143E-04	2.79489841E-06		3
-3.85091153E-09	1.68741719E-12	4.60040401E+04	4
1.56253185E+00			4
CH2(S)	L S/93C	1H 2 G 200.000 3500.000 1000.000	1
2.29203842E+00	4.65588637E-03-2.01191947E-06	4.17906000E-10-3.39716365E-14	2
5.09259997E+04	8.62650169E+00	4.19860411E+00-2.36661419E-03	3
8.23296220E-06			3
-6.68815981E-09	1.94314737E-12	5.04968163E+04-7.69118967E-01	4
CH3	L11/89C	1H 3 G 200.000 3500.000 1000.000	1

2.28571772E+00	7.23990037E-03	-2.98714348E-06	5.95684644E-10	-4.67154394E-14	2
1.67755843E+04	8.48007179E+00	3.67359040E+00	2.01095175E-03	5.73021856E-06	3
-6.87117425E-09	2.54385734E-12	1.64449988E+04	1.60456433E+00		4
CH4	L 8/88C	1H	4	G 200.000 3500.000 1000.000	1
7.48514950E-02	1.33909467E-02	-5.73285809E-06	1.22292535E-09	-1.01815230E-13	2
-9.46834459E+03	1.84373180E+01	5.14987613E+00	-1.36709788E-02	4.91800599E-05	3
-4.84743026E-08	1.66693956E-11	-1.02466476E+04	-4.64130376E+00		4
CO	TPIS79C	10	1	G 200.000 3500.000 1000.000	1
2.71518561E+00	2.06252743E-03	-9.98825771E-07	2.30053008E-10	-2.03647716E-14	2
-1.41518724E+04	7.81868772E+00	3.57953347E+00	-6.10353680E-04	1.01681433E-06	3
9.07005884E-10	-9.04424499E-13	-1.43440860E+04	3.50840928E+00		4
CO2	L 7/88C	10	2	G 200.000 3500.000 1000.000	1
3.85746029E+00	4.41437026E-03	-2.21481404E-06	5.23490188E-10	-4.72084164E-14	2
-4.87591660E+04	2.27163806E+00	2.35677352E+00	8.98459677E-03	-7.12356269E-06	3
2.45919022E-09	-1.43699548E-13	-4.83719697E+04	9.90105222E+00		4
HCO	L12/89H	1C	10	1 G 200.000 3500.000 1000.000	1
2.77217438E+00	4.95695526E-03	-2.48445613E-06	5.89161778E-10	-5.33508711E-14	2
4.01191815E+03	9.79834492E+00	4.22118584E+00	-3.24392532E-03	1.37799446E-05	3
-1.33144093E-08	4.33768865E-12	3.83956496E+03	3.39437243E+00		4
CH20	L 8/88H	2C	10	1 G 200.000 3500.000 1000.000	1
1.76069008E+00	9.20000082E-03	-4.42258813E-06	1.00641212E-09	-8.83855640E-14	2
-1.39958323E+04	1.36563230E+01	4.79372315E+00	-9.90833369E-03	3.73220008E-05	3
-3.79285261E-08	1.31772652E-11	-1.43089567E+04	6.02812900E-01		4
CH20H	GUNL93C	1H	30	1 G 200.000 3500.000 1000.000	1
3.69266569E+00	8.64576797E-03	-3.75101120E-06	7.87234636E-10	-6.48554201E-14	2
-3.24250627E+03	5.81043215E+00	3.86388918E+00	5.59672304E-03	5.93271791E-06	3
-1.04532012E-08	4.36967278E-12	-3.19391367E+03	5.47302243E+00		4
CH30	121686C	1H	30	1 G 300.00 3000.00 1000.000	1
0.03770799E+02	0.07871497E-01	-0.02656384E-04	0.03944431E-08	-0.02112616E-12	2
0.12783252E+03	0.02929575E+02	0.02106204E+02	0.07216595E-01	0.05338472E-04	3
-0.07377636E-07	0.02075610E-10	0.09786011E+04	0.13152177E+02		4
CH30H	L 8/88C	1H	40	1 G 200.000 3500.000 1000.000	1
1.78970791E+00	1.40938292E-02	-6.36500835E-06	1.38171085E-09	-1.17060220E-13	2
-2.53748747E+04	1.45023623E+01	5.71539582E+00	-1.52309129E-02	6.52441155E-05	3
-7.10806889E-08	2.61352698E-11	-2.56427656E+04	-1.50409823E+00		4

C2H	L 1/91C	2H	1	G	200.000	3500.000	1000.000	1	
	3.16780652E+00	4.75221902E-03	-1.83787077E-06	3.04190252E-10	-1.77232770E-14			2	
	6.71210650E+04	6.63589475E+00	2.88965733E+00	1.34099611E-02	-2.84769501E-05			3	
	2.94791045E-08	-1.09331511E-11	6.68393932E+04	6.22296438E+00				4	
C2H2	L 1/91C	2H	2	G	200.000	3500.000	1000.000	1	
	4.14756964E+00	5.96166664E-03	-2.37294852E-06	4.67412171E-10	-3.61235213E-14			2	
	2.59359992E+04	-1.23028121E+00	8.08681094E-01	2.33615629E-02	-3.55171815E-05			3	
	2.80152437E-08	-8.50072974E-12	2.64289807E+04	1.39397051E+01				4	
C2H3	L 2/92C	2H	3	G	200.000	3500.000	1000.000	1	
	3.01672400E+00	1.03302292E-02	-4.68082349E-06	1.01763288E-09	-8.62607041E-14			2	
	3.46128739E+04	7.78732378E+00	3.21246645E+00	1.51479162E-03	2.59209412E-05			3	
	-3.57657847E-08	1.47150873E-11	3.48598468E+04	8.51054025E+00				4	
C2H4	L 1/91C	2H	4	G	200.000	3500.000	1000.000	1	
	2.03611116E+00	1.46454151E-02	-6.71077915E-06	1.47222923E-09	-1.25706061E-13			2	
	4.93988614E+03	1.03053693E+01	3.95920148E+00	-7.57052247E-03	5.70990292E-05			3	
	-6.91588753E-08	2.69884373E-11	5.08977593E+03	4.09733096E+00				4	
C2H5	L12/92C	2H	5	G	200.000	3500.000	1000.000	1	
	1.95465642E+00	1.73972722E-02	-7.98206668E-06	1.75217689E-09	-1.49641576E-13			2	
	1.28575200E+04	1.34624343E+01	4.30646568E+00	-4.18658892E-03	4.97142807E-05			3	
	-5.99126606E-08	2.30509004E-11	1.28416265E+04	4.70720924E+00				4	
C2H6	L 8/88C	2H	6	G	200.000	3500.000	1000.000	1	
	1.07188150E+00	2.16852677E-02	-1.00256067E-05	2.21412001E-09	-1.90002890E-13			2	
	-1.14263932E+04	1.51156107E+01	4.29142492E+00	-5.50154270E-03	5.99438288E-05			3	
	-7.08466285E-08	2.68685771E-11	-1.15222055E+04	2.66682316E+00				4	
CH2CD	L 5/90C	2H	20	1	G	200.000	3500.000	1000.000	1
	4.51129732E+00	9.00359745E-03	-4.16939635E-06	9.23345882E-10	-7.94838201E-14			2	
	-7.55105311E+03	6.32247205E-01	2.13583630E+00	1.81188721E-02	-1.73947474E-05			3	
	9.34397568E-09	-2.01457615E-12	-7.04291804E+03	1.22156480E+01				4	
HCCO	SRIC91H	1C	20	1	G	300.00	4000.00	1000.000	1
	0.56282058E+01	0.40853401E-02	-0.15934547E-05	0.28626052E-09	-0.19407832E-13			2	
	0.19327215E+05	-0.39302595E+01	0.22517214E+01	0.17655021E-01	-0.23729101E-04			3	
	0.17275759E-07	-0.50664811E-11	0.20059449E+05	0.12490417E+02				4	
HCCOH	SRI91C	20	1H	2	G	300.000	5000.000	1000.000	1
	0.59238291E+01	0.67923600E-02	-0.25658564E-05	0.44987841E-09	-0.29940101E-13			2	
	0.72646260E+04	-0.76017742E+01	0.12423733E+01	0.31072201E-01	-0.50866864E-04			3	

	0.43137131E-07-0.14014594E-10	0.80316143E+04	0.13874319E+02						4
H2CN	41687H	2C	1N	1	G	300.00	4000.000	1000.000	1
	0.52097030E+01	0.29692911E-02-0.28555891E-06-0.16355500E-09	0.30432589E-13						2
	0.27677109E+05-0.44444780E+01	0.28516610E+01	0.56952331E-02	0.10711400E-05					3
	-0.16226120E-08-0.23511081E-12	0.28637820E+05	0.89927511E+01						4
HCN	GRI/98H	1C	1N	1	G	200.000	6000.000	1000.000	1
	0.38022392E+01	0.31464228E-02-0.10632185E-05	0.16619757E-09-0.97997570E-14						2
	0.14407292E+05	0.15754601E+01	0.22589886E+01	0.10051170E-01-0.13351763E-04					3
	0.10092349E-07-0.30089028E-11	0.14712633E+05	0.89164419E+01						4
HNO	And93 H	1N	10	1	G	200.000	6000.000	1000.000	1
	0.29792509E+01	0.34944059E-02-0.78549778E-06	0.57479594E-10-0.19335916E-15						2
	0.11750582E+05	0.86063728E+01	0.45334916E+01-0.56696171E-02	0.18473207E-04					3
	-0.17137094E-07	0.55454573E-11	0.11548297E+05	0.17498417E+01					4
N	L 6/88N	1			G	200.000	6000.000	1000.000	1
	0.24159429E+01	0.17489065E-03-0.11902369E-06	0.30226245E-10-0.20360982E-14						2
	0.56133773E+05	0.46496096E+01	0.25000000E+01	0.00000000E+00	0.00000000E+00	0.00000000E+00			3
	0.00000000E+00	0.00000000E+00	0.56104637E+05	0.41939087E+01					4
NNH	T07/93N	2H	1		G	200.000	6000.000	1000.000	1
	0.37667544E+01	0.28915082E-02-0.10416620E-05	0.16842594E-09-0.10091896E-13						2
	0.28650697E+05	0.44705067E+01	0.43446927E+01-0.48497072E-02	0.20059459E-04					3
	-0.21726464E-07	0.79469539E-11	0.28791973E+05	0.29779410E+01					4
N2O	L 7/88N	2O	1		G	200.000	6000.000	1000.000	1
	0.48230729E+01	0.26270251E-02-0.95850874E-06	0.16000712E-09-0.97752303E-14						2
	0.80734048E+04-0.22017207E+01	0.22571502E+01	0.11304728E-01-0.13671319E-04						3
	0.96819806E-08-0.29307182E-11	0.87417744E+04	0.10757992E+02						4
NH	And94 N	1H	1		G	200.000	6000.000	1000.000	1
	0.27836928E+01	0.13298430E-02-0.42478047E-06	0.78348501E-10-0.55044470E-14						2
	0.42120848E+05	0.57407799E+01	0.34929085E+01	0.31179198E-03-0.14890484E-05					3
	0.24816442E-08-0.10356967E-11	0.41880629E+05	0.18483278E+01						4
NH2	And89 N	1H	2		G	200.000	6000.000	1000.000	1
	0.28347421E+01	0.32073082E-02-0.93390804E-06	0.13702953E-09-0.79206144E-14						2
	0.22171957E+05	0.65204163E+01	0.42040029E+01-0.21061385E-02	0.71068348E-05					3
	-0.56115197E-08	0.16440717E-11	0.21885910E+05-0.14184248E+00						4
NH3	J 6/77N	1H	3		G	200.000	6000.000	1000.000	1
	0.26344521E+01	0.56662560E-02-0.17278676E-05	0.23867161E-09-0.12578786E-13						2

-0.65446958E+04	0.65662928E+01	0.42860274E+01	-0.46605230E-02	0.21718513E-04						3
-0.22808887E-07	0.82638046E-11	-0.67417285E+04	-0.62537277E+00							4
NO	RUS 78N	10	1		G	200.000	6000.000	1000.000		1
0.32606056E+01	0.11911043E-02	-0.42917048E-06	0.69457669E-10	-0.40336099E-14						2
0.99209746E+04	0.63693027E+01	0.42184763E+01	-0.46389760E-02	0.11041022E-04						3
-0.93361354E-08	0.28035770E-11	0.98446230E+04	0.22808464E+01							4
NO2	L 7/88N	10	2		G	200.000	6000.000	1000.000		1
0.48847542E+01	0.21723956E-02	-0.82806906E-06	0.15747510E-09	-0.10510895E-13						2
0.23164983E+04	-0.11741695E+00	0.39440312E+01	-0.15854290E-02	0.16657812E-04						3
-0.20475426E-07	0.78350564E-11	0.28966179E+04	0.63119917E+01							4
HCNO	BDEA94H	1N	1C	10	1G	300.000	5000.000	1382.000		1
6.59860456E+00	3.02778626E-03	-1.07704346E-06	1.71666528E-10	-1.01439391E-14						2
1.79661339E+04	-1.03306599E+01	2.64727989E+00	1.27505342E-02	-1.04794236E-05						3
4.41432836E-09	-7.57521466E-13	1.92990252E+04	1.07332972E+01							4
HOCN	BDEA94H	1N	1C	10	1G	300.000	5000.000	1368.000		1
5.89784885E+00	3.16789393E-03	-1.11801064E-06	1.77243144E-10	-1.04339177E-14						2
-3.70653331E+03	-6.18167825E+00	3.78604952E+00	6.88667922E-03	-3.21487864E-06						3
5.17195767E-10	1.19360788E-14	-2.82698400E+03	5.63292162E+00							4
HNCO	BDEA94H	1N	1C	10	1G	300.000	5000.000	1478.000		1
6.22395134E+00	3.17864004E-03	-1.09378755E-06	1.70735163E-10	-9.95021955E-15						2
-1.66599344E+04	-8.38224741E+00	3.63096317E+00	7.30282357E-03	-2.28050003E-06						3
-6.61271298E-10	3.62235752E-13	-1.55873636E+04	6.19457727E+00							4
NCO	EA 93 N	1C	10	1	G	200.000	6000.000	1000.000		1
0.51521845E+01	0.23051761E-02	-0.88033153E-06	0.14789098E-09	-0.90977996E-14						2
0.14004123E+05	-0.25442660E+01	0.28269308E+01	0.88051688E-02	-0.83866134E-05						3
0.48016964E-08	-0.13313595E-11	0.14682477E+05	0.95504646E+01							4
CN	HBH92 C	1N	1		G	200.000	6000.000	1000.000		1
0.37459805E+01	0.43450775E-04	0.29705984E-06	-0.68651806E-10	0.44134173E-14						2
0.51536188E+05	0.27867601E+01	0.36129351E+01	-0.95551327E-03	0.21442977E-05						3
-0.31516323E-09	-0.46430356E-12	0.51708340E+05	0.39804995E+01							4
HCNN	SRI/94C	1N	2H	1	G	300.000	5000.000	1000.000		1
0.58946362E+01	0.39895959E-02	-0.15982380E-05	0.29249395E-09	-0.20094686E-13						2
0.53452941E+05	-0.51030502E+01	0.25243194E+01	0.15960619E-01	-0.18816354E-04						3
0.12125540E-07	-0.32357378E-11	0.54261984E+05	0.11675870E+02							4
N2	121286N	2			G	300.000	5000.000	1000.000		1

0.02926640E+02	0.14879768E-02	-0.05684760E-05	0.10097038E-09	-0.06753351E-13	2
-0.09227977E+04	0.05980528E+02	0.03298677E+02	0.14082404E-02	-0.03963222E-04	3
0.05641515E-07	-0.02444854E-10	-0.10208999E+04	0.03950372E+02		4
AR	120186AR	1	G	300.000 5000.000 1000.000	1
0.02500000E+02	0.00000000E+00	0.00000000E+00	0.00000000E+00	0.00000000E+00	2
-0.07453750E+04	0.04366000E+02	0.02500000E+02	0.00000000E+00	0.00000000E+00	3
0.00000000E+00	0.00000000E+00	-0.07453750E+04	0.04366000E+02		4
C3H8	L 4/85C	3H 8	G	300.000 5000.000 1000.000	1
0.75341368E+01	0.18872239E-01	-0.62718491E-05	0.91475649E-09	-0.47838069E-13	2
-0.16467516E+05	-0.17892349E+02	0.93355381E+00	0.26424579E-01	0.61059727E-05	3
-0.21977499E-07	0.95149253E-11	-0.13958520E+05	0.19201691E+02		4
C3H7	L 9/84C	3H 7	G	300.000 5000.000 1000.000	1
0.77026987E+01	0.16044203E-01	-0.52833220E-05	0.76298590E-09	-0.39392284E-13	2
0.82984336E+04	-0.15480180E+02	0.10515518E+01	0.25991980E-01	0.23800540E-05	3
-0.19609569E-07	0.93732470E-11	0.10631863E+05	0.21122559E+02		4
CH3CHO	L 8/88C	2H 40 1	G	200.000 6000.000 1000.000	1
0.54041108E+01	0.11723059E-01	-0.42263137E-05	0.68372451E-09	-0.40984863E-13	2
-0.22593122E+05	-0.34807917E+01	0.47294595E+01	-0.31932858E-02	0.47534921E-04	3
-0.57458611E-07	0.21931112E-10	-0.21572878E+05	0.41030159E+01		4
CH2CHO	SAND86D	1H 3C 2	G	300.000 5000.000 1000.000	1
0.05975670E+02	0.08130591E-01	-0.02743624E-04	0.04070304E-08	-0.02176017E-12	2
0.04903218E+04	-0.05045251E+02	0.03409062E+02	0.10738574E-01	0.01891492E-04	3
-0.07158583E-07	0.02867385E-10	0.15214766E+04	0.09558290E+02		4
S	S	1 0 0	OG	300.00 5000.00 1000.00	1
2.90214800E+00	-5.48454600E-04	2.76457600E-07	-5.01711500E-11	3.15068500E-15	2
3.24942300E+04	3.83847100E+00	3.18732900E+00	-1.59577600E-03	2.00553100E-06	3
-1.50708100E-09	4.93128200E-13	3.24225900E+04	2.41444100E+00		4
SH	H	1S 1 0	OG	300.00 5000.00 1000.00	1
3.05381000E+00	1.25888400E-03	-4.24916900E-07	6.92959100E-11	-4.28169100E-15	2
1.61325805E+04	5.97355100E+00	4.13332700E+00	-3.78789300E-04	-2.77785400E-06	3
5.37011200E-09	-2.39400600E-12	1.58089505E+04	1.61153500E-01		4
H2S	H	2S 1 0	OG	300.00 5000.00 1000.00	1
2.88314700E+00	3.82783500E-03	-1.42339800E-06	2.49799900E-10	-1.66027300E-14	2
-3.48074300E+03	7.25816200E+00	3.07102900E+00	5.57826100E-03	-1.03096700E-05	3
1.20195300E-08	-4.83837000E-12	-3.55982600E+03	5.93522600E+00		4

S0	0	1S	1	0	OG	300.00	5000.00	1000.00	1
4.02107800E+00	2.58485600E-04	8.94814200E-08	-3.58014500E-11	3.22843000E-15					2
-7.11962000E+02	3.45252300E+00	3.08040100E+00	1.80310600E-03	6.70502200E-07					3
-2.06900500E-09	8.51465700E-13	-3.98616300E+02	8.58102800E+00						4
S0*	0	1S	1	0	OG	300.00	5000.00	1000.00	1
4.02107800E+00	2.58485600E-04	8.94814200E-08	-3.58014500E-11	3.22843000E-15					2
9.51175703E+03	3.45252300E+00	3.08040100E+00	1.80310600E-03	6.70502200E-07					3
-2.06900500E-09	8.51465700E-13	9.82510273E+03	8.58102800E+00						4
S02	0	2S	1	0	OG	300.00	5000.00	1000.00	1
5.25449800E+00	1.97854500E-03	-8.20422600E-07	1.57638300E-10	-1.12045100E-14					2
-3.75688600E+04	-1.14605600E+00	2.91143900E+00	8.10302200E-03	-6.90671000E-06					3
3.32901600E-09	-8.77712100E-13	-3.68788200E+04	1.11174000E+01						4
S03	0	3S	1	0	OG	300.00	5000.00	1000.00	1
7.05066800E+00	3.24656000E-03	-1.40889700E-06	2.72153500E-10	-1.94236500E-14					2
-5.02066800E+04	-1.10644300E+01	2.57528300E+00	1.51509200E-02	-1.22987200E-05					3
4.24025700E-09	-5.26681200E-13	-4.89441100E+04	1.21951200E+01						4
HS02	H	10	2S	1	OG	300.00	2000.00	1000.00	1
0.15627374E+01	0.20691389E-01	-0.23112073E-04	0.12670203E-07	-0.27274176E-11					2
-0.18214824E+05	0.17556820E+02	0.15627374E+01	0.20691389E-01	-0.23112073E-04					3
0.12670203E-07	-0.27274176E-11	-0.18214824E+05	0.17556820E+02						4
H0SD	H	10	2S	1	OG	300.00	2000.00	1000.00	1
9.60146992E+00	-2.53592657E-02	6.76829409E-05	-6.34954136E-08	1.95893537E-11					2
-3.12540147E+04	-1.56740934E+01	9.60146992E+00	-2.53592657E-02	6.76829409E-05					3
-6.34954136E-08	1.95893537E-11	-3.12540147E+04	-1.56740934E+01						4
HS00	H	10	2S	1	OG	300.00	5000.00	1000.00	1
5.87948232E+00	4.58580173E-03	-2.93621833E-06	1.10178148E-09	-1.86219122E-13					2
1.41706015E+04	-1.04622817E+00	3.04640372E+00	1.52114268E-02	-1.84762707E-05					3
1.13862234E-08	-2.72421836E-12	1.48073744E+04	1.28748017E+01						4
H0SD2	H	10	3S	1	OG	300.00	2000.00	1000.00	0 1
7.62277304E+00	-4.19908990E-03	3.52054969E-05	-4.12715317E-08	1.40006629E-11					2
-4.69478133E+04	-7.80787503E+00	7.62277304E+00	-4.19908990E-03	3.52054969E-05					3
-4.12715317E-08	1.40006629E-11	-4.69478133E+04	-7.80787503E+00						4
S2	tpis89S	2	0	0	OG	200.000	6000.000		1
3.83249656E+00	8.88970881E-04	-2.59080844E-07	3.63847115E-11	-1.72606371E-15					2
1.42836134E+04	5.33000845E+00	2.87736627E+00	5.00301430E-03	-6.04370732E-06					3

	3.04738962E-09-3.87017618E-13	1.44342379E+04	9.79873919E+00	1.54669367E+04	4
S3	tpis89S 3.	0.	0.	0.G 200.000 6000.000	1
	6.53302278E+00 4.89117086E-04-1.94120477E-07	3.34257105E-11-2.09106833E-15			2
	1.53186530E+04-4.42378063E+00 2.67426151E+00	1.85725510E-02-3.39241252E-05			3
	2.89518256E-08-9.41515882E-12 1.60320458E+04	1.37269667E+01 1.74079204E+04			4
S4	tpis89S 4.	0.	0.	0.G 200.000 6000.000	1
	9.12781762E+00 9.13784446E-04-3.62719239E-07	6.24637076E-11-3.90794764E-15			2
	1.33309374E+04-1.74976107E+01 1.62124479E+00	3.69694158E-02-6.92243749E-05			3
	6.03240791E-08-1.99529262E-11 1.46879795E+04	1.76312033E+01 1.63127271E+04			4
S5	tpis89S 5.	0.	0.	0.G 200.000 6000.000	1
	1.33325960E+01 2.09782536E-04-3.36431685E-07	8.53311588E-11-6.48294924E-15			2
	1.13787913E+04-3.48611560E+01 3.27621083E+00	4.32967838E-02-8.47662885E-05			3
	8.12574426E-08-2.97793536E-11 1.36965078E+04	1.41196663E+01 1.59953327E+04			4
S6	tpis89S 6.	0.	0.	0.G 200.000 2500.000	1
	1.34043558E+01 3.42127317E-03-1.12816145E-06	1.46420087E-10-6.61286087E-15			2
	8.10860569E+03-3.42545590E+01 2.69715935E+00	6.86818730E-02-1.43788282E-04			3
	1.35427080E-07-4.71805554E-11 9.35349932E+03	1.24775267E+01 1.21853457E+04			4
S7	tpis89S 7.	0.	0.	0.G 200.000 6000.000	1
	1.78534018E+01 1.21114205E-03-4.83082305E-07	8.34576672E-11-5.23294619E-15			2
	7.80776842E+03-5.40618730E+01 2.91732736E+00	8.29649517E-02-1.73743030E-04			3
	1.63959287E-07-5.74388498E-11 1.01380200E+04	1.37221660E+01 1.34572415E+04			4
S8	tpis89S 8.	0.	0.	0.G 200.000 6000.000	1
	2.04307658E+01 5.18092908E-03-2.91895357E-06	5.97574588E-10-4.13758389E-14			2
	5.11843364E+03-6.74373075E+01 4.13158109E+00	9.43298552E-02-2.05775943E-04			3
	2.05747851E-07-7.51844045E-11 8.20318834E+03	7.83537207E+00 1.21807686E+04			4
HSD	H 10 1S 1	OG 300.00 2000.00 1000.00			1
	3.27128857E+00 5.44981982E-03-3.73779021E-06	1.30021471E-09-1.83113895E-13			2
	-3.80855081E+03 9.02814507E+00 2.69499130E+00	8.52436765E-03-9.67990492E-06			3
	6.24321861E-09-1.68282268E-12-3.72466188E+03	1.16328382E+01			4
HOS	H 10 1S 1	OG 300.00 5000.00 1442.00			1
	2.63736730E+00 7.89119090E-03-8.11726030E-06	4.24833820E-09-8.57901160E-13			2
	-1.89058621E+03 1.17096820E+01 2.63736730E+00	7.89119090E-03-8.11726030E-06			3
	4.24833820E-09-8.57901160E-13-1.89058621E+03	1.17096820E+01			4
HSDH	H 20 1S 1	OG 300.00 5000.00 1388.00			1
	0.25676441E+01 0.11380521E-01-0.58667324E-05-0.59470041E-09	0.87438329E-12			2

-0.15571256E+05	0.11766399E+02	0.25676441E+01	0.11380521E-01	-0.58667324E-05					3
-0.59470041E-09	0.87438329E-12	-0.15571256E+05	0.11766399E+02						4
HSS	H	1S	2	OG	300.00	2000.00	1000.00		1
3.59075969E+00	4.98506901E-03	-3.43045513E-06	1.19341826E-09	-1.67403033E-13					2
1.17649789E+04	8.92475572E+00	2.81672268E+00	1.03969679E-02	-1.55535096E-05					3
1.24197562E-08	-3.90834999E-12	1.18156870E+04	1.21143632E+01						4
HSS0	H	10	1S	2	OG	300.00	2000.00	1000.00	1
6.11859237E+00	5.59523243E-03	-3.70626629E-06	1.22524738E-09	-1.62789560E-13					2
-6.05886590E+03	-1.97720682E+00	2.70484711E+00	2.32126968E-02	-3.77894894E-05					3
3.04178811E-08	-9.47692405E-12	-5.52811032E+03	1.36259179E+01						4
HSSH	H	2S	2	OG	300.00	2000.00	1000.00		1
4.69311463E+00	6.01993785E-03	-3.01832133E-06	7.52297526E-10	-7.91533129E-14					2
1.72179592E+02	2.47728860E+00	2.07852476E+00	1.94742814E-02	-2.93966240E-05					3
2.37295586E-08	-7.52058161E-12	5.96292301E+02	1.44741864E+01						4
SS02	0	2S	2	OG	300.00	2000.00	1000.00		1
6.34280650E+00	6.05027505E-03	-4.24571996E-06	1.40852829E-09	-1.81318004E-13					2
-2.27684952E+04	-3.78737520E+00	2.80168627E+00	1.99919280E-02	-2.56401242E-05					3
1.65559742E-08	-4.33620009E-12	-2.20225598E+04	1.34189370E+01						4
HSS02	H	10	2S	2	OG	300.00	2000.00	1000.00	1
7.76282262E+00	7.02637234E-03	-4.08428794E-06	1.12459784E-09	-1.18489230E-13					2
-2.33271862E+04	-9.48284274E+00	3.49856646E+00	2.50749289E-02	-3.40614452E-05					3
2.40531480E-08	-6.85626593E-12	-2.24794312E+04	1.09552126E+01						4
OSS0	0	2S	2	OG	300.00	2000.00	1000.00		1
8.06932897E+00	2.78600929E-03	-1.65788135E-06	4.55717434E-10	-4.76687943E-14					2
-1.68597542E+04	-1.12637659E+01	4.27684328E+00	1.71764292E-02	-2.30032367E-05					3
1.50850596E-08	-3.93335889E-12	-1.60275576E+04	7.31095245E+00						4
VDW1	H	20	3S	1	G	300.00	5000.00	1000.00	1
1.01262222E+01	3.57132793E-03	-7.13009073E-09	-5.82222901E-10	1.37375969E-13					2
-6.93881691E+04	-1.74036743E+01	8.13179120E+00	8.32444914E-03	-2.04192137E-06					3
-2.95153810E-09	1.78217150E-12	-6.88287103E+04	-6.98378761E+00						4
H2S202	H	20	2S	2	G	300.00	5000.00	1000.00	1
1.16213004E+01	3.43806006E-03	-5.74448284E-07	-3.13293096E-10	1.00662179E-13					2
-3.91048380E+04	-2.90177401E+01	8.28112013E-01	4.74477762E-02	-6.95648159E-05					3
4.87812487E-08	-1.32222441E-11	-3.69287907E+04	2.29903159E+01						4
S20	S	20	1	G	300.00	5000.00	1000.00		1


```

5.69256178E+00 1.42823665E-03-3.95223981E-07-9.64670639E-11 4.47355230E-14 2
-8.82970515E+03-1.14896126E+00 2.89887583E+00 1.15443527E-02-1.46502127E-05 3
9.19411666E-09-2.31495134E-12-8.19312607E+03 1.26535745E+01 4
H2S3O          H   20   1S   3   G   300.00  5000.00 1000.00 1
1.18514105E+01 3.33850673E-03-6.86562800E-07-2.02600304E-10 7.47780445E-14 2
-1.28853402E+04-2.85026663E+01 3.67805059E+00 4.07191390E-02-6.67990246E-05 3
5.28547092E-08-1.60811288E-11-1.13979874E+04 9.98571106E+00 4
HSSSOH          H   20   1S   3   G   300.00  5000.00 1000.00 1
1.10809208E+01 3.73387762E-03-2.44411342E-07-6.13453741E-10 1.64649581E-13 2
-1.78355780E+04-2.35331548E+01 2.93988478E+00 4.05695638E-02-6.59918573E-05 3
5.33283075E-08-1.67311298E-11-1.63029028E+04 1.49845285E+01 4
O3              L 5/900  3   0   0   OG  200.000  6000.000 1000. 1
1.23302914E+01-1.19324783E-02 7.98741278E-06-1.77194552E-09 1.26075824E-13 2
1.26755831E+04-4.08823374E+01 3.40738221E+00 2.05379063E-03 1.38486052E-05 3
-2.23311542E-08 9.76073226E-12 1.58644979E+04 8.28247580E+00 1.70545228E+04 4
HE              120186HE 1           G 0300.00  5000.00 1000.00 1
0.02500000E+02 0.00000000E+00 0.00000000E+00 0.00000000E+00 0.00000000E+00 2
-0.07453750E+04 0.09153489E+01 0.02500000E+02 0.00000000E+00 0.00000000E+00 3
0.00000000E+00 0.00000000E+00-0.07453750E+04 0.09153488E+01 4
END

```

A.2.2 Chemical Kinetic Data

The chemical kinetic data is given in CHEMKIN format. The pre-exponential factor A is given in units of cm-mol-s-K. The activation energy E is given in units of cal/mol.

```

! Sour Gas Mechanism 9/30/2013 by Dominik Bongartz (dominikb@mit.edu)
! Composed of:
!
! 1. GRI-Mech Version 3.0 7/30/99 CHEMKIN-II format
! See README30 file at anonymous FTP site unix.sri.com, directory gri;
! WorldWideWeb home page http://www.me.berkeley.edu/gri_mech/ or
! through http://www.gri.org , under 'Basic Research',
! for additional information, contacts, and disclaimer
!
! 2. Sulfur mechanism by Zhou et.al. Proc. Comb. Inst. 2013

```

! (deleted reactions 217-248 from the Zhou mechanism
! because these are O-H reactions which should be
! covered by the GRI mech)
!
! 3. Since the heat of formation of SH was changed to 33.8kcal/mol, the
! high pressure rate parameters for 2SH(+M)=HSSH(+M) had to be adjusted
! (9/14/2013)
!
! 4. Ten sulfur reactions were modified in a systematic optimization
! ('Optimization 1-12')

ELEMENTS

O H C N AR S HE

END

SPECIES

H2	H	O	O2	OH	H2O	H02	H2O2
C	CH	CH2	CH2(S)	CH3	CH4	CO	CO2
HCO	CH2O	CH2OH	CH3O	CH3OH	C2H	C2H2	C2H3
C2H4	C2H5	C2H6	HCCO	CH2CO	HCCOH	N	NH
NH2	NH3	NNH	NO	NO2	N2O	HNO	CN
HCN	H2CN	HCNN	HCNO	HOCN	HNCO	NCO	N2
AR	C3H7	C3H8	CH2CHO	CH3CHO	S	SH	H2S
SO	SO*	SO2	SO3	HSO2	HOSO	HSO0	HOSO2
S2	S3	S4	S5	S6	S7	S8	HSO
HOS	HSOH	HSS	HSSH	SSO2	HSSO2	OSSO	VDW1
H2S2O2	S2O	H2S3O	HSSO	HSSSOH	O3	HE	

END

REACTIONS

!----- GRI Mech 3.0 -----
2O+M<=>O2+M 1.200E+17 -1.000 .00
H2/ 2.40/ H2O/15.40/ CH4/ 2.00/ CO/ 1.75/ CO2/ 3.60/ C2H6/ 3.00/ AR/ .83/
O+H+M<=>OH+M 5.000E+17 -1.000 .00
H2/2.00/ H2O/6.00/ CH4/2.00/ CO/1.50/ CO2/2.00/ C2H6/3.00/ AR/ .70/
O+H2<=>H+OH 3.870E+04 2.700 6260.00
O+H02<=>OH+O2 2.000E+13 .000 .00

O+H2O2<=>OH+HO2	9.630E+06	2.000	4000.00
O+CH<=>H+CO	5.700E+13	.000	.00
O+CH2<=>H+HCO	8.000E+13	.000	.00
O+CH2(S)<=>H2+CO	1.500E+13	.000	.00
O+CH2(S)<=>H+HCO	1.500E+13	.000	.00
O+CH3<=>H+CH2O	5.060E+13	.000	.00
O+CH4<=>OH+CH3	1.020E+09	1.500	8600.00
O+CO(+M)<=>CO2(+M)	1.800E+10	.000	2385.00
LOW/ 6.020E+14	.000	3000.00/	
H2/2.00/ O2/6.00/ H2O/6.00/ CH4/2.00/ CO/1.50/ CO2/3.50/ C2H6/3.00/ AR/ .50/			
O+HCO<=>OH+CO	3.000E+13	.000	.00
O+HCO<=>H+CO2	3.000E+13	.000	.00
O+CH2O<=>OH+HCO	3.900E+13	.000	3540.00
O+CH2OH<=>OH+CH2O	1.000E+13	.000	.00
O+CH3O<=>OH+CH2O	1.000E+13	.000	.00
O+CH3OH<=>OH+CH2OH	3.880E+05	2.500	3100.00
O+CH3OH<=>OH+CH3O	1.300E+05	2.500	5000.00
O+C2H<=>CH+CO	5.000E+13	.000	.00
O+C2H2<=>H+HCCO	1.350E+07	2.000	1900.00
O+C2H2<=>OH+C2H	4.600E+19	-1.410	28950.00
O+C2H2<=>CO+CH2	6.940E+06	2.000	1900.00
O+C2H3<=>H+CH2CO	3.000E+13	.000	.00
O+C2H4<=>CH3+HCO	1.250E+07	1.830	220.00
O+C2H5<=>CH3+CH2O	2.240E+13	.000	.00
O+C2H6<=>OH+C2H5	8.980E+07	1.920	5690.00
O+HCCO<=>H+2CO	1.000E+14	.000	.00
O+CH2CO<=>OH+HCCO	1.000E+13	.000	8000.00
O+CH2CO<=>CH2+CO2	1.750E+12	.000	1350.00
O2+CO<=>O+CO2	2.500E+12	.000	47800.00
O2+CH2O<=>HO2+HCO	1.000E+14	.000	40000.00
H+O2+M<=>HO2+M	2.800E+18	-.860	.00
O2/ .00/ H2O/ .00/ CO/ .75/ CO2/1.50/ C2H6/1.50/ N2/ .00/ AR/ .00/			
H+2O2<=>HO2+O2	2.080E+19	-1.240	.00
H+O2+H2O<=>HO2+H2O	11.26E+18	-.760	.00
H+O2+N2<=>HO2+N2	2.600E+19	-1.240	.00

H+O2+AR<=>H02+AR	7.000E+17	-.800	.00
H+O2<=>O+OH	2.650E+16	-.6707	17041.00
2H+M<=>H2+M	1.000E+18	-1.000	.00
H2/ .00/ H2O/ .00/ CH4/2.00/ CO2/ .00/ C2H6/3.00/ AR/ .63/			
2H+H2<=>2H2	9.000E+16	-.600	.00
2H+H2O<=>H2+H2O	6.000E+19	-1.250	.00
2H+CO2<=>H2+CO2	5.500E+20	-2.000	.00
H+OH+M<=>H2O+M	2.200E+22	-2.000	.00
H2/ .73/ H2O/3.65/ CH4/2.00/ C2H6/3.00/ AR/ .38/			
H+H02<=>O+H2O	3.970E+12	.000	671.00
H+H02<=>O2+H2	4.480E+13	.000	1068.00
H+H02<=>2OH	0.840E+14	.000	635.00
H+H2O2<=>H02+H2	1.210E+07	2.000	5200.00
H+H2O2<=>OH+H2O	1.000E+13	.000	3600.00
H+CH<=>C+H2	1.650E+14	.000	.00
H+CH2(+M)<=>CH3(+M)	6.000E+14	.000	.00
LOW /	1.040E+26	-2.760	1600.00/
TROE/	.5620	91.00	5836.00 8552.00/
H2/2.00/ H2O/6.00/ CH4/2.00/ CO/1.50/ CO2/2.00/ C2H6/3.00/ AR/ .70/			
H+CH2(S)<=>CH+H2	3.000E+13	.000	.00
H+CH3(+M)<=>CH4(+M)	13.90E+15	-.534	536.00
LOW /	2.620E+33	-4.760	2440.00/
TROE/	.7830	74.00	2941.00 6964.00 /
H2/2.00/ H2O/6.00/ CH4/3.00/ CO/1.50/ CO2/2.00/ C2H6/3.00/ AR/ .70/			
H+CH4<=>CH3+H2	6.600E+08	1.620	10840.00
H+HCO(+M)<=>CH2O(+M)	1.090E+12	.480	-260.00
LOW /	2.470E+24	-2.570	425.00/
TROE/	.7824	271.00	2755.00 6570.00 /
H2/2.00/ H2O/6.00/ CH4/2.00/ CO/1.50/ CO2/2.00/ C2H6/3.00/ AR/ .70/			
H+HCO<=>H2+CO	7.340E+13	.000	.00
H+CH2O(+M)<=>CH2OH(+M)	5.400E+11	.454	3600.00
LOW /	1.270E+32	-4.820	6530.00/
TROE/	.7187	103.00	1291.00 4160.00 /
H2/2.00/ H2O/6.00/ CH4/2.00/ CO/1.50/ CO2/2.00/ C2H6/3.00/			
H+CH2O(+M)<=>CH3O(+M)	5.400E+11	.454	2600.00

LOW / 2.200E+30 -4.800 5560.00/
 TROE/ .7580 94.00 1555.00 4200.00 /
 H2/2.00/ H2O/6.00/ CH4/2.00/ CO/1.50/ CO2/2.00/ C2H6/3.00/
 H+CH2O<=>HCO+H2 5.740E+07 1.900 2742.00
 H+CH2OH(+M)<=>CH3OH(+M) 1.055E+12 .500 86.00
 LOW / 4.360E+31 -4.650 5080.00/
 TROE/ .600 100.00 90000.0 10000.0 /
 H2/2.00/ H2O/6.00/ CH4/2.00/ CO/1.50/ CO2/2.00/ C2H6/3.00/
 H+CH2OH<=>H2+CH2O 2.000E+13 .000 .00
 H+CH2OH<=>OH+CH3 1.650E+11 .650 -284.00
 H+CH2OH<=>CH2(S)+H2O 3.280E+13 -.090 610.00
 H+CH3O(+M)<=>CH3OH(+M) 2.430E+12 .515 50.00
 LOW / 4.660E+41 -7.440 14080.0/
 TROE/ .700 100.00 90000.0 10000.00 /
 H2/2.00/ H2O/6.00/ CH4/2.00/ CO/1.50/ CO2/2.00/ C2H6/3.00/
 H+CH3O<=>H+CH2OH 4.150E+07 1.630 1924.00
 H+CH3O<=>H2+CH2O 2.000E+13 .000 .00
 H+CH3O<=>OH+CH3 1.500E+12 .500 -110.00
 H+CH3O<=>CH2(S)+H2O 2.620E+14 -.230 1070.00
 H+CH3OH<=>CH2OH+H2 1.700E+07 2.100 4870.00
 H+CH3OH<=>CH3O+H2 4.200E+06 2.100 4870.00
 H+C2H(+M)<=>C2H2(+M) 1.000E+17 -1.000 .00
 LOW / 3.750E+33 -4.800 1900.00/
 TROE/ .6464 132.00 1315.00 5566.00 /
 H2/2.00/ H2O/6.00/ CH4/2.00/ CO/1.50/ CO2/2.00/ C2H6/3.00/ AR/ .70/
 H+C2H2(+M)<=>C2H3(+M) 5.600E+12 .000 2400.00
 LOW / 3.800E+40 -7.270 7220.00/
 TROE/ .7507 98.50 1302.00 4167.00 /
 H2/2.00/ H2O/6.00/ CH4/2.00/ CO/1.50/ CO2/2.00/ C2H6/3.00/ AR/ .70/
 H+C2H3(+M)<=>C2H4(+M) 6.080E+12 .270 280.00
 LOW / 1.400E+30 -3.860 3320.00/
 TROE/ .7820 207.50 2663.00 6095.00 /
 H2/2.00/ H2O/6.00/ CH4/2.00/ CO/1.50/ CO2/2.00/ C2H6/3.00/ AR/ .70/
 H+C2H3<=>H2+C2H2 3.000E+13 .000 .00
 H+C2H4(+M)<=>C2H5(+M) 0.540E+12 .454 1820.00

LOW /	0.600E+42	-7.620	6970.00/		
TROE/	.9753	210.00	984.00	4374.00 /	
H2/2.00/ H2O/6.00/ CH4/2.00/ CO/1.50/ CO2/2.00/ C2H6/3.00/ AR/ .70/					
H+C2H4<=>C2H3+H2			1.325E+06	2.530	12240.00
H+C2H5(+M)<=>C2H6(+M)			5.210E+17	-.990	1580.00
LOW /	1.990E+41	-7.080	6685.00/		
TROE/	.8422	125.00	2219.00	6882.00 /	
H2/2.00/ H2O/6.00/ CH4/2.00/ CO/1.50/ CO2/2.00/ C2H6/3.00/ AR/ .70/					
H+C2H5<=>H2+C2H4			2.000E+12	.000	.00
H+C2H6<=>C2H5+H2			1.150E+08	1.900	7530.00
H+HCCO<=>CH2(S)+CO			1.000E+14	.000	.00
H+CH2CO<=>HCCO+H2			5.000E+13	.000	8000.00
H+CH2CO<=>CH3+CO			1.130E+13	.000	3428.00
H+HCCOH<=>H+CH2CO			1.000E+13	.000	.00
H2+CO(+M)<=>CH2O(+M)			4.300E+07	1.500	79600.00
LOW /	5.070E+27	-3.420	84350.00/		
TROE/	.9320	197.00	1540.00	10300.00 /	
H2/2.00/ H2O/6.00/ CH4/2.00/ CO/1.50/ CO2/2.00/ C2H6/3.00/ AR/ .70/					
OH+H2<=>H+H2O			2.160E+08	1.510	3430.00
2OH(+M)<=>H2O2(+M)			7.400E+13	-.370	.00
LOW /	2.300E+18	-.900	-1700.00/		
TROE/	.7346	94.00	1756.00	5182.00 /	
H2/2.00/ H2O/6.00/ CH4/2.00/ CO/1.50/ CO2/2.00/ C2H6/3.00/ AR/ .70/					
2OH<=>O+H2O			3.570E+04	2.400	-2110.00
OH+HO2<=>O2+H2O			1.450E+13	.000	-500.00
DUPLICATE					
OH+H2O2<=>HO2+H2O			2.000E+12	.000	427.00
DUPLICATE					
OH+H2O2<=>HO2+H2O			1.700E+18	.000	29410.00
DUPLICATE					
OH+C<=>H+CO			5.000E+13	.000	.00
OH+CH<=>H+HCO			3.000E+13	.000	.00
OH+CH2<=>H+CH2O			2.000E+13	.000	.00
OH+CH2<=>CH+H2O			1.130E+07	2.000	3000.00
OH+CH2(S)<=>H+CH2O			3.000E+13	.000	.00

OH+CH3(+M)<=>CH3OH(+M)	2.790E+18	-1.430	1330.00
LOW / 4.000E+36	-5.920	3140.00/	
TR0E/ .4120	195.0	5900.00	6394.00/
H2/2.00/ H2O/6.00/ CH4/2.00/ CO/1.50/ CO2/2.00/ C2H6/3.00/			
OH+CH3<=>CH2+H2O	5.600E+07	1.600	5420.00
OH+CH3<=>CH2(S)+H2O	6.440E+17	-1.340	1417.00
OH+CH4<=>CH3+H2O	1.000E+08	1.600	3120.00
OH+CO<=>H+CO2	4.760E+07	1.228	70.00
OH+HCO<=>H2O+CO	5.000E+13	.000	.00
OH+CH2O<=>HCO+H2O	3.430E+09	1.180	-447.00
OH+CH2OH<=>H2O+CH2O	5.000E+12	.000	.00
OH+CH3O<=>H2O+CH2O	5.000E+12	.000	.00
OH+CH3OH<=>CH2OH+H2O	1.440E+06	2.000	-840.00
OH+CH3OH<=>CH3O+H2O	6.300E+06	2.000	1500.00
OH+C2H<=>H+HCCO	2.000E+13	.000	.00
OH+C2H2<=>H+CH2CO	2.180E-04	4.500	-1000.00
OH+C2H2<=>H+HCCOH	5.040E+05	2.300	13500.00
OH+C2H2<=>C2H+H2O	3.370E+07	2.000	14000.00
OH+C2H2<=>CH3+CO	4.830E-04	4.000	-2000.00
OH+C2H3<=>H2O+C2H2	5.000E+12	.000	.00
OH+C2H4<=>C2H3+H2O	3.600E+06	2.000	2500.00
OH+C2H6<=>C2H5+H2O	3.540E+06	2.120	870.00
OH+CH2CO<=>HCCO+H2O	7.500E+12	.000	2000.00
2HO2<=>O2+H2O2	1.300E+11	.000	-1630.00
DUPLICATE			
2HO2<=>O2+H2O2	4.200E+14	.000	12000.00
DUPLICATE			
HO2+CH2<=>OH+CH2O	2.000E+13	.000	.00
HO2+CH3<=>O2+CH4	1.000E+12	.000	.00
HO2+CH3<=>OH+CH3O	3.780E+13	.000	.00
HO2+CO<=>OH+CO2	1.500E+14	.000	23600.00
HO2+CH2O<=>HCO+H2O2	5.600E+06	2.000	12000.00
C+O2<=>O+CO	5.800E+13	.000	576.00
C+CH2<=>H+C2H	5.000E+13	.000	.00
C+CH3<=>H+C2H2	5.000E+13	.000	.00

CH+O2<=>O+HCO	6.710E+13	.000	.00
CH+H2<=>H+CH2	1.080E+14	.000	3110.00
CH+H2O<=>H+CH2O	5.710E+12	.000	-755.00
CH+CH2<=>H+C2H2	4.000E+13	.000	.00
CH+CH3<=>H+C2H3	3.000E+13	.000	.00
CH+CH4<=>H+C2H4	6.000E+13	.000	.00
CH+CO(+M)<=>HCCO(+M)	5.000E+13	.000	.00
LOW /	2.690E+28	-3.740	1936.00/
TR0E/	.5757	237.00	1652.00 5069.00 /
H2/2.00/ H2O/6.00/ CH4/2.00/ CO/1.50/ CO2/2.00/ C2H6/3.00/ AR/ .70/			
CH+CO2<=>HCO+CO	1.900E+14	.000	15792.00
CH+CH2O<=>H+CH2CO	9.460E+13	.000	-515.00
CH+HCCO<=>CO+C2H2	5.000E+13	.000	.00
CH2+O2=>OH+H+CO	5.000E+12	.000	1500.00
CH2+H2<=>H+CH3	5.000E+05	2.000	7230.00
2CH2<=>H2+C2H2	1.600E+15	.000	11944.00
CH2+CH3<=>H+C2H4	4.000E+13	.000	.00
CH2+CH4<=>2CH3	2.460E+06	2.000	8270.00
CH2+CO(+M)<=>CH2CO(+M)	8.100E+11	.500	4510.00
LOW /	2.690E+33	-5.110	7095.00/
TR0E/	.5907	275.00	1226.00 5185.00 /
H2/2.00/ H2O/6.00/ CH4/2.00/ CO/1.50/ CO2/2.00/ C2H6/3.00/ AR/ .70/			
CH2+HCCO<=>C2H3+CO	3.000E+13	.000	.00
CH2(S)+N2<=>CH2+N2	1.500E+13	.000	600.00
CH2(S)+AR<=>CH2+AR	9.000E+12	.000	600.00
CH2(S)+O2<=>H+OH+CO	2.800E+13	.000	.00
CH2(S)+O2<=>CO+H2O	1.200E+13	.000	.00
CH2(S)+H2<=>CH3+H	7.000E+13	.000	.00
CH2(S)+H2O(+M)<=>CH3OH(+M)	4.820E+17	-1.160	1145.00
LOW /	1.880E+38	-6.360	5040.00/
TR0E/	.6027	208.00	3922.00 10180.0 /
H2/2.00/ H2O/6.00/ CH4/2.00/ CO/1.50/ CO2/2.00/ C2H6/3.00/			
CH2(S)+H2O<=>CH2+H2O	3.000E+13	.000	.00
CH2(S)+CH3<=>H+C2H4	1.200E+13	.000	-570.00
CH2(S)+CH4<=>2CH3	1.600E+13	.000	-570.00

CH2(S)+CO<=>CH2+CO	9.000E+12	.000	.00
CH2(S)+CO2<=>CH2+CO2	7.000E+12	.000	.00
CH2(S)+CO2<=>CO+CH2O	1.400E+13	.000	.00
CH2(S)+C2H6<=>CH3+C2H5	4.000E+13	.000	-550.00
CH3+O2<=>O+CH3O	3.560E+13	.000	30480.00
CH3+O2<=>OH+CH2O	2.310E+12	.000	20315.00
CH3+H2O2<=>HO2+CH4	2.450E+04	2.470	5180.00
2CH3(+M)<=>C2H6(+M)	6.770E+16	-1.180	654.00

LOW / 3.400E+41 -7.030 2762.00/

TROE/ .6190 73.20 1180.00 9999.00 /

H2/2.00/ H2O/6.00/ CH4/2.00/ CO/1.50/ CO2/2.00/ C2H6/3.00/ AR/ .70/

2CH3<=>H+C2H5	6.840E+12	.100	10600.00
CH3+HCO<=>CH4+CO	2.648E+13	.000	.00
CH3+CH2O<=>HCO+CH4	3.320E+03	2.810	5860.00
CH3+CH3OH<=>CH2OH+CH4	3.000E+07	1.500	9940.00
CH3+CH3OH<=>CH3O+CH4	1.000E+07	1.500	9940.00
CH3+C2H4<=>C2H3+CH4	2.270E+05	2.000	9200.00
CH3+C2H6<=>C2H5+CH4	6.140E+06	1.740	10450.00
HCO+H2O<=>H+CO+H2O	1.500E+18	-1.000	17000.00
HCO+M<=>H+CO+M	1.870E+17	-1.000	17000.00

H2/2.00/ H2O/ .00/ CH4/2.00/ CO/1.50/ CO2/2.00/ C2H6/3.00/

HCO+O2<=>HO2+CO	13.45E+12	.000	400.00
CH2OH+O2<=>HO2+CH2O	1.800E+13	.000	900.00
CH3O+O2<=>HO2+CH2O	4.280E-13	7.600	-3530.00
C2H+O2<=>HCO+CO	1.000E+13	.000	-755.00
C2H+H2<=>H+C2H2	5.680E+10	0.900	1993.00
C2H3+O2<=>HCO+CH2O	4.580E+16	-1.390	1015.00
C2H4(+M)<=>H2+C2H2(+M)	8.000E+12	.440	86770.00

LOW / 1.580E+51 -9.300 97800.00/

TROE/ .7345 180.00 1035.00 5417.00 /

H2/2.00/ H2O/6.00/ CH4/2.00/ CO/1.50/ CO2/2.00/ C2H6/3.00/ AR/ .70/

C2H5+O2<=>HO2+C2H4	8.400E+11	.000	3875.00
HCCO+O2<=>OH+2CO	3.200E+12	.000	854.00
2HCCO<=>2CO+C2H2	1.000E+13	.000	.00
N+NO<=>N2+O	2.700E+13	.000	355.00

N+O2<=>NO+O	9.000E+09	1.000	6500.00
N+OH<=>NO+H	3.360E+13	.000	385.00
N2O+O<=>N2+O2	1.400E+12	.000	10810.00
N2O+O<=>2NO	2.900E+13	.000	23150.00
N2O+H<=>N2+OH	3.870E+14	.000	18880.00
N2O+OH<=>N2+HO2	2.000E+12	.000	21060.00
N2O(+M)<=>N2+O(+M)	7.910E+10	.000	56020.00
LOW / 6.370E+14	.000	56640.00/	
H2/2.00/ H2O/6.00/ CH4/2.00/ CO/1.50/ CO2/2.00/ C2H6/3.00/ AR/ .625/			
HO2+NO<=>NO2+OH	2.110E+12	.000	-480.00
NO+O+M<=>NO2+M	1.060E+20	-1.410	.00
H2/2.00/ H2O/6.00/ CH4/2.00/ CO/1.50/ CO2/2.00/ C2H6/3.00/ AR/ .70/			
NO2+O<=>NO+O2	3.900E+12	.000	-240.00
NO2+H<=>NO+OH	1.320E+14	.000	360.00
NH+O<=>NO+H	4.000E+13	.000	.00
NH+H<=>N+H2	3.200E+13	.000	330.00
NH+OH<=>HNO+H	2.000E+13	.000	.00
NH+OH<=>N+H2O	2.000E+09	1.200	.00
NH+O2<=>HNO+O	4.610E+05	2.000	6500.00
NH+O2<=>NO+OH	1.280E+06	1.500	100.00
NH+N<=>N2+H	1.500E+13	.000	.00
NH+H2O<=>HNO+H2	2.000E+13	.000	13850.00
NH+NO<=>N2+OH	2.160E+13	-.230	.00
NH+NO<=>N2O+H	3.650E+14	-.450	.00
NH2+O<=>OH+NH	3.000E+12	.000	.00
NH2+O<=>H+HNO	3.900E+13	.000	.00
NH2+H<=>NH+H2	4.000E+13	.000	3650.00
NH2+OH<=>NH+H2O	9.000E+07	1.500	-460.00
NNH<=>N2+H	3.300E+08	.000	.00
NNH+M<=>N2+H+M	1.300E+14	-.110	4980.00
H2/2.00/ H2O/6.00/ CH4/2.00/ CO/1.50/ CO2/2.00/ C2H6/3.00/ AR/ .70/			
NNH+O2<=>HO2+N2	5.000E+12	.000	.00
NNH+O<=>OH+N2	2.500E+13	.000	.00
NNH+O<=>NH+NO	7.000E+13	.000	.00
NNH+H<=>H2+N2	5.000E+13	.000	.00

NNH+OH<=>H2O+N2	2.000E+13	.000	.00
NNH+CH3<=>CH4+N2	2.500E+13	.000	.00
H+NO+M<=>HNO+M	4.480E+19	-1.320	740.00
H2/2.00/ H2O/6.00/ CH4/2.00/ CO/1.50/ CO2/2.00/ C2H6/3.00/ AR/ .70/			
HNO+O<=>NO+OH	2.500E+13	.000	.00
HNO+H<=>H2+NO	9.000E+11	.720	660.00
HNO+OH<=>NO+H2O	1.300E+07	1.900	-950.00
HNO+O2<=>HO2+NO	1.000E+13	.000	13000.00
CN+O<=>CO+N	7.700E+13	.000	.00
CN+OH<=>NCO+H	4.000E+13	.000	.00
CN+H2O<=>HCN+OH	8.000E+12	.000	7460.00
CN+O2<=>NCO+O	6.140E+12	.000	-440.00
CN+H2<=>HCN+H	2.950E+05	2.450	2240.00
NCO+O<=>NO+CO	2.350E+13	.000	.00
NCO+H<=>NH+CO	5.400E+13	.000	.00
NCO+OH<=>NO+H+CO	0.250E+13	.000	.00
NCO+N<=>N2+CO	2.000E+13	.000	.00
NCO+O2<=>NO+CO2	2.000E+12	.000	20000.00
NCO+M<=>N+CO+M	3.100E+14	.000	54050.00
H2/2.00/ H2O/6.00/ CH4/2.00/ CO/1.50/ CO2/2.00/ C2H6/3.00/ AR/ .70/			
NCO+NO<=>N2O+CO	1.900E+17	-1.520	740.00
NCO+NO<=>N2+CO2	3.800E+18	-2.000	800.00
HCN+M<=>H+CN+M	1.040E+29	-3.300	126600.00
H2/2.00/ H2O/6.00/ CH4/2.00/ CO/1.50/ CO2/2.00/ C2H6/3.00/ AR/ .70/			
HCN+O<=>NCO+H	2.030E+04	2.640	4980.00
HCN+O<=>NH+CO	5.070E+03	2.640	4980.00
HCN+O<=>CN+OH	3.910E+09	1.580	26600.00
HCN+OH<=>HOCN+H	1.100E+06	2.030	13370.00
HCN+OH<=>HNCO+H	4.400E+03	2.260	6400.00
HCN+OH<=>NH2+CO	1.600E+02	2.560	9000.00
H+HCN(+M)<=>H2CN(+M)	3.300E+13	.000	.00
LOW /	1.400E+26	-3.400	1900.00/
H2/2.00/ H2O/6.00/ CH4/2.00/ CO/1.50/ CO2/2.00/ C2H6/3.00/ AR/ .70/			
H2CN+N<=>N2+CH2	6.000E+13	.000	400.00
C+N2<=>CN+N	6.300E+13	.000	46020.00

CH+N2<=>HCN+N	3.120E+09	0.880	20130.00
CH+N2(+M)<=>HCNN(+M)	3.100E+12	.150	.00
LOW /	1.300E+25	-3.160	740.00/
TROE/	.6670	235.00	2117.00 4536.00 /
H2/2.00/ H2O/6.00/ CH4/2.00/ CO/1.50/ CO2/2.00/ C2H6/3.00/ AR/ 1.0/			
CH2+N2<=>HCN+NH	1.000E+13	.000	74000.00
CH2(S)+N2<=>NH+HCN	1.000E+11	.000	65000.00
C+NO<=>CN+O	1.900E+13	.000	.00
C+NO<=>CO+N	2.900E+13	.000	.00
CH+NO<=>HCN+O	4.100E+13	.000	.00
CH+NO<=>H+NCO	1.620E+13	.000	.00
CH+NO<=>N+HCO	2.460E+13	.000	.00
CH2+NO<=>H+HNCO	3.100E+17	-1.380	1270.00
CH2+NO<=>OH+HCN	2.900E+14	-.690	760.00
CH2+NO<=>H+HCNO	3.800E+13	-.360	580.00
CH2(S)+NO<=>H+HNCO	3.100E+17	-1.380	1270.00
CH2(S)+NO<=>OH+HCN	2.900E+14	-.690	760.00
CH2(S)+NO<=>H+HCNO	3.800E+13	-.360	580.00
CH3+NO<=>HCN+H2O	9.600E+13	.000	28800.00
CH3+NO<=>H2CN+OH	1.000E+12	.000	21750.00
HCNN+O<=>CO+H+N2	2.200E+13	.000	.00
HCNN+O<=>HCN+NO	2.000E+12	.000	.00
HCNN+O2<=>O+HCO+N2	1.200E+13	.000	.00
HCNN+OH<=>H+HCO+N2	1.200E+13	.000	.00
HCNN+H<=>CH2+N2	1.000E+14	.000	.00
HNCO+O<=>NH+CO2	9.800E+07	1.410	8500.00
HNCO+O<=>HNO+CO	1.500E+08	1.570	44000.00
HNCO+O<=>NCO+OH	2.200E+06	2.110	11400.00
HNCO+H<=>NH2+CO	2.250E+07	1.700	3800.00
HNCO+H<=>H2+NCO	1.050E+05	2.500	13300.00
HNCO+OH<=>NCO+H2O	3.300E+07	1.500	3600.00
HNCO+OH<=>NH2+CO2	3.300E+06	1.500	3600.00
HNCO+M<=>NH+CO+M	1.180E+16	.000	84720.00
H2/2.00/ H2O/6.00/ CH4/2.00/ CO/1.50/ CO2/2.00/ C2H6/3.00/ AR/ .70/			
HCNO+H<=>H+HNCO	2.100E+15	-.690	2850.00

HCNO+H<=>OH+HCN	2.700E+11	.180	2120.00
HCNO+H<=>NH2+CO	1.700E+14	-.750	2890.00
HOCN+H<=>H+HNCO	2.000E+07	2.000	2000.00
HCCO+NO<=>HCNO+CO	0.900E+13	.000	.00
CH3+N<=>H2CN+H	6.100E+14	-.310	290.00
CH3+N<=>HCN+H2	3.700E+12	.150	-90.00
NH3+H<=>NH2+H2	5.400E+05	2.400	9915.00
NH3+OH<=>NH2+H2O	5.000E+07	1.600	955.00
NH3+O<=>NH2+OH	9.400E+06	1.940	6460.00
NH+CO2<=>HNO+CO	1.000E+13	.000	14350.00
CN+NO2<=>NCO+NO	6.160E+15	-0.752	345.00
NCO+NO2<=>N2O+CO2	3.250E+12	.000	-705.00
N+CO2<=>NO+CO	3.000E+12	.000	11300.00
O+CH3=>H+H2+CO	3.370E+13	.000	.00
O+C2H4<=>H+CH2CHO	6.700E+06	1.830	220.00
O+C2H5<=>H+CH3CHO	1.096E+14	.000	.00
OH+HO2<=>O2+H2O	0.500E+16	.000	17330.00
DUPLICATE			
OH+CH3=>H2+CH2O	8.000E+09	.500	-1755.00
CH+H2(+M)<=>CH3(+M)	1.970E+12	.430	-370.00
LOW/ 4.820E+25 -2.80 590.0 /			
TROE/ .578 122.0 2535.0 9365.0 /			
H2/2.00/ H2O/6.00/ CH4/2.00/ CO/1.50/ CO2/2.00/ C2H6/3.00/ AR/ .70/			
CH2+O2=>2H+CO2	5.800E+12	.000	1500.00
CH2+O2<=>O+CH2O	2.400E+12	.000	1500.00
CH2+CH2=>2H+C2H2	2.000E+14	.000	10989.00
CH2(S)+H2O=>H2+CH2O	6.820E+10	.250	-935.00
C2H3+O2<=>O+CH2CHO	3.030E+11	.290	11.00
C2H3+O2<=>HO2+C2H2	1.337E+06	1.610	-384.00
O+CH3CHO<=>OH+CH2CHO	2.920E+12	.000	1808.00
O+CH3CHO=>OH+CH3+CO	2.920E+12	.000	1808.00
O2+CH3CHO=>HO2+CH3+CO	3.010E+13	.000	39150.00
H+CH3CHO<=>CH2CHO+H2	2.050E+09	1.160	2405.00
H+CH3CHO=>CH3+H2+CO	2.050E+09	1.160	2405.00
OH+CH3CHO=>CH3+H2O+CO	2.343E+10	0.730	-1113.00

H02+CH3CHO=>CH3+H2O2+CO	3.010E+12	.000	11923.00
CH3+CH3CHO=>CH3+CH4+CO	2.720E+06	1.770	5920.00
H+CH2CO(+M)<=>CH2CHO(+M)	4.865E+11	0.422	-1755.00

LOW/ 1.012E+42 -7.63 3854.0/

TROE/ 0.465 201.0 1773.0 5333.0 /

H2/2.00/ H2O/6.00/ CH4/2.00/ CO/1.50/ CO2/2.00/ C2H6/3.00/ AR/ .70/

O+CH2CHO=>H+CH2+CO2	1.500E+14	.000	.00
O2+CH2CHO=>OH+CO+CH2O	1.810E+10	.000	.00
O2+CH2CHO=>OH+2HCO	2.350E+10	.000	.00
H+CH2CHO<=>CH3+HCO	2.200E+13	.000	.00
H+CH2CHO<=>CH2CO+H2	1.100E+13	.000	.00
OH+CH2CHO<=>H2O+CH2CO	1.200E+13	.000	.00
OH+CH2CHO<=>HCO+CH2OH	3.010E+13	.000	.00
CH3+C2H5(+M)<=>C3H8(+M)	.9430E+13	.000	.00

LOW/ 2.710E+74 -16.82 13065.0 /

TROE/ .1527 291.0 2742.0 7748.0 /

H2/2.00/ H2O/6.00/ CH4/2.00/ CO/1.50/ CO2/2.00/ C2H6/3.00/ AR/ .70/

O+C3H8<=>OH+C3H7	1.930E+05	2.680	3716.00
H+C3H8<=>C3H7+H2	1.320E+06	2.540	6756.00
OH+C3H8<=>C3H7+H2O	3.160E+07	1.800	934.00
C3H7+H2O2<=>H02+C3H8	3.780E+02	2.720	1500.00
CH3+C3H8<=>C3H7+CH4	0.903E+00	3.650	7154.00
CH3+C2H4(+M)<=>C3H7(+M)	2.550E+06	1.600	5700.00

LOW/ 3.00E+63 -14.6 18170./

TROE/ .1894 277.0 8748.0 7891.0 /

H2/2.00/ H2O/6.00/ CH4/2.00/ CO/1.50/ CO2/2.00/ C2H6/3.00/ AR/ .70/

O+C3H7<=>C2H5+CH2O	9.640E+13	.000	.00
H+C3H7(+M)<=>C3H8(+M)	3.613E+13	.000	.00

LOW/ 4.420E+61 -13.545 11357.0/

TROE/ .315 369.0 3285.0 6667.0 /

H2/2.00/ H2O/6.00/ CH4/2.00/ CO/1.50/ CO2/2.00/ C2H6/3.00/ AR/ .70/

H+C3H7<=>CH3+C2H5	4.060E+06	2.190	890.00
OH+C3H7<=>C2H5+CH2OH	2.410E+13	.000	.00
H02+C3H7<=>O2+C3H8	2.550E+10	0.255	-943.00
H02+C3H7=>OH+C2H5+CH2O	2.410E+13	.000	.00

CH3+C3H7<=>2C2H5	1.927E+13	-0.320	.00
! ----- Zhou Mechanism -----			
! w/o H-0 reactions			
H2S+M=H2+S+M	1.60E+24	-2.6	89170.0
H2S+H=SH+H2	3.49E+07	1.9	904.0
H2S+S=2SH	8.47E+06	2.3	9007.0 !opt
DUPLICATE			
H2S+S=2SH	8.85e+17	-1.7	5975.0 !opt
DUPLICATE			
S+H2=SH+H	1.35E+14	0.0	19290.0
S+SH=S2+H	3.20E+12	0.5	-29.0 !opt
H+S2+M=HSS+M	1.15E+25	-2.8	1665.0
H2S/1.100E+00/ AR/8.800E-01/ HE/1.390E+00/			
H+HSS=2SH	2.72E+08	1.6	-1030.0 !opt
DUPLICATE			
H+HSS=2SH	1.81E+18	-1.0	261.0 !opt
DUPLICATE			
SH+SH(+M)=HSSH(+M)	6.34E+11	0.23	-829.3 !opt
LOW /	8.5874e+30	-0.49430E+01	0.19980E+04 / !opt
TR0E /	0.10000E+01	0.25400E+03	0.23730E+04 /
SH+HSS=H2S+S2	6.27E+03	3.0	-1105.0
H+HSS=H2+S2	1.05E+08	1.8	-877.0
DUPLICATE			
H+HSS=H2+S2	2.91E+16	-0.9	-56.0
DUPLICATE			
H+HSS=H2S+S	1.50E+08	1.6	2259.0
DUPLICATE			
H+HSS=H2S+S	4.19E+18	-1.6	472.0
DUPLICATE			
S+HSS=S2+SH	4.17E+06	2.2	-600.0
HSS+HSS=HSSH+S2	9.56E+00	3.4	-1672.0
HSSH+H=HSS+H2	4.99E+07	1.9	-1408.0
HSSH+H=H2S+SH	3.66E+08	1.7	467.0
HSSH+SH=H2S+HSS	6.40E+03	3.0	-1480.0
HSSH+S=HSS+SH	2.85E+06	2.3	1204.0

H+S+M=SH+M		6.20E+16	-0.6	0.0
S+S+M=S2+M		1.89E+13	0.0	-1788.0
H2S+S(+M)=HSSH(+M)		6.38E+07	1.3	-478.0
LOW /	0.24000E+22	-0.16120E+01		0.16730E+04 /
TROE /	0.50000E+00	0.72600E+03		0.72600E+03 /
N2/1.300E+00/				
SH+H02=H2S+O2		3.31E+04	2.8	-1529.5 !opt
H2S+O2=HSO+OH		1.00E+11	0.0	49100.0
H2S+OH=SH+H2O		8.70E+13	-0.7	0.0
DUPLICATE				
H2S+OH=SH+H2O		4.07E+07	1.8	0.0
DUPLICATE				
H2S+O=SH+OH		1.80E+05	2.6	2532.0
H2S+O=HSO+H		1.36E+09	1.1	5099.0
H2O2+SH=H2S+H02		5.57E+04	2.8	8668.0
H2O2+SH=HSOH+OH		9.49E+03	2.8	9829.0
H2S+H02=HSO+H2O		1.03E+00	3.3	6224.0
H2S+HSO=SH+HSOH		1.00E+13	0.0	17300.0
H2S+HOS=SH+HSOH		1.00E+13	0.0	12500.0
H2S+S0=HSO+SH		5.38E+03	3.2	26824.0
H2S+S0=HOS+SH		1.00E+13	0.0	36500.0
SH+O2=H02+S		4.72E+06	2.0	36913.0
SH+O2=HSO+O		2.29E+06	1.8	20008.0
SH+O2=SO+OH		7.50E+04	2.1	16384.0
SH+O2=H+S02		6.50E+11	0.0	15000.0
SH+O=OH+S		1.80E+12	0.0	0.0
DUPLICATE				
SH+O=OH+S		4.32E+06	2.1	3582.7
DUPLICATE				
SH+O=SO+H		4.25E+11	0.7	-1027.0
SH+OH=S+H2O		1.67E+05	2.5	-1637.0
SH+OH=HOS+H		1.00E+13	0.0	7400.0
H2O2+S=SH+H02		4.14E+06	2.2	12619.0
SH+H02=HSO+OH		2.46E+08	1.5	-2169.0
SH+H02=H2O+S0		3.20E+02	2.6	-2071.0

SH+HSO=S+HSOH	1.00E+11	0.0	11000.0
SH+HSO=S2O+H2	1.00E+14	0.0	14250.0
H2+S2O=SH+HOS	1.00E+13	0.0	46000.0
SH+S0=HSO+S	1.00E+13	0.0	25000.0
SH+S0=HOS+S	1.00E+13	0.0	30000.0
SH+S0=S2O+H	1.00E+12	0.0	5000.0
HSSO2+M=SH+S02+M	1.00E+17	0.0	3000.0
SH+O3=HSO+O2	5.72E+08	0.0	280.0
S+OH=S0+H	1.46E+13	0.2	-1361.4
S+O2=S0+O	5.39E+05	2.06	-1593.9 !opt
S+HO2=S0+OH	5.66E+13	0.0	0.0
S+HO2=HOS+O	1.00E+13	0.0	0.0
SSO2+M=S+S02+M	1.00E+15	0.0	30000.0
S+SSO2=S2+S02	1.00E+13	0.0	0.0
S+HSO0=SH+S02	1.00E+13	0.0	0.0
S+HSO0=S0+HSO	1.00E+13	0.0	0.0
S+HOS02=SH+S03	1.00E+13	0.0	0.0
S+S03=S0+S02	1.00E+13	0.0	0.0
S+O3=S0+O2	7.23E+12	0.0	0.0
H2O2+S=HOS+OH	1.00E+12	0.0	0.0
HSO+O2=HO2+S0	6.44E+05	2.6	19013.0
HOS+O2=HO2+S0	6.44E+05	2.6	19013.0
HSO+O2=S02+OH	3.70E+01	2.8	6575.0
HOS+O2=S02+OH	3.70E+01	2.8	6575.0
HSO+O2=HSO2+O	8.40E-07	5.1	11312.0
HSO+S2=HSS+S0	1.00E+12	0.0	3000.0
HOS+S2=HSS+S0	1.00E+12	0.0	1000.0
HOS+S2=S3+OH	1.00E+13	0.0	13000.0
H+S0+M=HSO+M	4.93E+29	-5.3	1815.2
N2/0.000E+00/			
H+S0+N2=HSO+N2	2.08E+27	-4.3	812.1
H+S0+M=HOS+M	3.62E+20	-1.9	-28.7
N2/0.000E+00/			
H+S0+N2=HOS+N2	2.03E+21	-2.1	-71.7
HOS+M=HSO+M	5.77E+11	0.0	32721.9

N2/0.000E+00/			
HOS+N2=HSO+N2	2.93E+11	0.0	24601.1
HSO+H=H2+S0	6.00E+13	0.0	0.0
HSO+H=SH+OH	4.90E+19	-1.9	1560.0
HSO+H=S+H2O	1.60E+09	1.4	-340.0
HOS+H=H2+S0	1.00E+13	0.0	0.0
HSO+OH=H2O+S0	1.70E+09	1.0	470.0
HOS+OH=H2O+S0	1.00E+13	0.0	0.0
HSO+OH=H2+S02	1.00E+11	0.0	0.0
HOS+OH=H2+S02	1.00E+11	0.0	0.0
HSO+O=OH+S0	1.40E+13	0.1	300.0
HOS+O=OH+S0	1.00E+14	0.0	0.0
HSO+O=H+S02	4.50E+14	-0.4	0.0
HOS+O=H+S02	1.00E+14	0.0	0.0
H+HSO=H+HOS	1.00E+14	0.0	4000.0
HSS+O2=HSSO+O	1.00E+13	0.0	26000.0
HSSO+O=S2O+OH	1.00E+13	0.0	0.0
HSSO+O=SH+S02	1.00E+13	0.0	0.0
HSSO+H=S2O+H2	1.00E+13	0.0	0.0
HSSO+H=HSS+OH	1.00E+13	0.0	0.0
HSSO+OH=S2O+H2O	1.00E+13	0.0	0.0
HSSO+OH=HSS+H02	1.00E+13	0.0	27000.0
HSSO+SH=S2O+H2S	1.00E+13	0.0	0.0
HSS+HSO=HSSO+SH	1.00E+13	0.0	7000.0
HSSO+S=HSS+S0	1.00E+13	0.0	0.0
HSSO+S=S2O+SH	1.00E+13	0.0	0.0
HSSO+HSS=S2O+HSSH	1.00E+13	0.0	0.0
HSSO+H02=S2O+H2O2	1.00E+13	0.0	0.0
HSSO+S2=S2O+HSS	1.00E+13	0.0	0.0
S2O+HS02=HSSO+S02	1.00E+13	0.0	32000.0
HSS+S03=HSSO+S02	1.00E+13	0.0	10000.0
S2O+H+M=HSSO+M	6.42E+22	-2.6	286.6
S0*+M=S0+M	1.00E+13	0.0	0.0
S0*+O2=S02+O	1.00E+13	0.0	0.0
S0+O2=S02+O	6.56E+06	1.42	3629 !opt

S0+0(+M)=S02(+M)		3.20E+13	0.0	0.0
LOW /	0.12000E+22	-0.15400E+01	0.00000E+00 /	
TROE /	0.55000E+00	0.10000E-29	0.10000E+31 /	
N2/1.500E+00/ S02/1.000E+01/ H2O/1.000E+01/				
S0+H02=S02+OH		3.70E+03	2.4	7660.0
S0+S0+M=OSS0+M		3.23E+32	-5.8	3044.2
OSS0+0=S0+S02		1.00E+13	0.0	0.0
OSS0+0=02+S20		1.00E+13	0.0	0.0
OSS0+H=OH+S20		1.00E+13	0.0	0.0
OSS0+H=S0+HS0		1.00E+13	0.0	0.0
OSS0+H=S0+HOS		1.00E+13	0.0	0.0
OSS0+H=H02+S2		1.00E+13	0.0	12570.0
OSS0+OH=H02+S20		1.00E+13	0.0	11350.0
OSS0+OH=HOS0+S0		1.00E+12	0.0	0.0
OSS0+S0=S02+S20		2.00E+10	0.0	0.0
OSS0+S=S20+S0		1.00E+13	0.0	0.0
OSS0+S=S2+S02		1.00E+13	0.0	0.0
OSS0+SH=HS0+S20		1.00E+13	0.0	0.0
OSS0+S2=S20+S20		1.00E+12	0.0	0.0
S+S02=2S0		5.88E+12	0.0	9034.0
H+S02(+M)=HS02(+M)		5.30E+08	1.6	2472.0
LOW /	0.14100E+32	-0.51900E+01	0.45130E+04 /	
TROE /	0.39000E+00	0.16700E+03	0.21910E+04 /	
N2/1.000E+00/ S02/1.000E+01/ H2O/1.000E+01/				
H+S02(+M)=HOS0(+M)		2.37E+08	1.6	7339.0
LOW /	0.18500E+38	-0.61400E+01	0.11075E+05 /	
TROE /	0.28300E+00	0.27200E+03	0.39950E+04 /	
N2/1.000E+00/ S02/1.000E+01/ H2O/1.000E+01/				
HOS0(+M)=HS02(+M)		1.00E+09	1.0	50000.0
LOW /	0.17000E+36	-0.56400E+01	0.55400E+05 /	
TROE /	0.40000E+00	0.10000E-29	0.10000E+31 /	
N2/1.500E+00/ S02/1.000E+01/ H2O/1.000E+01/				
HOS0(+M)=OH+S0(+M)		9.94E+21	-2.5	75891.0
LOW /	0.11600E+47	-0.90200E+01	0.52953E+05 /	
TROE /	0.95000E+00	0.29890E+04	0.11000E+01 /	

H+S02=OH+S0		6.74E+21	-2.2	30736.0
S02+O(+M)=S03(+M)		3.70E+11	0.0	1689.0
LOW /	0.24000E+28	-0.36000E+01		0.51860E+04 /
TROE /	0.44200E+00	0.31600E+03		0.74420E+04 /
N2/0.000E+00/ S02/1.000E+01/ H2O/1.000E+01/				
S02+O(+N2)=S03(+N2)		3.70E+11	0.0	1689.0
LOW /	0.29000E+28	-0.35800E+01		0.52060E+04 /
TROE /	0.43000E+00	0.37100E+03		0.74420E+04 /
S02+OH(+M)=HOS02(+M)		5.70E+12	-0.3	0.0
LOW /	0.17000E+28	-0.40900E+01		0.00000E+00 /
TROE /	0.10000E+00	0.10000E-29		0.10000E+31 /
H2O/5.000E+00/ S02/5.000E+00/ N2/1.000E+00/				
HOS02+O2=S03+H02		7.83E+11	0.0	656.0
S03+S0=2S02		7.60E+03	2.4	2980.0
S03+O=S02+O2		2.80E+04	2.6	29230.0
S03+H=S02+OH		8.40E+09	1.2	3322.0
S03+OH=S02+H02		4.80E+04	2.5	27271.0
O3+S02=O2+S03		1.80E+12	0.0	14000.0
HS02+O2=S02+H02		1.10E+03	3.2	3.2
HS02+O=S02+OH		1.00E+13	0.0	0.0
HS02+H=S02+H2		5.00E+12	0.5	0.5
HS02+OH=S02+H2O		1.00E+13	0.0	0.0
HS02+SH=S02+H2S		1.00E+13	0.0	0.0
HS02+S=S02+SH		1.00E+13	0.0	0.0
HS02+H02=S02+H2O2		1.00E+13	0.0	0.0
HS02+HSS=S02+HSSH		1.00E+13	0.0	0.0
HS02+S2=S02+HSS		1.00E+13	0.0	0.0
HS02+S0=S02+HSO		1.00E+13	0.0	0.0
HS02+S0=S02+HOS		1.00E+13	0.0	0.0
HS02+HSO=S02+HSOH		1.00E+13	0.0	0.0
HOS0+O2=S02+H02		9.60E+01	2.4	2.4
HOS0+O=S02+OH		1.00E+13	0.0	0.0
HOS0+H=S02+H2		1.80E+07	1.7	1.7
HOS0+H=S0*+H2O		2.40E+14	0.0	0.0
HOS0+OH=S02+H2O		6.00E+12	0.0	0.0

HOSO+SH=S02+H2S	1.00E+13	0.0	0.0
HOSO+S=S02+SH	1.00E+13	0.0	0.0
HOSO+H02=S02+H202	1.00E+13	0.0	0.0
HOSO+HSS=S02+HSSH	1.00E+13	0.0	0.0
HOSO+S2=S02+HSS	1.00E+13	0.0	0.0
HOSO+S0=S02+HSO	1.00E+13	0.0	0.0
HOSO+S0=S02+HOS	1.00E+13	0.0	0.0
HOSO+HSO=S02+HSOH	1.00E+13	0.0	0.0
HOSO+HOS=S02+HSOH	1.00E+13	0.0	0.0
S2+O=S0+S	1.43E+11	0.7	0.7
S0+SH=S2+OH	1.00E+12	0.0	0.0
S2+O2=S20+O	1.71E+04	2.5	2.5
S2+O2=S0+S0	2.30E+03	2.5	2.5
S2+O+M=S20+M	1.88E+21	-2.8	-2.8
S20+O=2S0	9.27E+11	0.0	0.0
S20+S=S0+S2	1.00E+13	0.0	0.0
S20+SH=HSO+S2	1.00E+12	0.0	0.0
S20+SH=HSS+S0	1.00E+13	0.0	0.0
S20+OH=H02+S2	1.00E+13	0.0	0.0
S20+H=OH+S2	1.00E+13	0.0	0.0
S20+S02=S2+S03	1.00E+13	0.0	0.0
HSS+O2=H02+S2	4.10E+03	2.5	2.5
HSS+O2=HSO+S0	6.61E+03	1.9	1.9
HSS+OH=H20+S2	1.00E+14	0.0	0.0
HSS+O=OH+S2	1.00E+14	0.0	0.0
HSS+O=SH+S0	1.00E+14	0.0	0.0
HSSH+O=HSS+OH	1.00E+14	0.0	0.0
HSSH+O=HSO+SH	1.00E+14	0.0	0.0
HSSH+OH=HSS+H20	1.00E+14	0.0	0.0
HSSH+O2=HSS+H02	1.00E+13	0.0	0.0
HSSH+H02=HSS+H202	1.00E+13	0.0	0.0
HSSH+S0=HSS+HSO	1.00E+13	0.0	0.0
HSSH+S0=HSS+HOS	1.00E+13	0.0	0.0
HSSH+HSO=HSS+HSOH	1.00E+13	0.0	0.0
HSSH+HOS=HSS+HSOH	1.00E+13	0.0	0.0

HSOH+H02=HSO+H2O2	1.00E+13	0.0	0.0
HSOH+H02=HOS+H2O2	1.00E+13	0.0	0.0
HSS+H02=S2+H2O2	1.00E+13	0.0	0.0
HSO+H02=SO+H2O2	1.00E+13	0.0	0.0
HOS+H02=SO+H2O2	1.00E+13	0.0	0.0
HSS+HSO=S2+HSOH	1.00E+13	0.0	0.0
HSS+HOS=S2+HSOH	1.00E+13	0.0	0.0
HSO+HSO=SO+HSOH	1.00E+13	0.0	0.0
HOS+HOS=SO+HSOH	1.00E+13	0.0	0.0
HSOH+O2=HSO+H02	1.00E+13	0.0	0.0
HSOH+O2=HOS+H02	1.00E+13	0.0	0.0
HSOH+O=HSO+OH	1.00E+14	0.0	0.0
HSOH+O=HOS+OH	1.00E+14	0.0	0.0
HSOH+H=HSO+H2	1.00E+14	0.0	0.0
HSOH+H=HOS+H2	1.00E+14	0.0	0.0
HSOH+OH=HSO+H2O	1.00E+14	0.0	0.0
HSOH+OH=HOS+H2O	1.00E+14	0.0	0.0
H2S+S02=S2O+H2O	1.67E+06	1.9	1.9
H2S+S02=H2S2O2	3.51E+18	-2.1	-2.1
H2S2O2+H2O=H2S+VDW1	3.89E+05	1.7	1.7
H2O+S02=VDW1	1.00E+14	0.0	0.0
H2S2O2+H2O=2H2O+S2O	3.64E+05	1.6	1.6
H2S2O2+SH=HSSH+HOSO	1.00E+13	0.0	0.0
H2S+S2O=H2S3O	2.38E+19	-2.3	-2.3
H2S+S2O=S3+H2O	8.01E+07	1.5	1.5
H2S+S2O=HSSSOH	2.85E+00	3.6	3.6
H2O+S3=HSSSOH	1.00E+14	0.0	0.0
S+S2+M=S3+M	1.89E+15	0.0	0.0
S2+S2+M=S4+M	1.89E+15	0.0	0.0
S2+S3+M=S5+M	1.89E+15	0.0	0.0
S3+S3+M=S6+M	1.89E+15	0.0	0.0
S3+S4+M=S7+M	1.89E+15	0.0	0.0
S4+S4+M=S8+M	1.89E+15	0.0	0.0
S02+SH=HSO+S0	1.00E+14	0.0	0.0
S02+SH=HOS+S0	1.00E+14	0.0	0.0

S02+SH=0H+S20	1.00E+14	0.0	0.0
S02+HSS=S20+HS0	1.00E+14	0.0	0.0
S02+S2=S20+S0	1.00E+14	0.0	0.0
S20+S2=S3+S0	1.00E+14	0.0	0.0
S20+S3=S4+S0	1.00E+14	0.0	0.0
S20+S20=S3+S02	1.00E+12	0.0	0.0
SH+S02=HSS02	1.00E+13	0.0	0.0
HSS02=S20+0H	1.00E+13	0.0	0.0
S20+SH=S3+0H	1.00E+13	0.0	0.0
S0+HSS=S3+0H	1.00E+13	0.0	0.0
H2S+S0*=HS0+SH	1.00E+13	0.0	0.0
END			